PRODUCTION ANALYSIS OF BIOFILM FERMENTATION UNDER HOMOGENEOUS SHEAR CONDITIONS

by

Hendrik Gideon Brink

A dissertation submitted in partial fulfilment of the requirements for the degree

Philosophiae Doctor in Chemical Engineering

In the

Department of Chemical Engineering

Faculty of Engineering, the Built Environment and Information Technology

University of Pretoria

Pretoria

March 2015

Production analysis of biofilm fermentation under homogeneous shear conditions

Author: Hendrik Gideon Brink

Supervisor: Professor W. Nicol

Department: Department of Chemical Engineering

University of Pretoria

Degree: Philosophiae Doctor (Chemical Engineering)

Synopsis

This thesis explores the behaviour of biofilm fermenters through the analysis of two individual biofilm fermentation case studies. The studies were performed in a novel tubular bioreactor with homogeneously controlled shear. The case studies included a two-phase (gas–liquid) study performed on the anaerobic, lactic acid-producing *Lactobacillus rhamnosus*, and a three-phase (gas–liquid–solid) study on the CO_2-fixating, succinic acid-producing *Actinobacillus succinogenes*. The studies focused specifically on four parameters, namely volumetric production rates, specific production rates, the metabolic product distributions with corresponding redox analysis, and the biofilm compositions as a function of shear conditions.

It was found that the volumetric production rates in both the biofilm case studies were highly dependent on the total biomass retained within the biofilm fermenters. In the *L. rhamnosus* biofilm case study, the volumetric production rates of lactic acid exhibited nearly a two-fold increase (4.46 $g.L^{-1}.h^{-1}$ vs 8.04 $g.L^{-1}.h^{-1}$) from chemostat to biofilm operation. In comparison, the volumetric production rates of succinic acid, in the case of the *A. succinogenes* case study, increased by nearly an order of magnitude (1.8 $g.L^{-1}.h^{-1}$ vs 17 $g.L^{-1}.h^{-1}$) when comparing the chemostat with the biofilm results. The significantly larger increase in the *A. succinogenes* study, when compared with the *L. rhamnosus* study, was attributed to a marked increase in biomass concentrations when comparing the chemostat and biofilm runs.

With regard to the specific production rates, both studies indicated their significant dependence on the metabolic state (growth- or non-growth-related metabolism) of the organism in

the fermenter. Under growth-related metabolic conditions, applicable to the entire *L. rhamnosus* study as well as the *A. succinogenes* study (succinic acid titres below 10 $g.L^{-1}$), the specific production rates were shown to be shear dependent. In the *L. rhamnosus* study, it was found that the specific production rates, based on the total biomass concentration (including extracellular polymeric substances – EPS), decreased with decreasing shear velocities. This indicated a change in the biofilm composition, i.e. a change in the fraction of inactive EPS in the biofilm. In the *A. succinogenes* study, the cell-based (EPS excluded) specific production rates under growth conditions were shown to be highly dependent on shear stresses. The case study revealed an unexplained split in the rate trends between the higher- and lower-shear conditions. The specific cellular production rates in the lower-shear biofilm run were as much as five times higher (2.5 $g.g^{-1}.h^{-1}$ vs 0.4 $g.g^{-1}.h^{-1}$) than those in the higher-shear fermentation. In contrast, under maintenance conditions (succinic acid titres greater than 10 $g.L^{-1}$) the cellular production rates of *A. succinogenes* were found to be independent of shear conditions in the biofilm fermenter. The specific cellular succinic acid and adenosine triphosphate (ATP) production rates decreased exponentially from values of approximately 1 $g.g^{-1}.h^{-1}$/30 mmol $ATP.(g.h)^{-1}$, at a succinic acid titre of 10 $g.L^{-1}$, to asymptotic values of 0.59 $g.g^{-1}.h^{-1}$/16.1 mmol $ATP.(g.h)^{-1}$ at significantly high succinic acid titres. These values represent the non-growth-related cellular production rates.

Regarding the metabolic product distributions in the respective case studies, it became apparent that the microbial metabolisms for both studies were extremely sensitive to redox requirements during operation. The *L. rhamnosus* study showed that it was possible to alter the yields during biofilm fermentations by manipulating the shear conditions in the reactor and subsequently changing the biofilm composition and metabolic fluxes. The yield of lactic acid on glucose increased from 0.75 to 0.90 $g.g^{-1}$ as a result of decreasing the shear from chemostat conditions to the lowest-shear biofilm run. This corresponded to a decrease in the acetoin yield on glucose from 0.074 to 0.017 $g.g^{-1}$. It is hypothesised that the change in metabolism is linked to a decrease in redox requirements due to a change in the biofilm composition; the production of acetoin is accompanied by a net production of nicotinamide adenine dinucleotide (NADH), while the production of lactic acid is redox neutral. The results from the *A. succinogenes* study showed that under growth conditions the metabolic product distribution was linked to the shear conditions in the biofilm fermenter. The chemostat metabolism

showed a significant anabolic consumption of NADH, which corresponded to the observations in the *L. rhamnosus* study. In contrast, a shear-independent metabolic product distribution was observed under maintenance conditions (succinic acid titres in excess of 10 $g.L^{-1}$) in the *A. succinogenes* study. The results indicated an underprediction of the glucose consumption, as well as an underproduction of NADH to account for the metabolic product distribution measured during fermentations. Pyruvic acid was identified as a candidate product that could account for the "missing" glucose and the shortage of NADH. The requirement for an NADH-producing fermentation product illustrates the difference between the growth and maintenance metabolisms with respect to the redox requirements.

Lastly, concerning the biofilm compositions, i.e. the EPS fractions in the biofilm, these were found to be highly dependent on the shear conditions in both case studies. In the *L. rhamnosus* study, the predicted EPS fraction increased (0.09 to 0.70 $g.g^{-1}$) with decreasing shear velocities (0.55 to 0.19 $m.s^{-1}$). Correspondingly, the results in the *A. succinogenes* study showed a similar trend, with an EPS fraction of 0.50 ± 0.05 $g.g^{-1}$ measured for the lower-shear condition and an EPS fraction of 0.16 ± 0.02 $g.g^{-1}$ measured for the higher-shear condition. These results indicate a significant change in the biofilm morphology as a result of the shear conditions in the fermenter.

From a general biofilm fermentation perspective, the work presented in this thesis yielded fresh insights into the characteristics of biofilm fermenters with respect to the underlying mechanisms that govern single-culture biofilm fermentation.

Acknowledgements

First of all, I humbly acknowledge my heavenly Father for the inspiration, courage and strength throughout a very difficult process. This thesis was built on a huge amount of prayer without which I believe this work might never have been completed.

I would like to convey my gratitude to my supervisor, Professor Willie Nicol. It has been a privilege to work with such an incredible academic and mentor for the best part of six years. His guidance and sometimes rough criticisms shaped me into the researcher and academic I am today. I know that I gave him a huge amount of anxiety and unnecessary frustration during my less productive spells, but I thank him for his perseverance in seeing the product to completion.

My colleagues in the Bioreactor design laboratories, Jean Saayman, Carel van Heerden, Joseph Mwakio, Michael Bradfield, Karishma Maharaj, André Naudé, Adolf Krige, as well as the two new ladies, Jolandi Herselman and Uma Vijayan – we have spent many nights working at unbelievably uncomfortable hours. You guys made it worth it, with social sessions at Oom Gert's, as well as the Square, and a huge amount of brainstorming during crunch time. Thank you all so very, very much.

My family, Ma, Pa, Gert and Ansa – you guys are the best. You were an inspiration and support during the times when I felt like this was just not worth it. Thank you so much for the love and motivation through it all.

Last, but definitely not least, I have to thank my beautiful wife Kim. You came into my life about halfway through this torturous journey they call a doctorate. You (and our lovely cat, Cadey) spent many hours in the lab with me, driving in at ridiculous hours for batch samples and for fixing blockages in the line, seeing the worst of me at times when the frustration just became too much. You carried me through so much of this process with your patience and love. You know the hours I didn't spend with you while writing up and I appreciate that I was able to do so. Thank you so very, very much for everything you did and continue to do for me every day.

Dedications

This thesis is dedicated to my heavenly Father for all His support, inspiration and courage throughout this incredible process. I also dedicate this thesis to my family for all their love and support.

Finally, I dedicate this thesis to my beautiful, incredible, loving, best friend and life co-pilot, my wife Kim Brink-Flores. Without you in my life I do not think I would be finishing this project. You gave me the support when I needed a strut, you gave me direction when I felt lost and you gave me motivation when I felt overwhelmed by the enormity of the mountain I was climbing. You are amazing and I love you more every day …

This is my belated Valentine's gift to you.

"Whereas there is nothing more necessary for promoting the improvement of Philosophical Matters, than the communication to such, as apply their Studies and Endeavours that way, such things are discovered or put in practise by others"

- Henry Oldenburg (1665)

(Introduction to Volume 1, Issue 1 of Philosophical Transactions of the Royal Society of London)

The respective chapters, sections, figures, tables and equations within the study are cross-referenced through hyperlinks within the portable document format (pdf) document. Any hyperlinks within the text are indicated by capitalised, underlined, italic formatting (e.g. TABLE 2-1) and clicking on these links within the text will redirect the reader to the referenced item. Within the software package "Adobe Acrobat Reader", the reader can return to the original departure point from which the link was referenced by either selecting the "Previous view" icon on the toolbar, or alternatively depressing the alt and the left arrow keys simultaneously on the keyboard.

Contents

List of Figures

List of Tables

Nomenclature

A/V	Area to volume ratio	($m^2.m^{-3}$)
$(A/V)_{max}$	Maximum A/V as calculated for a tube only	($m^2.m^{-3}$)
AA	Acetic acid	
ABS_{560}	Absorbance of light with a wavelength of 560 nm	(-)
ABS_{660}	Absorbance of light with a wavelength of 660 nm	(-)
a_{cap}	Specific area of the cap	($m^2.m^{-3}$)
a_{film}	Specific area of the film	($m^2.m^{-3}$)
AcCoA	Acetyl-CoA	
AcLac	Acetolactate	
Acn	Acetoin	
ADP	Adenosine diphosphate	
ATP	Adenosine triphosphate	
C	Chisholm parameter used to determine two-phase pressure drop	
C_3	Section of *A. succinogenes* metabolism producing three-carbon products	
C_4	Section of *A. succinogenes* metabolism producing four-carbon products	
CA	Citric acid	
C_{CO2}^{sat}	CO_2 saturation concentration in the medium	($mol.L^{-1}$)
C_{Glc0}	Feed glucose concentration	($g.L^{-1}$)
C_i	Concentration of component i in the reactor	($g.L^{-1}$)
$C_{LA(t)}$	Concentration of LA at time t	($g.L^{-1}$)
$C_{LA,steady}$	Predicted concentration of LA at steady state	($g.L^{-1}$)
C_o	C_{xt} in the reactor prior to washout	($g.L^{-1}$)
CoA	Co-enzyme A	
C_S	C_{xt} in the sample vial after washout	($g.L^{-1}$)
C_{AA}	AA titre	($g.L^{-1}$)
C_{FA}	FA titre	($g.L^{-1}$)
C_{SA}	SA titre	($g.L^{-1}$)
C_{xt}	Total biomass concentration in the reactor	($g.L^{-1}$)

C_{xt}*	Total cellular biomass concentration in the reactor (excluding EPS)	($g.L^{-1}$)
CSTR	Continuously stirred tank reactor	
CPS	Capsular polysaccharides	
$C_R(t)$	Concentration of biomass in the reactor at time t	($g.L^{-1}$)
CSL	Corn steep liquor	
C_x	Concentration of suspended biomass in reactor	($g.L^{-1}$)
d	Tube inner diameter	(m)
d_i	Impeller diameter	(m)
d_T	Vessel diameter	(m)
D	Overall dilution rate through the reactor	(h^{-1})
$\mathfrak{D}$	Diffusivity of gas species in liquid	($m^2.s^{-1}$)
Diac	Diacetyl	
DNA	Deoxyribonucleic acid	
DOR	Degree of reduction	
EPS	Extracellular polymeric substances	
EpsE	Protein encoding for *gtf* and inhibits motility; used during biofilm formation	
ET	Ethanol	
f	Darcy-Weisbach friction factor	
F6P	Fructose-6-phosphate	
FA	Formic acid	
FA/AA	FA to AA ratio	($g.g^{-1}$)
ftf	Fructosyltransferase	
FuA	Fumaric acid	
G6P	Glucose-6-phosphate	
Gal	Galactose	
Glc	Glucose	
GlcNAc	N-Acetylglucosamine	
GLS	Gas–liquid separator	
gtf	Glucosyltransferase	
ΔGlc	Glucose consumed	($g.L^{-1}$)

HePS	Heteropolysaccharides	
HETPP	Hydroxyethyl-TPP	
HoPS	Homopolysaccharides	
k_i	Stirrer/impeller/system-dependent constant	(Pa.s)
k_La	Gas–liquid mass transfer coefficient	(h^{-1})
L	Tube length	(m)
L_{UC}	Sum of bubble and slug lengths in slugging flow	(m)
LA	Lactic acid	($g.L^{-1}$)
L_{min}	Minimum tube length to negate entrance effects	(m)
MA	Malic acid	
m_{ATP}	Specific ATP production rate during maintenance	($g.g^{-1}.h^{-1}$)
m_{ATP}*	Specific maintenance production of ATP based on x_t*	($mmol.g^{-1}.h^{-1}$)
m_{Glc}	Specific Glc consumption rate during maintenance	($g.g^{-1}.h^{-1}$)
m_P	Specific maintenance production of product P	($g.g^{-1}.h^{-1}$)
m_{SA}	Specific maintenance production of SA	($g.g^{-1}.h^{-1}$)
m_{SA}*	Maintenance production of SA based on x_t*	($g.g^{-1}.h^{-1}$)
MRS	de Man, Rogosa and Sharpe	
n	Number of repeated polymer units	
N	Stirring speed of the impeller	(s^{-1})
NAD+/NADH	Nicotinamide adenine dinucleotide	
$NADH_{consumed}$	Catabolically consumed NADH	($mol.C\text{-}mol^{-1}$)
$NADH_{produced}$	Catabolically produced NADH	($mol.C\text{-}mol^{-1}$)
NADPH	Nicotinamide adenine dinucleotide phosphate	
NS	Complex nitrogen sources	
OAA	Oxaloacetic acid	
PA	Pyruvic acid	
PCS	Plastic composite support	
pdh/fdh	Pyruvate/formate dehydrogenase	
PEP	Phosphoenolpyruvate	
pfl	Pyruvate formate lyase	
ΔP_G	Pressure drop in a single-phase gas system	(bar)

ΔP_L	Pressure drop in a single-phase liquid system	(bar)
ΔP_{min}	Minimum pressure drop as a result of the tube length, i.e. excluding pressure losses due to equipment	(bar)
PP	Polypropylene	
PPP	Pentose phosphate pathway	
ΔP_{total}	Total pressure drop including losses due to equipment	(bar)
Py	Pyruvate	
$q_{CO2}^{t,max}$	Maximum CO_2 transfer rate	($g.L^{-1}.h^{-1}$)
$q_{LA}(t)$	Volumetric production rate of LA at time t	($g.L^{-1}.h^{-1}$)
q_{SA}	Volumetric production rate of SA	($g.L^{-1}.h^{-1}$)
q_{SA}^{max}	Maximum volumetric production rate of SA/productivity boundary	($g.L^{-1}.h^{-1}$)
$Q_{NaOH}(t)$	Volumetric flow rate of NaOH at time t	($L.h^{-1}$)
Q_R	Volumetric flow rate of liquid through reactor during washout procedure	($L.h^{-1}$)
R/Q	Recycle to through-flow ratio	
R5P	Pentose-phosphates	
Rha	Rhamnose	
r	Distance from the centre to radial point r in the tube	(m)
R	Total radius of the tube	(m)
r_{ATP}*	Specific production rate of ATP based on x_t*	($mmol.g^{-1}h^{-1}$)
r_{Glc}	Specific consumption rate of Glc in the system	($g.g^{-1}.h^{-1}$)
r_P	Specific production rate of product	($g.g^{-1}.h^{-1}$)
r_{SA}	Specific production rate of SA	($g.g^{-1}.h^{-1}$)
r_{SA}*	Specific production rate of SA based on x_t*	($g.g^{-1}.h^{-1}$)
Re	Reynolds number ($\rho u_{avg} d/\mu_L$)	
Re_i	Impeller Reynolds number ($\rho N d_i^2/\mu_L$)	
S7P	Sedoheptulose-7-phosphate	
SA	Succinic acid	
SA/AA	SA to AA ratio	($g.g^{-1}$)
Δt	Sampling period of data logging system	(h)
t_f	Time at which the experimental run was terminated	(h)
TPP	Thiamine pyrophosphate	

u	Superficial recycle velocity or shear velocity	$(m.s^{-1})$
u_{avg}	Average superficial recycle velocity or shear velocity	$(m.s^{-1})$
u_G	Gas superficial velocity	$(m.s^{-1})$
u_L	Liquid superficial velocity	$(m.s^{-1})$
$u(r)$	Liquid velocity profile as a function of the tube radius	$(m.s^{-1})$
u_δ	Velocity at the edge of the viscous sublayer	(m)
v_1	Metabolic flux of Glc to LA (Chapter 5)/SA (Chapter 6)	$(C\text{-}mol.C\text{-}mol^{-1})$
v_2	Metabolic flux of Glc to Acn (Chapter 5)/ AA (Chapter 6), CO_2 and NADH	$(C\text{-}mol.C\text{-}mol^{-1})$
v_3	Metabolic flux of Glc and YE to x_t* and NADH (Chapter 5) / Glc to AA, FA and NADH (Chapter 6)	$(C\text{-}mol.C\text{-}mol^{-1})$
v_4	Metabolic flux of Glc to EPS and NADH (Chapter 5)/ Glc and NS to x_t and NADH (Chapter 6)	$(C\text{-}mol.C\text{-}mol^{-1})$
v_5	Metabolic flux of Glc to PA and NADH	$(C\text{-}mol.C\text{-}mol^{-1})$
V_R	Volume of reactor	(L)
$V_S(t)$	Volume captured in the sample vial at time t, during the washout procedure	(L)
vvm	Volume of gas per volume of reactor per minute	
x	Suspended/anabolically produced biomass	
X^2	Ratio of ΔP_L to ΔP_G	(-)
x_t	Total biomass	
x_t*	Cellular biomass (excluding EPS)	
y	Distance from tube surface	(m)
Y_3	NADH requirements for biomass production	$(mol.C\text{-}mol^{-1})$
Y_4	NADH production for EPS production	$(mol.C\text{-}mol^{-1})$
$Y_{Glc,x}^{obs}$	Observed yield of x to ΔGlc	$(g.g^{-1})$
$Y_{Glc,AA}$	Yield of AA on ΔGlc	$(g.g^{-1})$
$Y_{Glc,Acn}$	Yield of Acn on ΔGlc	$(g.g^{-1})$
$Y_{Glc,FA}$	Yield of FA on ΔGlc	$(g.g^{-1})$
$Y_{Glc,Glc}$	Theoretical ΔGlc consumption on measured ΔGlc	$(g.g^{-1})$
$Y_{Glc,P}$	Yield of metabolite P on ΔGlc	$(g.g^{-1})$
$Y_{Glc,PA}$	Yield of PA on ΔGlc	$(g.g^{-1})$
$Y_{Glc,SA}$	Yield of SA on ΔGlc	$(g.g^{-1})$

$Y_{x,ATP}^{obs}$	Observed yield coefficient of ATP on biomass	$(g.g^{-1})$
$Y_{x,Glc}$	Yield coefficient of ΔGlc on biomass	$(g.g^{-1})$
$Y_{x,Glc}^{true}$	True yield of ΔGlc to x	$(g.g^{-1})$
$Y_{x,NADH}^{obs}$	Observed yield coefficient of NADH on biomass	$(g.g^{-1})$
$Y_{x,NS}^{obs}$	Observed yield coefficient of NS on biomass	$(g.g^{-1})$
$Y_{x,SA}^{true}$	True yield coefficient of SA on biomass	$(g.g^{-1})$
$Y_{xt,x}$	Yield of x to x_t in the system	$(g.g^{-1})$
YE	Yeast extract	
y_δ	Thickness of the viscous sublayer in turbulent flow	(m)

Greek lettered abbreviations

α	Yield of CO_2 production to biomass	$(g.g^{-1})$
α_m	Actual void fraction in the reactor	$(m^3.m^{-3})$
Θ_M	Mixing time	(s)
μ	Specific growth rate of biomass	(h^{-1})
μ_{max}	Maximum specific growth rate	(h^{-1})
μ_L	Liquid viscosity	(Pa.s)
ρ	Liquid density	$(kg.m^{-3})$
ρ_i	Density of component i	$(kg.m^{-3})$
σ	Gas–liquid surface tension	$(N.m^{-1})$
τ_W	Shear stresses at the wall in a vessel or tube	(Pa)
τ_{Wo}	Wall shear stress in a single phase under equivalent conditions	(Pa)
φ_L^2	Multiplier used to determine two-phase pressure drop	(-)

CHAPTER 1
INTRODUCTION

For the past 80 to 90 years the production of fuels and platform chemicals has, almost exclusively, remained the domain of the petrochemical industry (Villadsen, Nielsen & Lidén, 2011: 7). Due to the exhaustible nature of oil and gas (i.e. non-renewable), a substitute source of raw materials for the production of these chemicals is required, creating a possible role for the biorefinery. Historically, the application of fermentation has been limited to the food and beverage industries. However, it is believed that the future of fermentation lies in bulk-scale bioprocessing (biorefinery) for the production of biofuels and value-added chemicals (Werpy & Petersen, 2004).

Currently, the main requirements for making bulk-scale bioprocessing economically viable are high-productivity fermentation, high titres and high metabolic flux towards the desired metabolites (Werpy & Petersen, 2004; Villadsen, Nielsen & Lidén, 2011: 52). Within suspended cell systems, high production rates have been traditionally achieved through separation of the biomass from the product stream by either containing the biomass behind a barrier (synthetic membrane) using a hydrocyclone (Karel, Libicki & Robertson, 1985).

Alternatively, the biomass concentration in bioreactors can be increased by immobilisation of the biomass within (entrapment) or on the surface (adsorption) of a solid support structure. Immobilisation of the microbes can be done by artificial (active) entrapment, adsorption or covalent bonding, or by natural (passive) means during which the microbe naturally adheres to the support surface (biofilms).

If an organism naturally possesses biofilm-formation properties, it is unavoidable that biofilm development will result during long-term continuous or repeat batch operation (Chapman et al., 2010). Therefore a wild organism that possesses an attractive metabolism, i.e. an appealing fermentation catalyst, yet has self-immobilisation properties predetermines the use of a biofilm reactor. A significant number of metabolically attractive fermentative organisms have

biofilm-forming properties. Examples of biofilm fermentation studies in the literature include *Clostridia beijerinckii* for the production of butanol, ethanol and acetone solvents (Huang, Ramey & Yang, 2004; Qureshi, Lai & Blaschek, 2004; Lee et al., 2008; Zhang et al., 2009), *Zymomonas mobilis* for ethanol production (Weuster-Botz, 1993; Kunduru & Pometto, 1996a), *Acetobacter* species used for acetic acid production (Kennedy et al., 1980; Park & Toda, 1992; Horiuchi et al., 2000), *Lactobacilli* species for lactic acid production (Krischke, Schröder & Trösch, 1991; Gonçalves et al., 1992; Silva & Yang, 1995; Bruno-Bárcena et al., 1999; Dagher et al., 2010) and *Actinobacillus succinogenes* for succinic acid production (Urbance et al., 2004; Van Heerden & Nicol, 2013; Bradfield & Nicol, 2014; Maharaj, Bradfield & Nicol, 2014; Yan, Zheng, Tao, et al., 2014).

There are three major modes of biofilm fermentation: the repeat batch, fed batch and continuous operation. The repeat batch involves the drainage and replenishment of the liquid fraction in the reactor while the solid catalyst fraction is retained in the reactor. The fed batch involves transient biofilm fermentation, during which a specific variable or variables are controlled by the addition of a feed stream, the composition of which depends on the control strategy employed. Continuous operation involves an inlet feed stream and an outlet product stream that continuously maintain a steady state within the biofilm fermenter, i.e. the various process parameters remain constant over time.

The major advantage of repeat batch and fed batch operation is that, in the case of severe catabolite repression, the integrated average production rates are higher than those of continuous operation. However, due to the transient nature of these modes of operation, the biofilm environment constantly changes, making the prediction and control of the biofilm fermenter problematic. Consequently, the stability of continuous biofilm fermentation is preferred for industrial bioprocessing. Continuous biofilm fermenters inherently regulate the concentration of the external metabolites and substrates in the reactor by constant removal/replenishment during operation, while retaining the biomass within the reactor. This stability does not, however, extend to the genetic stability of recombinant organisms. The continuous removal of biomass can cause these organisms to revert back to the parent strain as genetic modifications tend to inhibit an organism's energy efficiency and growth rate.

Fundamental studies of biofilm reactors are extremely rare due to the difficulty in quantifying the total and cellular biomass in the biofilm fermenter. With biofilm reactors, most of the

biomass is retained within the reactor volume and therefore the fermentation has to be completely terminated in order to remove all the biomass (Maharaj, Bradfield & Nicol, 2014). Currently, the preferred tool used for fundamental continuous fermentation analysis is the classic chemostat, as the outlet biomass concentration represents the biomass concentration in the bioreactor.

Fundamental understanding of biofilm fermentation requires proper quantification of the producing biomass and of the biofilm composition, i.e. the extracellular polymeric substances and cellular biomass distributions, as a function of operational conditions. From a yield perspective, analysis of the metabolic flux distribution is essential. These parameters are required for upscaling of laboratory-scale biofilm reactors to pilot plant and eventually industrial-scale applications.

The objective of this study was to address the shortage of fundamental investigations into biofilm fermentation by designing a fermenter with the ability to remove biofilm biomass *in situ*. This was to be done either by increased wall shear due to shear velocity increases or by mechanical friction through the soft silicone tubing. The *in situ* removal of biofilm enabled biomass analysis (total and cellular fractions), which could be used to analyse the production process within the biofilm fermenter.

In addition to the removal of biofilm, the controlled shear velocity allowed chemostat operation as well as the study of biofilms under varying homogeneous shear conditions. During fermentation studies on organisms with biofilm-producing capabilities, the microbe tends to adhere to the inside of traditional bioreactor surfaces. In this study, it was possible to increase the shear stress within the reactor sufficiently to inhibit biofilm formation and therefore chemostat analysis was possible. The chemostat results were required to establish a baseline for comparison of the biofilm results. The control of the shear velocities, and by extension the shear stresses experienced by the biofilm in the bioreactor, allowed the study of shear influences on the biofilm morphology and composition as a function of shear conditions. These results would contribute to further fundamental understanding of the biofilm fermentation.

The study was limited to two case studies, the first being a two-phase (liquid–solid) and the second a three-phase (gas–liquid–solid) biofilm fermenter system. The first case study in-

volved an anaerobic gram-positive organism, *Lactobacillus rhamnosus*, known for its extracellular polymeric substance producing (biofilm producing) capabilities (Dupont, Roy & Lapointe, 2000; Van Calsteren et al., 2002; Bergmaier, Champagne & Lacroix, 2005; Kim et al., 2006) as well as negligible gas production during fermentation. The second case study was performed using *Actinobacillus succinogenes*, a CO_2 fixating gram negative species; *A. succinogenes* is reported to self-immobilise on various support structures (Urbance et al., 2003; Van Heerden & Nicol, 2013; Bradfield & Nicol, 2014; Maharaj, Bradfield & Nicol, 2014). These two organisms are considered as biofilm fermentation "guinea pigs" with the ultimate aim of broadening the fundamental understanding of biofilm fermentation.

The scope and layout of the study was arranged as follows. Initially, general theoretical knowledge on biofilms in nature, biofilm formation and the dynamic structure of biofilms is presented in Section 2.1. This is followed by the literature concerning the two microbial species used in the case studies, which are presented in Sections 2.2 (*L. rhamnosus*) and 2.3 (*A. succinogenes*). Subsequently, the design and experimental operation of the respective two-phase (Chapter 3) and three-phase (Chapter 4) reactors are discussed, as well as the results from the respective case studies (Chapters 5 and 6). Finally the conclusions from the entire study are presented (Chapter 7).

A significant portion of the work presented in this thesis has been published in peer-reviewed articles. The work presented in Chapters 3 and 5 was published in the journal *New Biotechnology* (Brink & Nicol, 2014a). Some of the work shown in Chapters 4 and 6 was published in the journal *Microbial Cell Factories* (Brink & Nicol, 2014b); this includes the chemostat analysis section (Section 6.2) and the results from the lower shear velocity of 0.09 $m.s^{-1}$ (TABLE 6-4). The batch results (Section 6.3.2), the higher shear velocity (0.36 $m.s^{-1}$) results (TABLE 6-5) and the metabolic flux analysis (Section 6.3.4) are yet to be submitted for publication.

CHAPTER 2
LITERATURE

2.1 Bacterial Biofilms

2.1.1 The poetry of biofilms

2.1.1.1 *Biofilm background*

Biofilms were first described late in the 17th century by the Dutch inventor and scientist Antonie van Leeuwenhoek when, using his simple microscope to analyse the dental plaque on the surface of his own teeth, he observed what he called “animalcules” within the plaque structure (Leewenhoeck, 1684). He observed that there were differences between the “animals” freely suspended in water and those in the “scurf” on his teeth. He noted that when treating the suspended “animals” with wine vinegar, “the Animals dyed [sic] presently”; by contrast, gargling with wine vinegar left “an innumerable quant’ty [sic] of Animals yet remaining in the scurf upon the Teeth”. He concluded that the vinegar only kills those microbes on the outside of the plaque layer and does not pass through the whole of the substance (Leewenhoeck, 1684).

The term “biofilm” was first coined and described in 1978 (Costerton, Geesey & Cheng, 1978; Costerton, 1989). Biofilms are defined as naturally occurring, multicellular communities which are irreversibly attached to solid surfaces by a self-produced extracellular matrix (Donlan, 2002; Dunne, 2002; Cheng, Demirci & Catchmark, 2010; López, Vlamakis & Kolter, 2010) and are observed universally. Virtually any surface, whether animal, mineral or vegetable, and has the potential to provide a biofilm formation site (Dunne, 2002; Vu et al., 2009; Flemming & Wingender, 2010; López, Vlamakis & Kolter, 2010). Biofilms are considered to represent the typical environment for most microbial cells in natural and artificial settings; more than 99%

of microbes in nature are estimated to exist in biofilms (Sutherland, 2001a; Donlan & Costerton, 2002; Vu et al., 2009; Goldstone et al., 2012).

Biofilms consist of complex associations of cells, extracellular products and debris left over during biofilm formation from cell excretion or from cell lysis as a result of aging. The main constituent of biofilms is typically water (> 90%), while the main structural components (> 70% of the dry weight) are ordinarily a mixture of exopolysaccharides secreted by the microbial cells themselves. This exopolysaccharide mixture maintains the biofilm's structural integrity in much the same way as the macromolecules in processed food provide a recognisable structure (Sutherland, 2001a). This edifice contains the cells, water, ions and soluble molecules contained in the biofilm. Biofilm thicknesses can vary from a few microns to several centimetres and depend on the microbes present, biofilm age, availability of nutrients and shear stresses present (Sutherland, 2001a; Vu et al., 2009; Cheng, Demirci & Catchmark, 2010).

Biofilms are characterised by significant differences, compared with their planktonic counterparts, with respect to various physiological features. These features include:

- Increased growth and activity as a result of the "bottle effect" (Donlan, 2002; Kokare et al., 2009). The "bottle effect" was first quantitatively analysed by Heukelekian and Heller (1940) and compares the microbial concentrations in batch reactors of different surface-to-volume ratios. They found that significant increases in microbial activity were apparent in bottles with glass beads as opposed to those without, if nutrient limitations were present in the reactors (Heukelekian & Heller, 1940).
- Increased tolerance to stress, protection against biocides, antibiotics, surfactants, bacteriophages, host immunological defences, as well as protozoan grazing (Whitfield, 1988; Dunne, 2002; Beloin, Roux & Ghigo, 2008; López, Vlamakis & Kolter, 2010). For example, the exopolysaccharides of the probiotic *Lactobacillus rhamnosus* GG (ATCC 53103) form a protective shield against innate defences within human intestines (Lebeer et al., 2011).
- Transcribed genes controlling for various physiological aspects of the microbes, e.g. the down-regulation of genes that transcribe for the flagellar apparatuses unnecessary after irreversible adhesion to surfaces. As well as the down-regulation of genes

required for the production of colanic acid, a polysaccharide acid which forms a capsule around bacterial cells. This is required during initial attachment as the capsule inhibits the preliminary association of the organism with the surface. The production of colanic acid is, however, up-regulated during biofilm maturation as this plays a role in mature biofilm architecture (Dunne, 2002; Beloin, Roux & Ghigo, 2008).

- Changes in the metabolism as a result of stationary-phase conditions within the biofilm (Beloin & Ghigo, 2005; Beloin, Roux & Ghigo, 2008; López, Vlamakis & Kolter, 2010). The stationary phase is defined as the condition in a reactor when the cellular population in the reactor remains constant (Cloete & Atlas, 2006: 40). The stationary phase can lead to a significant change in microbial physiology and a subsequent increase in the production of secondary metabolites, such as antibiotics, pigments, etc. (Beloin & Ghigo, 2005; Beloin, Roux & Ghigo, 2008; López, Vlamakis & Kolter, 2010)

2.1.1.2 *Formation of biofilms*

The formation of biofilms typically involves the following three stages and is shown in *FIGURE 2-1* (Cheng, Demirci & Catchmark, 2010):

1. **Attachment**. This stage is dictated by surface properties such as roughness and charge, as well as the rate of transportation of the microbe to the surface (Cheng, Demirci & Catchmark, 2010; Dagher et al., 2010). Dunne (2002) explains that the process of initial microbial adhesion is analogous to the initial docking of a space shuttle to a space station, which is followed by a secondary locking phase. The docking phase involves the chance interaction between a surface and a microorganism, during which the interactions are weak and reversible, dictated by various physicochemical variables resulting from the microbe-surface interactions. The planktonic microbes are transported to the substratum by diffusion, convection or self-motility and there form a weak, reversible adhesion with the substratum. Generally, the adhesion takes place by non-specific interactions (e.g. hydrophobic) in the case of abiotic surfaces, while specific molecular docking mechanisms (e.g. lectin, ligand or adhesion) are observed on biological surfaces (Dunne, 2002; Beloin & Ghigo, 2005; Beloin, Roux & Ghigo, 2008; Cheng, Demirci & Catchmark, 2010; Petrova & Sauer, 2012).

Certain genes are regulated (by, e.g., a σ-factor) upon initial interaction with surfaces, phenotypically differentiating the sessile cells from their planktonic equivalent (Costerton et al., 1995; López, Vlamakis & Kolter, 2010). These include the derepressing of genes that induce exopolysaccharide production, as well as repressed genes that encode for flagella which is unnecessary for sessile lifestyle (Costerton et al., 1995; Beloin & Ghigo, 2005; Beloin, Roux & Ghigo, 2008). Guttenplan, Blair and Kearns (2010) found that the same protein, EpsE, is bifunctional, acting as a flagellar clutch as well as an exopolysaccharide biosynthesis glycosyltransferase enzyme. This protein disengages (working as a clutch) the flagellum while aiding in exopolysaccharide production, thereby promoting biofilm formation (Guttenplan, Blair & Kearns, 2010). In the case of high shear environments, various organisms react by inducing a global genetic response causing a complete modification of surface constituents, including flagella, fimbriae, pili, capsule and cell-wall polysaccharides (Dagher et al., 2010).

2. **Colonisation**. The colonisation phase starts with the locking procedure in the Dunne (2002) analogy. The microbes are anchored irreversibly (in the absence of physical or chemical interventions) to the surface by the actions of specific adhesins to the surface (Dunne, 2002), also referred to as “polymer bridges” (Cheng, Demirci & Catchmark, 2010; Dagher et al., 2010). Loosely bound organisms unify the initial structure by producing exopolysaccharides which form links between the surface and specific ligands on the pili, fimbriae and fibrillae (Dunne, 2002; Dagher et al., 2010). During this stage, planktonic organisms may agglomerate, forming aggregates on the substratum or in the medium. It is widely accepted that all bacteria produce multiple adhesins used for attachment and that these are regulated via transcriptional controls. This permits the bacteria to switch between sessile and planktonic lifestyles under different environmental conditions (Dunne, 2002; Cheng, Demirci & Catchmark, 2010).
3. **Growth**. After colonisation, the biofilm growth phase, also termed the biofilm maturation phase, starts. This phase involves an increase in biofilm density and complexity as sessile organisms replicate and die within the biofilm matrix and the extracellular components, excreted by the microbes, interact with the environment, creating an exopolymeric matrix or glycocalyx (Dunne, 2002; Dagher et al., 2010). The growth of biofilms is limited by the availability of nutrients in the environment, the diffusion of nutrients to the cells in the biofilm and the removal of waste from the biofilm. The cells within the biofilm become

inactive or die as a result of the unfavourable environment (Wimpenny & Colasanti, 1997; Dunne, 2002; Cheng, Demirci & Catchmark, 2010; Dagher et al., 2010). The growth of biofilms is further limited by hydrodynamic forces which balance the growth and erosion or sloughing of the biofilm's outer layer (van Loosdrecht et al., 2002; Cheng, Demirci & Catchmark, 2010; Dagher et al., 2010).

There have been indications that cells within the biofilm matrix form channels within the biofilm used for substrate or product delivery, as well as for waste removal (Dagher et al., 2010; Gloag et al., 2013). The matured biofilms have been observed to control bacterial growth, intercellular cooperation and metabolism in such a manner that they resemble primitive eukaryotic tissue (Wimpenny & Colasanti, 1997; Dunne, 2002). At a certain point in the life cycle a dynamic equilibrium is reached during which the biofilm's outer layer starts producing microorganisms able to break free of the biofilm. These organisms have the ability to move on and colonise a new or established biofilm (Dunne, 2002; Cheng, Demirci & Catchmark, 2010; Dagher et al., 2010).

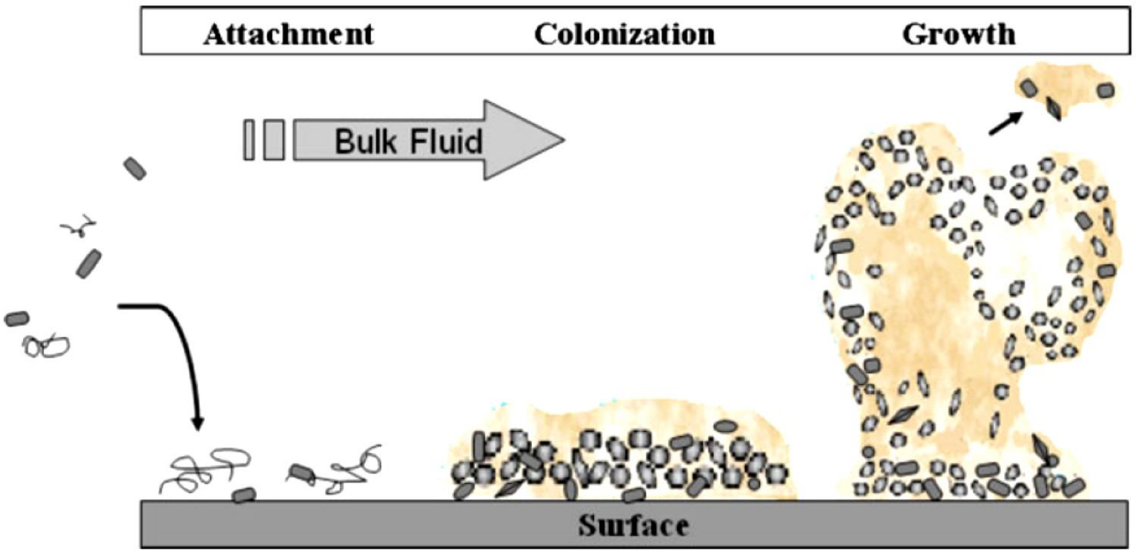

Figure 2-1: The typical life-cycle of biofilm formation and dispersion (Cheng, Demirci & Catchmark, 2010)

2.1.1.3 *Dynamic biofilm structure*

The structures of biofilms are widely reported to vary significantly in space and over time (van Loosdrecht et al., 2002; Cheng, Demirci & Catchmark, 2010). These structures are believed to

reflect the function of the biofilms and are affected by a combination of several factors (Costerton et al., 1995; Van Loosdrecht et al., 1995; Cheng, Demirci & Catchmark, 2010):

- Nutrient availability or diffusional limitation
- Adhesive capabilities or exopolysaccharide production
- Shear forces
- Growth rate of microorganisms
- Environmental conditions (e.g. temperature, pH and external metabolite concentrations)

The exact structure of biofilms and their relation to function are not currently well understood due to their immense complexity. However, at least three models have been proposed to account for biofilm structures, developed from the visual analysis of the biofilms of various microbes (Wimpenny & Colasanti, 1997; Cheng, Demirci & Catchmark, 2010; Ercan & Demirci, 2015). It has been reported that combinations of different biofilm structures have been observed in the same environment (Ercan & Demirci, 2015):

1. **The heterogeneous, water-channel or mushroom model** (Costerton et al., 1995)**:**
   The heterogeneous model describes the biofilm as consisting of proliferated mushroom forms, which are attached to "stalks" of exopolysaccharides. Some of the stalks coalesce to form water channels that penetrate deep within the biofilm structure, with smaller channels observed within the mushroom structures themselves. The channels act as a form of primitive circulatory system comparable to that in higher order animals and are effective in exchanging substrate for waste products, as well as regulating the internal conditions within the biofilm (Costerton et al., 1995; Wimpenny & Colasanti, 1997; Dunne, 2002).
2. **The heterogeneous mosaic or pseudo-homogeneous model** (Walker et al., 1995)**:**
   The heterogeneous mosaic or pseudo-homogeneous model is similar to the heterogeneous model in that it describes the biofilm as micro-colonies forming stacks which are attached to the surface at their base; they are, however, seen to be well separated from each other. In addition, there is a background film (≈5 µm) of individual cells covering the surface between the stacks. The main difference between this

model and the heterogeneous model is that the stacks are spread apart and therefore not connected to form channels (Wimpenny & Colasanti, 1997).

3. **Dense or homogeneous biofilm model** (Nyvad & Fejerskov, 1989)**:**

   The dense or homogeneous model was originally developed as a means to describe dental plaque biofilm. It is seen as a dense biofilm without the macroscopic structural characteristics, such as channels or significant protrusions from the surface, observed in heterogeneous biofilms. There is still structural organisation present, with various micro-colonies of similarly shaped bacteria populating various areas on the surface. This model also describes the biofilm present in internal medical devices such as catheters which lacks evidence of channelling within the biofilm (Wimpenny & Colasanti, 1997).

The theory in explaining the underlying mechanisms that govern the biofilm structure as described in the models above revolves around the interplay of various phenomena within the system (Van Loosdrecht et al., 1995). These phenomena can be summarised as a simultaneous balance between various intrinsic and extrinsic factors (Sutherland, 2001b; Flemming & Wingender, 2010). The extrinsic factors are the supply of substrate (diffusional effects) and detachment forces (shear effects) (Van Loosdrecht et al., 1995; Dunne, 2002), and the intrinsic forces are global microbial regulation, as well as the exopolymeric and protein-producing capabilities of the bacteria (genetic effects) (Sutherland, 2001b; Dunne, 2002; Flemming & Wingender, 2010):

1. **Diffusional effects:**

   Diffusional gradients result from a higher rate of substrate consumption/metabolite production than their corresponding diffusional rate of substrate supply or metabolite removal. If the concentration gradients are high, strongly porous or filamentous biofilms result. This is due to the difference in growth rates in high substrate/low metabolite environments (at the tips) and low substrate/high metabolite environments (at the base). In the case of a biofilm grown in an environment with a low concentration gradient, the microbes grow at a more unified rate and are therefore likely to form a more homogeneously distributed biofilm (van Loosdrecht, Picioreanu & Heijnen, 1997). The supply of substrate is considered the main effect dominating the formation of biofilms (Wimpenny & Colasanti, 1997).

2. **Shear effects:**

   High shear results in the removal of biofilm layers from the outside of the biofilm and, by extension, the removal of filamentous appendages as a result of uneven growth and diffusional gradients; this results in smoother biofilm surfaces which tend to exhibit a more two-dimensional geometry. Higher shear also increases the turbulence and therefore mixing in the environment, which inherently leads to smaller external concentration gradients. The combination of smoother biofilm surfaces and smaller concentration gradients means that high shear tends to result in less porous and denser biofilms (Van Loosdrecht et al., 1995; Liu & Tay, 2002).

3. **Genetic effects:**

   Global microbial regulation

   It has been found that the initial development, maturation and breakdown of biofilms are regulated by population density-dependent gene expressions which are controlled by quorum sensing cell-to-cell signalling molecules (Donlan, 2002; Laspidou & Rittmann, 2002; van Loosdrecht et al., 2002; Vu et al., 2009; Dagher et al., 2010; May & Okabe, 2011; Terada et al., 2012; Tan et al., 2014), examples being acylated homoserine lactones (Laspidou & Rittmann, 2002; Beloin & Ghigo, 2005; Beloin, Roux & Ghigo, 2008; Vu et al., 2009; Goldstone et al., 2012; Petrova & Sauer, 2012) in Gram-negative species and oligopeptides in Gram-positive species (Vu et al., 2009; Goldstone et al., 2012; Petrova & Sauer, 2012).

   As a result of the heterogeneity of most biofilms with respect to time and space, significant differences can arise in phenotypes between sub-populations in a biofilm. This is a result of differences in gene expression and not necessarily gene composition (López, Vlamakis & Kolter, 2010). In addition to quorum sensing, several studies (Whitchurch et al., 2002; Vilain et al., 2009; Das et al., 2010; López, Vlamakis & Kolter, 2010; Petrova & Sauer, 2012; Gloag et al., 2013) observed the importance of extracellular DNA (eDNA) in regulating biofilm properties and controlling cellular interactions. It was originally believed that the eDNA was residual DNA from lysed cells (López, Vlamakis & Kolter, 2010). However, it has recently been discovered that the eDNA was also excreted by living cells to act as biofilm regulators (Whitchurch et al.,

2002). Biofilm sensitivity to certain secondary metabolites, including antibiotics, pigments and siderophores, also acted as regulators which, at low concentrations, act as trigger signals for gene expression changes.

Exopolysaccharide and protein production capabilities

Biofilm characteristics are significantly affected by the extracellular polysaccharides and protein production capabilities of the specific bacterial population present. This was demonstrated in biofilm construction significantly altered by mutans that lacked certain exopolysaccharide production genes, as compared with their parent strains (Flemming & Wingender, 2010).

2.1.1.4 *Extracellular polymeric substances (EPS)*

EPS background

Flemming, Neu and Wozniak (2007) described a biofilm, metaphorically, as a "city of microbes" with the EPS being the "house of the biofilm cells". The abbreviation EPS originally denoted extracellular polysaccharides (Whitfield, 1988) or exopolysaccharides (Sutherland, 2001a) but was subsequently renamed extracellular polymeric substances (Wingender, Neu & Flemming, 1999; Laspidou & Rittmann, 2002; Vu et al., 2009; Flemming & Wingender, 2010). EPS of bacterial origin consist of an intricate combination of biopolymers, the usual composition being polysaccharides, proteins, nucleic acids, lipids and humic substances, as well as intracellular (from lysed cells) and intercellular (excreted from cells) DNA (Wingender, Neu & Flemming, 1999; Flemming, Neu & Wozniak, 2007; Vu et al., 2009; Flemming & Wingender, 2010).

EPS generally refer to the organic substances that provide initial adhesion to the surface, provides protection against environmental stress and dehydration, and keep the exopolymeric matrix (glycocalyx) architecture intact (Ruas-Madiedo & De los Reyes-Gavilán, 2005; Vu et al., 2009; Flemming & Wingender, 2010; López, Vlamakis & Kolter, 2010). The nature and composition of the EPS differ greatly and are dependent on the growth conditions, medium, substrates, age of the biofilm and the species under consideration (Whitfield, 1988; Czaczyk & Myszka, 2007; Vu et al., 2009; López, Vlamakis & Kolter, 2010). EPS have been referred to as

"the dark matter of biofilms" due to the diversity of biopolymers present and the difficulty in analysing them (Flemming, Neu & Wozniak, 2007; Flemming & Wingender, 2010).

EPS are considered to contribute significantly to the physical attributes of biofilms as a result of their ability to interact with other polysaccharides, macromolecules, cells, ions and small solutes (Sutherland, 2001a; Flemming, Neu & Wozniak, 2007; Flemming & Wingender, 2010; Ercan & Demirci, 2015). *TABLE 2-1* summarises the main functions of EPS as identified by Flemming and Wingender (2010).

The influence of EPS on biofilm architecture

Most of the volume in a biofilm is usually occupied by EPS and therefore the microbial environment is significantly affected by the characteristics of the specific EPS in the biofilm matrix (Flemming & Wingender, 2010). The EPS matrix has been found to separate the biofilm into discrete micro-domains (Lawrence et al., 2007); this provides an almost infinite range of micro-environments within a biofilm structure which are enzymatically adapted to localised conditions (Sutherland, 2001a; Flemming, Neu & Wozniak, 2007; Flemming & Wingender, 2010; Ercan & Demirci, 2015). *FIGURE 2-2* shows the biofilm as visualised by De Beer et al. (1994) at various dimensions (Flemming & Wingender, 2010). This figure shows the various interactions within the biofilm, from the microbial scale (*FIGURE 2-2*a) to the macromolecular scale (*FIGURE 2-2*b), the molecular scale with the corresponding intermolecular forces (*FIGURE 2-2*c), and then finally a molecular modelling simulation of the interaction of alginate with lipase within a *Pseudomonas aeruginosa* biofilm system (*FIGURE 2-2*d). From this figure can be seen that the biofilm system exhibits significant heterogeneity throughout its structure.

There are various factors that influence the internal structure of biofilms (see *DYNAMIC BIOFILM STRUCTURE* on page *2-5*). Among these are the EPS production capabilities of the specific biofilm strain or consortium under investigation. These influences were investigated by analysing the differences between the biofilms with and without (parent strains vs. mutans) various EPS production genes (Flemming & Wingender, 2010). Examples of these are:

- Exopolysaccharides of *Vibrio cholerae* (Watnick, Kolter & Watnik, 1999)
- Colanic acid production in *Escherichia coli* K-12 (Danese, Pratt & Kolter, 2000)
- Exopolysaccharide and protein production in *Bacillus subtilis* (Branda et al., 2006)

- "Fruiting body" formation during starvation in *Myxococcus xanthus* (Lux et al., 2004)
- Alginate production in *Pseudomonas aeroginosa* (Franklin & Ohman, 1993; Tielen et al., 2005)
- Interaction of anion EPS with carboxylic substituents with multivalent ions, e.g. Ca^{+2}, Mg^{+2}, etc. The ions act as bridges between the carboxylic substituents, providing structural stability (Franklin & Ohman, 1993; Tielen et al., 2005).

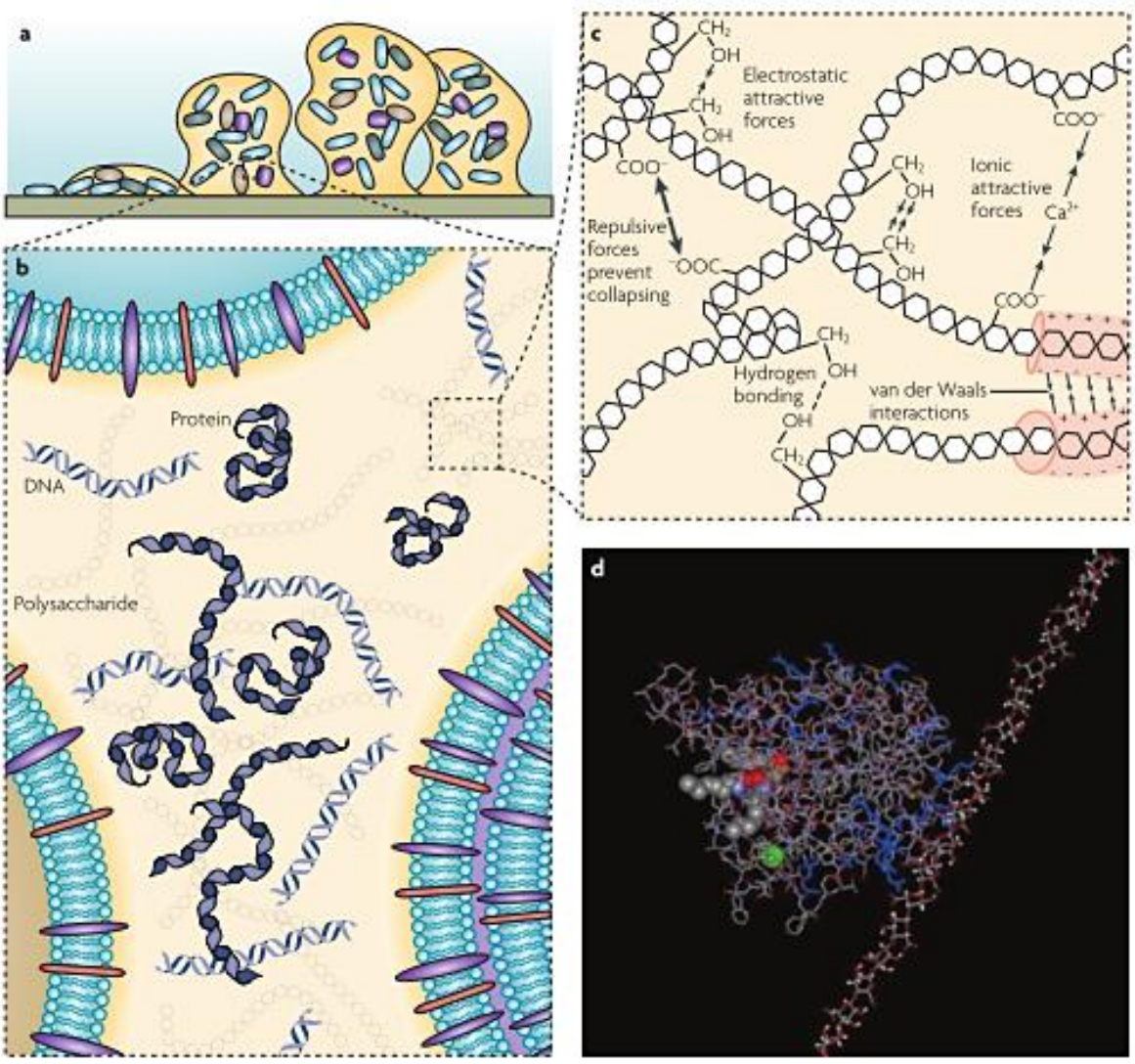

Figure 2-2: The biofilm as visualised by De Beer et al. (1994) at various dimensions (Flemming & Wingender, 2010), showing various interactions and the significant heterogeneity throughout the biofilm structure. a) microbial scale, b) macromolecular scale, c) molecular scale with the corresponding intermolecular force d) a molecular modelling simulation of the interaction of alginate with lipase within a *Pseudomonas aeruginosa* biofilm system.

Table 2-1: The main functions of EPS as identified by Flemming and Wingender (2010). EPS are considered to contribute significantly to the physical attributes of biofilms as a result of their ability to interact with other polysaccharides, macromolecules, cells, ions and small solutes.

Function	Application in the biofilm	EPS components involved
Adhesion	Aids in the initial colonisation of surfaces by planktonic cells and long-term attachment of biofilm	Polysaccharides, protein, DNA, amphiphilic compounds
Aggregation	Allows cellular bridging, temporary immobilisation, increased cellular densities and cell–cell recognition	Polysaccharides, proteins, DNA
Cohesion	Forms the biofilm matrix, provides mechanical stability and determines biofilm architecture	Charged and neutral polysaccharides, protein, DNA
Water retention	Maintains a water-rich milieu for microbes, increasing tolerance to water-scarce environments	Hydrophilic polysaccharides
Protection	Provides various forms of protection, including resistance to antibiotics, antiseptics, protozoan predation or host immune defences	Polysaccharides, proteins
Organic sorption	Enhances the absorption of environmental nutrients, aiding in environmental decontamination	Charged and hydrophobic polysaccharides, proteins
Inorganic sorption	Enhances the absorption of inorganic ions which promotes polysaccharides production, ion exchange, and removal of unwanted metal ions in the environment	Charged polysaccharides, proteins, phosphates, sulphates
Enzyme action	Digestion of extracellular macromolecules as nutrient source for cells, degradation of structural EPS which releases sessile biofilm cells	Proteins
Source of nutrients	Stores carbon, nitrogen and phosphate for use by biofilm inhabitants	All EPS components
Cell–cell communication	Increases proximity of biofilms cells, aiding in horizontal gene transfer and communication	DNA, quorum sensing molecules
Electron transfer	Aids in redox reactions within the biofilm	Proteins, humic substances
Cell component expulsion	Removes unwanted cellular material from cell lysis and metabolism	Nucleic acids, enzymes, lipopolysaccharides, phospholipids
Energy sink	Stores excess carbon during nitrogen-limited conditions	Polysaccharides
Enzyme binding	Concentrates and stabilises enzymes through enzyme–polysaccharide interaction	Polysaccharides, enzymes

The EPS production genes have been found to be regulated by "megaplasmids" rather than chromosomally in various *Escherichia, Streptococcus* and *Lactobacillus* subspecies. The section of genes controlling EPS production can therefore be replaced by genes from other bacteria, thereby manipulating the EPS and, by extension, the biofilm properties (Czaczyk & Myszka, 2007).

Exopolysaccharides

Exopolysaccharides are considered to constitute a significant portion of the EPS in biofilms. Most are long, linear or branched molecules of molecular mass 5×10^5–2×10^6 daltons (Flemming & Wingender, 2010). Exopolysaccharides can be classified according to their intrinsic and extrinsic properties. Intrinsically, the polysaccharides are divided into:

- Homopolysaccharides (HoPS), which are polysaccharides with identical monosaccharide units (Flemming & Wingender, 2010; Harutoshi, 2013: 516),
- Heteropolysaccharides (HePS) which, with the exception of alginate, usually consist of repeating units of 2-8 monosaccharides composed mostly of D-glucose, D-galactose, and L-rhamnose (Sutherland, 2001a; Vu et al., 2009; Harutoshi, 2013: 516).

Some bacteria are able to manufacture both types of exopolysaccharides (HoPS and HePS) (Ercan & Demirci, 2015)

Extrinsically, exopolysaccharides are classified with respect to the cellular association after production (Whitfield, 1988; Cerning, 1990; Laspidou & Rittmann, 2002; Kim et al., 2006; Cuthbertson et al., 2009):

- As capsular (Whitfield, 1988; Cerning, 1990) or cell-bound (Kim et al., 2006) polysaccharides (CPS) (K-antigen), which are intimately associated with the cell surface. CPS are mostly covalently bonded to the phospholipid lipid-A molecules on the cellular surface (Whitfield, 1988; Roberts, 1996; Fajardo-Solache, 1999).
- As slime polysaccharides (Whitfield, 1988; Degeest, Vaningelgem & De Vuyst, 2001; Broadbent et al., 2003) or released polysaccharides (Cerning, 1990; Fajardo-Solache, 1999; Kim et al., 2006), which are only tentatively associated with the cellular surface.

The differences between these polysaccharides are often only defined as the observable cell association following centrifugation; in some cases both types of EPS are produced by the same microbe (Cerning, 1990). CPS and lipopolysaccharides (O-antigen) are sometimes difficult to distinguish. It has been suggested by Lee at al. (2013) that the presence of CPS is detrimental during the formative stage of a biofilm, but is required during the maturation stage and that CPS therefore mostly form at later stages of biofilm lifecycles.

It was found for *L. rhamnosus* that during maturation the fractions of each of these respective types of exopolysaccharide changed from initially a higher amount of cell-bound exopolysaccharide (61%) during exponential growth to a much lower fraction of cell-bound exopolysaccharide (23%) during the stationary phase (Kim et al., 2006).

- *Homopolysaccharides (HoPS)*

  The most common HoPS can be classified as either glucans, from D-glucose, or fructans, from L-fructose (Czaczyk & Myszka, 2007; Flemming & Wingender, 2010; Badel, Bernardi & Michaud, 2011). The HoPS can be further classified according to the linkages present in the polysaccharide chains (Czaczyk & Myszka, 2007; Badel, Bernardi & Michaud, 2011; Harutoshi, 2013: 516).

  The biosynthesis of HoPS occurs outside the cell surface and requires a specific substrate, e.g. sucrose or similar oligosaccharide, indicating requirement for very specific enzymes (glycosyltransferases (*gtf*) or fructosyltransferases (*ftf*)) (Whitfield, 1988; Cerning, 1990; Badel, Bernardi & Michaud, 2011; Harutoshi, 2013: 520). The biosynthesis of HoPS are considered significantly low in terms of energy requirements, the only energy requirement from the cell is the initial enzyme production, after which extracellular synthesis of the polysaccharides take place (Badel, Bernardi & Michaud, 2011; Harutoshi, 2013: 520).

- *Heteropolysaccharides (HePS)*

  HePS are polysaccharides assembled from significantly varied repeating units. The repeating units are usually oligosaccharides of D-glucose, D-galactose, L-fructose, L-rhamnose, D-glucuronic acid, L-guluronic acid and D-mannuronic acid, composed of two to eight monosaccharides in length. Additional substituents of succinates, pyruvates and formates are found in most HePS (Czaczyk & Myszka, 2007; Ercan &

Demirci, 2015). Bacterial alginate, produced by *Pseudomonas aeruginosa* and *Azotobacter vinelandii*, is a notable exception. Alginate is a HePS of irregular structure in which vestiges of D-mannurosyl and L-guluronosyl are present (Sutherland, 2001a; Czaczyk & Myszka, 2007).

The physical properties of HePS are dependent on the inter-monosaccharide linkages present and on branching of the polysaccharides chain (Czaczyk & Myszka, 2007). These properties can even differ between strains of the same bacterium (Ercan & Demirci, 2015). Both the production quantity and type of HePS are dependent on the growth conditions, i.e. medium composition, temperature, pH, oxygen tension and growth phase play a role in the production and types of HePS produced (Degeest, Vaningelgem & De Vuyst, 2001; Czaczyk & Myszka, 2007).

HePS, in contrast to HoPS, are synthesised by intracellular enzymes which polymerise oligosaccharide repeating units. These repeating units are, in turn, built from monosaccharides, at the cytoplasmic membrane. The biosynthesis of HePS is an energy-intensive process as both the polymerisation and transport of polysaccharides through the cell membranes require a significant amount of energy (Whitfield, 1988; Harutoshi, 2013: 522).

2.1.2 Industrial application of cell immobilisation technology

Cell immobilisation is defined as “the physical confinement or localisation of intact cells to a certain defined region of space with the preservation of some desired catalytic activity” (Karel, Libicki & Robertson, 1985) and can occur naturally (biofilms) or artificially by chemical or physical means (Dervakos & Webb, 1991; Dagher et al., 2010). *TABLE 2-2* shows the various methods employed in cell immobilisation (Karel, Libicki & Robertson, 1985), as well as prominent studies from the literature employing the specific methods.

Cell immobilisation is considered to improve the bioreactor performance as a result of various factors (Dervakos & Webb, 1991):

- Enhanced biological stability
- High biomass concentration
- Advantageous partition effects
- Increased product yields

- Increased product stability
- Integration with downstream processing
- Advantages due to cell proximity
- Increased reaction selectivity
- Versatility in the selection of the reactor.

The selection of cell immobilisation method is extremely important in the overall performance of industrial bioreactors. The method selected has the ability to influence cell physiology, metabolism and bacterial distribution within the immobilisation matrix (Dagher et al., 2010).

The industrial application of biofilms has been successfully exploited in various bioprocessing industries as a natural form of cell immobilisation with increased tolerances, and to impart long-term stability in bioprocess operations (Li, Hauer & Rosche, 2007; Rosche et al., 2009). A thorough understanding of biofilm formation and infrastructure is imperative as this dictates the reactor start-up and operation. Start-up times of between four and nine months have been reported (Annachhatre & Bhamidimarri, 1992)

The industrial applications of biofilms include industries as diverse as (Annachhatre & Bhamidimarri, 1992; Li, Hauer & Rosche, 2007; Rosche et al., 2009):

- Bioremediation (Meyer & Wallis, 1997; Ebihara & Bishop, 2002; Singh, Paul & Jain, 2006; Vu et al., 2009; Edwards & Kjellerup, 2013)
- Wastewater treatment (Hall, 1987; Nicolella, Van Loosdrecht & Heijnen, 2000a,b; An & Lo, 2001; Botrous, Dahab & Mihăltz, 2004; Manolov, Kristina & Benoit, 2005)
- Biosynthesis (Zhang et al., 2004; Ürküt, Dağbağlı & Göksungur, 2007; West, 2011; Jarpa et al., 2012),
- Fermentation (Andries et al., 1996; Tay & Yang, 2002; Huang, Ramey & Yang, 2004; Qureshi, Lai & Blaschek, 2004; Zhang et al., 2009; Ercan & Demirci, 2015)

Table 2-2: The various methods employed in cell immobilisation (Karel, Libicki & Robertson, 1985) as well as prominent studies from literature employing the specific methods.

Attachment type		Support		References
Surface attachment	Natural Adsorption	Wood chips		(Krischke, Schröder & Trösch, 1991)
		Porous bricks and cotton cloth		(Gonçalves et al., 1992)
		Poraver®		(Guoqiang, Kaul & Mattiasson, 1992; Bradfield & Nicol, 2014; Maharaj, Bradfield & Nicol, 2014)
		Plastic composite support		(Ho et al., 1997b; Cotton, Pometto & Gvozdenovic-Jeremic, 2001; Urbance et al., 2003, 2004)
	Chemically bound	Chelation/metal-link		(Rogl et al., 1998; Fischer et al., 2009)
		Glutaraldehyde cross-linking		(Olde Damink et al., 1995; Migneault et al., 2004; Stojkovič & Žnidaršič-Plazl, 2012)
Entrapment within porous matrix	Gel	Alginate		(Roy, Goulet & Le Duy, 1987; Ryu & Wee, 2001; Tielen et al., 2005; Idris & Suzana, 2006)
		κ-carrageenan		(Audet, Paquin & Lacroix, 1988; Mostafa, 1996; Ryu & Wee, 2001)
		Polyacrylamide		(Tuli et al., 1985; Raihan et al., 1997; Petrov, Yankov & Beschkov, 2005; Petrov, Petrova & Beschkov, 2007)
		Collagen		(Saini & Vieth, 2007; Wang et al., 2008)
		PTFE		(Hyde, Hunt & Errede, 1991)
	Preformed Support	Controlled pore glass		(Bruno-Bárcena et al., 1999; Martin et al., 2006; Rieder et al., 2011)
		Bricks		(Gonçalves et al., 1992)
		Cordierite		(De Lathouder et al., 2004; Moreno-Castilla & Pérez-Cadenas, 2010)
Containment behind a barrier	Phase entrainment	Micro en-capsula-tion	Polylysine	(Ma et al., 2013; Chen et al., 2014)
			Ethylcellulose	(Chowdary & Panguluri, 2008; Prasertmanakit et al., 2009; Murtaza, 2012)
		Two-phase emulsions		(Katzbauer, Narodoslawsky & Moser, 1995; Sajc, Grubisic & Vunjak-Novakovic, 2000; Schmid et al., 2001)
	Preformed barriers	Synthetic membranes		(Mehaia & Cheryan, 1987; Reij & Hartmans, 1996; Lee, Lee & Chang, 2008; Kim et al., 2009)
Self-aggregation	Natural	Mycelia pellets		(Cao et al., 1997; Du et al., 1997; Riscaldati et al., 2002; Yu et al., 2007)
		Microbial flocs		(Katzbauer, Narodoslawsky & Moser, 1995; Stewart, 1998; Khezry, 2012)
	Artificially induced	Polyelectrolytes		(Stenroos, Linko & Linko, 1982; Yahiro et al., 1995; Xu et al., 2006; Zhang et al., 2011)
		Glutaraldehyde cross-linking		(McCarthy et al., 1985; Wang, Hayter & Wilson, 1996)

In this study the main application of interest is the fermentation of a sugar substrate to yield value-added products. The next section is dedicated to several single-species biofilm studies in the production of these value-added products.

2.1.3 Continuous biofilm fermentation studies

In order to produce industrially important chemicals continuously from fermentation, single-species biofilms are generally preferred. This is due to the ease of control, as well as to maximising the desired product during fermentation; a single species is inoculated into a sterile environment with the goal of forming a biofilm and subsequently producing a specific fermentation product (Qureshi et al., 2005).

Most continuous single-culture biofilm fermentation studies are currently still at the bench-scale or pilot-scale research level, in stark contrast to the intensive research being done with respect to the application of biofilm reactors to water treatment (Cheng, Demirci & Catchmark, 2010; Gross, Schmid & Buehler, 2012: 208). However, despite the lack of industrial application, biofilm reactors have been shown to improve the production of various value-added products, including alcohol, organic acids, enzymes, antibiotics and polysaccharides (Qureshi et al., 2005; Cheng, Demirci & Catchmark, 2010; Ercan & Demirci, 2015). These reactors have the ability to improve the volumetric productivity rates within the reactor due to significantly enhanced biomass concentrations within the bioreactors (Qureshi, Lai & Blaschek, 2004; Qureshi et al., 2005; Cheng, Demirci & Catchmark, 2010; Gross, Schmid & Buehler, 2012: 214; Ercan & Demirci, 2015). In addition to the productivity of bioreactors, factors such as product titre, product yield and length of reactor operation affect the overall process economics of a fermentation process (Qureshi et al., 2005).

Some examples of the above products from fermentation studies are summarised in *TABLE 2-3*. This table compares the maximum suspended cell production rates, product concentrations and yields with the same parameters in biofilm reactors at the same conditions and using the same culture. In addition, it shows the length of operation of the various biofilm reactors. From *TABLE 2-3* it can be seen that these parameters appear to increase significantly from the suspended cell to the biofilm reactor for most of the studies. The observed production rate increases were expected due to the significant increase in the cellular concentrations in the biofilm reactors as compared with the suspended cell reactors (Qureshi, Lai & Blaschek,

2004; Qureshi et al., 2005; Cheng, Demirci & Catchmark, 2010; Gross, Schmid & Buehler, 2012: 214; Ercan & Demirci, 2015). The general increase in product yield is, however, interesting: increases in yield of as much as 45% for acetone/butanol/ethanol (Lee et al., 2008) and ethanol (Kunduru & Pometto, 1996a,b) production were reported. This indicates a change in the metabolism of the bacterium, which could possibly involve an increase in the non-growth or maintenance-related production with a corresponding decrease in the growth-related production (Qureshi et al., 2005; Gross, Schmid & Buehler, 2012: 195).

The final column in *TABLE 2-3* shows the maximum operational biofilm fermentation time during each run. It can be seen that the operational times for the biofilm runs were significant, with online fermentation times as long as 180 days reported for continuous acetic acid fermentation (Horiuchi et al., 2000).

Table 2-3: Examples of results from continuous biofilm fermentation studies in the literature, comparing the maximum volumetric productivities, product concentrations and product yields between suspended cell and biofilm studies. The table also shows the longest continuous operational time reported in the various studies.

Product type	Product	Microbial species	Reference	Maximum volumetric productivity ($g.L^{-1}.h^{-1}$)		Maximum product concentration ($g.L^{-1}$)		Maximum product yield ($g.g^{-1}$)		Continuous operation time (d)
				Suspended cell	Biofilm	Suspended cell	Biofilm	Suspended cell	Biofilm	
Alcohol	Ace-tone/ butanol/ ethanol	*Clostridium bei-jerinckii* BA101	(Qureshi, Lai & Blaschek, 2004)	0.38	16.13	9.7	12.0	0.36	0.43	96
		Clostridium acetobutylicum ATCC 55025	(Huang, Ramey & Yang, 2004)	-	6.0	-	5.1	-	0.53[1]	46
		Clostridium beijerinckii NCIMB 8052	(Lee et al., 2008)	0.22	0.40	7.1	22.1	0.24	0.44	> 12
		Clostridium beijerinckii ATCC 55025	(Zhang et al., 2009)	0.22	5.06	9.4	9.0	0.24	0.32	20
	Ethanol	*Zymomonas mobilis* ATCC 31821	(Weuster-Botz, 1993; Weuster-Botz, Aivasidis & Wandrey, 1993)	11.8	53	60	58	0.48	0.51	120
		Zymomonas mobilis ATCC 31821	(Kunduru & Pometto, 1996a,b)	5	536	10	47	0.24	0.5	60

[1]Max theoretical yield is 0.44 $g.g^{-1}$, i.e. this value is questionable and could indicate unsteady behaviour

Table 2-3: ***continued***

Product type	Product	Microbial species	Reference	Maximum volumetric productivity ($g.L^{-1}.h^{-1}$)		Maximum product concentration ($g.L^{-1}$)		Maximum product yield ($g.g^{-1}$)		Continuous operation time (d)
				Suspended cell	Biofilm	Suspended cell	Biofilm	Suspended cell	Biofilm	
Alcohol	Ethanol	*Saccharomyces cerevisiae* ATCC 24859	(Kunduru & Pometto, 1996a,b)	5	76	10	38	0.26	0.47	60
		Escherichia coli KO11	(Dumsday et al., 1997)	1.27	1.12	21.2	18.7	0.44	0.40	27
		Kluyveromyces marxianus DSMZ-7239	(Ozmihci & Kargi, 2007, 2008, 2009)	0.745	1.58	40	22.5	0.4	0.54	> 21
	Butanol	*Clostridium acetobutylicum* P262	(Qureshi & Maddox, 1988)	0.1	6.5	-	13.0	-	0.4	> 83
		Clostridium beijerinckii BA101	(Qureshi & Schripsema, 2000)	0.38	15.8	-	7.9	-	0.45	> 23
	1,3-butanediol	Recombinant *Escherichia coli*	(Itoh et al., 2007)	12.5	75	-	49.5	-	-	21
	2,3-butanediol	*Klebsiella pneumonia* NCIB 8017	(Lee & Maddox, 1986)	0.028	2.3	2.7	3.0	0.27	0.40	49

Table 2-3: ***continued***

Product type	Product	Microbial species	Reference	Maximum volumetric productivity ($g.L^{-1}.h^{-1}$)		Maximum product concentration ($g.L^{-1}$)		Maximum product yield ($g.g^{-1}$)		Continuous operation time (d)
				Suspended cell	Biofilm	Suspended cell	Biofilm	Suspended cell	Biofilm	
Enzyme	**Cellulase**	*Trichoderma viride* QM 9123	(Webb, Fukuda & Atkinson, 1986)	53% volumetric productivity increase, 31% yield increase						
	Amylase	*Escherichia coli* EC147	(Oriel, 1988; Ercan & Demirci, 2015)	Fivefold production increase						
Organic acid	**Acetic acid**	*Acetobacter* species	(Kennedy et al., 1980)	1.45 - 2.34	4.38 – 5.0	49.3-63.3	92.1	-	-	75
		Acetobacter aceti M7	(Park & Toda, 1992)	-	7	-	98	-	0.98	39
		Acetobacter pasteurianus	(Horiuchi et al., 2000)	-	6.45	-	38	-	0.85	180
	Lactic acid	*Streptococcus thermophilus*	(Andrews & Fonta, 1989)	-	12	-	-	-	-	58
		Lactobacillus casei ssp. *casei* DSM 20244	(Krischke, Schröder & Trösch, 1991)	5.5	13.5	30	25	-	-	-
		Lactobacillus casei ssp. *casei* CRL 686	(Bruno-Bárcena et al., 1999)	2.42	9.72	48	57.5	0.79	0.6	-

Table 2-3: ***continued***

Product type	Product	Microbial species	Reference	Maximum volumetric productivity ($g.L^{-1}.h^{-1}$)		Maximum product concentration ($g.L^{-1}$)		Maximum product yield ($g.g^{-1}$)		Continuous operation time (d)
				Suspended cell	Biofilm	Suspended cell	Biofilm	Suspended cell	Biofilm	
Organic acid	Lactic acid	*Lactobacillus helveticus* ATCC 15009	(Silva & Yang, 1995)	1.4	4.8	48.7	50.8	0.99	0.99	14
		Lactobacillus casei ssp. *casei* CRL 686	(Bruno-Bárcena et al., 1999)	2.42	9.72	48	57.5	0.79	0.6	-
		Lactobacillus casei ADNOX95	(Dagher et al., 2010)	-	11.9	-	27.7	-	1.00	30
		Lactobacillus rhamnosus NRRL B445	(Gonçalves et al., 1992)	7.64	20.1	23.15	51.4	0.71	0.76	-
		Lactobacillus rhamnosus ATCC 11443	(Demirci, Pometto & Johnson, 1993)	8.8	16	8	13.9	1.00	1.00	5
			(Cotton, Pometto & Gvozdenovic-Jeremic, 2001)	5.8	9.0	21.68	23.37	0.7	0.75	90
		Lactobacillus rhamnosus RW-9595M	(Bergmaier, Champagne & Lacroix, 2005)	9.9	14.4	51.4	38.1	-	-	32

Table 2-3: ***continued***

Product type	Product	Microbial species	Reference	Maximum volumetric productivity ($g.L^{-1}.h^{-1}$)		Maximum product concentration ($g.L^{-1}$)		Maximum product yield ($g.g^{-1}$)		Continuous operation time (d)
				Suspended cell	Biofilm	Suspended cell	Biofilm	Suspended cell	Biofilm	
Organic acid	Lactic acid	*Lactobacillus rhamnosus* RS93	(Dagher et al., 2010)	-	10.4	-	25.7	-	1.00	30
	Fumaric acid	*Rhizopus arrhizus* NRRL 1526	(Frederici & Petruccioli, 1996: 659)	0.119	0.215	42	6	0.17	0.27	10
	Citric acid	*Aspergillus niger* ATCC 1015	(Sankpal, Joshi & Kulkarni, 2001)	0.125	2.08	35-50	65	-	1.00	26
		Aspergillus niger ATCC 9142	(Kim, Park & Byun, 2002)	0.063	0.16	4.7	4.5	0.51	0.70	20
	Succinic acid	*Enterococcus faecalis* RKY1	(Wee et al., 2002)	9.9	17.1	95.0	72.7	0.95	0.91	15
		Actinobacillus succinogenes ATCC 55618	(Urbance et al., 2003, 2004)	-	8.8	-	10.4	-	0.76	5
			(Van Heerden & Nicol, 2013)	-	6.35	-	13.39	-	0.73	8
			(Bradfield & Nicol, 2014)	-	9.5	-	48.5	-	0.89	54

Table 2-3: ***continued***

Product type	Product	Microbial species	Reference	Maximum volumetric productivity ($g.L^{-1}.h^{-1}$)		Maximum product concentration ($g.L^{-1}$)		Maximum product yield ($g.g^{-1}$)		Continuous operation time (d)
				Suspended cell	Biofilm	Suspended cell	Biofilm	Suspended cell	Biofilm	
Organic acid	Succinic acid	*Actinobacillus succinogenes* ATCC 55618	(Maharaj, Bradfield & Nicol, 2014)	-	10.7	-	32.5	-	0.90	> 12
		Actinobacillus succinogenes M2012036	(Yan, Zheng, Tao, et al., 2014)	-	2.77	-	55.3	-	0.80	18
Miscella-neous	(S) – styrene oxide	*Pseudomonas* sp. VLB12ΔDC	(Gross et al., 2007; Park et al., 2007)	1.95	0.7-1.9	-	12.4	0.68	0.09	> 68
			(Park et al., 2007; Gross et al., 2010)		2.9	-	60		0.3	50
			(Park et al., 2007; Halan, Schmid & Buehler, 2010)		1.2	-	42		-	30

2.2 *Lactobacillus rhamnosus*

The bacterial species *Lactobacillus rhamnosus* is considered to be a ubiquitously adaptable Gram-positive organism, recovered from various bodily orifices and openings, as well as fermented milk products (Kant et al., 2014). *Lactobacillus rhamnosus* was originally designated as *Lactobacillus casei* subsp. *rhamnosus* (Hansen, 1968: 76); the *L. casei* group consisted of one species, which were subdivided into five subspecies – *casei, alactosus, pseudoplantarum, tolerans* and *rhamnosus* (Collins, Phillips & Zanoni, 1989; Ryu et al., 2001). Collins et al. (1989) reclassified these subspecies, using DNA-DNA hybridisations, as belonging to four elevated species with subspecies– *L. casei, L. paracasei* subsp*. paracasei, L. paracasei* subsp*. tolerans* and *L. rhamnosus. L. rhamnosus* was given the type strain ATCC 7469^T which was easily differentiable from the other *L. casei* group members due to a rhamnose-containing cell wall and to an ability to metabolise rhamnose (Collins, Phillips & Zanoni, 1989; Ryu et al., 2001; Sakai et al., 2010).

L. rhamnosus and *L. casei* are well-studied organisms and are currently the species most widely used for lactic acid fermentation (Dagher et al., 2010). Lactic acid bacteria are, however, known to be fastidious organisms, of which *L. rhamnosus* is no exception (Ho et al, 1997a; Lebeer, De Keersmaecker, et al., 2007; Dagher et al., 2010). This is problematic as the downstream processing during lactic acid production is severely affected by the addition of rich media during fermentation; e.g. a yeast extract (YE) concentration in excess of 1% would affect the optical purity of the lactic acid produced due to the presence of lactic acid in the YE medium (Dagher et al., 2010).

2.2.1 Metabolism

According to the group who published the complete genome of *L.* rhamnosus GG, *L. rhamnosus* is a facultatively heterofermentative lactic acid bacterium (Morita et al., 2009). However, in the literature *L. rhamnosus* is generally considered to be homofermentative (Nakamura, 1982; Benito de Cárdenas, Ledesma & Oliver, 1987; Berry et al., 1999; Kwon et al., 2000; Petrov, Yankov & Beschkov, 2005; Mel et al., 2008; Dagher et al., 2010). It has been observed that the metabolism changed to heterofermentative in the presence of oxygen (Manderson & Doelle, 1972), for pH > 6.5 (Senthuran et al., 1999), and during the fermentation of pentoses

via the phosphoketolase pathway which produces equimolar amounts of lactic acid and acetic acid (Marques et al., 2008; Abdel-Rahman, Tashiro & Sonomoto, 2011; Lazzi et al., 2014). In addition, it has been observed that in fermentations containing excess citrate or pyruvate, the flavour compounds acetoin (Acn) and diacetyl (Diac) were produced (Benito de Cárdenas, Ledesma & Oliver, 1987; Benito de Cardenas, Ledesma & Oliver, 1989; Medina de Figueroa, Oliver & Benito de Cárdenas, 2001). It was theorised that the production of the flavour compounds in fermentations without added pyruvate was a result of nicotinamide adenine dinucleotide (NADH) oxidation (by an increased activity of NADH oxidase), which led to an increased amount of pyruvate in the medium and subsequently an increase in flavour compound production (Medina de Figueroa, Oliver & Benito de Cárdenas, 2001).

Lactic acid fermentation by *L. rhamnosus* has been found to involve both growth-related and non-growth-related catabolism (Ho et al., 1997b; Berry et al., 1999; Cotton, Pometto & Gvozdenovic-Jeremic, 2001; Ling et al., 2006; Choi, Al-Zahrani & Lee, 2014).

The L. rhamnosus metabolism as reported in the literature (Jyoti, Suresh & Venkatesh, 2004; Poolman et al., 2004; Gayen, Gupta & Venkatesh, 2007) is presented in *FIGURE 2-3*, and shows that there are seven possible catabolic products, namely pyruvic acid (PA), lactic acid (LA), acetoin (Acn), diacetyl (Diac), acetic acid (AA), citric acid (CA) and oxaloacetic acid (OAA), as well as anabolically produced biomass (x).

2.2.2 Biofilm

The biofilm formation capabilities of *L. rhamnosus* have been studied extensively in the literature (Gonçalves et al., 1992; Ho et al., 1997b; Millsap et al., 1997; Pelletier et al., 1997; Cotton, Pometto & Gvozdenovic-Jeremic, 2001; Lebeer, De Keersmaecker, et al., 2007; Lebeer, Verhoeven, et al., 2007; Djukić-Vuković et al., 2013; Kant et al., 2014) and it was found to have a natural affinity for biofilm formation: biofilms provide natural protection to the *in vitro* probiotic action of *L. rhamnosus* GG, one of the most intensively studied probiotic organisms (Lebeer, Verhoeven, et al., 2007).

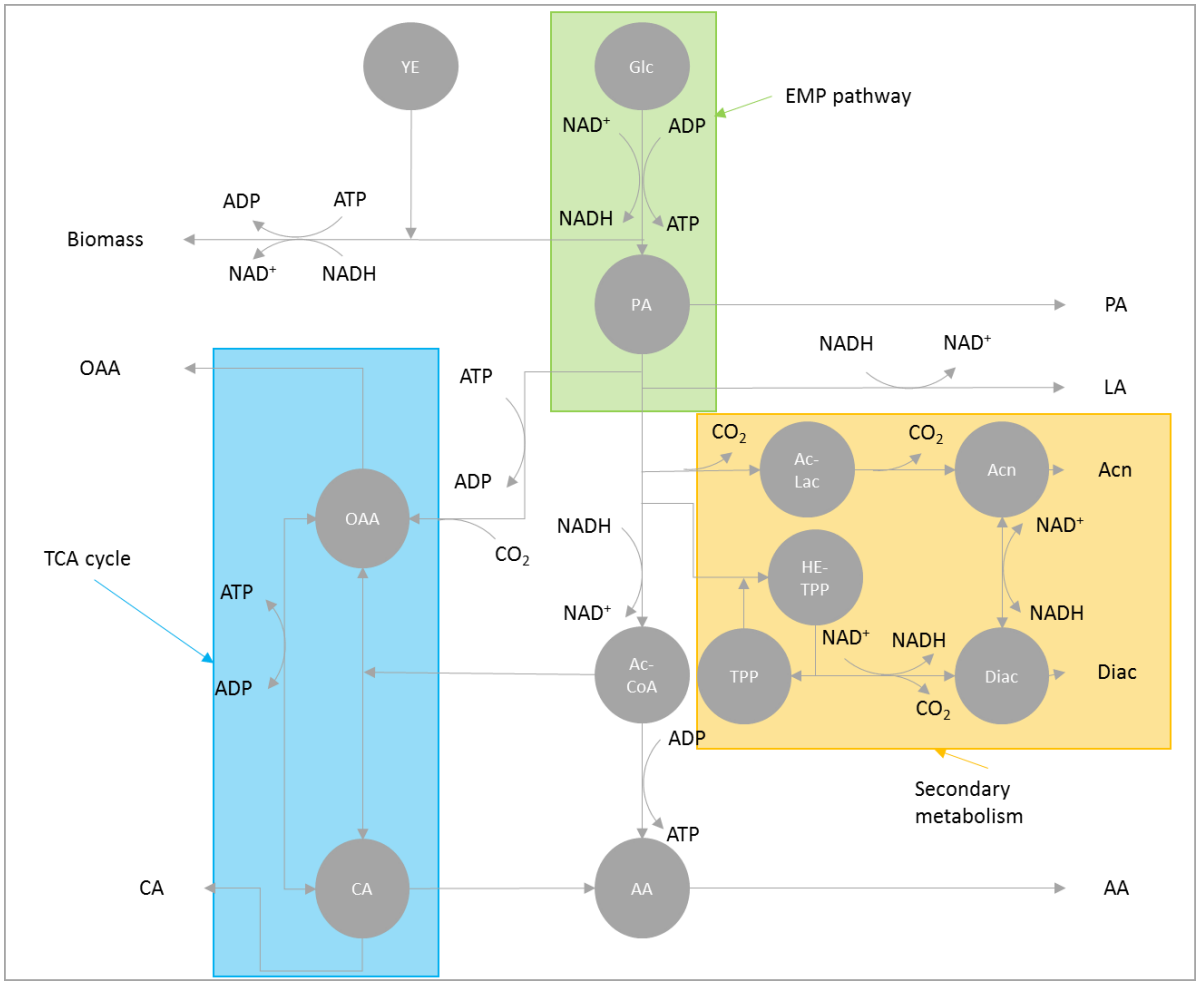

Figure 2-3: *L. rhamnosus* metabolism from the literature (Jyoti, Suresh & Venkatesh, 2004; Poolman et al., 2004; Gayen, Gupta & Venkatesh, 2007). The metabolism consists of mainly an energy metabolism on the left and a secondary metabolism on the right. Metabolites represented by: AA, acetic acid; AcCoA, acetyl-CoA; AcLac, acetolactate; Acn, acetoin; CA, citric acid; CoA, co-enzyme A; Diac, diacetyl; Glc, glucose; HETPP, hydroxyethyl-TPP; LA, lactic acid; OAA, oxaloacetic acid; PA, pyruvic acid; TPP, thiamine pyrophosphate; YE, yeast extract.

As discussed in Section 2.1.1.4 (page 2-9), the ability of any organism to produce a biofilm is dependent on its ability to produce an extracellular matrix or glycocalyx which would form a stable structure for the biofilm. This glycocalyx is composed mostly of exopolysaccharides, meaning that the exopolysaccharide production capabilities of the organism dictate its biofilm construction (Costerton, Geesey & Cheng, 1978; Dunne, 2002; Cheng, Catchmark & Demirci, 2009; Dagher et al., 2010). The exopolysaccharide production ability of *L. rhamnosus* has been extensively studied and it has been reported to be among the highest for any lactobacilli in the literature (Dupont, Roy & Lapointe, 2000; Pham et al., 2000; Van Calsteren et al., 2002; Landersjö et al., 2002; Macedo et al., 2002; Bergmaier, Champagne & Lacroix, 2005; Péant et al., 2005; Champagne, Gardner & Lacroix, 2007; Lebeer et al., 2009, 2011; Bleau et al., 2010; Yang et al., 2010). In *L. rhamnosus* it was found that no plasmids were present in the cells,

which is a strong indication that the genes necessary for exopolysaccharide production are chromosomal, meaning they are phenotypically more stable and therefore industrially preferred (Dupont, Roy & Lapointe, 2000).

According to Van Calsteren et al. (2002), the structure of the exopolysaccharide of *L. rhamnosus* ATCC-9595M consists of a heptasaccharide repeating unit (equation *(2-1)*) and a general formula of $C_nH_{1.6n}O_{0.89n}$.

$$\{-3Rha - 3Glc - 3[Gal4,6(R)Py - 2]Rha - 3Rha - 2Glc -\}_n \quad (2\text{-}1)$$

This repeating unit was supported by Kim et al. (2006) and Bergmaier, Champagne and Lacroix (2005) who found that major constituents of the exopolysaccharide of *L. rhamnosus* ATCC 9595 to be glucose, galactose and rhamnose. The exopolysaccharide repeating unit for the strain *L. rhamnosus* GG, as determined by Landersjö et al. (2002), was slightly different and is described by equation *(2-2)*:

$$\{-3Gal - 3Gal - 4[Gal - 6]GlcNAc - 3Rha - 2Gal -\}_n \quad (2\text{-}2)$$

However, the repeating unit as shown in equation *(2-1)* can be assumed to represent the exopolysaccharide of *L. rhamnosus* ATCC 9595 as it was determined by Péant et al. (2005) that the same genes encoded for exopolysaccharides in both strains, *L. rhamnosus* RW-9595M and 9595.

2.2.3 Continuous *L. rhamnosus* Biofilm Fermentation Studies

There are several studies in the literature on the use of *L. rhamnosus* in continuous biofilm fermentation (Gonçalves et al., 1992; Demirci, Pometto & Johnson, 1993; Cotton, Pometto & Gvozdenovic-Jeremic, 2001; Bergmaier, Champagne & Lacroix, 2005; Dagher et al., 2010). These studies highlight the potential for increasing the volumetric productivity of the bioreactor by increasing the total biomass in the reactor.

Gonçalves et al. (1992) studied the production of lactic acid by *L. rhamnosus* using four inert supports. These four supports were Raschig rings of sintered glass, beads of sintered glass, Poraver® and irregular ceramic particles. The best support was found to be the beads of sintered glass based on lactic acid volumetric productivity. The authors found from batch and continuous results using the biofilm reactors that extrapolating from batch results to obtain

continuous (predicted) behaviour can introduce significant errors. It was found that the influence of pH in the biofilm system was reduced because the productivity remained constant for pH values higher or lower than the optimum obtained in the chemostat system. The highest volumetric productivity was reported as 20.8 $g.L^{-1}.h^{-1}$, with a maximum lactic acid concentration of 51.4 $g.L^{-1}$ and a maximum yield of 0.76 $g.g^{-1}$. The maximum productivity was almost three times the maximum value obtained in the chemostat of 7.64 $g.L^{-1}.h^{-1}$.

Demirci, Pometto and Johnson (1993) used a novel plastic composite support (PCS) blended with various agricultural materials, on which a biofilm of *L. rhamnosus* was established. The PCS compositions were varied to determine the optimum composition for biofilm formation. The study observed production rates between two and five times higher than those of suspended culture, with a maximum productivity of 16 $g.L^{-1}.h^{-1}$, a lactic acid yield of 100% and a maximum lactic acid titre of 13.9 $g.L^{-1}$. The authors commented that lignocellulosic supports (corn fibre, oat hulls and soy hulls) perfomed better than single polymers (cellulose or starch) at immobilising *L. rhamnosus*. The pH was not controlled during fermentations, which might have led to the relatively low lactic acid titre reported.

Building on the work by Demirci, Pometto and Johnson (1993), Cotton, Pometto and Gvozdenovic-Jeremic (2001) studied the production of lactic acid using PCS stacked in a grid and bound to an agitator shaft of a standard laboratory-scale bioreactor. The PCS consisted of 50% lignocellulosic agricultural products and YE and 50% polypropylene (PP). The results showed a maximum production rate of 9.0 $g.L^{-1}.h^{-1}$, a maximum product yield of 75% and a maximum final lactic acid concentration of 23.4 $g.L^{-1}$. Between runs the biofilm was removed using concentrated NH_4OH. However, the effluent from this was not analysed for total cellular biomass. From the significant scatter in the results it can be assumed that the washing procedure was not completely effective. The results show that the productivity and yields of the agitated PCS system decreased significantly compared with the results obtained by Demirci, Pometto and Johnson (1993). However, this could very well be a result of increased shear on the biofilm as the agitator shaft was rotated at 100–125 $r.min^{-1}$ in the study by Cotton, Pometto and Gvozdenovic-Jeremic (2001), while Demirci, Pometto and Johnson (1993) employed a packed bed reactor.

The aim of the study by Bergmaier, Champagne & Lacroix (2005) was to quantify the EPS production of *L. rhamnosus* RW-9595M, but since the production of lactic acid is an inherent

catabolic characteristic of *L. rhamnosus*, it was therefore also reported. During free-cell chemostat cultures, the authors of the study observed lactic acid production of 10.0 $g.L^{-1}.h^{-1}$, with a maximum lactic acid titre of 33.2 $g.L^{-1}$ and a lactic acid yield of 77.9% on lactose. The cells were immobilised on a food-grade porous silicone rubber support (ImmobaSil®) and the fermentation was done in a two-stage system (Bergmaier, Champagne & Lacroix, 2005). The first stage consisted of the biofilm reactor with immobilisation support, and the second stage was operated as a free-cell reactor in series with the first and using the released cells from the first reactor. Morpholigically, the cultures appeared to change from short-chain cells of up to four cells in length in the chemostat to long chains of cells, which were densely packed and with EPS observable on the surface. Aggregates were observed in the second stage of the reactor as the short chains observed in the free-cell chemostat cultures were replaced by long network-like stuctures. This indicated that the suspended cells in stage two derived from the biofilm in stage one, as opposed to growth in the medium (Bergmaier, Champagne & Lacroix, 2005). The maximum volumetric productivity in the two-stage system was reported to be as high as 49.5 $g.L^{-1}.h^{-1}$, with maximum lactic acid concentrations of 38.1 $g.L^{-1}$ in stage one and 51.4 $g.L^{-1}$ in the outlet of the reactor.

Dagher et al. (2010) used an upflow, recycle, packed bed reactor with Poraver® beads and polyurethane foam as support to test the biofilm production capability of *L. rhamnosus* RS93 (an adherent variant of *L. rhamnosus* DSM 20021). The stability of the biofilm was tested by repeating the initial dilution rate after a month of operation. The results from the study showed a maximum volumetric productivity of 10.4 $g.L^{-1}.h^{-1}$ for the Poraver® and a maximum productivity of 9.2 $g.L^{-1}.h^{-1}$ for the polyurethane. A maximum product yield of 100% lactic acid to glucose was obtained for both packing methods and maximum lactic acid concentrations of 23.7 $g.L^{-1}$ and 25.7 $g.L^{-1}$ were obtained for the Poraver® and polyurethane, respectively.

2.3 *Actinobacillus succinogenes*

Actinobacillus succinogenes is a proteobacterium which forms part of the *Pasteurellaceae* family, the *Actinobacillus* genera and has the species designation of *succinogenes* (Guettler, Rumler & Jain, 1999). *A. succinogenes* is a capnophilic, chemo-organotrophic, facultatively anaerobic, non-fastidious, Gram-negative, non-motile rod or coccobacillus (0.8 × 1 µm) isolated from bovine rumen (Guettler, Rumler & Jain, 1999). It has the ability to produce high

concentrations of succinate (> 100 $g.L^{-1}$) as fermentation product. However, due to mixed acid fermentation, formate, acetate and ethanol are also formed (Guettler, Jain & Rumler, 1996; Van der Werf et al., 1997; Guettler, Rumler & Jain, 1999).

The organism has the ability to produce acid from a variety of different substrates, including L-arabinose, D-ribose, D-xylose, galactose, D-glucose, D-fructose, D-mannose, D-mannitol, D-sorbitol, glycerol, amygdalin, arbutin, aesculin, salicin, cellobiose, maltose, lactose, sucrose, raffinose, P-gentiobiose, D-arabitol, gluconate, idonate, ascorbate, glucarate, galactarate, pectin, β-glucoside and 5-ketogluconate (Guettler, Jain & Rumler, 1996; Guettler, Rumler & Jain, 1999; McKinlay et al., 2010). Substrates other than glucose are taken up via pentose phosphate pathway (PPP) intermediates, as well as through various other mechanisms prior to degradation and fermentation (McKinlay et al., 2010). Due to the saccharolytic succinogenic nature of the organism, it has been hypothesised that the organism is adapted to a symbiotic relationship within the bovine rumen. In the rumen the organism converts various non-metabolisable sugars to succinic acid, which in turn is decarboxylated to propionic acid and then utilised by the ruminant host in the gluconeogenic pathway (Guettler, Rumler & Jain, 1999).

2.3.1 Metabolism

*Actinobacillus succinogene*s produces as major products succinate, acetate and formate and as a minor product, ethanol. No lactic acid was observed in buffered or unbuffered fermentation media (Van der Werf et al., 1997; McKinlay et al., 2010; Vlysidis et al., 2011). In order to produce succinate the fermentation requires CO_2 fixation; under CO_2-limiting conditions more ethanol and less succinate are formed during fermentation (Van der Werf et al., 1997; McKinlay, Zeikus & Vieille, 2005; Vlysidis et al., 2011). Fermentation product ratios were found to remain constant at pH values between 6.0 and 7.4. More succinate was produced with the addition of hydrogen in the gas phase, as well as when more reduced substrates were used, such as D-sorbitol or glycerol (Van der Werf et al., 1997; Vlysidis et al., 2011; Schindler, Joshi & Vieille, 2014). *A. succinogenes* grew at the expense of fumarate and L-malate reduction (Van der Werf et al., 1997).

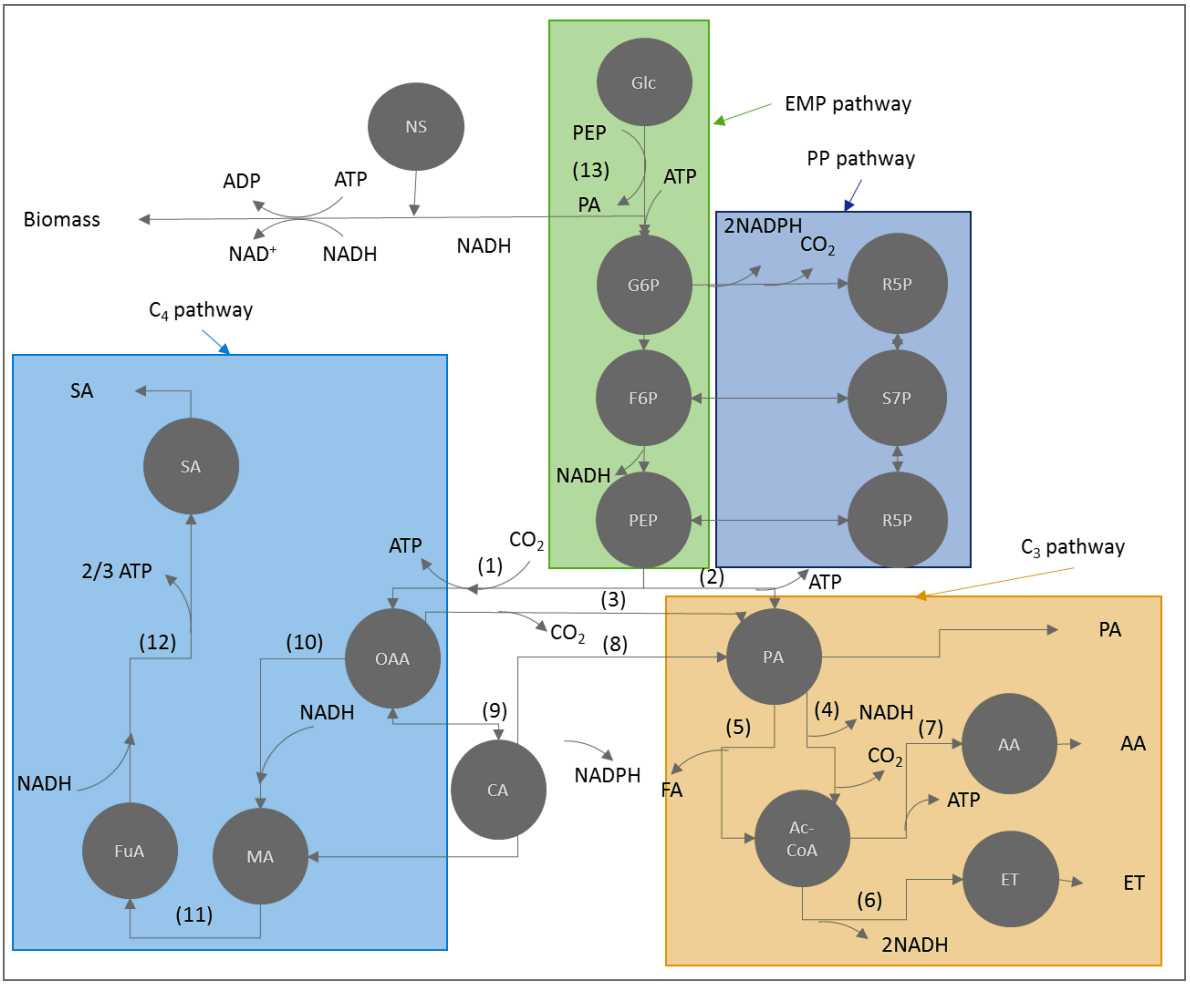

Figure 2-4: The metabolism of *A. succinogenes* as determined by enzyme assays (Van der Werf et al., 1997), through growth in defined minimal media (McKinlay, Zeikus & Vieille, 2005), ^{13}C metabolic analysis (McKinlay et al., 2007) and through genome analysis (McKinlay et al., 2010). Metabolites represented are: AcCoA, acetyl-co-enzymeA; AA, acetic acid; CA, citric acid; ET, ethanol; FA, formic acid; FuA, fumaric acid; F6P, fructose-6-phosphate; Glc, glucose; G6P, glucose-6-phosphate; MA, malic acid; OAA, oxaloacetic acid; PEP, phosphoenolpyruvate; PA, pyruvic acid; R5P, pentose-phosphates, SA, succinic acid; S7P, sedoheptulose-7-phosphate. Enzymes are: (1) phosphoenolpyruvate (PEP) carboxykinase, (2) pyruvate kinase, (3) oxaloacetate decarboxylase, (4) pyruvate dehydrogenase or pyruvate formate-lyase linked to formate lyase, (5) pyruvate formate-lyase, (6) alcohol dehydrogenase, (7) acetate kinase, (8) malic enzyme, (9) citrate lyase, (10) malate dehydrogenase, (11) fumarase, (12) fumarate reductase.

A. succinogenes contains the fundamental enzymes involved in the Embden-Meyerhof-Parnas and PPP, although the organism possesses only a partial citric acid cycle. The following enzymes were found to be active in *A. succinogenes* (Van der Werf et al., 1997; McKinlay et al., 2007): phosphoenolpyruvate (PEP) carboxykinase, pyruvate kinase, oxaloacetate decarboxylase, pyruvate dehydrogenase/formate dehydrogenase (*pdh/fdh)*, pyruvate formate-lyase (*pfl*), alcohol dehydrogenase, acetate kinase, malic enzyme, citrate lyase, malate dehydrogenase, fumarase, fumarate reductase, glucose:PEP phosphotransferase and phosphotransacetylase. The overall metabolism can be represented by *FIGURE 2-4* (Guettler, Rumler & Jain,

1999; McKinlay, Zeikus & Vieille, 2005; McKinlay et al., 2007, 2010), with the numbers in brackets representing the enzymes present in the organism as stated above.

The metabolism starts with the uptake of glucose through a permease and subsequent phosphorylation by hexokinase, as well as through a PEP-dependent phosphotransferase (13) system to G6P, which in turn is converted to PEP by glycolysis (McKinlay et al., 2010). During glycolysis it was found that a minor involvement of the PPP was measured using ^{13}C metabolic flux analysis (McKinlay et al., 2007). From PEP the metabolism can be divided into two separate sections, designated the C_3 (leading to PA, AA, FA and ET) and C_4 (leading to SA) pathways. It was found that the malic enzyme (8) and oxaloacetate decarboxylase (3) formed reversible shunts between the respective pathways.

2.3.2 Product and substrate inhibition from batch studies

Kinetic analyses of *A. succinogenes* are limited to batch fermentations in the absence of cell immobilisation (Corona-González et al., 2008; Lin et al., 2008). Numerous authors have reported batch profiles using various substrates (see *FIGURE 2-5* for notable studies on glucose (Glc) (Du et al., 2007; McKinlay et al., 2007; Corona-González et al., 2008; Lin et al., 2008; Liu et al., 2008; Chen et al., 2010; Corona-Gonzalez et al., 2010; Li, Jiang, et al., 2010; Xi et al., 2012; Zheng et al., 2013; Yan, Zheng, Dong, et al., 2014). All these studies are characterised by a point in time at which cell growth terminates while metabolite production continues beyond the termination point.

FIGURE 2-5 represents some of the prominent studies using Glc with the specific growth rates (μ), estimated from biomass curves, plotted against the SA titre. All these experiments were started without the external addition of metabolites to the medium and with different medium formulations. SA was chosen as the indicator for growth inhibition, although all metabolically produced acids (SA, AA and FA) are known to contribute to inhibition (Corona-Gonzalez et al., 2010). The catabolite ratios vary to some extent and SA can only be used as a relative indicator. Most of the data in *FIGURE 2-5* fall within the blue 'data cloud' and drastic growth inhibition is reflected by lower growth rates between 8 and 14 $g.L^{-1}$ of SA. Surprisingly, the SA titre in *FIGURE 2-5* does not correspond to the terminal SA titre when succinate is externally added prior to the fermentation (Corona-Gonzalez et al., 2010; Li, Wang, et al., 2010).

In both these studies, growth was observed above SA titres of 30 g.L^{-1}, indicating a difference between the influences of external and produced succinate on *A. succinogenes*.

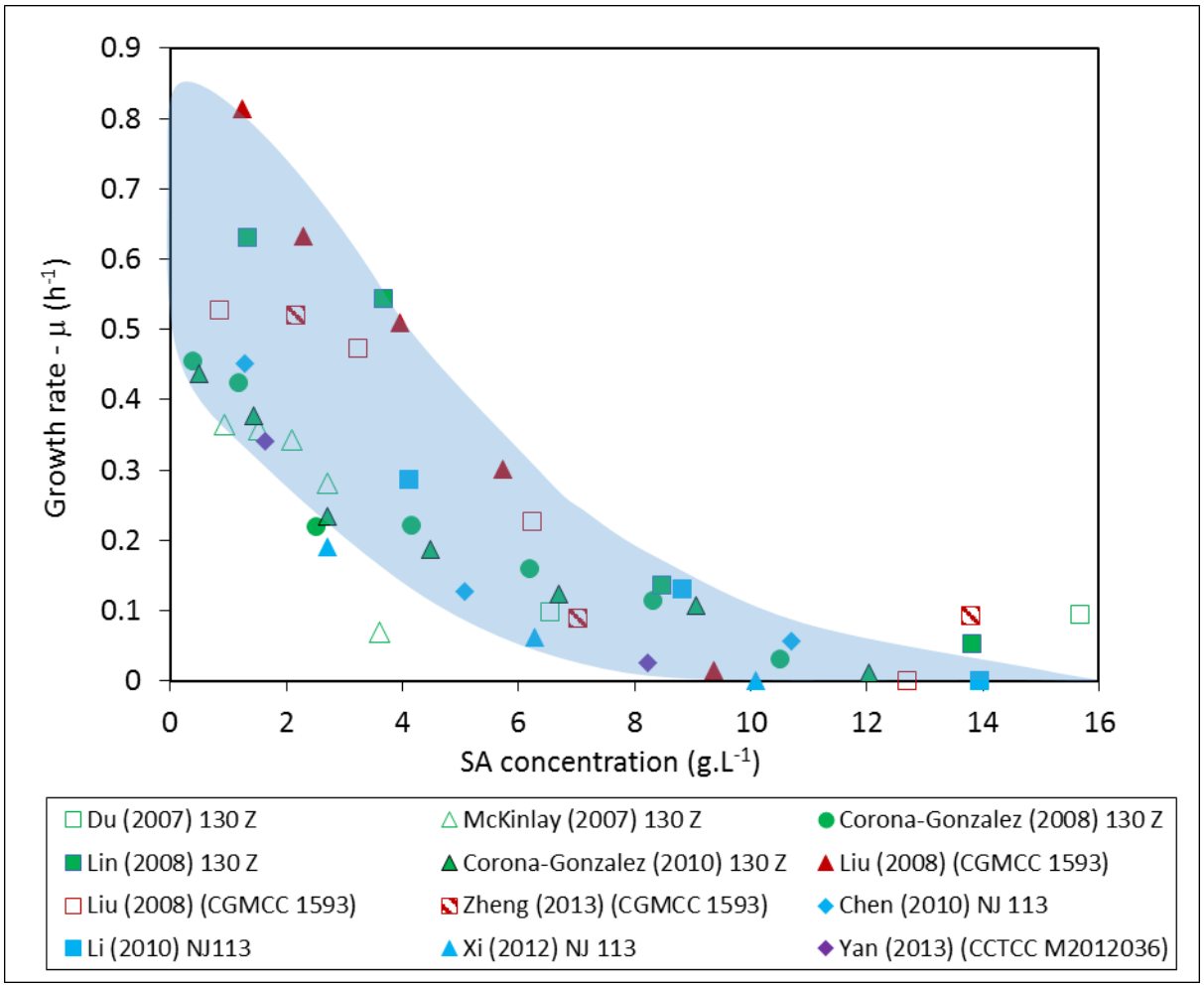

Figure 2-5: Notable batch studies from the literature on *A. succinogenes* on glucose (Du et al., 2007; McKinlay et al., 2007; Corona-González et al., 2008; Lin et al., 2008; Liu et al., 2008; Chen et al., 2010; Corona-Gonzalez et al., 2010; Li, Jiang, et al., 2010; Xi et al., 2012; Zheng et al., 2013; Yan, Zheng, Dong, et al., 2014)**. The figure shows that most of the results fall within the blue "data cloud" and indicates severe growth inhibition as a function of SA titres. It appears that growth terminates for SA concentrations between 8 g.L^{-1} and 14 g.L^{-1}.**

Another striking similarity between the various batch runs is that the production rates of the by-products (AA and FA) decrease after the growth termination point, while SA production appears to be unaffected. This clearly indicates that non-growth or maintenance production of SA plays an important role and that there are yield differences between the growth and maintenance modes. In some studies, the consumption of FA is reported in the non-growth phase of the batch fermentation (Du et al., 2008; Xi et al., 2012; Zheng et al., 2013).

With regard to substrate inhibition, differences between biofilm and suspended cultures are reported (Yan, Zheng, Dong, et al., 2014), with established biofilms appearing to be unaffected by the initial Glc concentration whereas the lag time of the suspended cultures (no lag for biofilm cultures) is clearly influenced by the initial Glc concentrations, with higher lag times reported for higher Glc concentrations (Lin et al., 2008).

2.3.3 Biofilm

A. succinogenes is well known to self-adhere to support surfaces and form biofilms under prolonged operation. According to Guettler, Rumler & Jain (1999), the observation of cells within an extracellular matrix is common in aerobically, chemo-organotrophic, yeast extract and CO_2-stimulated growth. There is currently no information available on the exopolysaccharide or EPS composition of *A. succinogenes*. However, during genome analysis (McKinlay et al., 2010) it was found that *A. succinogenes* possesses several large open-reading frames that could encode for the high-molecular-weight adhesins necessary for cellular immobilisation, but it does not possess the required genes for capsule formation and is therefore most probably non-capsulated.

All continuous studies on *A. succinogenes* resulted in unavoidable biofilm formation (Urbance et al., 2004; Van Heerden & Nicol, 2013; Bradfield & Nicol, 2014; Maharaj, Bradfield & Nicol, 2014; Yan, Zheng, Tao, et al., 2014), except for the study by Kim *et al.* (2009) in which a membrane-separation recycle system was implemented. The limited fermentation times in the Kim study were most probably caused by biofilms blocking the filter. Accordingly, self-immobilisation would appear to be the only cell retainment option for achieving high cell densities. The biofilm mode of operation is not limited to continuous fermenters and can also be employed in repeat batch fermentations where the attached biomass is retained after a batch cycle is completed (Urbance et al., 2004; Yan, Zheng, Dong, et al., 2014). In addition, the repeat batch fermentation can be supplemented with substrate (fed-batch) during the fermentation cycle (Yan, Zheng, Dong, et al., 2014).

2.3.4 Continuous *A. succinogenes* biofilm fermentation studies

Currently, only a limited number of continuous biofilm fermentation studies on *A. succinogenes* have been done and reported, with the majority published since 2013 (Urbance et

al., 2004; Van Heerden & Nicol, 2013; Bradfield & Nicol, 2014; Maharaj, Bradfield & Nicol, 2014; Yan, Zheng, Tao, et al., 2014). These studies tested the potential of using biofilm reactors for continuous production of *A. succinogenes* and highlight the substantial biofilm production capabilities of the organism.

Urbance et al. (2004) immobilsed *A. succinogenes* 130Z^T on PCS with a composition specifically optimised for the organism (Urbance et al., 2003) and consisting of 50% PP, 35% dried soybean hulls and 15% complex nitrogen sources (bovine albumin, soybean flour, yeast extract, bovine red blood cells, bacto peptone). As in the study by Demirci, Pometto and Johnson (1993) (*CONTINUOUS L. RHAMNOSUS BIOFILM FERMENTATION STUDIES* section on page *2-29*), the PCS were stacked in a grid and attached to the agitation shaft. During fermentations large amounts of biofilm were formed, at D < 0.8 h^{-1} suspended biomass concentrations as high as 160 $g.L^{-1}$ were reported. At D ≥ 0.8 h^{-1} large aggregates were formed inside the reactor, and therefore suspended values were not reported. It was found that for increasing D, the SA concentrations and yields decreased, while the volumetric productivity increased. A maximum volumetric productivity in the PCS biofilm reactor of 8.8 $g.L^{-1}.h^{-1}$ was measured, as well as a maximum SA concentration of 10.4 $g.L^{-1}$ and a maximum SA yield of 0.72 $g.g^{-1}$.

In the study by Van Heerden and Nicol (2013), *A. succinogenes* 130Z^T was immobilised on Genulite™ Groperl packing, in a packed bed reactor with external recycle. The authors noted that due to extreme biofilm formation, it was impossible to perform suspended cell fermentations as significant biofilm formation was observed inside the reactor surfaces during runs without packing present. The study was limited to D < 0.8 h^{-1}, with a highest volumetric productivity of 6.35 $g.L^{-1}.h^{-1}$ measured and a constant yield of SA on glucose of 0.69 ± 0.02 $g.g^{-1}$, which was found to be independent of dilution rate, transient state or biofilm amount. All AA formation took place via the pyruvate-formate lyase route as an equimolar amount of FA and AA was measured for almost all fermentations. It was found that at D > 0.35 h^{-1}, which corresponded to an SA titre < 10 $g.L^{-1}$, rapid cellular growth with corresponding biofilm growth was observed; this corresponds well to the observed growth termination SA concentration (*FIGURE 2-5*) of 8 $g.L^{-1}$ to 14 $g.L^{-1}$.

Bradfield & Nicol (2014) investigated the metabolic characteristics of *A. succinogenes* 130Z^T immobilised in a biofilm grown on stainless steel wool. The yields of SA to glucose were found to have an increasing dependence on the glucose consumed (negatively proportional to D),

with a maximum value of 0.91 $g.g^{-1}$ measured at a maximum SA titre of 48.5 $g.L^{-1}$. This observation was echoed by an increased SA to AA ratio with increasing glucose consumption; the values measured started at 2.4 $g.g^{-1}$ at a glucose consumption of 10 $g.L^{-1}$ and increased to an unprecendented value of 5.7 $g.g^{-1}$ at a glucose consumption of 50 $g.L^{-1}$. It should be noted that the SA titre in this study was significantly higher than that in the study by Van Heerden and Nicol (2013), which could explain the different observations in metabolic behaviour between the two studies.

The ratios of SA to AA corresponded to the FA to AA ratios which decreased from the equimolar values of 0.77 $g.g^{-1}$ to close to 0 $g.g^{-1}$, indicating a metabolic shift from the *pfl* to *pdh/fdh* route of AA production. This metabolic shift is, however, not sufficient to explain the SA to AA ratios observed as an FA to AA ratio of 0.77 $g.g^{-1}$ would match an SA to AA ratio of 1.97 $g.g^{-1}$, while an FA to AA ratio of 0 $g.g^{-1}$ would predict an SA to AA ratio of 3.93 $g.g^{-1}$. These results indicated the presence of an additional unknown source of NADH during fermentation or within the fermentation medium. A maximum SA productivity of 9.50 $g.L^{-1}.h^{-1}$ was measured during the fermentation.

Maharaj, Bradfield and Nicol (2014) studied the immobilisation and biofilm formation capability of *A. succinogenes* 130Z^T on Poraver®, within a packed bed reactor with external recycle. The reactor had the same dimensions as that used in the study by Van Heerden and Nicol (2013). Dilution rates were limited to 0.054–0.72 h^{-1} and it was found that steady states were repeatable and independent of the operational history. The stability of biofilm production capabilities was tested for periods of more than 80 h and it was found that steady states remained constant to within 5% and no deactivation of the biofilm was observed. The total biomass was measured and determined to be independent of D, with a dry weight concentration of 23.8 ± 2.9 $g.L^{-1}$, which indicated that the attachment is controlled by the reactor geometry. SA productivity increased with increasing D and a maximum SA productivity of 10.8 $g.L^{-1}.h^{-1}$ was measured. It was found that the yield of SA on glucose and the concentration of SA decreased with increasing D, starting at yields of 0.9 $g.g^{-1}$ and 32.5 $g.L^{-1}$ respectively at D = 0.054 h^{-1}. The authors observed minor substrate inhibition at glucose concentrations higher than 50 $g.L^{-1}$ for D > 0.32 h^{-1}, as well as significant product inhibition at low D values.

In contrast to the observations by Van Heerden and Nicol (2013), Maharaj, Bradfield and Nicol (2014) found that the *pdh/fdh* route to AA was predominant at low D and changed to the *pfl* route with increasing D. This agrees with the observations by Bradfield and Nicol (2014) if it is assumed that an increase in glucose consumption indicates a decrease in dilution rate. As was the case in the Bradfield and Nicol (2014) study, the observed change in the AA production route could partially explain the significant improvement in yield of SA on glucose as this resulted in a higher NADH production and a more favourable yield of SA (0.9 $g.g^{-1}$) on glucose at low D. However, the ratios of SA to AA exceeded the theoretically possible value of 3.93 $g.g^{-1}$, which indicated that an additional source of NADH was required to account for the higher SA to AA ratio.

In the study by Yan et al. (2014), *A. succinogenes* CCTCC M2012036 (a genetically modified strain (Zheng et al., 2013)) was immobilised in a fibrous bed bioreactor which consisted of a cotton fibrous matrix bonded to a cylindrical stainless steel screen mounted to the agitation shaft of a commecially available laboratory bioreactor (Yan, Zheng, Dong, et al., 2014). In this study two separate glucose feed concentrations, 50 $g.L^{-1}$ and 80 $g.L^{-1}$, were tested. In the 50 $g.L^{-1}$ case, the D values were limited to between 0.1 h^{-1} and 0.4 h^{-1}, while for the 80 $g.L^{-1}$ study the values were maintained between 0.01 h^{-1} and 0.11 h^{-1}. In both cases it was found that the biomass levels remained almost constant for all dilution rates tested, which is in agreement with the findings of Maharaj, Bradfield and Nicol (2014). The SA titres decreased with increasing D, and maximum SA titres of 39.6 $g.L^{-1}$ and 63.6 $g.L^{-1}$ were measured, for the 50 $g.L^{-1}$ and 80 $g.L^{-1}$ feed concentrations, respectively. The SA productivity increased with increasing D, with maximum measured values of 7.5 $g.L^{-1}$ and 4.22 $g.L^{-1}.h^{-1}$ reported for the two glucose feed concentrations of 50 $g.L^{-1}$ and 80 $g.L^{-1}$ respectively. The SA yield increased from 0.84 to 0.92 $g.g^{-1}$ in the 50 $g.L^{-1}$ case and decreased from 0.85 to 0.72 $g.g^{-1}$ in the case of the 80 $g.L^{-1}$ glucose feed. The biofilm stability was investigated by running the biofilm reactor at a constant D for a period of 18 days and it was determined that the SA titre, productivity and yield varied by less then 5% over the course of the test. Using the Ierusalimskii equation (Egamberdiev & Ierusalimskii, 1968) to determine product inhibition, the authors found a critical SA concentration of 60 $g.L^{-1}$, at which point all SA production (including non-growth-related production) appeared to cease.

The measured ratios of SA to AA in the study by Yan et al. (Yan, Zheng, Tao, et al., 2014) exceeded the maximum theoretical value of 3.93 $g.L^{-1}$ by a significant margin in all of the tested conditions; values between 4.8 $g.g^{-1}$ and 7.2 $g.g^{-1}$ were reported for the 50 $g.L^{-1}$ glucose feed and 5.4 $g.g^{-1}$ to 6.7 $g.g^{-1}$ for the 80 $g.L^{-1}$ gucose feed. These values were significantly similar to those in a previous study by the same authors in batch (7.0 $g.g^{-1}$) and fed-batch (6.5 $g.g^{-1}$) conditions (Yan, Zheng, Dong, et al., 2014). The values reported are significantly higher than those of Bradfield and Nicol (2014) or Maharaj, Bradfield and Nicol (2014). However, the observations are similar and therefore it can be concluded that an additional unknown source of NADH is either produced during fermentation or present within the medium.

CHAPTER 3
TWO-PHASE REACTOR: DESIGN, OPERATION AND ANALYSES

3.1 Introduction

The academic study of biofilm reactors has been largely neglected as a result of the difficulty in quantifying the biomass in a biofilm reactor; in a suspended cell reactor the outlet biomass concentration is representative of the total biomass concentration in the reactor, but in the biofilm reactor this is never the case (Karel, Libicki & Robertson, 1985; Agathos et al., 1997; Stoodley et al., 1997; Beyenal & Lewandowski, 2002; Maharaj, Bradfield & Nicol, 2014).

The main objective in the design of the biofilm fermentation bioreactor was to control homogeneously distributed shear in a two-phase (liquid–solid) microbial system by manipulating the superficial liquid velocity for a sufficiently wide range of values. This biofilm fermentation reactor had to facilitate a low shear environment for biofilm growth while being capable of high shear *in situ* removal of the biofilm, or alternatively inhibiting biofilm growth completely for chemostat studies.

This chapter addresses the initial design of the liquid–solid fermentation system, as well as the operational conditions and analyses used to perform the biofilm case study on the anaerobic, lactic acid-producing organism *Lactobacillus rhamnosus*. The results from this study are reported in Chapter 5.

3.2 Two-phase reactor design requirements

3.2.1 Two-phase reactor: Hydrodynamic requirements

The main hydrodynamic requirements in the design of the two-phase biofilm fermenter were:

- Homogeneously distributed and controlled shear throughout the reaction volume
- The maximum possible area to volume (A/V) ratio to ensure sufficient area for bacterial adhesion
- A wide shear range to ensure biofilm growth at low shears with subsequent biofilm removal at a high shear rate, as well as being able to run in chemostat mode at high shear
- Near-ideal mixing (continuously stirred tank reactor – CSTR) to prevent gradients throughout the reactor which would influence biofilm formation
- A sufficiently low pressure drop in the reactor to prevent mechanical failure.

3.2.2 Two-phase reactor: Material requirements

The material used for the bioreactor system had to be transparent so that the biofilm could be observed during biofilm runs and for inspection after high shear removal of the biofilms. The material had to be flexible enough to allow the significant length of tubing to be kept within a reasonable space, while controlling the heating of the reactor as well as minimising heat losses. The idea was to keep as much of the reactor surface as possible submerged within a single water bath while the temperature of the water was controlled by measuring the temperature in the reactor. The material had to be heat resistant to over 121 ℃ as the entire reactor would be autoclaved in order to sterilise it prior to inoculation. The material also had to be predisposed to microbial adhesion and subsequent biofilm formation.

3.3 Two-phase biofilm fermentation: Bioreactor design

In order for the shear in the reactor to be homogeneously distributed, the reactor required a uniform cross-sectional area throughout most of its volume and had to be long enough for any entrance effects, as a result of instrumentation in-line, to become insignificant (see *HYDRODYNAMIC ENTRY LENGTH CRITERIA* in *APPENDIX A*). This implicitly required a design in which the

reactor would consist of a long tube of significantly small diameter so as to produce the required superficial velocity as well as a significantly large A/V (see section on *AREA TO VOLUME RATIO OF A TUBE* in *APPENDIX A*), while simulating a perfectly mixed reactor similar to a CSTR.

To control the shear in the experimental study it was required that the average superficial velocity through the tube be controlled: low shear biofilm studies with subsequent high shear biofilm removal, as well as high shear chemostat studies could then be performed in the same unit. In order to perform the chemostat studies on adhesive bacteria, i.e. bacteria that usually form biofilms, the shear stresses on the inner walls of the reactor had to be high enough to inhibit initial attachment of microbial cells. For the biofilm studies the shear stresses had to be high enough to remove the microbial cells that were already attached to the surface. For a more in-depth discussion on wall shear stresses within tubes, as well as the calculation of wall shear stresses within a tube, see the section on *WALL SHEAR STRESSES IN A TUBE* on page *A-2* of *APPENDIX A*.

The reactor type chosen was based on the well-known tubular loop reactor (Andries et al., 1996; Papagianni, Mattey & Kristiansen, 2003; Yazdian et al., 2009, 2010; Kilonzo, Margaritis & Bergougnou, 2010; Mousavi et al., 2010). This reactor type has been found to simulate CSTRs in a laboratory setting by achieving near-perfect mixing through sufficiently large recycle to through-flow ratios (R/Q). R/Q values of more than 20 were found to be sufficient to ensure near-ideal CSTR conditions (Bakke, Kommedal & Kalvenes, 2001; Papagianni, Mattey & Kristiansen, 2003).

It was found that the only material that fitted the above criteria (*TWO-PHASE REACTOR: MATERIAL* requirements section on page *3-2*) was silicone tubing. Silicone tubing has been used extensively for biomedical devices due to its biocompatibility and biodurability in various implantable biomedical devices (Wang, Neoh, et al., 2012). This material is highly transparent, significantly flexible, is heat resistant to over 121 ℃ and has been reported to be prone to bacterial adhesion and biofilm formation in various studies (Millsap et al., 1997; Gross et al., 2007; Li, Hauer & Rosche, 2007; Kokare et al., 2009; Tang et al., 2009; Teodósio et al., 2011; Wang, Neoh, et al., 2012). Li, Hauer & Rosche (2007) found that the biofilm attachment of *Zymomonas mobilis* to silicone tubing outperforms that of glass, polypropylene and smooth stainless steel.

The choice of pump for this study was limited to the Watson Marlow (Falmouth, UK) 323S peristaltic pump with 314D pump head. According to the manufacturer's specifications, the maximum peristaltic tube diameter one can place in this pump is 8 mm, which corresponds to a volumetric flow rate range of 12–1 600 mL.min^{-1}. The diameter of the reactor tubing would dictate the maximum linear velocity possible within the reactor. However, this linear velocity needs to be greater than 2.2 m.s^{-1} to ensure a shear stress of more than the required 12 Pa (see *SHEAR STRESS REQUIREMENTS TO INHIBIT MICROBIAL ATTACHMENT OR BIOFILM REMOVAL* section in *APPENDIX A*).

A significant parameter in the design of most piping systems is the pressure drop across the length of tubing as this dictates the pumping requirements in the system (Çengel & Cimbala, 2006: 329). However, in this case the pressure drop would indicate the pressure in the system immediately after the pump and it could therefore possibly cause material failure in the system. The maximum safe operating pressure of silicone tubing is approximately 3.5 bar and the burst pressure is between 7 and 17 bar (Malczewski, Inman & Cadieux, 2003, 2004; Colas, Malczewski & Ulman, 2004).

TABLE 3-1 shows several commercially available silicone tube diameters, with their corresponding maximum superficial velocities (calculated from the maximum volumetric flow rate of 1 600 mL.min^{-1}), estimated wall shear stresses (calculated using equation *(B-14)* in *APPENDIX B*), minimum tube lengths in order to ensure negligible entrance effects (calculated using the criteria of Bahrami (Bahrami, 2011), L_{min} = 1 000d), the corresponding minimum pressure drop (ΔP_{min}) (calculated using equation *(A-2)* in *APPENDIX A*) and the $(A/V)_{max}$ values for the respective tube diameters (calculated using equation *(A-1)* in *APPENDIX A*).

This table shows that the optimum tube diameter for this study would be 3 mm ID tubing. The linear velocity is much greater than the required 2.2 m.s^{-1}, and has an estimated $\tau_W \gg 12$ Pa required for biofilm removal (Bakker et al., 2003; Teodósio et al., 2011). *TABLE 3-1* shows that the ΔP_{min} (calculated from equation *(A-2)* in *APPENDIX A*) of the 3 mm tube is within the maximum operating pressure of silicone. A smaller diameter tubing of 2 mm has a ΔP_{min} significantly greater than 3.5 bar.

Table 3-1: Commercially available silicone tube diameters with the corresponding average linear velocities (u_{avg}), L_{min}, ΔP_{min} calculated from equation *(A-2)* and $(A/V)_{max}$ calculated from equation *(A-1)*. The parameter values were determined using the maximum volumetric flow rate of 1.6 $L.min^{-1}$ for the marprene tubing of 8 mm ID.

d (m)	u_{avg} ($m.s^{-1}$)	τ_W (Pa)	L_{min} (m)	ΔP_{min} (bar)	$(A/V)_{max}$ (m^{-1})
0.002	8.49	80.1	2.0	10.8	2 000
0.003	3.77	27.0	3.0	2.01	1 333
0.004	2.12	12.5	4.0	0.68	1 000
0.005	1.36	6.89	5.0	0.28	800

Even though the $(A/V)_{max}$ remains constant for a given tube diameter (equation *(A-1)*), the total volume of the reactor setup consists of various ancillary components which make up a fraction of the total volume of the reactor. Therefore the reactor tubing had to be as long as possible to ensure that a value as close as possible to the $(A/V)_{max}$ was obtained in the experimental setup, while remaining below the safe operating pressure limit. The experimental setup used in the investigation is shown in *FIGURE 3-1*. *TABLE 3-2* gives a theoretical analysis of the experimental setup, showing the theoretical total pressure drop (ΔP_{total}), the A/V ratio and the percentage of the $(A/V)_{max}$. The ΔP_{total} was calculated as the sum of minor losses in the system as a result of constrictions, expansions, elbows and measurement equipment placed in-line and the pressure loss as a result of the pipe length. L corresponds to the length of tube in *FIGURE 3-1* from the temperature controller to the recycle pump.

TABLE 3-2 shows that the longest possible tube length that is still within the 3.5 bar pressure limit is L = 5 m. When analysing the percentage of $(A/V)_{max}$ it can be seen that at L = 5m the A/V is approximately 78 % of the $(A/V)_{max}$. Therefore a maximum tube length of 5 m was chosen. The A/V was calculated as the quotient of the internal area of the tubing, i.e. the area available for biofilm attachment, and the measured total volume of the reactor. The total volume included additional equipment, such as the temperature-control sleeve and the pH-probe housing, as well as a section of peristaltic tubing.

The final reactor (*FIGURE 3-1*) consisted of a silicone tube of approximately 5 m in length with an active volume of 46.1 mL (average inner diameter of 3.1 mm) in which the reaction takes place (shown in bold), a feed line, an NaOH dosing line, an inoculation line and a waste line. Nitrogen gas (Afrox, Johannesburg, South Africa) was connected to the feed sample line and

the outlet line to prevent infection from the environment via the sampling point, and to maintain anaerobic conditions.

Table 3-2: Theoretically calculated ΔP using equation *(A-2)* and a volumetric flow rate of 1.6 L.min^{-1} at various tube lengths. The area to volume ratios (A/V) show that at 5 m length the A/V reaches 80% of $(A/V)_{max}$. However, an A/V value of more than 1 000 m^2/m^3 is reached. The maximum safe operating pressure (3.5 bar) is exceeded at a length greater than 5 m.

L	ΔP_{total} (bar)	A/V (m^2/m^3)	% of $(A/V)_{max}$
4.00	2.68	985	74
4.50	3.01	1 014	76
5.00	3.35	1 039	78
5.50	3.68	1 061	80

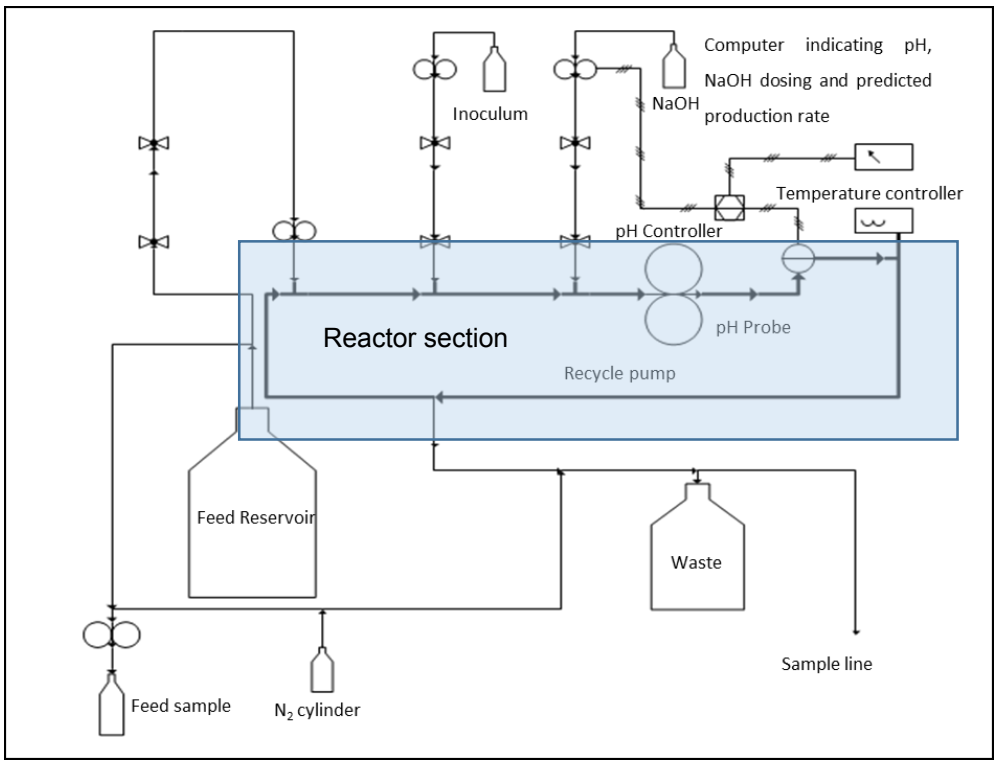

Figure 3-1: The reactor setup used during two-phase fermentations. The setup consists of a silicone loop (shown in bold) in which the reaction takes place (indicated by the enclosed blue rectangle), a feed line, inoculation line, NaOH dosing line (for pH control) and waste line.

Temperature was controlled at 37 °C using a hotplate coupled to a thermocouple, which was housed in an aluminium sheath connected within the reactor. The pH was controlled at 6.25 by dosing unsterilised 4 M NaOH through a peristaltic pump 120U (Watson Marlow, Falmouth, UK) with a relay connected to a Liquiline CM442 controller and a Tophit CPS471D ISFET probe (Endress+Hauser, Gerlingen, Germany) housed within an in-line stainless steel

holder. The CM442 was connected to a data logging system NI USB-6008 (National Instruments, Austin, Texas) and the pH, relay position and temperature were recorded continuously during fermentations.

3.4 Two-phase bioreactor experimental operation

3.4.1 Shear velocities and shear stress

The experimental shear velocities (the quotient of the volumetric recycle rate ($m^3.s^{-1}$) and the cross-sectional area (m^2) of the tube), corresponding Reynolds number (Re) (equation *(A-3)*), wall shear stresses (τ_W), dilution rate ranges and recycle to through-flow ratios are shown in *TABLE 3-3*. The τ_W for the highest linear velocity (turbulent regime) was inferred from the work of Liu (1997), Su et al. (2010) and Teodósio et al. (2011) (see *WALL SHEAR IN A TAYLOR FLOW SYSTEM* section on page *B-6* in *APPENDIX B*) using equation *(B-14)*, while τ_W values for the three biofilm runs (Re < 2 300, i.e. laminar regime) were calculated using equation *(A-6)*.

Table 3-3: The experimental conditions chosen for the two-phase fermentation runs. The independent variables were the average superficial recycle velocities, which related to a given τ_W, and the dilution rate. The ratios of recycle to through-flow (related to D) of between 200 and 3 700 (much greater than the minimum criterion of 20 (Bakke, Kommedal & Kalvenes, 2001)) indicate that the system has near-ideal mixing and therefore approximates a CSTR.

u_{avg} ($m.s^{-1}$)	Re	Regime	τ_W (Pa)	Dilution rates (h^{-1})	Minimum R/Q
3.65	15 600	Turbulent	26.1	0.12–0.54	3 731
0.55	2 290	Laminar	1.03	0.23–0.65	467
0.37	1 590	Laminar	0.70	0.24–0.61	335
0.19	814	Laminar	0.35	0.11–0.54	194

Due to the high recycle rate, as compared with the reactor through-flow, it was assumed that the reactor section acts as a perfectly mixed reactor with negligible axial and radial concentration profiles. As seen in *TABLE 3-3*, the minimum recycle to through-flow (R/Q) was between 194 and 3 731, which is significantly greater than the minimum requirement of R/Q > 20 (Bakke, Kommedal & Kalvenes, 2001). This was confirmed by residence time distribution tests performed *in situ* by applying a pulse change to the NaOH for pH control and measuring the change in pH over time.

3.4.2 Microorganism and growth medium

The microorganism used for the study was *L. rhamnosus* ATCC 9595. Stock cultures were stored at 6 °C on MRS agar slopes (Merck KgaA, Darmstadt, Germany). The growth medium for the seed culture was the same as that used for the fermentation (Section *3.4.3*), with 2 g $CaCO_3$ as a buffer agent, incubated for 18–24 hours at 37 °C.

3.4.3 Fermentation medium

All chemicals were sourced from Merck KgaA (Darmstadt, Germany), unless specified differently. The medium used for the experimental runs was based on the medium used by Senthuran et al. (1999) for immobilised fermentation of *L. rhamnosus* and consisted of ($g.L^{-1}$): glucose (Glc): 40; yeast extract (YE): 10; $MgSO_4.7H_2O$: 0.05; $MnSO_4.7H_2O$: 0.02; sodium acetate: 1.5; K_2HPO_4: 1; KH_2PO_4: 1; $FeSO_4.7H_2O$: 0.02; and ascorbic acid: 0.005. The Glc was diluted in 1.5 L of distilled water and the YE and mineral salts were diluted in 3.5 L of distilled water and separately sterilised by autoclaving at 121 °C for 40 min. Prior to use, the solutions were left to cool to room temperature, after which the glucose solution was aseptically added to the balance of the medium. To ensure no abiotic factors influenced the substrate removal the fermentation medium was tested, together with the product from the fermenter, using the method described in the *PRODUCT ANALYSIS* section. No significant changes in the medium composition were observed.

3.4.4 Product analysis

The bacterium possesses seven distinct metabolic products, as shown in the overall metabolic map (*FIGURE 2-3*) (Jyoti, Suresh & Venkatesh, 2004; Poolman et al., 2004; Gayen, Gupta & Venkatesh, 2007): lactic acid (LA), acetoin (Acn), diacetyl (Diac), pyruvic acid (PA), citric acid, oxaloacetic acid and acetic acid, the concentrations of which were measured, along with residual Glc, using an Infinity 1260 *high-performance liquid chromatograph* (Agilent Technologies, USA) with an Aminex HPX-87H ion-exclusion organic acid column (Bio-Rad Laboratories, Berkeley, California). The column was pre-calibrated using > 99% purity standards sourced from Merck KgaA (Darmstadt, Germany) and (Sigma–Aldrich, St. Louis, Missouri). Only two products, LA and Acn, were measured in appreciable quantities (> 0.1 $g.L^{-1}$). A simplified metabolic flux diagram (Jyoti, Suresh & Venkatesh, 2004; Poolman et al., 2004; Gayen, Gupta &

Venkatesh, 2007) for *L. rhamnosus* is presented in FIGURE 3-2 which shows that the carbon from Glc can be diverted towards the suspended biomass (x) and both the anabolic CO_2 (α) and catabolic products LA and Acn, as well as the catabolically produced CO_2. The system was assumed to be fully anaerobic due to the absence of Diac in the product. Diac is produced by non-enzymatic oxidation of 2-acetolactate (Park, Xing & Whitman, 1995; Oliveira, Nielsen & Förster, 2005), the direct precursor to Acn, and therefore in the presence of oxygen one would expect the presence of Diac and *vice versa*.

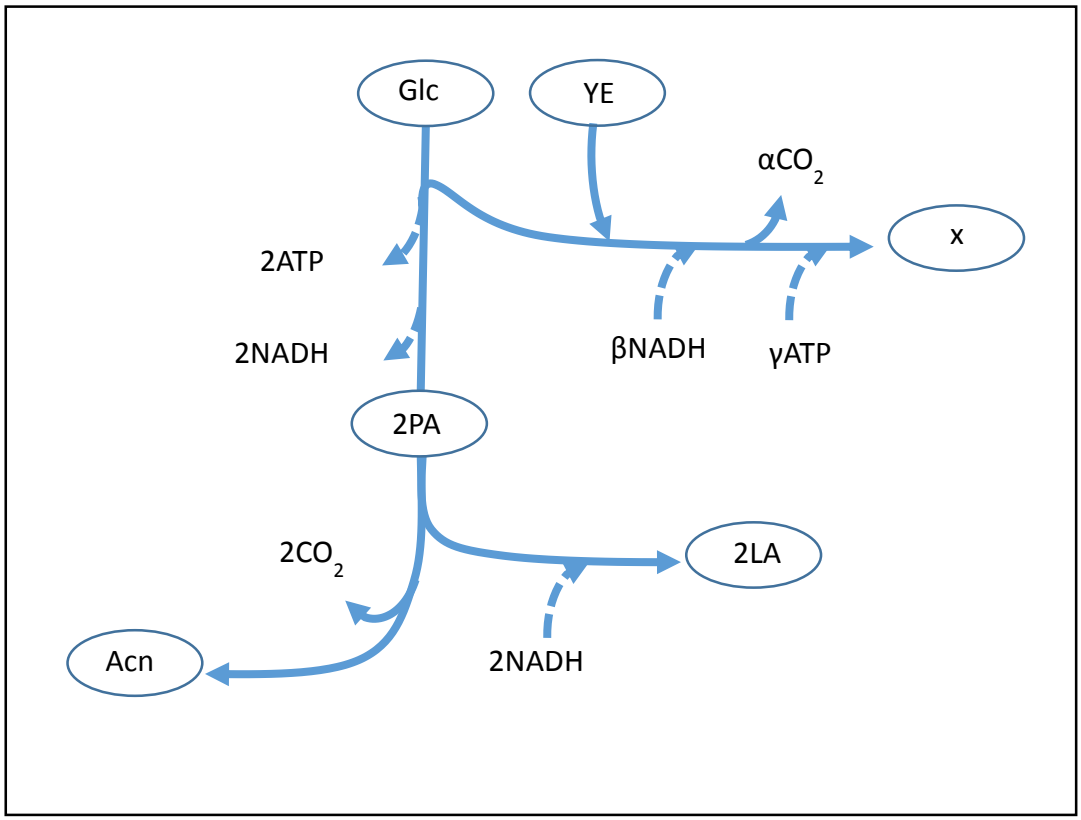

Figure 3-2: A simplified metabolic flow map of *L. rhamnosus*, based on the measured product concentrations. The map is based on the metabolism in the literature (Jyoti, Suresh & Venkatesh, 2004; Poolman et al., 2004; Gayen, Gupta & Venkatesh, 2007) shown in FIGURE 2-3

3.4.5 Steady-state criteria

The production of LA was continuously monitored by measuring the amount of NaOH dosed for pH control. This amount was assumed to be directly proportional to the production of LA. The steady state in the system was predicted by an algorithm programmed in the data logging system, which integrated the accumulation rate of LA over time ($C_{LA}(t)$) (equation (3-1)) and compared that with the theoretical concentration of LA at steady state ($C_{LA,steady}$) (equation (3-2)). The $C_{LA,steady}$ (equation (3-3)) only has physical meaning at values where equations (3-1)

and *(3-2)* have corresponding values. The value for $C_{LA}(0)$ was determined at the initiation of each run by measuring the initial concentration of LA in the reactor effluent.

$$C_{LA}(t) = C_{LA}(0) + \sum_{0}^{t_f} \left(q_{LA}(t) - DC_{LA}(t)\right) \Delta t \tag{3-1}$$

$$C_{LA,steady} = \frac{q_{LA}(t)}{D} \tag{3-2}$$

$$q_{LA}(t) = \frac{(4)(90)Q_{NaOH}(t)}{V_R} \tag{3-3}$$

FIGURE 3-3 shows a typical profile of the calculated values of C_{LA} and $C_{LA,steady}$, from which it can be seen that despite the $C_{LA}(t)$ fluctuating throughout the run, the $C_{LA,steady}$ matches the $C_{LA}(t)$. This indicates that a metabolic steady state was reached despite fluctuations in the total biomass content (suspended and attached cells). As a precaution, the reactor effluent was analysed at 48 h after initiation for D > 0.2 h^{-1} and after 96 h for D < 0.2 h^{-1} since temporary pseudo-steady states were observed in the initial stages of biofilm development. The longer times allowed at low dilution were due to slow growth at higher LA titres. Samples were taken after the mentioned periods when the predicted $C_{LA}(t)$ and $C_{LA,steady}$ were equal.

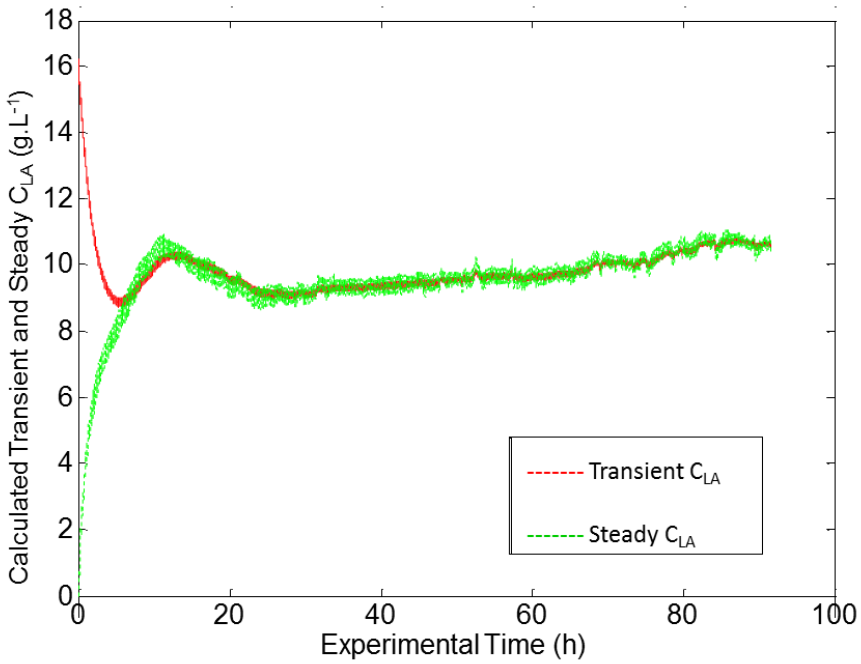

Figure 3-3: The transient C_{LA} (equation *(3-1)*) and steady state C_{LA} (equation *(3-2)*) during an experimental run at D ≈ 0.32 h^{-1} and at a recycle velocity of 0.55 m.s^{-1}. The figure clearly shows that the values coincide at a point during the fermentation, indicating a metabolic steady state within the reactor.

3.4.6 Biomass quantification

Calibration curves of dry weight to absorbance were determined by measuring the absorbance of outlet samples from the reactor at different biomass outlet concentrations for wavelengths of 560 nm (T60 UV/VIS Spectrophotometer, PG Instruments, Leicestershire, UK). The samples were washed twice with distilled water, resuspended in distilled water and dried overnight at 70 °C. The dry weights were calibrated to the measured absorbance of the samples (*FIGURE 3-4*) and the biomass concentrations were subsequently inferred by comparing them with these pre-calibrated concentration-absorbance curves for the C_x (equation *(3-4)*) and sample biomass (C_S) measured after the washout procedure described in Section *3.4.7* below (equation *(3-5)*). Equations *(3-4)* and *(3-5)* fitted the experimentally determined ABS_{560} to dry cell weight with r^2 values of 0.92 and 0.90 respectively, in the ABS_{560} range between 1.90 and 2.65.

$$C_x = 3.82(ABS_{560}) - 6.11 \quad (3\text{-}4)$$

$$C_S = 3.12(ABS_{560}) - 4.52 \quad (3\text{-}5)$$

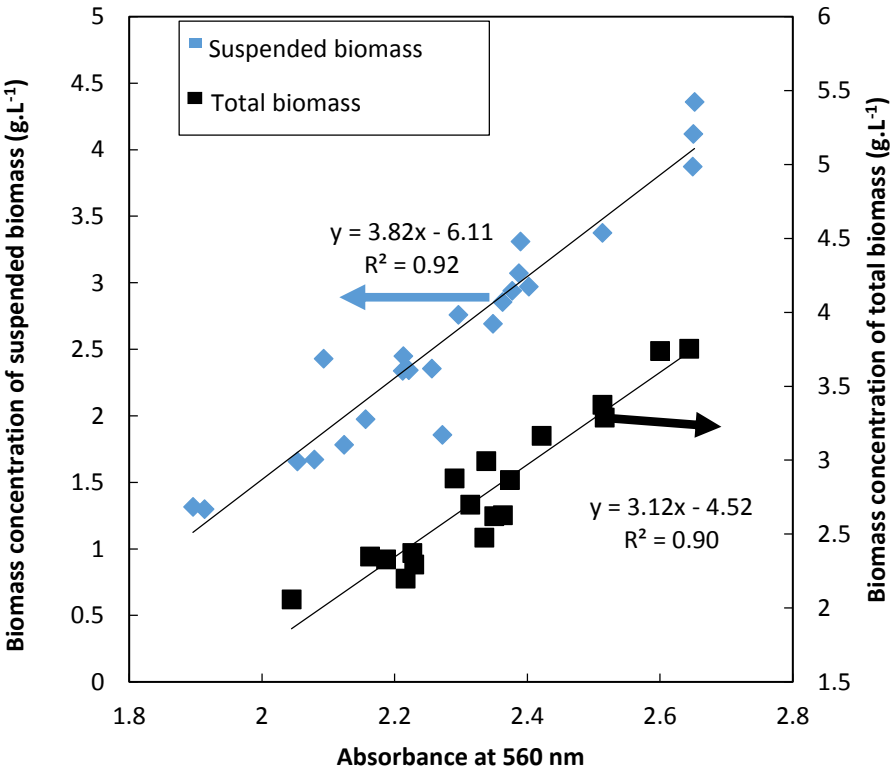

Figure 3-4: Calibration curves used to correlate the suspended and total biomass in the reactor to the absorbance of the sample at 560 nm

3.4.7 Calculation of total biomass

Biofilm quantification was achieved by physically removing the biofilm from the internal surface of the bioreactor. All feed to the bioreactor was ceased while the shear velocity in the bioreactor was simultaneously increased to 3.65 $m.s^{-1}$ for 30 min to ensure total removal of the biofilm. During this period, the biofilm was "scrubbed" from the internal surface of the reactor section and thoroughly mixed due to the significant shear and turbulence in the reactor. In order to keep the reactor ready for subsequent experiments, without the need for a complete restart, the reactor was not completely drained. Rather, after 30 min the feed rate was increased to the maximum flow of 8.6 $mL.min^{-1}$ while the recycle velocity was kept at 3.65 $m.s^{-1}$ and a sample of approximately 20 mL was taken from the reactor. The exact sample size (V_S) was determined by weight.

Assuming negligible growth of cells during the washout procedure, the initial biomass concentration (C_o) in the reactor was determined by solving a mass balance over the system. The system was modelled as a two-tank system with flow of liquid through the first constant-volume tank (fermenter V_R) and accumulation of liquid in the second tank (sample V_S). A diagram of the proposed model is shown in *FIGURE 3-5*.

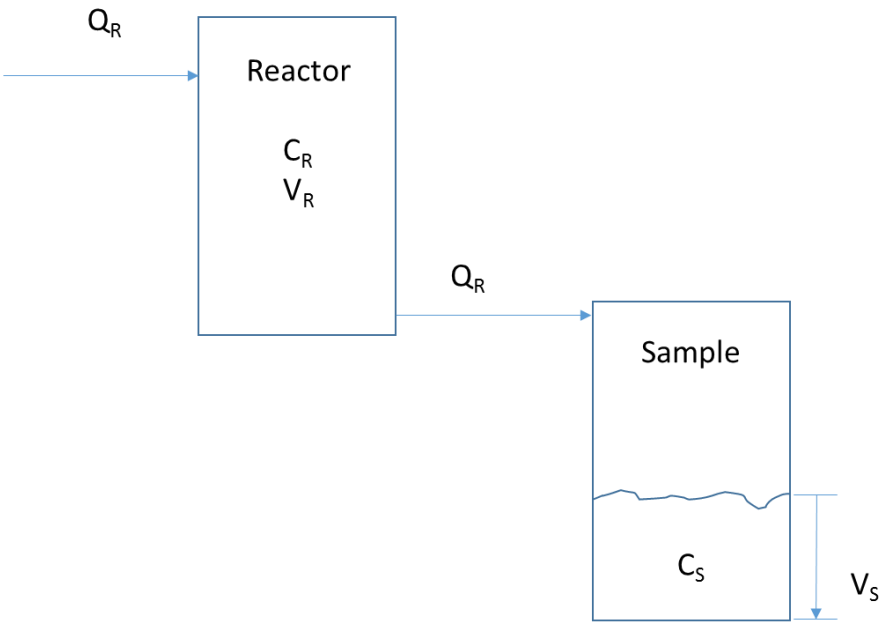

Figure 3-5: Diagrammatic representation of the two-tank system used to model the sampling procedure during washout and subsequent calculation of the initial biomass concentration (C_0) in the reactor

From this the C_o was estimated by applying a mass balance across the system (equation *(3-6)*) and solving for the dilution of the reactor during the washout procedure (equation *(3-7)*):

$$C_S(t)V_S(t) = C_0V_R - C_R(t)V_R$$
$$C_S(t) = \frac{V_R}{V_S(t)}\left(C_0 - C_R(t)\right) \quad (3\text{-}6)$$

$$\frac{dC_R(t)}{dt} = -\frac{Q_R}{V_R}C_R(t)$$
$$C_R(t) = C_0e^{-\frac{Q_Rt}{V_R}} = C_0e^{-\frac{V_S}{V_R}} \quad (3\text{-}7)$$

Combining equations *(3-6)* and *(3-7)* and solving for C_0 yields equation *(3-8)*, which was subsequently used to determine the biomass concentration in the reactor.

$$C_o = \frac{C_S}{\frac{V_R}{V_S(t)}\left(1 - e^{-\frac{V_S}{V_R}}\right)} \quad (3\text{-}8)$$

CHAPTER 4
THREE-PHASE REACTOR: DESIGN, OPERATION AND ANALYSES

4.1 Introduction

The main objective in the design of the three-phase biofilm fermentation bioreactor was to control homogeneously distributed shear in the reaction system by manipulating the gas–liquid superficial velocity in the reactor for a sufficiently wide range of values. This capability would facilitate the study of the effect of shear on biofilms in continuous and batch fermentation work. It would also aid in the inhibition of biofilm growth for chemostat operation of three-phase (gas–liquid–solid) fermentation with specific application to the case of succinic acid (SA) production by the proteobacterium *Actinobacillus succinogenes* with CO_2 as the gaseous reagent. This is very similar to the objective as described in Chapter 3 (*TWO-PHASE REACTOR: DESIGN, OPERATION AND ANALYSES*); this reactor also had to facilitate a low shear environment for biofilm growth while being capable of high shear *in situ* removal of the biofilm or alternatively inhibiting biofilm growth completely for chemostat studies.

This chapter addresses the initial design of the gas–liquid–solid biofilm fermentation system, as well as the operational conditions and analyses used to perform a biofilm case study on the CO_2-fixating, SA-producing organism *Actinobacillus succinogenes*. The results from this study are reported in Chapter 6.

4.2 Three-phase reactor requirements

4.2.1 Three-phase reactor: Hydrodynamic requirements

The hydrodynamic requirements for this reactor were the same as those for the two-phase reactor described in the *TWO-PHASE REACTOR: HYDRODYNAMIC REQUIREMENTS* section on page *3-2*. In summary the requirements were:

- Homogeneously distributed and controlled shear throughout the reaction volume
- The maximum possible area to volume (A/V) ratio to ensure sufficient area for bacterial adhesion
- A wide shear range to ensure biofilm growth at low shears with subsequent biofilm removal at a high shear rate, as well as being able to run in chemostat mode at high shear
- Near-ideal mixing (CSTR) to prevent gradients throughout the reactor which would influence biofilm formation
- A sufficiently low pressure drop in the reactor to prevent mechanical failure.

The main difference between the reactors was the addition of the gas phase to the system. It was required that the gas phase be sufficiently distributed within the liquid phase to prevent any rate effects as a result of gas–liquid mass transfer limitation.

A final addition to the reactor was an in-line sampling port for use during batch operation. During continuous operation, sampling was done by measuring at the outlet from the gas–liquid separator (GLS). It was assumed that this sample represented the reactor contents due to near-ideal mixing. During the batch runs, the flow from the GLS was stopped and therefore any sample from the product line during operation could not be assumed to represent the contents of the reactor. The batch sampling requirements were:

- The sample had to be representative of the reactor contents and therefore stagnant liquid in the sample line needed to be expelled before sampling.
- The volume of sample had to be small enough for the influence on the reactor operation to be minimal.

4.2.2 Gas–liquid separation considerations

In order for the system to operate for extended periods of time, a method had to be developed to separate the gas and liquid phases during operation. The reason for this was that the gas was continuously added to the system at a significantly higher volumetric flow rate than the addition of liquid, which would result in an accumulation of gas in the system during operation. For the steady state operation of the reactor system it was required that the liquid and gas hold-up remain constant during operation, necessitating the continued recycling of the liquid in the reactor while the excess gas from the system was continuously removed. Industrially, this is achieved by the use of a GLS; this system is discussed in Section *B.VI* on page *B-9*.

The operational considerations for the GLS in this system were:

- The volume of liquid in the GLS had to be small compared with the rest of the reactor volume to ensure that the reaction taking place in the GLS was insignificant compared with that in the rest of the reactor. The total volume of the GLS system had to be large enough so that during biofilm removal the reactor tube volume could be emptied into the GLS and the tube inspected. The contents of the reactor system (biofilm and suspended biomass) had to be thoroughly mixed in the GLS prior to removal and analysis.
- The gas–liquid separation had to be good enough to ensure that no gas recycling took place, as this would eventually cause the system to accumulate gas and become empty of liquid.
- The mixing in the vessel had to be sufficient to ensure complete mixing in the GLS system, thereby ensuring that the entire system remained an approximation of a CSTR.
- The GLS had to consist of a transparent material to allow for visual observation of the GLS operation, specifically with respect to the gas–liquid separation.
- There had to be no biofilm growth on the inner walls of the GLS system. This meant that either the wall shear in the GLS system had to be sufficient to inhibit any biofilm formation on the inner surface of the GLS system, or an alternative method of biofilm removal was required.

4.2.3 Three-phase reactor: Material requirements

The material requirements for the bioreactor system were the same as those for the two-phase system (*TWO-PHASE REACTOR: MATERIAL REQUIREMENTS* section on page *3-2*):

- The material had to be transparent so that the biofilm could be observed during biofilm runs and for inspection after high shear removal of the biofilms.
- The material had to be flexible enough to keep the significant length of tubing, to be kept within a reasonable space, while controlling the heating of the reactor as well as minimising heat losses.
- The material had to be heat resistant to over 121 ℃ as the entire reactor was autoclaved in order to sterilise it prior to inoculation.
- The material had to be predisposed to microbial adhesion and subsequent biofilm formation.

4.3 Three-phase biofilm fermentation: Bioreactor design

In order to compare the two-phase and three-phase case studies, it was decided to keep the final three-phase reactor design as near as possible to that of the two-phase reactor (*TWO-PHASE BIOFILM FERMENTATION: BIOREACTOR DESIGN* section on page *3-2*). The design was limited with regard to the choice of peristaltic pump: the Watson Marlow (Falmouth, UK) 323S peristaltic pump with 314D pump head and a maximum volumetric liquid flow rate of 1 600 mL/min was used. As in the two-phase reactor, the liquid recycle rate was controlled by the recycle pump, but in this case gas was added to the system and controlled independently. This meant that the gas inlet into the system had to be placed just after the recycle pump, and the gas–liquid separation vessel had to be placed just before the recycle pump. This would ensure that most of the reactor length would be exposed to gas–liquid flow, thereby ensuring an adequate supply of all required substrates. As was the case for the two-phase reactor, a silicone tube with a fixed diameter of 3 mm and a tube length at 5 m was chosen. The reactor was modified by adding a GLS, a gas inlet and a batch sampling line to the system.

With regard to the batch sampling line, it was decided to add a sampling line to the reactor at the point where CO_2 was added to the system. This meant that a small sample could be taken from the reactor even when using a sample line of significant length, as the sample was

followed by a slug of CO_2. In addition, the line could be flushed by using sterile CO_2 before and after sampling to ensure that it was free from stagnant liquid that could contaminate the samples.

The process of adding the GLS to the loop required cold-flow operational testing as the unit had to be custom-made, modified and tested specifically for this purpose. *FIGURE 4-1* shows a diagram of the final design obtained. The system was based on the industrial design of a GLS (*FIGURE B-6*). The mixture of gas and liquid entered the system and was separated by allowing the liquid to collect at the bottom of the vessel while the gas was removed through a vent at the top. The liquid was thoroughly mixed and recycled through the system or removed from the vessel as product.

It can be seen that the height of the liquid outlet line from the reactor was set at 12 mm above the bottom of the bottle. This value was determined experimentally during cold-flow operation as the minimum height at which

1. the line inlet was above the splash zone of the stirrer at 500 $r.min^{-1}$, shown in Section *B.VII* on page *B-10* to be the value at which the mixing time becomes independent of the stirring rate.
2. the liquid recycle was far enough below the level of the liquid to prevent any entrainment of gas into the recycle line from the GLS.

Table 4-1: The main components, respective dimensions and materials used for the GLS system

Component	Dimensions	Material
100 mL Duran® GL 45 glass bottle with cap	Max Ø 56 mm × 105 mm (outside) Max Ø 46 mm × 100 mm (inside)	Glass (bottle) PP (cap)
Magnetic stirrer	Ø 8 mm × 25 mm	PTFE coating
Gas vent	Ø 5 mm × 30 mm	Stainless steel
Liquid line to recycle	Ø 1.5 mm × 105 mm	Stainless steel
Liquid and gas line from recycle	Ø 1.5 mm × 50 mm	Stainless steel
Liquid outlet from reactor	Ø 10 mm × 100 mm	Stainless steel

For this design, the volume of liquid hold-up in the GLS, during normal operation, was determined as 10 ± 0.6 mL. The volume in the GLS was correlated to the measured liquid height in

the GLS. This correlation is shown in Section *B.IX* on page *B-13*. It was used to determine the working volume of liquid in the reactor. *TABLE 4-1* shows the main components, dimensions and materials of the GLS system.

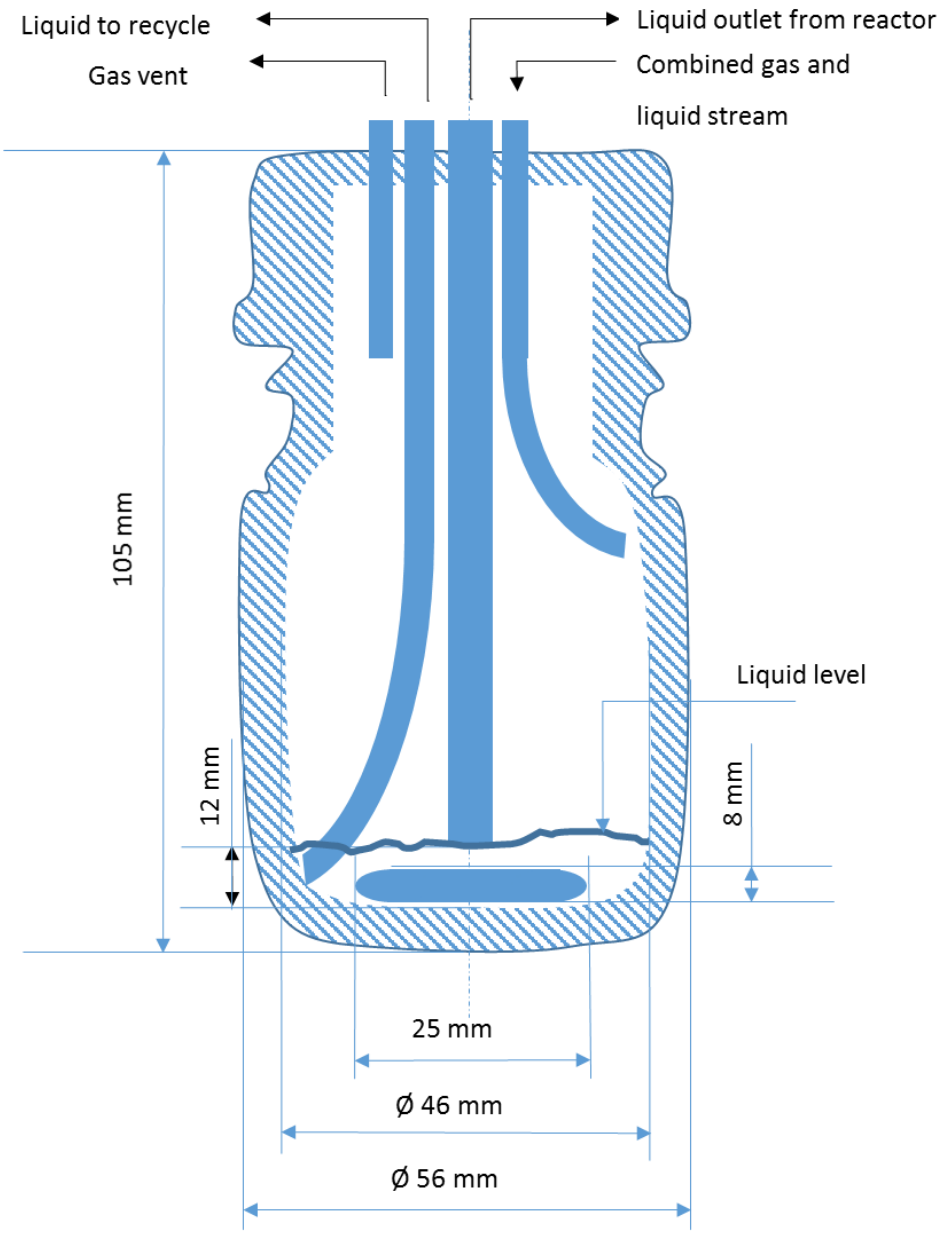

Figure 4-1: The GLS design implemented in the reactor setup. The system was based on the industrial design of a GLS (*FIGURE B-6*). The mixture of gas and liquid entered the system and was separated by allowing the liquid to collect at the bottom of the vessel while the gas was removed through a vent at the top. The liquid was thoroughly mixed and recycled through the system or removed from the vessel as product.

From a comparison of the design of the GLS to the requirements as described in the *GAS–LIQUID SEPARATION* considerations section on page *4-3*, it is clear that all requirements were fulfilled in the design, except for the requirement for the wall shear to be sufficient to prevent

biofilm growth during operation. This was shown to be an unrealistic requirement (Section *B.VIII* on page *B-11* in *APPENDIX B*) as the wall shear could not be increased sufficiently by merely increasing the mixing rate. Therefore the removal of biofilm from the glass surface had to be done by another means. In the case of biofilm build-up in the GLS, the inside surface of the GLS was mechanically scrubbed with the magnetic stirrer by physically moving the GLS over the magnetic stirrer plate.

The final reactor design used in the investigation is shown in *FIGURE 4-2*; the reactor section is shown in bold and contains an in-line gas trap to remove CO_2 continuously from the reactor, therefore preventing CO_2 accumulation. The reactor consisted of a 3 mm silicone tube of approximately 5 m in length with an active volume of 50–60 mL, depending on the amount of gas holdup in the reactor. A feed line (L-2), an NaOH dosing line (L-7), an inoculation line (L-5), a CO_2 (Afrox, Johannesburg, South Africa) line (G-1), a batch sampling line (L-8) and a product line (L-3) were connected to the reactor section as shown in *FIGURE 4-2*. Compressed air (G-2) was connected to the feed sample line (L-4), the product line (L-3) and the batch sample line (L-8), directly after the peristaltic pumps, to establish positive pressure which assisted in maintaining aseptic conditions. Anaerobic conditions were maintained by the peristaltic pumps which prevented inflow of air from the compressed air lines. The CO_2 gas vent from the GLS (G-3) was connected to the feed reservoir to ensure that the feed was completely saturated with CO_2 prior to entering the reactor.

Temperature was controlled at 37 °C using a hotplate coupled to a thermocouple, housed in an aluminium sheath connected within the reactor. pH was controlled at 6.80 ± 0.05 by dosing unsterilised 10 M NaOH through a peristaltic pump 120U (Watson Marlow, Falmouth, UK) with a relay connected to a Liquiline CM442 controller (Endress+Hauser, Gerlingen, Germany). The controller was connected to a Tophit CPS471D ISFET pH probe (Endress+Hauser, Gerlingen, Germany) housed within an in-line stainless-steel holder. The CO_2 flow rate to the reactor was continuously controlled at a constant flow rate of 6 NmL.min^{-1} (approximately 10% vvm) with a Brooks SLA5850S thermal mass flow controller (Brooks Instrument, Hatfield, Pennsylvania). The CM442 and the SLA5850S were connected to a data logging system NI USB-6008 (National Instruments, Austin, Texas) whereby pH, relay position, temperature and CO_2 flow rate were recorded continuously during fermentations.

The time-averaged rate of NaOH dosed, for pH control, was monitored continuously and used as an indication of steady state in the system. In order to verify steady state in the reactor, the effluent was analysed twice with at least two volume turnovers between samples, when the rate of NaOH dosing fluctuated less than 5%.

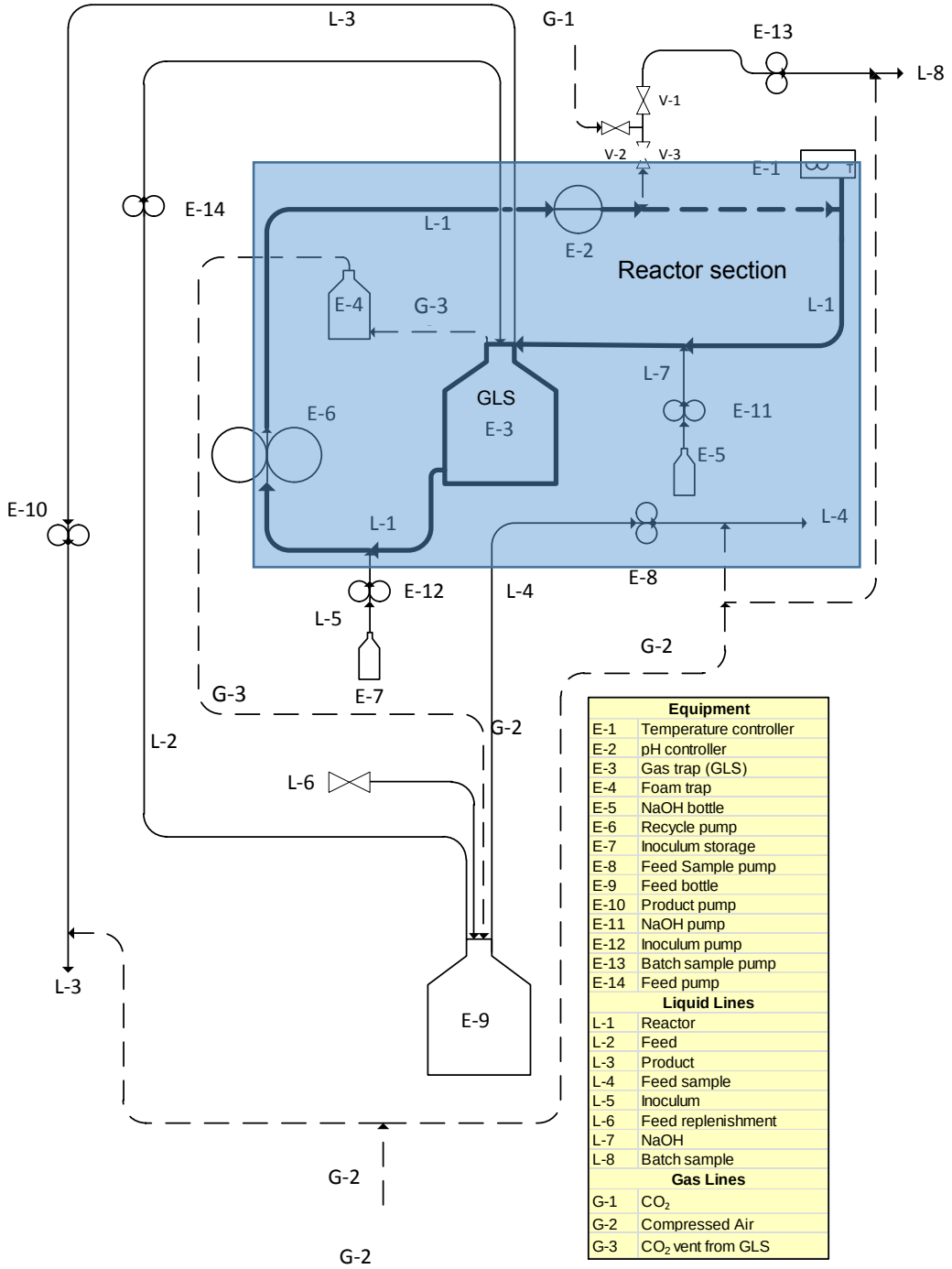

Figure 4-2: The fermenter setup used during three-phase fermentations. The fermentation took place in the reactor section (bold, L-1, enclosed by blue rectangle). The reactor included a feed line (L-2), a product line (L-3), a feed sample line (L-4), an inoculation line (L-5), an NaOH dosing line (L-7), a CO_2 line (G-1) and a batch sampling line (L-8).

4.4 Hydrodynamic verification of the three-phase bioreactor design

Hydrodynamic flow in gas–liquid systems is different from homogeneous single-phase flow. The characteristics of gas–liquid flow are explained in more detail in the section on *GAS–LIQUID FLOW IN* tubes on page *B-1* in *APPENDIX B*. It was verified in Section *B.II* on page *B-3* that the system can be defined as small-channel, two-phase flow capable of Taylor flow at medium to low superficial velocities (Salman, Gavriilidis & Angeli, 2006). Therefore the system should not be affected by gravitational effects and the gas–liquid flow regime map (*FIGURE B-2*) is applicable.

From the flow regime map (*FIGURE B-2*) it can be seen that the gas superficial velocity in the system plays an important role in defining the hydrodynamic flow regime and therefore in determining the shear stresses in the system. It was therefore imperative that the gas flow and, by extension, the gas superficial velocity be fixed in order to determine the reactor hydrodynamics. A study of the effect of a CO_2 donor on the SA production of *A. succinogenes* was performed by Zou et al. (2011) and it was found that at a volumetric rate of CO_2 addition of 10% vvm (volume of gas per volume of reactor per minute), the production of succinic acid remains independent of the CO_2 partial pressure and therefore an increase in CO_2 addition had no discernible effect on the SA production rates. In addition, there were several other studies that used CO_2 addition rates of 10% vvm (Zheng et al., 2009, 2013; Galaction et al., 2012; Wang, Zhu, et al., 2012). In this case a CO_2 addition rate of 10% vvm translates to approximately 6 NmL.min^{-1} or a u_G of approximately 0.014 m.s^{-1}.

The gas–liquid mass transfer coefficient (k_La) of CO_2 to the medium was modelled using correlations from the literature (Berčič & Pintar, 1997; Vandu, Liu & Krishna, 2005; Cai et al., 2013) at the minimum required recycle of 0.09 m.s^{-1} liquid flow (controlled by the peristaltic pump as there was no gas present in the pump section) and various gas superficial velocities (see Section *B.III* on page *B-4* in *APPENDIX B*). It was determined that the k_La value remained within a narrow band of between 0.02 and 0.04 s^{-1} for u_G values of 0.014–0.078 m.s^{-1}. These values correspond to 10% vvm – 70% vvm CO_2 addition.

Assuming a k_La = 0.02 s^{-1} = 72 h^{-1}, the maximum SA production rate can be calculated from the maximum CO_2 transfer rate ($q_{CO2}^{t,max}$) using equations *(4-1)* and *(4-2)*, with $C_{CO2}^{sat} = P_r/H_{CO2}$ = 100/3 901 = 0.0256 mol.L^{-1} (Lísal, Smith & Aim, 2004; Sander, 2014). The $q_{CO2}^{t,max}$ (equation *(4-1)*) was derived by assuming all CO_2 in the medium to be depleted, and therefore the mass transfer of CO_2 becomes the rate-limiting step in the production of SA.

$$q_{CO_2}^{t,max} = k_L a\left(C_{CO_2}^{sat}\right) \quad (4\text{-}1)$$

$$q_{CO_2}^{t,max} = q_{SA}^{max} \quad (4\text{-}2)$$

The resulting q_{SA}^{max} = 1.84 mol SA.L^{-1}.h^{-1} = 217 gSA.L^{-1}.h^{-1}, which is more than an order of magnitude higher than the highest reported volumetric SA production in the literature of 10.8 g.L^{-1}.h^{-1} (Maharaj, Bradfield & Nicol, 2014), indicating that the CO_2 will always be in excess during fermentation if a CO_2 addition rate of 10 vvm is used, and assuming that the correlations predicted the k_La value correctly.

The reactor design was subject to the same pressure drop limitation as in Chapter *3*: the maximum safe operating pressure of silicone tubing is approximately 3.5 bar, while the burst pressure is between 7 and 17 bar (Malczewski, Inman & Cadieux, 2003, 2004; Colas, Malczewski & Ulman, 2004). *TABLE 4-2* shows the total pressure drop (ΔP_{total}) as well as the corresponding parameters used for the calculation to evaluate equations *(B-15)* to *(B-18)* (Section *B.V* on page *B-8*) in the gas–liquid system at a gas flow rate of approximately 10 vvm (6 NmL.min^{-1}) and various u_L. This table shows that the pressure drop in the gas–liquid system is significantly higher than in the liquid system in Chapter *3* (*TABLE* 3-2). The maximum operational pressure of 3.5 bar is reached between liquid velocities of 1.5 and 2 m.s^{-1}. The maximum liquid velocity chosen for the chemostat runs was 1.83 m.s^{-1} (200 r.min^{-1} on the peristaltic pump) as this was the highest liquid velocity achieved during cold-flow testing without significant observable deformation of the silicone. This liquid velocity is also still higher than the required 1.2–1.5 m.s^{-1} (6–8 Pa) (equation *(B-14)*) to ensure inhibition of microbial biofilm on the surface (a τ_w = 10.25 Pa was calculated for a u_L = 1.83 m.s^{-1} using equation *(B-14)*). It was, however, too low for thorough biofilm removal (> 12 Pa), which necessitated mechanical removal of the biofilm as will be explained in the *MEASUREMENT OF TOTAL BIOMASS* section (Section *4.5.8*).

Table 4-2: The total pressure drop (ΔP_{total}) in the three-phase reactor and the parameters used to calculate these values (equations *(B-15)* to *(B-18)*), at various superficial liquid velocities (u_L).

U_L	ΔP_{total} (bar)	ΔP_L (bar) *1	ΔP_G ($\times 10^{-3}$ bar)	X^2	φ^2
3.66	6.17	4.62	2.96	1 130	1.40
3	4.92	3.52	3.13	719	1.50
2.5	4.17	2.83	3.55	440	1.63
2	3.50	2.27	3.78	265	1.82
1.5	3.10	1.83	4.93	114	2.25

*1 The ΔP_L included a pressure drop of 1.27 bar that took into account the pressure drop as a result of additional tubing in the GLS system

4.5 Three-phase bioreactor experimental operation

4.5.1 Shear velocities and dilution rates used during continuous operation

The shear velocities (the quotient of the volumetric recycle rate ($m^3.s^{-1}$) and the cross-sectional area (m^2) of the tube) used for the experiments were 1.83 $m.s^{-1}$ for the chemostat experiments and 0.36 $m.s^{-1}$ and 0.09 $m.s^{-1}$ for the biofilm experiments. *TABLE 4-3* shows the u_L values and the dilution rate (D) ranges used during the experimental runs. In addition, the corresponding hydrodynamic flow regime (*FIGURE B-2*) and the predicted wall shear (τ_W) using equations *(B-12)* and *(B-14)* are shown. Due to the high recycle rate, as compared with the reactor through-flow (R/Q), it was assumed that the reactor section acted as a perfectly mixed reactor with negligible axial and radial concentration profiles. Typical R/Q were between 90 and 8 850, which is significantly higher than the minimum criterion of R/Q > 20 (Bakke, Kommedal & Kalvenes, 2001). This was confirmed by residence time distribution tests performed *in situ* by applying a pulse change to the NaOH flowrate for pH control and measuring the pH change over time.

The GLS vessel was stirred at a constant rate of 500 $r.min^{-1}$, shown to be the minimum rate above which a negligible difference in mixing is observed (*MIXING IN A STIRRED VESSEL* section on page *B-10*). This stirring rate was, however, found to produce a wall shear stress inside the GLS significantly lower than that required for biofilm inhibition or removal, which meant that

a mechanical biofilm removal method had to be devised to remove biofilm in the GLS prior to sampling. The method is described in Section 4.5.2.

Table 4-3: The superficial liquid velocities (u_L) and dilution rate (D) ranges used for the experimental study. The table also shows the corresponding hydrodynamic flow regimes (FIGURE B-2) and the calculated wall shear stresses from equation (B-12) and (B-14).

u_L (m.s^{-1})	D range (h^{-1})	Regime	τ_W (Pa)
1.83	0.10–0.80	Bubble	10.5
0.36	0.51–2.22	Slugging/Taylor	0.70
0.09	0.44–2.59	Slugging/Taylor	0.18

4.5.2 Steady state sampling during continuous operation

As a result of the extremely high dilution rates used during continuous operation in the biofilm reactor, the biofilm was observed to grow extremely fast. This was most probably a result of a much lower C_{SA} in the reactor at a higher D, which was shown to promote a much faster microbial growth rate (FIGURE 2-5). This meant that the biofilm reached an apparent steady state in the reactor, as confirmed by NaOH dosing profiles, within a period of between 16 and 36 h. At this time an initial sample was taken and analysed. To confirm steady state in the reactor, another sample was taken after one volume turnover; if the analysis was within 5% of the first sample, the results were logged as the system was assumed to be at steady state.

It was decided to sample, scrub the reactor and continue the run after each first apparent steady-state value due to significant shedding of biofilm as a result of aging biofilm in the tubular reactor during extended runs. It appeared that due to the adhesive properties of the support (silicone tubing), the long-term biofilm stability was compromised. This phenomenon was also observed by Maharaj, Bradfield & Nicol (2014) and resulted in oscillatory behaviour, which could have compromised the results in this study. This did, however, mean that the extremely high SA titres (C_{SA} > 30 g.L^{-1}) as reported in the literature (Bradfield & Nicol, 2014; Maharaj, Bradfield & Nicol, 2014) were not achieved.

An example of an NaOH dosing profile is presented in FIGURE 4-3 and clearly shows that the time at which the apparent steady-state conditions (constant dosing of NaOH) were reached was after approximately 18 h of operation. The respective samples are indicated on the figure.

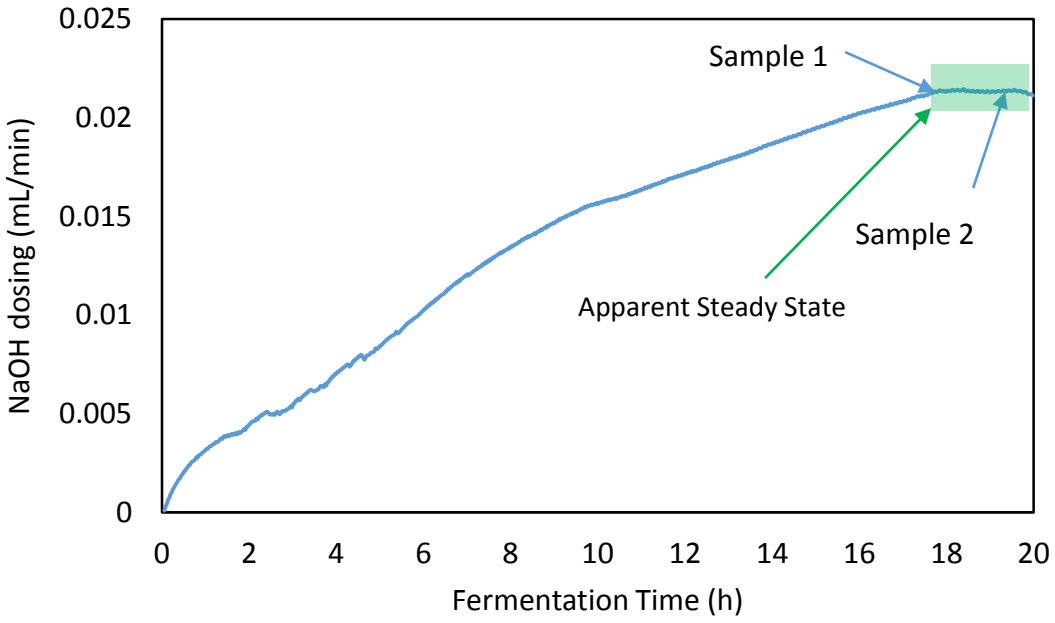

Figure 4-3: Typical dosing profile during a continuous biofilm run. The specific conditions were D = 1.0 h^{-1}, recycle velocity = 0.09 $m.s^{-1}$. In addition, the apparent steady-state region and the sample times to ensure steady state are shown.

When there was found to be biofilm build-up in the GLS, the inside surface of the GLS was mechanically scrubbed with the magnetic stirrer by physically moving the GLS over the magnetic stirrer plate. After this procedure, the system was left to stabilise for at least three volume turnovers and confirmed to be at steady state through observation of the NaOH dosing profile and of two consecutive samples, one volume turnover apart.

4.5.3 Batch operation

The bioreactor setup was used to perform four separate batch runs, all at a u_L = 0.09 $m.s^{-1}$ and u_G = 0.014 $m.s^{-1}$. At these operational conditions a wall shear stress of τ_w = 0.18 Pa was calculated from equation *(B 12)*. Prior to batch operation, a biofilm was grown continuously inside the reactor tube. The preparation conditions for biofilm growth, as well as the measured concentrations of total biomass (C_{xt}) and cellular biomass (C_{xt*}), are summarised in *TABLE 4-4*. A negative trend was observed in terms of the total and cellular biomass with regard to feed glucose concentrations (C_{Glc0}).

Table 4-4: Continuous biofilm growth conditions of all batch runs and final biomass concentrations measured after completion of the respective runs. From the table can be seen that the C_{xt} and C_{xt*} values maintained a downward trend as a function of the C_{Glc0}.

Batch	1	2	3	4
D (h^{-1})	1.22	0.97	0.76	1.07
C_{Glc0} ($g.L^{-1}$)	70	100	100	120
u_{avg} ($m.s^{-1}$)	0.09	0.09	0.09	0.09
Δt (h)	46.33	66.88	41.00	45.51
C_{xt} ($g.L^{-1}$)	12.01	7.32	8.25	5.84
C_{xt*} ($g.L^{-1}$)	5.04	7.12	4.83	3.42

At the end of the initial continuous biofilm growth period, a sample of the contents of the reactor was taken and analysed. This was used as the starting point of the batch fermentation. The batch run was initiated by stopping both the feed (E-14) and product pumps (E-10) (*FIGURE 4-2*) simultaneously, and starting the NaOH dosing log. During fermentation, samples were periodically taken by first closing the valve to the reactor (V-3) and opening the sample valve (V-1). The line was flushed with CO_2 by switching on the batch sample pump (E-13). The sample was then taken by closing the CO_2 valve (V-2) and simultaneously opening the valve to the reactor (V-3) and letting approximately 1 mL of sample accumulate in the sample line. The valve to the reactor (V-3) was closed while opening the CO_2 valve (V-2), allowing CO_2 to fill the line while the sample was pumped to the sample vial for analysis. The sample was weighed to determine the exact amount of sample taken from the reactor. Normal operation was continued by switching off the sample pump (E-13), closing the sample valve (V-1) and reopening the valve to the reactor (V-3) to allow CO_2 into the reactor. The sample procedure took approximately 5 min to complete, an interval that was assumed to have a minimal effect on normal operation of the reactor.

4.5.4 Microorganism and growth medium

A. succinogenes 130Z (DSM 22257 or ATCC 55618) was acquired from the German Collection of Microorganisms and Cell Cultures (DSMZ). Seed cultures in 30 mL McCartney bottles containing 15 mL of sterilised tryptone soy broth (TSB) were incubated for 16–24 h at 37°C and 150 $r.min^{-1}$ prior to use (for stock cultures or reactor inoculation). Short-term (< 3 weeks)

stock cultures were stored at 4 °C in TSB from Merck KgaA (Darmstadt, Germany). For long-term storage (> 3 weeks) 1 g, 66.6% glycerol, solutions were inoculated with 0.5 mL of stock culture and stored at −40°C.

4.5.5 Medium

All chemicals were sourced from Merck KgaA (Darmstadt, Germany), unless specified differently. The growth medium and phosphate buffer used for the experimental runs were the same as those used by Bradfield and Nicol (2014). The growth medium consisted of ($g.L^{-1}$): YE: 6; clarified CSL [15] (Sigma–Aldrich, St. Louis, Missouri): 10; NaCl: 1.0; $MgCl_2 \cdot 6H_2O$: 0.2; $CaCl_2 \cdot 2H_2O$: 0.2; sodium acetate: 1.36; $Na_2S \cdot 9H_2O$: 0.16 (for anaerobic conditions); and 1 $mL.L^{-1}$ Antifoam A (Sigma-Aldrich. St. Louis, Missouri). The phosphate buffer consisted of ($g.L^{-1}$): KH_2PO_4: 3.2 and K_2HPO_4: 1.6. A D-glucose (Futaste Pharmaceutical Co. Ltd., Shandong, China) concentration of 40 $g.L^{-1}$ was used for all continuous fermentations. The feed concentrations that were used in the batch runs are summarised in *TABLE 4-4*.

The growth medium was diluted in 8 L of distilled water (10 L bottle), the phosphate buffer in 0.5 L of distilled water (1 L bottle) and Glc in 1.5 L of distilled water (2 L bottle), and separately sterilised by autoclaving at 121 °C for 40 min. Prior to use, the solutions were left to cool to room temperature to prevent unwanted reactions among the components, after which the Glc solution and phosphate buffer were aseptically added to the growth medium.

To ensure no abiotic factors influenced the substrate removal, the fermentation medium was tested, together with the product from the reactor, using the method described in the *PRODUCT ANALYSIS* section. No significant changes in the medium composition were observed.

4.5.6 Product analysis

The bacterium produces four distinct metabolic products: SA, AA, FA and ET as shown in the *A. succinogenes* metabolic map in *FIGURE 2-4* (McKinlay, Zeikus & Vieille, 2005; McKinlay et al., 2007; McKinlay & Vieille, 2008).The concentrations of the products were measured, along with residual Glc, using an Infinity 1260 high-performance liquid chromatograph (Agilent Technologies, Santa Clara, California) with an Aminex HPX-87H ion-exclusion organic acid column (Bio-Rad Laboratories, Berkeley, California). The column was pre-calibrated using > 99%

purity standards sourced from Merck KgaA (Darmstadt, Germany) and Sigma–Aldrich (St. Louis, Missouri).

4.5.7 Biomass quantification

The relationship between biomass and absorbance was determined, using the method in by measuring the absorbance (ABS_{660}), at a wavelength of 660 nm (CE 1021 Spectrophotometer, Cecil Instruments, Cambridge, UK), of 46 individual samples from various reaction conditions and biomass concentrations. Suspended and total biomass measurements were done on the samples (*MEASUREMENT OF TOTAL BIOMASS* – Section *4.5.8*). The samples were washed twice with distilled water, resuspended in distilled water, the ABS_{660} was measured and the samples were dried overnight at 70 °C (Liu et al. 2008; Zheng et al. 2013). It was determined that an absorbance value of 1 relates to 645 ± 36 mg L^{-1} of biomass with a correlation coefficient of 0.9701. *FIGURE 4-4* shows the data and the linear regression obtained. The biomass concentrations were inferred from this relationship and from the ABS_{660} measurements. It was assumed that the drying temperature of 70 °C was low enough to avoid any loss of mass, apart from the evaporation of water.

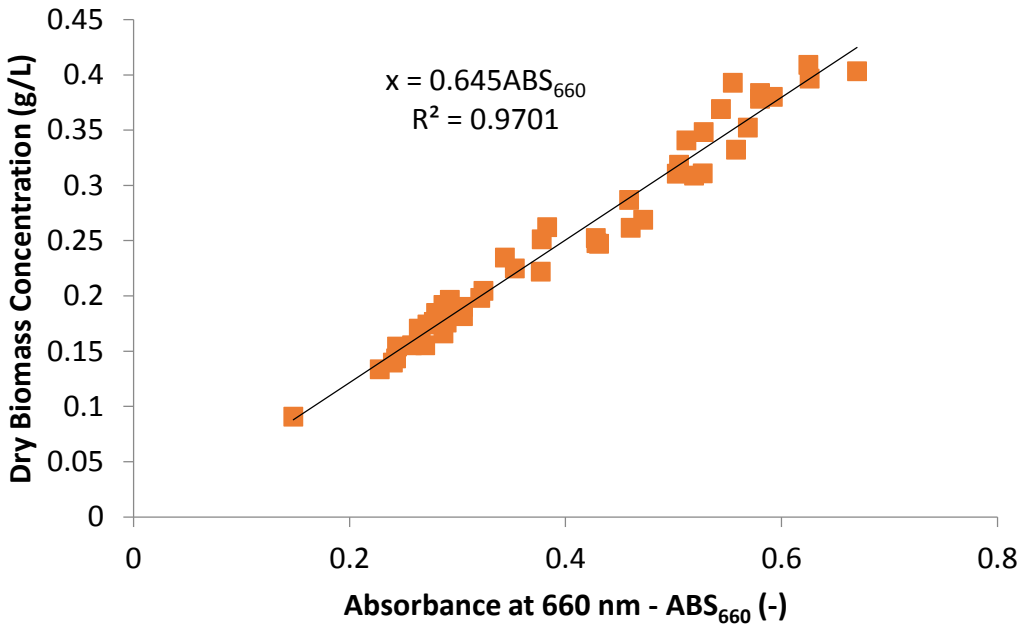

Figure 4-4: Correlation between the absorbance measurement at 660 nm and the weighed dry biomass measurements. This correlation showed that an ABS = 1 relates to a dry biomass measurement of 645 mg.L^{-1}. The correlation was limited to the absorbance range between 0.15 and 0.67.

4.5.8 Measurement of total biomass

Biofilm quantification was achieved by physically removing the biofilm from the internal surface of the bioreactor. All feed to the bioreactor and recycling in the bioreactor were ceased and, using mechanical friction through the soft silicone tubing, the biofilm was loosened and subsequently removed by increased shear (1.83 $m.s^{-1}$). This procedure differed from that in Chapter 3, where the recycle stream was used to remove the biofilm. The pressure drop in the reactor was too great (ΔP_{total} > 3.5 bar for u_{avg} > 2 $m.s^{-1}$) in the system (TABLE 4-2), which caused mechanical failure of the silicone tubing during cold-flow testing. To ensure total removal of the biofilm, the reactor volume was emptied into the gas trap to prepare the silicone tubing for inspection. The process was repeated until all observable traces of biofilm had been removed from the tubing. During this process, the removed biofilm was thoroughly mixed with the medium due to the significant shear and turbulence in the reactor.

In order to keep the reactor ready for subsequent experiments, without the need for a complete restart, the reactor was incompletely drained after removal of the biofilm. The silicone-tube section of the reactor was emptied into the gas-trap section of the reactor. A sample of approximately 40 mL was taken from the gas trap, the biomass concentration was determined by ABS_{660} (FIGURE 4-4) and the sample was diluted to within the absorbance range of 0.15–0.67. The removed volume was then replaced with clean feed to allow the re-initialisation of the reactor for the next run.

4.5.9 EPS quantification

EPS quantification was done by alkaline hydrolysis and subsequent removal of the EPS fraction from the biofilm by dissolution in distilled water (Nielsen & Jahn, 1999). For preliminary tests, the samples were treated with pH 9 and pH 11 buffers, using the procedure described below. However, it was found that the difference in results between the two pH buffers was negligible, and therefore only the pH 9 buffer was subsequently used. The pH 9 buffer consisted of 1 $g.L^{-1}$ KH_2PO_4 and 79 $g.L^{-1}$ K_2HPO_4, and the pH 11 buffer of 0.01 $g.L^{-1}$ KH_2PO_4 and 79 $g.L^{-1}$ K_2HPO_4 (ratios of 0.0162 mol KH_2PO_4.(mol K_2HPO_4)$^{-1}$ and 0.000162 mol KH_2PO_4.(mol K_2HPO_4)$^{-1}$, respectively). The buffers were prepared by initially adding the KH_2PO_4 to a 1 L mixing vial and then adding the K_2HPO_4 while monitoring the pH (Alpha pH 190 pH controller, Eutech Instruments, Singapore).

For EPS removal, a known volume of the total biomass sample after ABS_{660} measurement (*MEASUREMENT OF TOTAL BIOMASS* section) was centrifuged and resuspended in a known volume of the required buffer solution (pH 9 or pH 11). The sample was ultrasonicated for 30 min (UMC 2, Integral Systems, Johannesburg, South Africa), centrifuged and washed twice with distilled water. Finally, the washed sample was resuspended in a known volume of distilled water and the ABS_{660} was measured. The ABS_{660} values of the pretreated and treated samples were converted to biomass concentrations and adjusted for dilution. The ratio of concentrations before and after treatment was assumed to represent the fraction of cellular-to-total biomass (including EPS).

CHAPTER 5
TWO-PHASE REACTOR: CASE STUDY

5.1 Introduction

This chapter is based on work published in the journal *New Biotechnology* (Brink & Nicol, 2014a) and addresses the effect of liquid shear rate on biofilm productivity and, more importantly, the product distribution. The expectation is that shear will affect the distribution of cells and EPS in the biofilm matrix (Beyenal & Lewandowski, 2002). Lactic acid (LA) fermentation was chosen in order to minimise gas formation in the novel, homogeneously distributed shear-control fermenter as described in Chapter 3 (*TWO-PHASE REACTOR: DESIGN, OPERATION AND ANALYSES* on page *3-1*). Numerous *Lactobacillus* species are known for their biofilm formation characteristics (Dagher et al., 2010) and *Lactobacillus rhamnosus* ATCC 9595 was chosen for the fermentation. The biofilm properties of this organism have been well studied (Dupont, Roy & Lapointe, 2000; Van Calsteren et al., 2002; Bergmaier, Champagne & Lacroix, 2005; Kim et al., 2006), making it an ideal bacterium for the investigation. The experimental procedures and methods are described in detail in Section *3.4* on page *3-7*. The experimental conditions are summarised in *TABLE 3-3*.

5.2 Experimental result obtained during the two-phase fermentation

The dataset represents 21 steady state conditions. Four velocity or shear conditions were investigated while the dilution rates (D) were varied between values of 0.1 and 0.7 h^{-1}. Each shear condition comprised four to six separate dilution rates. The concentrations of LA (C_{LA}), Acetoin (C_{Acn}), suspended biomass (C_x) and total biomass (C_{xt}), i.e. sum of attached and suspended biomass (x_t), were quantified at each of the 21 steady states. All D values resulted in

only partial glucose (Glc) conversion, with the C_{Glc} in the outlet always exceeding 5 g/L. The experimental results obtained during the individual runs are shown in *TABLE 5-1*.

5.2.1 Biofilm characteristics

The C_{xt} and C_x biomass measurements are given as a function of D in *FIGURE 5-1*. The chemostat run, consisting of only suspended biomass, exhibits the expected behaviour with a decline in the C_x as D increases. The C_{xt} measurements do not appear to exhibit a clear trend, despite prolonged operation of the biofilm runs. The biofilm runs measured C_x in close proximity to that of the chemostat run, while the C_{xt} generally increased as shear velocities decreased. Repeat runs at similar dilution rates (u_{avg} = 0.37 m.s^{-1}, D = 0.2 and 0.6 h^{-1}) did not result in repeatable C_{xt}, although steady state was established. This is in agreement with the work of Peyton & Characklis (1993) and Peyton (1996), who observed significant variation in biofilm thickness, roughness and density for constant substrate loadings (analogous to dilution rate) and shear conditions.

In *FIGURE 5-2* the C_x to C_{xt} are shown, with the fitted average ratio of suspended-to-total biomass (C_x/C_{xt}) for each shear condition given as the slope and expressed as a yield ($Y_{xt,x}$). The independent variable D is not obvious in *FIGURE 5-2* due to the random variations observed in the measured concentrations (*FIGURE 5-1*). However, despite the fluctuations in the C_x and C_{xt} (*FIGURE 5-1*), the $Y_{xt,x}$ remains strikingly constant at a specific shear. In addition, the $Y_{xt,x}$ clearly decreases as the average superficial recycle velocity (u_{avg}) decreases. The fact that even at the lowest u_{avg} of 0.19 m s^{-1}, the fitted $Y_{xt,x}$ remains 0.61 indicates that the C_x is greater than the attached biomass concentration, even at the lowest-shear condition. This is supported by the visual observation that the biofilm appeared thin and non-evenly dispersed over the internal tube area.

Table 5-1: Experimental results obtained during all fermentations of *L. rhamnosus* within the biofilm fermentation bioreactor

Shear velocity ($m.s^{-1}$)	Run No	D (h^{-1})	Glc out ($g.L^{-1}$)	ΔGlc ($g.L^{-1}$) *1	C_{LA} ($g.L^{-1}$)	C_{Acn} ($g.L^{-1}$)	C_x ($g.L^{-1}$)	C_{xt} ($g.L^{-1}$) *2	$Y_{xt,x}$	$Y_{Glc,LA}$ ($g.g^{-1}$)	q_{LA} ($g.L^{-1}h^{-1}$)	r_{LA} ($g.g^{-1}h^{-1}$) *3
Chemostat 3.66	1	0.12	5.02	32.4	22.7	2.84	3.98	3.98	1.00	0.70	2.64	0.66
	2	0.22	13.2	24.5	19.9	1.30	3.57	3.57	1.00	0.81	4.46	1.25
	3	0.34	24.7	14.1	10.7	0.94	3.11	3.11	1.00	0.76	3.60	1.16
	4	0.44	28.4	10.7	8.42	0.76	2.53	2.53	1.00	0.79	3.67	1.45
	5	0.54	32.3	7.07	5.90	0.55	1.35	1.35	1.00	0.83	3.20	2.36
0.55	1	0.23	11.6	26.5	21.9	1.19	3.54	4.25	0.83	0.83	4.98	1.17
	2	0.32	21.0	17.8	15.5	0.75	2.88	3.47	0.83	0.87	4.97	1.43
	3	0.34	19.9	18.4	15.6	0.88	2.43	3.05	0.80	0.85	5.27	1.73
	4	0.42	26.5	13.0	10.8	0.61	2.36	2.89	0.82	0.83	4.50	1.56
	5	0.55	26.6	13.0	10.9	0.46	2.34	2.92	0.80	0.84	5.97	2.05
	6	0.65	32.5	6.93	5.86	0.44	1.36	1.59	0.85	0.85	3.78	2.37
0.36	1	0.24	11.7	27.0	22.7	1.01	3.38	4.94	0.68	0.84	5.45	1.10
	2	0.24	5.57	32.3	26.8	1.23	3.78	5.70	0.66	0.83	6.48	1.14
	3	0.31	19.4	19.8	16.7	0.69	3.01	3.95	0.76	0.84	5.26	1.33
	4	0.46	27.7	12.6	10.1	0.50	2.47	3.42	0.72	0.80	4.65	1.36
	5	0.57	28.6	11.4	9.69	0.47	2.36	3.38	0.70	0.85	5.52	1.63
	6	0.58	26.7	13.2	11.0	0.49	2.99	4.04	0.74	0.84	6.45	1.60
0.19	1	0.21	6.88	30.3	27.3	0.57	3.57	5.09	0.70	0.90	5.66	1.11
	2	0.30	7.32	29.9	27.1	0.37	4.26	6.75	0.63	0.91	8.04	1.19
	3	0.44	21.5	17.1	14.8	0.39	3.03	4.74	0.64	0.86	6.44	1.36
	4	0.54	30.0	9.54	8.36	0.23	1.81	2.95	0.62	0.88	4.52	1.54

*1 Effect of NaOH dosing incorporated into calculation
*2 Including scrubbed biofilm and suspended cells
*3 Based on x_t

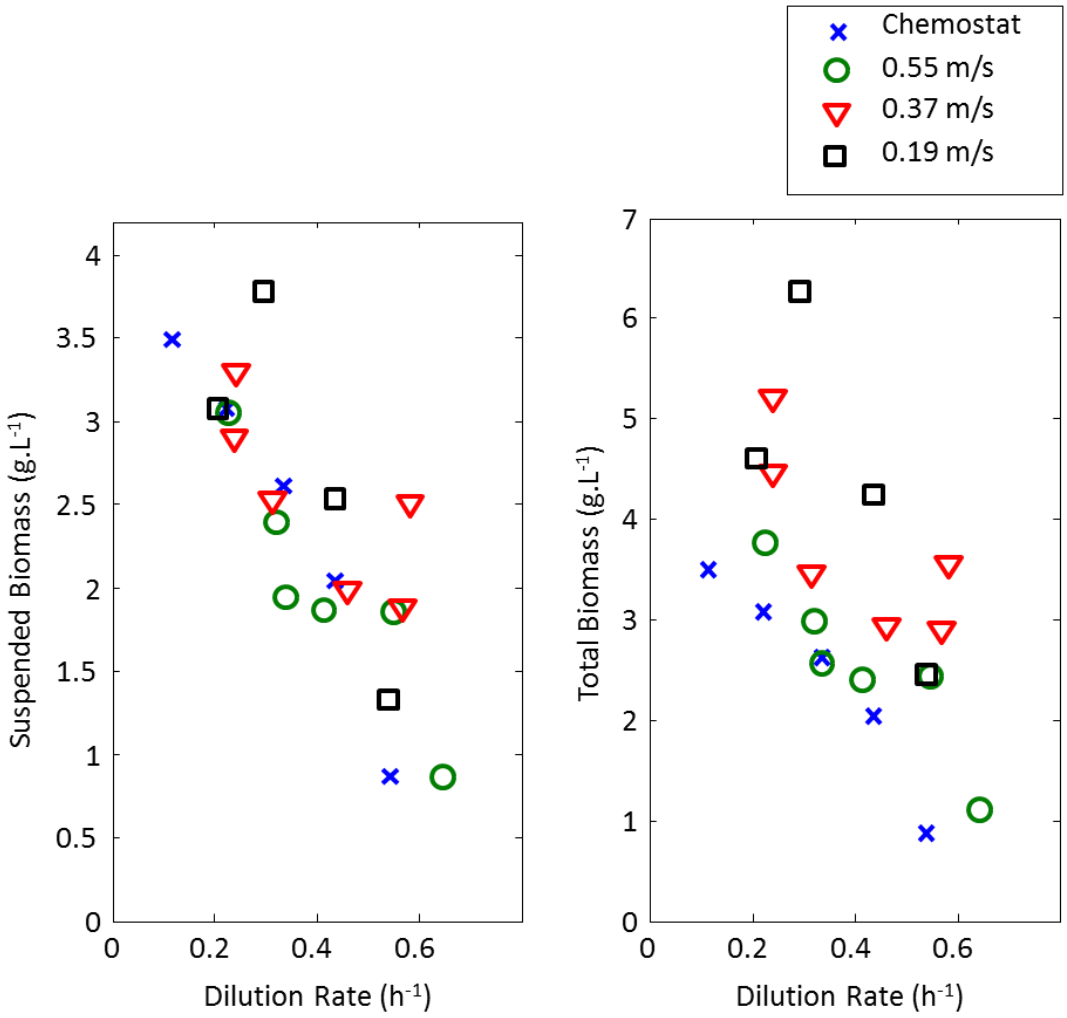

Figure 5-1: Suspended (C_x) and total (C_{xt}) biomass concentrations measured during the chemostat and biofilm fermentation runs as a function of dilution rate (D). The biofilm C_{xt} results do not exhibit a clear and repeatability during the biofilm runs, for a given D and u_{avg}, was not achieved.

The constant $Y_{xt,x}$ at a given shear condition was attributed to a constant balance between the biofilm growth and detachment. The balance is clearly related to the u_{avg}, where higher shear increase the rate of detachment (Van Loosdrecht et al., 1995; van Loosdrecht, Picioreanu & Heijnen, 1997; van Loosdrecht et al., 2002). Given the rapid detachment rate of biofilm and the relatively low ratio of suspended to total biomass (between 0.61 and 0.79 $g.g^{-1}$), it was assumed that the composition of the suspended and immobilised biomass for each respective shear condition was identical and remained constant irrespective of D.

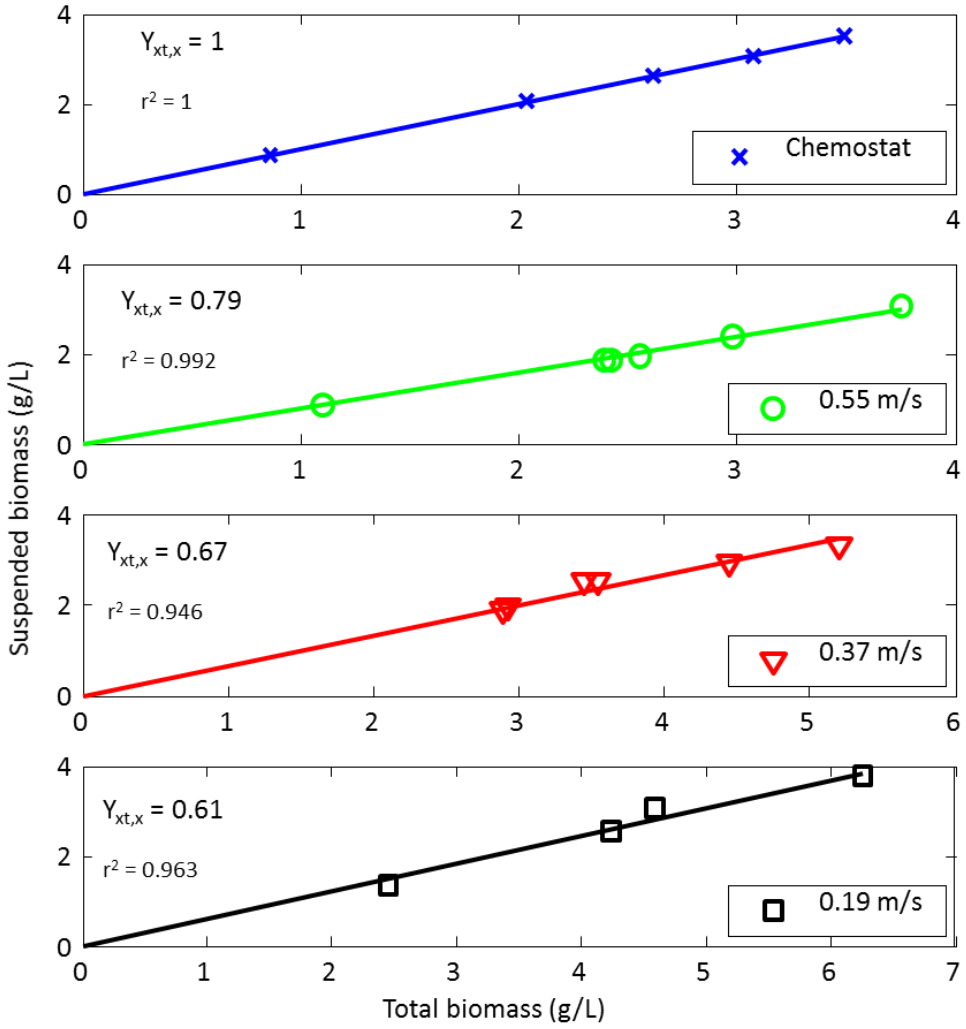

Figure 5-2: Suspended biomass (C_x) vs. total biomass (C_{xt}) to determine $Y_{xt,x}$. The constant $Y_{xt,x}$ values found in this study was attributed to the balance between biofilm growth and detachment; the balance appeared to be positively related to u_{avg}. The lowest $Y_{xt,x}$ corresponded to the lowest u_{avg} and increased as u_{avg} increased.

5.2.2 Yield and rate analysis

The observed product and biomass yields are given in *FIGURE 5-3*, *FIGURE 5-4* and *FIGURE 5-5*. Glc consumption was used as the basis for all yield determinations and plotted on the horizontal axes of *FIGURE 5-3* to *FIGURE 5-5*. The linear fits on these graphs give the observed yield coefficients with the regression analysis indicated on the graphs. The independent variable D is not directly observable in these figures but can be inferred from the fact that high D will result in low Glc consumption.

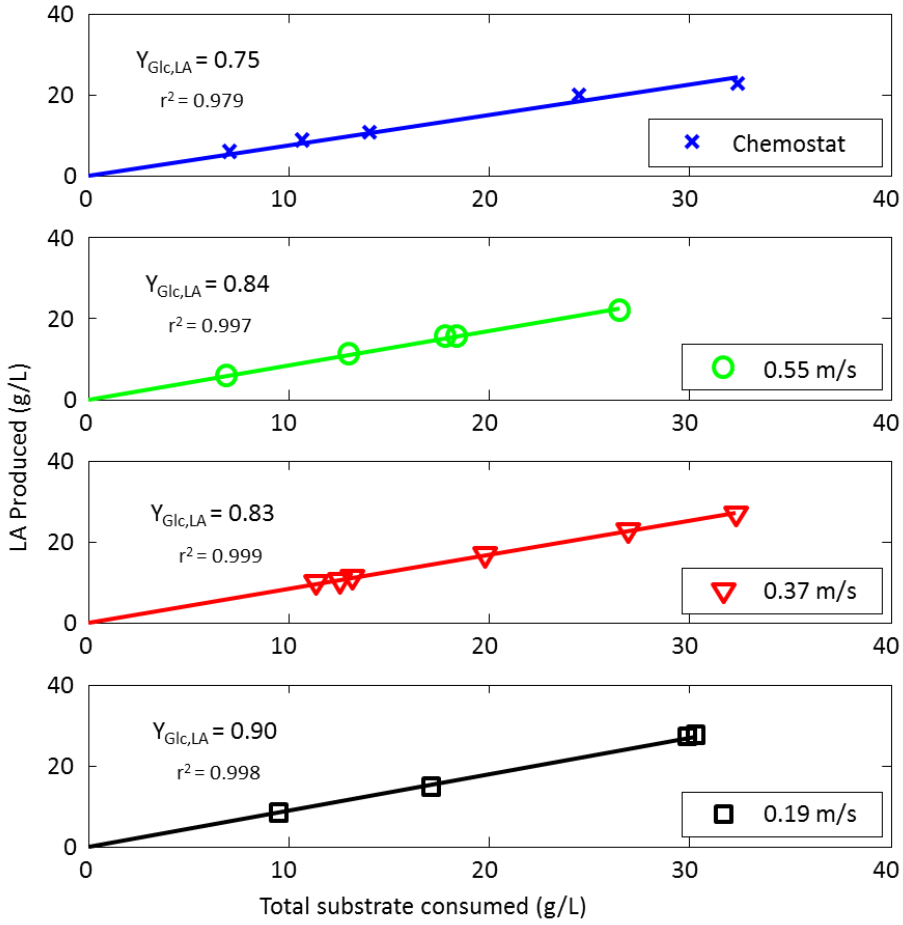

Figure 5-3: LA concentration (C_{LA}) vs. Glc consumption (ΔGlc) to determine $Y_{Glc,LA}$ for the four individual shear velocities. The individual data points were for the respective dilution rates (D), with the lowest D corresponding to the highest ΔGlc. The figure indicates an increase in $Y_{Glc,LA}$ with decreasing u_{avg}.

A significant change in the LA and Acn yields ($Y_{Glc,LA}$ and $Y_{Glc,Acn}$) is observed with a change in shear (*FIGURE 5-3* and *FIGURE 5-4*), while the biomass yield based on the suspended biomass exiting the fermenter ($Y_{Glc,x}$) remains more or less constant with shear variation (*FIGURE 5-5*). The Acn yield quadrupled from the lowest-shear biofilm run ($Y_{Glc,Acn}$ = 0.017 g.g^{-1}) to the chemostat run ($Y_{Glc,Acn}$ = 0.074 g.g^{-1}), with a corresponding increase in the LA yield of 20% from the chemostat run ($Y_{Glc,LA}$ = 0.75 g.g^{-1}) to the highest value obtained in the lowest-shear biofilm run ($Y_{Glc,LA}$ = 0.9 g.g^{-1}).

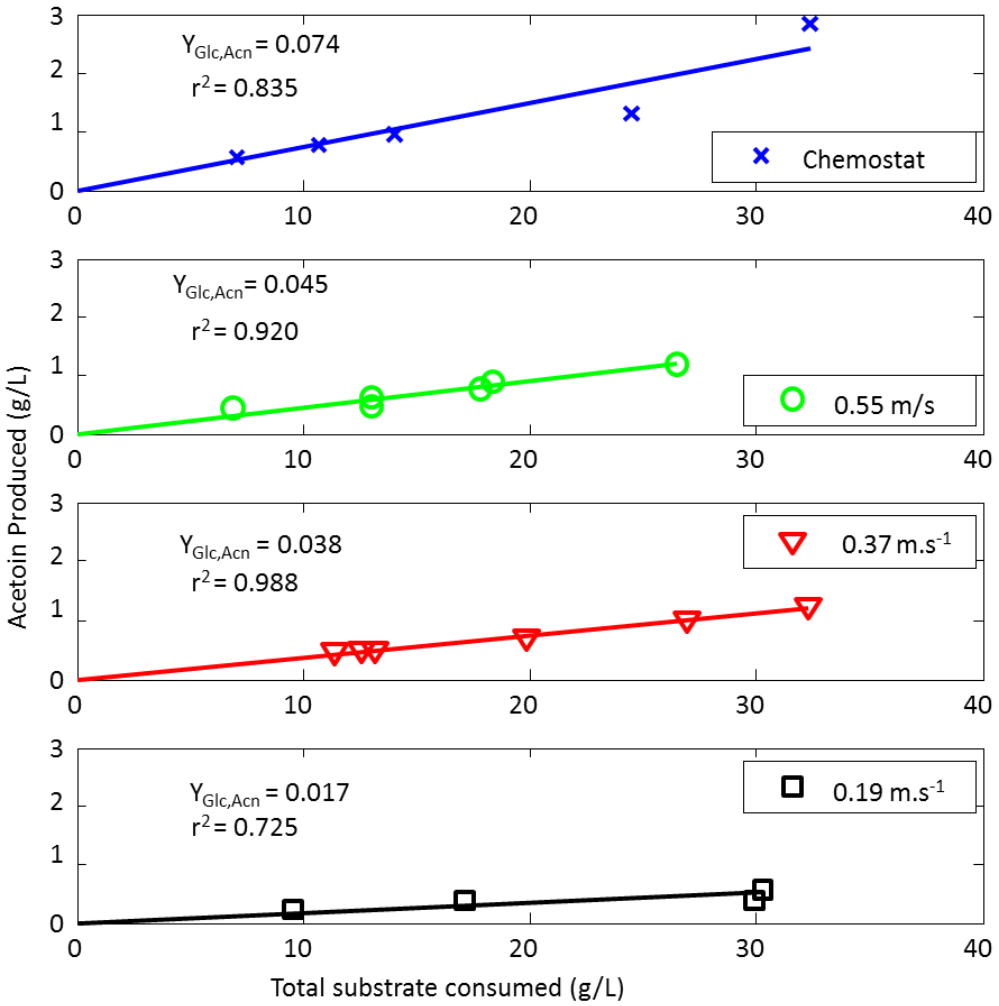

Figure 5-4: Acn concentration (C_{Acn}) vs. Glc consumption (ΔGlc) to determine $Y_{Glc,Acn}$ for the four individual shear velocities. The individual data points were for the respective dilution rates (D), with the lowest D corresponding to the highest ΔGlc. The $Y_{Glc,Acn}$ exhibited a positive relationship with the u_{avg}, an increase in $Y_{Glc,Acn}$ was observed with increasing u_{avg}.

From *FIGURE 5-3* and *FIGURE 5-4*, it is clear from the coefficient of determination (r^2) that the yields of the metabolic products remained remarkably constant for each respective u_{avg}. Since both growth and maintenance (Luedeking & Piret, 1959; Villadsen, Nielsen & Lidén, 2011) are expected to contribute to metabolite production, the measured or observed yield can be described by the following equation:

$$Y_{Glc,P}^{obs} = \frac{r_P}{r_{Glc}} = \frac{Y_{x,P}^{true}\mu + m_P}{Y_{x,Glc}^{true}\mu + m_{Glc}} \approx \frac{Y_{x,P}^{true}}{Y_{x,Glc}^{true}} \qquad (5\text{-}1)$$

For LA production the maintenance constants m_{Pi} and m_{Glc} are identical since no loss of mass occurs in the formation of LA. The growth rate (μ) will vary according to different amounts of

LA in the broth causing varying degrees of inhibition. Since the observed yield ($Y_{Glc,P}^{obs}$) remains constant while the LA titre (and μ) is changing, it is evident that m_P (and m_{Glc}) is negligibly small in order for μ to cancel out of the equation. Accordingly, maintenance or non-growth effects can be ignored within the dilution rate range of the study.

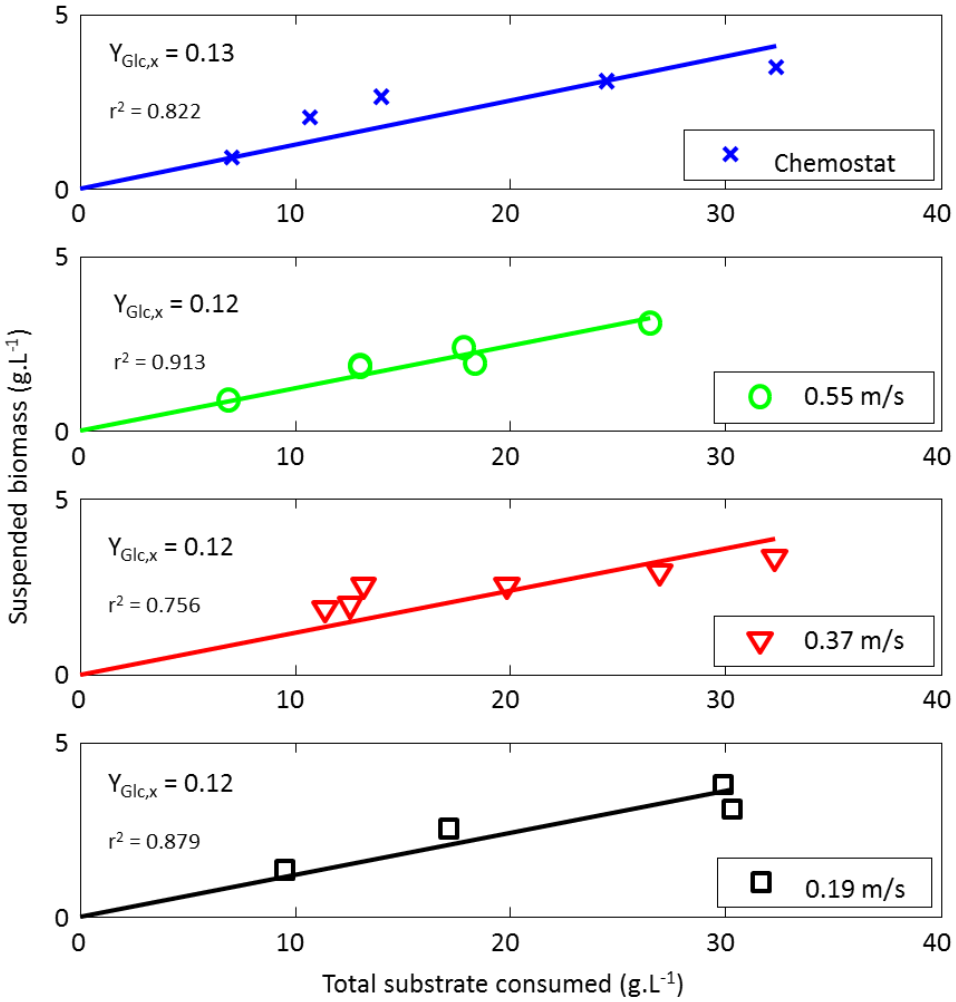

Figure 5-5: Suspended biomass (C_x) vs. Glc consumption (ΔGlc) to determine $Y_{Glc,x}$ for the four individual shear velocities. The individual data points were for the respective dilution rates (D), with the lowest D corresponding to the highest ΔGlc. The $Y_{Glc,x}$ appear unaffected by the u_{avg}, the $Y_{Glc,x}$ remained constant with changes in u_{avg}.

FIGURE 5-6 shows the biomass-based rates of Glc consumption (r_{Glc}) and LA production (r_{LA}). Note that the C_{xt} was used for the calculation of the specific rates. At high D a distinct decrease in biomass productivity is observed at lower u_{avg}. At high D, where the biomass productivity differences are observed, LA titres are low and product inhibition is at a minimum.

The cellular part of the biomass (x_t*) at these conditions is expected to have similar metabolite production characteristics, irrespective of the shear on the biofilm (*BIOFILM CHARACTERISTICS*

section). Accordingly, the decrease in biomass productivity can only be attributed to metabolically inactive biomass, such as EPS. The rate results therefore suggest that the EPS fraction of the biomass increases with a decrease in shear.

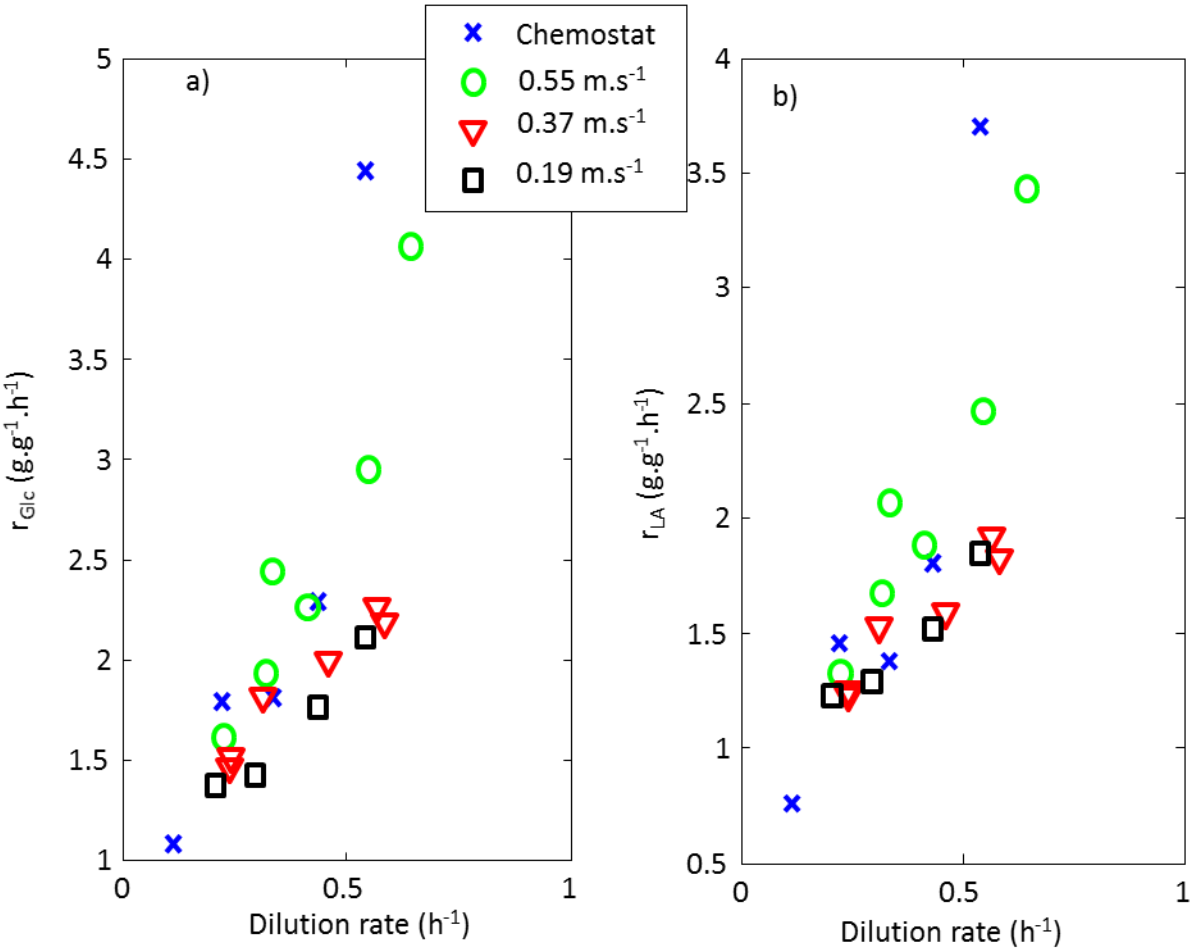

Figure 5-6: a) Specific Glc consumption rate (r_{Glc}); b) Specific LA production rate (r_{LA}) against dilution rate. The differences in production rates between the u_{avg} conditions can only be attributed to differences in the biofilm composition, i.e. EPS content.

5.2.3 NADH balance for elucidating flux variation

Insight into the major differences in metabolite yields as a function of the shear might be gained from the redox difference between lactic acid and acetoin. The overall metabolic pathway from glucose to acetoin is associated with the generation of NADH and it is well accepted that acetoin production is linked to the regulation of NAD^+/NADH in a microbial system (Xiao & Xu, 2007). In comparison with acetoin production from glucose, lactic acid production is redox neutral. Since the net NADH production in the cell should be zero, it is clear that NADH consumption is related to the shear condition in the fermenter where less NADH is consumed

at low shear conditions. NADH consumption can only proceed via the anabolism or via the direct oxidation of NADH since all the catabolites are quantified. The direct oxidation option is unlikely since the system was proven to be completely anaerobic (Section 3.4.4 on page 3-8). It is well established that biomass growth on inorganic nitrogen is associated with the formation of NADH, while growth on complex and undefined organic nitrogen is considered to be redox neutral (Villadsen, Nielsen & Lidén, 2011). For purposes of analysis it was decided to associate the apparent NADH consumption with the formation of cellular biomass.

From this assumption it follows that biomass formation under lower u_{avg} would necessarily consume less redox (NADH). This is because the $Y_{Glc,Acn}$ drastically decreased at lower shear conditions, while the $Y_{Glc,x}$ remained unchanged. The rate data in FIGURE 5-6 support this observation, namely that one can attribute the rate decrease to a change in the biomass composition where more inactive EPS are present at lower shear conditions, thus lowering the productivity of the x_t. This observation can be used to explain the redox consumption changes – it is proposed that EPS formation is different from cellular biomass formation in terms of NADH consumption/production. *L. rhamnosus* is known to produce EPS with the following repeating unit: {3Rha-3Glc-3[Gal4,6(R)Py-2]Rha-3Rha-3Rha-2Glc-}$_n$ (Van Calsteren et al., 2002). This can be used to calculate the overall NADH consumption/production when forming EPS from Glc. The underlying assumption is that the EPS fraction in the biomass is independent of dilution rate due to the fact that the substrate is always present in excess. Variations in EPS content have been reported at substrate inhibition conditions (Looijesteijn et al., 2000).

The complete metabolism can be represented by two catabolic reactions (lactic acid and acetoin) and two anabolic reactions (x_t* and EPS). The carbon flux of these reactions was converted to a carbon mole basis (C-mol.L^{-1}) and the degree of reduction (DOR) of the components was determined by using H_2O, CO_2 and NH_3 as the defined neutral compounds. The metabolism can be written as equations (5-2) to (5-5) indicating four separate fluxes (v_1 – v_4). The cellular biomass (x_t*) flux (v_3) is separated from the EPS flux (v_4).

$$v_1: CH_2O\ (Glc) \rightarrow CH_2O\ (LA) \tag{5-2}$$

$$v_2: CH_2O\ (Glc) \rightarrow \frac{2}{3}CH_2O_{0.5}\ (Acn) + \frac{1}{3}CO_2 + \frac{1}{3}NADH \tag{5-3}$$

$$v_3: CH_2O\ (Glc) + 0.59YE \rightarrow 1.59x_t^* + Y_3NADH \tag{5-4}$$

$$v_4: CH_2O\ (Glc) \rightarrow EPS + Y_4NADH \tag{5-5}$$

The chemostat run was used as the baseline scenario with the assumption that zero EPS formed during this run ($v_4 = 0$, $x_t^* = x$). Given the measured values of lactic acid and acetoin produced, and glucose consumed, the sum of the fluxes v_1 and v_2 were determined to be 0.9 (C-mol Glc)/(total C-mol Glc consumed). Y_3 was determined to be −0.42, using the known fluxes and an NADH balance. CO_2 formation during biomass synthesis was not considered ($\alpha = 0$). Note that the Glc flux in v_3, expressed as a fraction of the total glucose consumed, was calculated by using only the C_{LA}, C_{Acn} and C_{Glc} measurements. The x_t^* and YE yield coefficients were determined from the $Y_{Glc,x}$, assuming a biomass composition of $CH_{1.8}O_{0.5}N_{0.2}$ (Villadsen, Nielsen & Lidén, 2011: 74).

When considering the biofilm runs, the combined ($v_3 + v_4$) flux was shown to vary between 0.06 and 0.09 (C-mol Glc)/(total C-mol Glc consumed). This value is slightly lower than expected and is most likely due to small inaccuracies in the Acn and LA yield fits. The yield coefficient (Y_3) of equation *(5-4)* was determined for the chemostat run and directly applied in the biofilm runs. Using the known EPS composition ($CH_{1.6}O_{0.89}$) from the repeating unit given above, a redox balance was used to calculate Y_4 (0.09 moles NADH ***formed*** per C-mol EPS).

Therefore the overall NADH balance dictated the increased yield of EPS (v_4) production and the decreased yield of cellular biomass production (v_3) with the decrease in Acn production (v_2). Using the proposed anabolic stoichiometry, the EPS fraction of the biomass was estimated using equation *(5-6)* from the values for v_3 and v_4 from *TABLE 5-2*. The results are reported in *TABLE 5-2*.

$$EPS\ fraction = \frac{v_4}{v_4 + 1.59v_3} \tag{5-6}$$

Table 5-2: Biomass flux distribution (v_3 and v_4) and the EPS fractions calculated for the respective shear velocities. The table clearly shows an increase in the EPS fraction with a decrease in the u_{avg}.

Shear velocity (m.s^{-1})	v_3 (C-mol.C-mol^{-1})	v_4 (C-mol.C-mol^{-1})	EPS fraction
3.65 (chemostat)	0.10	0.00	0.00
0.55	0.06	0.01	0.09
0.37	0.04	0.05	0.43
0.19	0.01	0.05	0.70

5.3 Conclusions

This study clearly illustrated that shear can affect the metabolite yields of *L. rhamnosus* biofilms. Increasing shear resulted in decreased acetoin formation and increased lactic acid formation, while the biomass yields remained constant. Rate data indicated a lower specific biomass productivity with a decrease in shear, suggesting a composition change in biomass where more inactive EPS forms part of the biomass at low shear velocities.

Redox analysis of the catabolic reactions revealed that the anabolic reactions are associated with the net consumption of NADH, despite the fact that EPS production was calculated to be an NADH producer. The decrease in acetoin formation with decreasing shear clearly indicated that the extent of anabolic NADH consumption was related to shear. The relationship was explained by varying the EPS content of the biomass as a function of shear velocity, which coincides with the rate findings. A simplified model was presented to estimate the distribution of EPS and cellular biomass as the shear varied. In order to determine whether the change in biofilm composition as a function of shear, determined using the simplified model, was applicable to the biofilm produced by a different microbial species, a method was required that could separate the EPS from the cellular biomass. The work in Chapter 6 attempted to address this by developing a method to separate EPS from the cellular biomass and in this way compare the EPS composition for different shear conditions.

This study postulated that it was possible to alter the yields during biofilm fermentations by manipulating the shear conditions in the reactor and subsequently changing the biofilm composition and metabolic fluxes. Chapter 6 attempts to scrutinise this postulate and its general applicability by analysing the influence of the shear on the metabolic flux of glucose in a biofilm system containing the microbe *Actinobacillus succinogenes*. Assuming the applicability of the mechanism proposed in this study, i.e. that the metabolism was regulated through requirements during biofilm formation, this mechanism would clearly present itself in the results reported in Chapter 6.

CHAPTER 6
THREE-PHASE REACTOR: CASE STUDY

6.1 Introduction

This chapter is partly based on work published in the journal *Microbial Cell Factories* (Brink & Nicol, 2014b), as well as additional unpublished work. It addresses the effect of gas–liquid shear on biofilm steady-state rate and yield characteristics. As in the previous chapter, the expectation is that shear will affect the distribution of cells and EPS in the biofilm matrix (Beyenal & Lewandowski, 2002). However, in this chapter a method was developed to remove the EPS from the biofilm cells (Section *4.5.9* on page *4-17*) and thereby quantify the cellular production characteristics. The system consisted of the proteobacterium *Actinobacillus succinogenes* and gas-phase CO_2 for the production of succinic acid (SA). *A. succinogenes* is an attractive production strain for the production of SA as it is able to metabolise most naturally occurring sugars (McKinlay et al., 2010) and to produce SA close to the saturation point of SA (> 95 $g.L^{-1}$) (Yan, Zheng, Tao, et al., 2014). In addition, volumetric productivities in excess of 10 $g.L^{-1}.h^{-1}$ have been reported (Maharaj, Bradfield & Nicol, 2014). *A. succinogenes* is well known to self-adhere to support surfaces during extended operation. All continuous fermentation studies on *A. succinogenes* resulted in unavoidable biofilm formation (Urbance et al., 2004; Kim et al., 2009; Van Heerden & Nicol, 2013; Bradfield & Nicol, 2014; Maharaj, Bradfield & Nicol, 2014; Yan, Zheng, Tao, et al., 2014). This experimental study included continuous chemostat runs, biofilm runs and batch biofilm runs. The reason for the batch biofilm runs was to assess the influence that the SA inhibition had on the transient behaviour of the biofilm immobilised organism.

The experiments were performed in the novel, gas–liquid shear-control fermenter as described in detail in Section *4.3* on page *4-4*. The experimental procedures and methods are

discussed in Section 4.5, the chemostat and continuous biofilm operational conditions are summarised in TABLE 4-3, and the continuous biofilm growth conditions prior to the individual batch runs are summarised in TABLE 4-4.

6.2 Chemostat analysis

Chemostat experiments were performed by running the three-phase *homoshear* bioreactor (Chapter 4) at a superficial velocity of 1.83 $m.s^{-2}$ (τ_W = 10.5 Pa, TABLE 4-3) until the NaOH dosing profile remained within a 5% fluctuation (Section 4.3 on page 4-4). Consecutive samples were taken, one volume turnover (1/D) apart to ensure steady operation. The absence of biofilm in the reactor was visually confirmed.

All steady-state chemostat data are given in TABLE 6-1. Dilution rates (D) varied between 0.1 and 0.8 h^{-1}. The Glc consumed (ΔGlc), SA titre and biomass (x) in the outlet are plotted as a function of D in FIGURE 6-1. Repeat runs were performed at six of the seven conditions and the standard errors are indicated in TABLE 6-1, as well as in FIGURE 6-1 and FIGURE 6-2. Mass balance checks at steady-state conditions indicated that the residual Glc and metabolites in the fermenter outlet accounted for more mass than that determined from the ΔGlc. The average overestimation of 127% indicates that a significant fraction of constituents from yeast extract (YE) and/or corn steep liquor (CSL) were incorporated into the formed biomass. The decline in the ΔGlc with an increase in D in FIGURE 6-1 suggests that washout will occur between a D of 0.8 h^{-1} and 0.85 h^{-1}, suggesting a maximum specific growth rate (μ_{max}) within this range.

Table 6-1: The experimentally measured chemostat results indicating the means and standard errors of the observations.

Run No.	1	2	3	4	5	6	7
D (h^{-1})	0.10	0.19	0.29	0.35	0.49	0.71	0.80
Glc out ($g.L^{-1}$)	27.56±0.9	30.9±0.1	31.1±0.4	33.1±0.39	34.4	34.7±0.1	38.3±0.1
ΔGlc ($g.L^{-1}$) *1	13.13±1.37	10.7±0.7	10.7±0.4	9.36±0.39	8.53	4.34±0.10	1.49±0.08
C_{SA} ($g.L^{-1}$)	6.43±0.48	5.31±0.09	5.37±0.06	4.25±0.15	3.76	1.99±0.02	0.69±0.01
C_{AA} ($g.L^{-1}$)	4.47±0.28	3.87±0.49	3.59±0.17	2.99±0.29	3.10	1.66±0.03	0.74±0.00
C_{FA} ($g.L^{-1}$)	0.03±0.01	0.82±0.28	1.88±0.05	1.86±0.10	1.54	1.19±0.01	0.33±0.01
C_x ($g.L^{-1}$)	2.22±0.09	2.20±0.24	2.65±0.23	2.35±0.30	1.74	1.58±0.02	0.71±0.04
SA/AA ($g.g^{-1}$)	1.44±0.06	1.37±0.19	1.50±0.05	1.42±0.09	1.22	1.20±0.02	0.93±0.00
FA/AA ($g.g^{-1)}$	0.01±0	0.21±0.05	0.52±0.04	0.62±0.03	0.50	0.72±0.01	0.45±0.02
$Y_{Glc,SA}$ ($g.g^{-1}$)	0.5±0.03	0.49±0.03	0.50±0.01	0.45±0	0.44	0.46±0.01	0.46±0.02
q_{SA} ($g.L^{-1}h^{-1}$)	0.62±0.04	0.99±0.01	1.54±0.02	1.50±0.05	1.83	1.41±0.01	0.55±0.01
r_{SA} ($g.g^{-1}h^{-1}$)	0.28±0.01	0.45±0.06	0.58±0.05	0.64±0.06	1.05	0.89±0.02	0.77±0.04
Mass Balance (%)	114±7	117±3	118±1	113±5	113	137±2	168±4
Measurements	6	3	2	2	1	3	2

*1 Effect of NaOH dosing incorporated into calculation

The chemostat product distribution can be seen in *FIGURE 6-2* on which $Y_{Glc,SA}$ and the by-product ratios are plotted. Overall, the $Y_{Glc,SA}$ values are fairly constant around the average value of 0.48 g SA.(g ΔGlc)$^{-1}$. The SA to AA ratio (SA/AA) was in the vicinity of 1.4 $g.g^{-1}$ for D values below 0.5 h^{-1}, while a slight decrease in the value is observed at higher D values. The formation of FA decreased at lower values of D where a negligible amount of FA was observed at

D = 0.1 h^{-1}. The maximum value of the FA to AA ratio (FA/AA) of 0.72 ± 0.02 $g.g^{-1}$ obtained at a high D is close to the equimolar value of 0.77 $g.g^{-1}$. This implies that the pyruvate formate lyase (*pfl*) route for the oxidation of pyruvate is dominant at high D. The decrease in the FA/AA with a reduction in D is linked to either pyruvate dehydrogenase or formate dehydrogenase, contributing to the formation of less FA. The FA/AA decrease corresponds to the observations of Bradfield & Nicol (2014) where low D in a biofilm reactor resulted in a similar trend. The decrease in FA is probably attributable to formate dehydrogenase converting FA to CO_2 and NADH since Zheng *et al.* (2013), Xi *et al.* (2012) and Du *et al.* (2008) observed an FA decrease against time after initial formation in a batch fermenter.

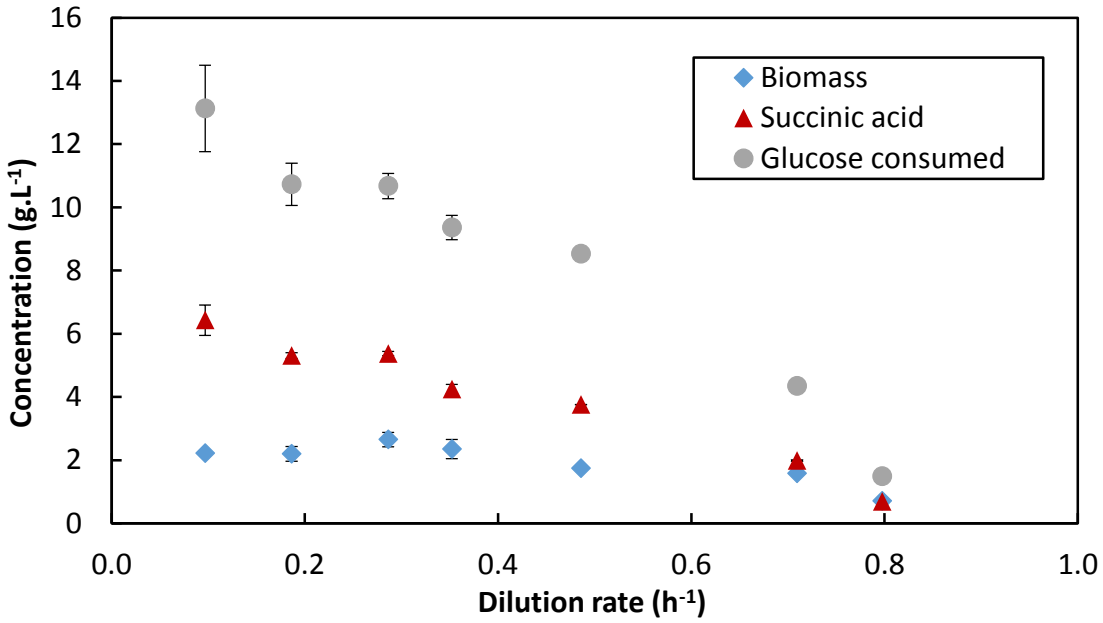

Figure 6-1: Chemostat measurements of biomass, SA concentrations and ΔGlc. The figure shows that the concentrations of the measured variables decreased significantly with increasing D; washout was expected at a D between 0.80 and 0.85 h^{-1}.

The SA/AA observed in *FIGURE 6-2* is lower than the expected values when redox closure of the catabolic pathways is considered, while ignoring the anabolic pathways responsible for biomass synthesis. The analysis by Bradfield and Nicol (2014) suggests that the SA/AA should vary between 1.97 $g.g^{-1}$ (for FA/AA = 0.77 $g.g^{-1}$) and 3.93 $g.g^{-1}$ (for FA/AA = 0 $g.g^{-1}$). The slight increase in the SA/AA ratio at lower D is probably linked to the decrease in the FA/AA, although the values are far below those expected.

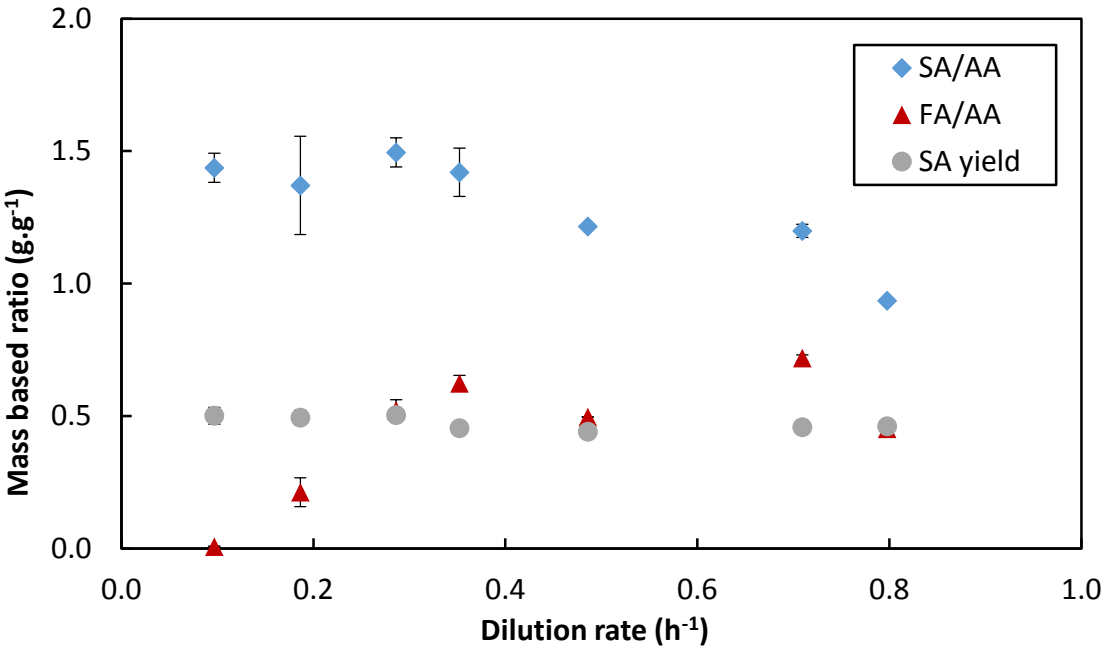

Figure 6-2: Ratios of products as well as SA to glucose measured during chemostat operation. The SA yield appeared to remain approximately constant at 0.48 g.g^{-1}, while the SA/AA decreased with a corresponding increase in FA/AA.

The chemostat metabolism (on a carbon mole basis) can be expressed as equations *(6-1)* to *(6-4)* (see *FIGURE 2-4* in section *2.3.1* on page *2-32*)

$$v_1: CH_2O\ (Glc) + \frac{1}{3}CO_2 + \frac{1}{3}NADH \rightarrow \frac{4}{3}CH_{\frac{3}{2}}O(SA) + \frac{5}{9}ATP \quad (6\text{-}1)$$

$$v_2: CH_2O\ (Glc) \rightarrow \frac{2}{3}CH_2O\ (AA) + \frac{1}{3}CO_2 + \frac{2}{3}NADH + \frac{2}{3}ATP \quad (6\text{-}2)$$

$$v_3: CH_2O\ (Glc) \rightarrow \frac{2}{3}CH_2O\ (AA) + \frac{1}{3}CH_2O_2(FA) + \frac{1}{3}NADH + \frac{2}{3}ATP \quad (6\text{-}3)$$

$$v_4: Y_{x,Glc}CH_2O\ (Glc) + Y^{obs}_{x,NS}NS + Y^{obs}_{x,ATP}ATP \rightarrow x + Y^{obs}_{x,NADH}NADH \quad (6\text{-}4)$$

This metabolism consists of a catabolic section (equations *(6-1)* to *(6-3)*) and an anabolic section (equation *(6-4)*). The catabolic section describes the formation of SA, AA, FA and CO_2 during fermentation, while the anabolic section shows the anabolic formation of biomass (x) from glucose and a complex nitrogen source (NS), which in this case is a mixture of YE and CSL.

From the average results shown in TABLE 6-1, the catabolic glucose fluxes ($v_1 - v_3$) were determined and are shown in TABLE 6-2. The final column in TABLE 6-2 shows the catabolically produced NADH relative to the catabolically consumed NADH ($NADH_{produced}/NADH_{consumed}$) during the catabolism (equations (6-1) to (6-3)), which was calculated using equation (6-5).

$$\frac{NADH_{produced}}{NADH_{consumed}} = \frac{\frac{2}{3}v_2 + \frac{1}{3}v_3}{\frac{1}{3}v_1} \tag{6-5}$$

Table 6-2: The catabolic flux of glucose to SA (v_1) and AA via the *pdh/fdh* (v_2) and *pfl* (v_3) routes

Run no.	D (h^{-1})	v_1 (C-mol/C-mol)	v_2 (C-mol/C-mol)	v_3 (C-mol/C-mol)	$NADH_{produced}/NADH_{consumed}$
1	0.10	0.37	0.51	0	2.72
2	0.19	0.38	0.39	0.15	2.47
3	0.29	0.38	0.16	0.34	1.74
4	0.35	0.35	0.09	0.39	1.64
5	0.49	0.34	0.19	0.35	2.19
6	0.71	0.35	0.04	0.54	1.74
7	0.80	0.35	0.3	0.44	2.97

From the values of $NADH_{produced}/NADH_{consumed}$, it is clear that the catabolically produced NADH exceeds the catabolically consumed NADH by a factor of 1.64–2.97. From this observation it can be concluded that the sign of $Y_{x,NADH}$ would be negative, which suggests that significant amounts of NADH are consumed in the anabolism since direct oxidation of NADH under anaerobic conditions is unlikely. The system was assumed to be completely anaerobic due to the addition of $Na_2S{\cdot}9H_2O$ to the feed medium (Lovley & Lonergan, 1990; Bradfield & Nicol, 2014), as well as the formation of formate during fermentation; the activity of the pyruvate formate lyase (*pfl*) enzyme is deactivated by the presence of even small amounts of oxygen in the system (Schindler, Joshi & Vieille, 2014).

TABLE 6-3 shows the anabolic flux parameters (equation (6-4)), as determined from the glucose flux values shown in TABLE 6-2, and assuming a standard biomass formula of $CH_{1.8}O_{0.5}N_{0.2}$ (Villadsen, Nielsen & Lidén, 2011: 74). The parameters were calculated using equations (6-6) to (6-9).

$$v_4 = Y_{Glc,x}^{obs} = \frac{C_x}{\Delta Glc} \quad (6\text{-}6)$$

$$Y_{x,NS} = 1 - \frac{1 - (v_1 + v_2 + v_3)}{v_4} \quad (6\text{-}7)$$

$$Y_{x,NADH} = \frac{NADH_{produced} - NADH_{consumed}}{v_4} = \frac{\frac{2}{3}v_2 + \frac{1}{3}v_3 - \frac{1}{3}v_1}{v_4} \quad (6\text{-}8)$$

$$Y_{x,ATP}^{obs} = \frac{ATP\ produced}{v_4} = \frac{\frac{5}{9}v_1 + \frac{2}{3}v_2 + \frac{2}{3}v_3}{v_4} \quad (6\text{-}9)$$

TABLE 6-3 shows that as the total flux (v_4) of biomass increases with increasing D, the fraction of that flux from NS increases, with a corresponding decrease in $Y_{x,Glc}$ ($Y_{x,NS}$ + $Y_{x,Glc}$ = 1). This observation indicates that as D increases, a larger fraction of glucose is consumed catabolically, with a corresponding increase in reliance on NS as building blocks for biomass. TABLE 6-3 indicates that the $Y_{x,NADH}$ was consumed throughout. However, the absolute values decreased continuously with increased D. The final column in TABLE 6-3 reports the ATP consumption per C-mol biomass produced and indicates a decreasing requirement for ATP per C-mol biomass, with increasing D.

Table 6-3: The anabolic flux parameters (equation (6-4)) as calculated from glucose fluxes (TABLE 6-2), using equations (6-6) to (6-9).

Run no.	D (h^{-1})	v_4 (C-mol/C-mol)	$Y_{x,NS}$ (C-mol/C-mol)	$Y_{x,NADH}$ (mol/C-mol)	$Y_{x,ATP}^{obs}$ (mmol/C-mol)
1	0.10	0.21	0.42	- 1.04	2658
2	0.19	0.25	0.64	- 0.74	2282
3	0.29	0.30	0.64	- 0.31	1815
4	0.35	0.31	0.41	- 0.24	1673
5	0.49	0.25	0.52	- 0.54	2210
6	0.71	0.44	0.84	- 0.20	1299
7	0.80	0.58	1.00	- 0.40	1182

The observations in the final two columns (decreasing ATP/NADH requirements with increasing D) could very well be linked to the relationship between biosynthesis and ATP/NAD(P)H requirements, i.e. the synthesis of amino acids, peptides and proteins requires significant

amounts of ATP/NAD(P)H (McKinlay et al., 2007; Villadsen, Nielsen & Lidén, 2011: 40). With an increased reliance on NS for biomass production, a corresponding decrease in ATP/NAD(P)H would be expected (Benthin et al., 1994; Villadsen, Nielsen & Lidén, 2011: 40). Alternatively, the possibility of an alternative oxidising agent being present in the NS cannot be excluded. In contrast to an aerobic system in which the *pfl* is effectively deactivated by oxygen, it was shown that the activity of the *pfl* enzyme, in the presence of alternative oxidation sources such as dimethyl sulphide oxide (DMSO) or yeast extract, was not affected significantly (Carvalho et al., 2014).

The observation of NADH requirement during biomass formation within a system containing yeast extract as an NS has been observed for the growth of *A. succinogenes* (Vlysidis et al., 2011; Carvalho et al., 2014) as well as for *L. rhamnosus* in YE-rich media (Brink & Nicol, 2014a).

FIGURE 6-3 reports the SA volumetric productivity (q_{SA}) and SA specific productivity (r_{SA}), i.e. productivity based on cell mass. The q_{SA} obeys the expected behaviour by reaching a maximum of 1.8 $g.L^{-1}h^{-1}$ at an intermediate D of 0.5 h^{-1}. The specific productivity is expected to fit a straight line where the slope gives the growth-associated yield coefficient of SA on biomass ($Y_{x,SA}^{true}$) (Villadsen, Nielsen & Lidén, 2011: 289). The data fit a straight line reasonably well (r^2 = 0.84) if the value at D = 0.49 h^{-1} is ignored. The straight-line fit is given as:

$$r_{SA} = 0.71D + 0.31 \qquad (6\text{-}10)$$

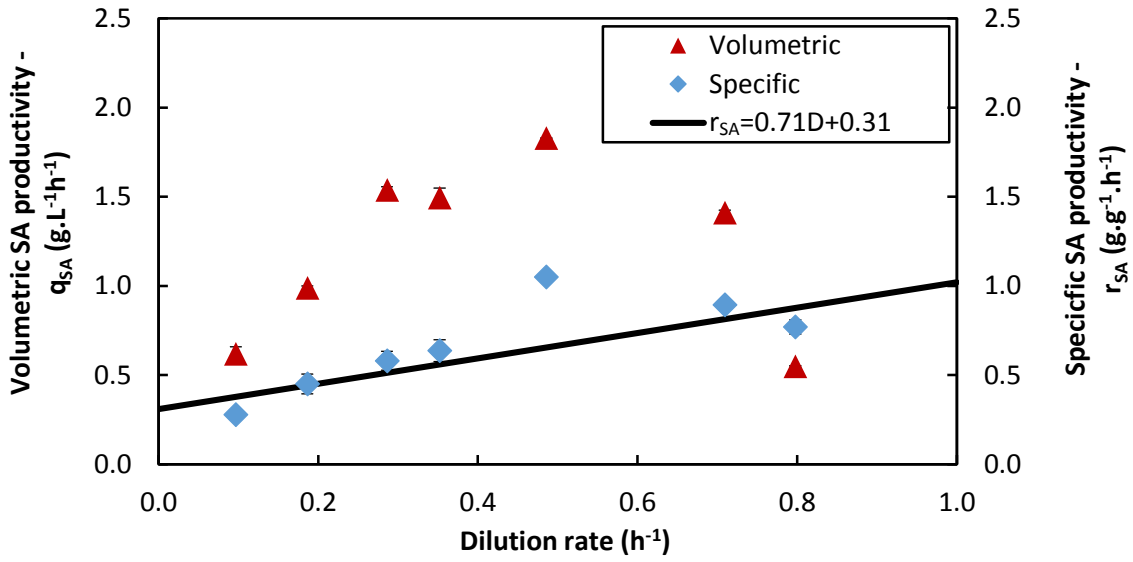

Figure 6-3: Volumetric (q_{SA}) and specific (r_{SA}) production rates of SA in the chemostat system against dilution rates. The q_{SA} results follow the expected trend, with a maximum at a D ≈ 0.5 h^{-1}. The r_{SA} results were used to determine the growth- and non-growth-associated SA production.

The growth-associated ATP consumption ($Y_{x,ATP}^{true}$) can be determined using a method similar to that shown above, by plotting the specific rate of ATP consumption (r_{ATP}) against D. The values for $Y_{x,ATP}^{obs}$ were the same as those in *TABLE 6-3*, converted to units of mmol ATP.(g x)$^{-1}$. This conversion involved the division of the value of $Y_{x,ATP}^{obs}$ in *TABLE 6-3* by the mass per C-mole of biomass, i.e. 24.6 g.C-mol^{-1} (Villadsen, Nielsen & Lidén, 2011: 74). The r_{ATP} is plotted against D in *FIGURE 6-4* and shows that the straight-line regression (equation *(6-11)*, r^2 = 0.98) fitted the experimental data significantly better than that for the r_{SA} (equation *(6-10)*), if the D = 0.49 h^{-1} point is ignored. The experimental point at D = 0.49 h^{-1} is possibly an outlier, because there was only one experimental measurement at this condition (*TABLE 6-1*).

$$r_{ATP} = Y_{x,ATP}^{obs} D = 36.4D + 10.4 \qquad (6\text{-}11)$$

In addition, the theoretical r_{ATP} is plotted against D. This line was derived from work done by McKinlay et al. (2007) in which a total $Y_{x,ATP}$ = 46.9 mmol/g was calculated from metabolic flow towards *A. succinogenes* biomass formation in a batch fermentation using minimal media. The $r_{ATP,theoretical}$ line is very close to the values obtained in this study, considering that the McKinlay et al. (2007) study represents batch flux results in a minimal medium.

Since maintenance or non-growth production of SA is considered to be prominent under conditions where cell growth has ceased (see Section *2.3.2* on page *2-34*), it is important to establish the maintenance contribution concurrent with growth that is prevalent in the chemostat. Estimates of the maintenance production of SA (m_{SA}) and the maintenance consumption of ATP (m_{ATP}) can be obtained from the y-axis intersection of the linear fit on *FIGURE 6-3* and *FIGURE 6-4* respectively (Villadsen, Nielsen & Lidén, 2011: 174, 289). The estimated values of m_{SA} = 0.31 g.g^{-1}.h^{-1} and m_{ATP} = 10.4 mmol.g^{-1}.h^{-1} correspond well with values from the literature: a value of m_{SA} = 0.299 g.g^{-1}.h^{-1} was estimated by Lin at al. (2008) for *A. succinogenes* during batch fermentations and values for m_{ATP} = 2–18 mmol.g^{-1}.h^{-1} have been reported for various bacterial species (Villadsen, Nielsen & Lidén, 2011: 176, 179). The values of these maintenance parameters are significant when compared with the total SA production rate/ ATP consumption rate.

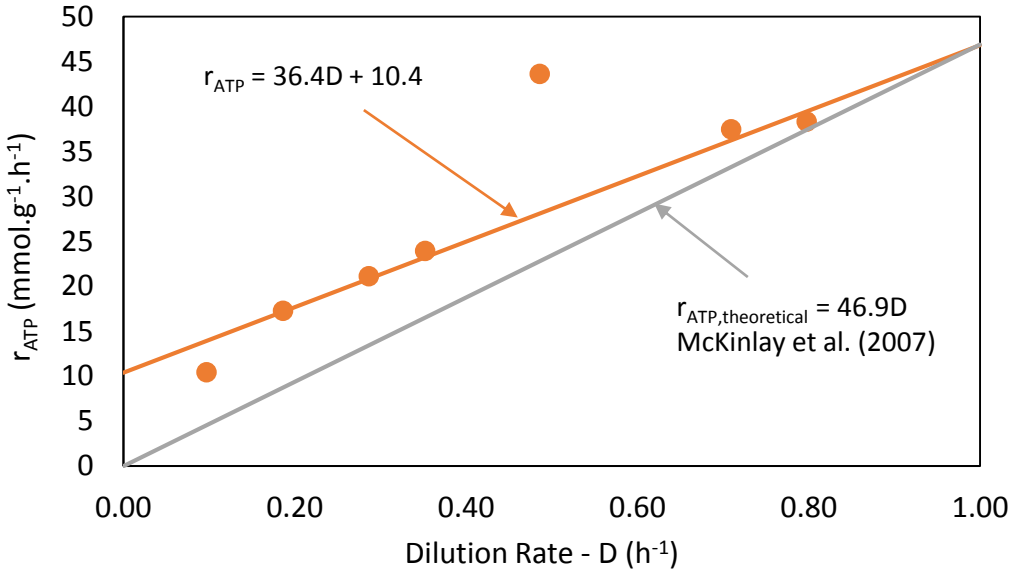

Figure 6-4: The experimentally determined rate of catabolic ATP production during fermentation vs. the dilution rate in the chemostat system. From the linear regression of the data, the ATP requirements for biomass synthesis (slope) and the maintenance (intercept) were detemined. In addition, the theoretical ATP requirements of *A. succinogenes* in a minimal medium (McKinlay et al., 2007) are shown.

In order to quantify the growth inhibition, μ (or D for a chemostat) is plotted against the SA titre in *FIGURE 6-5* and compared with the data cloud given in *FIGURE 2-5*. It should be noted that SA is not the only inhibitor and that the other acids (AA and FA) also contribute to growth inhibition (Corona-Gonzalez et al., 2010). Due to the observation that the by-product relationships exhibit a consistent trend with D, the choice of the inhibition variable is irrelevant. The chemostat data compare remarkably well with batch data from the literature, with the severity of inhibition being clearly evident. Equation *(6-12)* represents a fit (r^2 = 0.98) of the chemostat data using a Gompertz asymmetrical sigmoid function (Gompertz, 1825), which incorporates the μ_{max} of 0.83 h^{-1} and the gradual tailing of the data cloud beyond the highest measured SA titre (C_{SA}) of this study. This μ_{max} value corresponded well to the value of 0.80 to 0.85 h^{-1} established from *FIGURE 6-1*.

$$\mu = 0.83exp(0.093(1 - exp(0.5C_{SA})) \qquad (6\text{-}12)$$

It is evident from *FIGURE 6-5* that growth inhibition is severe since the growth rate is reduced eightfold by merely increasing the SA titre from 0 g.L^{-1} to 7 g.L^{-1}. The asymptotic behaviour of the inhibition function beyond an SA titre of 14 g.L^{-1} is uncertain, but it is evident that growth beyond this point is extremely slow. This supports the notion presented by Maharaj,

Bradfield and Nicol (2014) that high titre production of SA (SA > 15 g.L^{-1}) is predominantly maintenance driven.

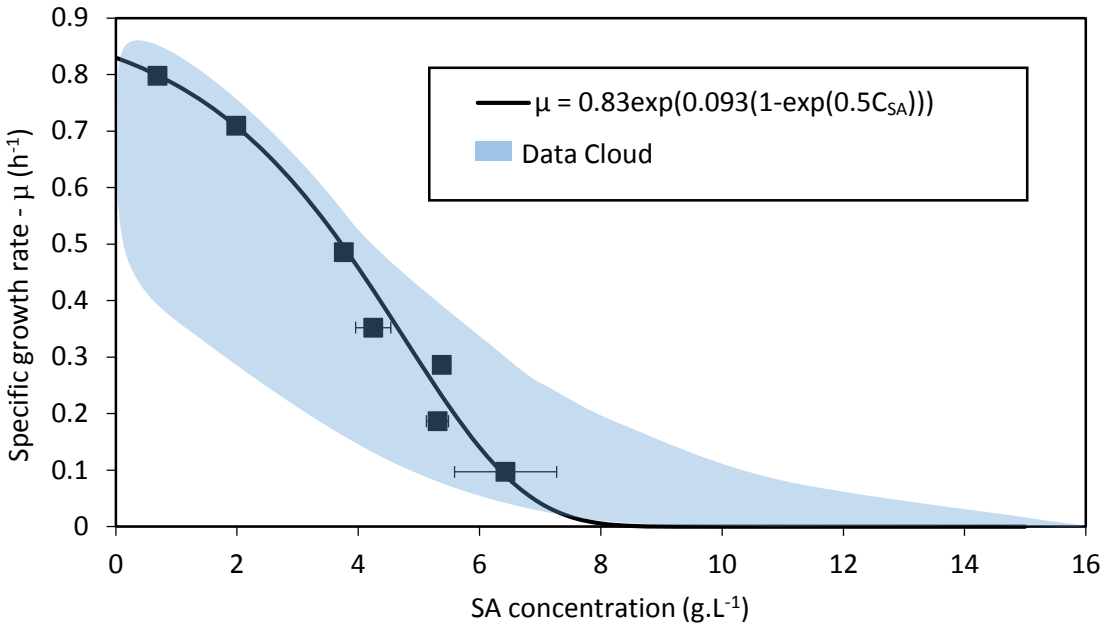

Figure 6-5: The specific growth rate as a function of SA titre to determine the influence of product inhibition on the growth rate in the chemostat system. The results were fitted by equation *(6-12)* and indicate the extreme inhibition experienced by the microbe as a result of the C_{SA}. The blue "data cloud" represents data from from the literature shown in *FIGURE 2-5*.

6.3 Biofilm analysis

6.3.1 Results obtained from continuous runs

The experimental procedures used during the continuous biofilm runs are summarised in *TABLE 4-3* (Section *4.5.1* on page *4-11*). For the biofilm runs, 11 separate steady-states were achieved for each of the shear velocities (0.09 m.s^{-1} and 0.36 m.s^{-1}) and for all of these runs both the total biomass and the cellular biomass (EPS removed) content were quantified. The dilution rates in the respective shear runs ranged from 0.51–2.2 h^{-1} for the 0.09 m.s^{-1} runs, and between 0.44 and 2.6 h^{-1} in the 0.36 m.s^{-1} runs. The measurements for the 11 steady-states obtained in the 0.09 m.s^{-1} and 0.36 m.s^{-1} runs are reported in *TABLE 6-4* and *TABLE 6-5* respectively.

For most of the steady states at a recycle velocity of 0.09 m.s^{-1}, the suspended biomass was not detected and a clear effluent was observed, although significant biomass concentrations were observed in runs 3 and 10. The suspended biomass measured in the higher shear 0.36

m.s^{-1} runs was slightly higher than that for the lower shear conditions. For both shear conditions, these occurrences appeared unrelated to D and were rather associated with natural biofilm-shedding phases.

Table 6-4: Results from the continuous biofilm runs at a shear velocity of 0.09 m.s^{-1}

Run No.	1	2	3	4	5	6	7	8	9	10	11
D (h^{-1})	0.51	0.55	0.61	0.71	0.93	0.98	1.0	1.7	1.9	1.9	2.2
Glc out ($g.L^{-1}$)	14.9	19.0	18.8	26.5	28.3	23.1	21.0	31.0	34.9	33.5	30.4
ΔGlc ($g.L^{-1}$) *1	26.1	21.9	22.8	15.1	13.1	15.2	17.1	11.1	6.78	8.38	11.2
C_{SA} ($g.L^{-1}$)	18.2	15.6	15.9	11.3	9.72	10.4	12.3	7.41	4.47	5.29	7.67
C_{AA} ($g.L^{-1}$)	5.56	5.12	5.29	3.40	3.23	4.21	4.59	2.63	1.90	2.23	2.79
C_{FA} ($g.L^{-1}$)	2.26	2.44	2.47	1.29	1.64	2.86	3.01	1.75	1.42	1.69	1.76
C_x ($g.L^{-1}$)	0.0	0.0	1.0	0.2	0.2	0.0	0.0	0.0	0.0	0.8	0.0
C_{xt} ($g.L^{-1}$) *2	26.1	28.9	28.3	15.5	15.0	17.0	27.3	17.0	13.2	25.3	25.7
C_{xt*} ($g.L^{-1}$)	13.5	18.9	16.7	8.8	8.2	9.9	17.5	8.4	3.4	5.1	12.9
Mass balance %	85	89	88	91	93	93	95	86	92	88	90
SA/AA ($g.g^{-1}$)	3.3	3.0	3.0	3.3	3.0	2.5	2.7	2.8	2.3	2.4	2.7
FA/AA ($g.g^{-1}$)	0.41	0.48	0.47	0.38	0.51	0.68	0.66	0.66	0.75	0.76	0.63
$Y_{SA,Glc}$ ($g.g^{-1}$)	0.70	0.71	0.70	0.75	0.74	0.68	0.71	0.67	0.66	0.63	0.69
q_{SA} ($g.L^{-1}h^{-1}$)	9.24	8.59	9.64	7.97	9.00	10.2	12.5	12.9	8.48	10.2	17.1
r_{SA} ($g.g^{-1}h^{-1}$) *3	0.35	0.30	0.34	0.52	0.60	0.60	0.46	0.76	0.64	0.40	0.66
r_{SA}^* ($g.g^{-1}h^{-1}$) *4	0.69	0.46	0.58	0.91	1.1	1.0	0.71	1.5	2.5	2.0	1.3

*1 Effect of NaOH dosing incorporated into calculation
*2 Including scrubbed biofilm and suspended cells
*3 Based on x_t
*4 Based on estimated cellular mass

Biofilm build-up is gradual and most of the biofilm is a former metabolic product that developed before steady state was achieved. The observation that the cellular fraction (C_{xt*}/C_{xt}) measured during the higher shear run (average 0.84 ± 0.02 from *Table 6-5*) was higher than that during the lower shear run (average 0.50 ± 0.05 from *Table 6-4*) could indicate that the

biofilm characteristics change as a result of the shear. This is supported by the model proposed by Van Loosdrecht et al. (1995; 2002) in which it is suggested that the biofilm changes from a thicker, heterogeneous to a thin homogeneous configuration as shear increases (see Section 2.1.1.3 on page 2-5). This observation correlates with the increase in the predicted EPS fractions with a decrease in shear velocities in the two-phase biofilm system using *L. rhamnosus* (TABLE 5-2 in Section 5.2.3 on page 5-9).

Table 6-5: Results from the continuous biofilm run at 0.36 m.s^{-1}

Run No.	1	2	3	4	5	6	7	8	9	10	11
D (h^{-1})	0.44	0.75	0.77	0.82	1.0	1.2	1.2	1.4	1.6	2.0	2.6
Glc out ($g.L^{-1}$)	13.6	20.7	22.1	28.9	25.4	24.1	25.3	23.3	28.3	32.9	35.9
ΔGlc ($g.L^{-1}$) *1	26.7	19.6	18.6	12.0	16.4	17.1	15.5	18.0	12.7	8.86	6.0
C_{SA} ($g.L^{-1}$)	17.6	13.7	12.8	7.55	9.5	11.5	9.65	10.9	7.50	4.67	3.35
C_{AA} ($g.L^{-1}$)	6.31	5.48	4.56	3.36	4.18	4.01	4.36	4.31	3.72	2.56	1.83
C_{FA} ($g.L^{-1}$)	3.79	3.32	2.13	2.50	3.19	2.02	3.46	2.93	3.08	2.14	1.40
C_x ($g.L^{-1}$)	0.34	1.1	1.2	1.7	0.33	0.69	0.38	1.7	0.48	0.60	1.16
C_{xt} ($g.L^{-1}$) *2	14.2	22.0	15.2	11.6	18.9	17.8	16.6	14.2	29.6	27.7	21.1
C_{xt*} ($g.L^{-1}$)	11.0	16.9	12.6	10.3	15.4	16.5	11.7	13.5	24.4	24.4	19.0
Mass balance %	86	95	89	90	83	86	91	82	92	87	88
SA/AA ($g.g^{-1}$)	2.8	2.5	2.8	2.3	2.3	2.6	2.2	2.5	2.0	1.8	1.8
FA/AA ($g.g^{-1}$)	0.60	0.61	0.47	0.74	0.76	0.47	0.79	0.68	0.83	0.84	0.8
$Y_{SA,Glc}$ ($g.g^{-1}$)	0.66	0.70	0.69	0.63	0.58	0.66	0.62	0.61	0.59	0.53	0.56
q_{SA} ($g.L^{-1}h^{-1}$)	7.75	10.3	9.87	6.20	9.68	13.3	12.0	15.2	12.1	9.28	8.8
r_{SA} ($g.g^{-1}h^{-1}$) *3	0.55	0.47	0.61	0.53	0.51	0.74	0.72	0.68	0.41	0.33	0.42
r_{SA}* ($g.g^{-1}h^{-1}$) *4	0.71	0.61	0.79	0.60	0.63	0.83	1.0	1.1	0.50	0.38	0.46

*1 Effect of NaOH dosing incorporated into calculation
*2 Including scrubbed biofilm and suspended cells
*3 Based on x_t
4 Based on estimated cellular mass (x_t)

A possible explanation for the significant drop in growth during the biofilm work is the extreme growth inhibition as a result of the product formation in the bioreactor (FIGURE 6-5).

This is consistent with observations made in the literature with regard to biofilms of *A. succinogenes* at high (> 10 $g.L^{-1}$) SA titres (Van Heerden & Nicol, 2013; Bradfield & Nicol, 2014; Maharaj, Bradfield & Nicol, 2014).

As a result, the suspended biomass was not included in the mass balance checks as most of the experimental results were obtained at SA titres of more than 10 $g.L^{-1}$ and it was shown in TABLE 6-3 that most of the carbon directed towards biomass is sourced from the NS. Mass balance checks on steady-state conditions averaged 90 ± 1% for the 0.09 $m.s^{-1}$ runs and 89 ± 1% for the 0.36 $m.s^{-1}$ runs. The mass balance was calculated using a "black box" mass balance as described by Villadsen, Nielsen and Lidén (2011: 96). A more comprehensive discussion on the mass balance method used can be found in Section B.x on page B-13.

The lower-than-expected mass balances were observed in *A. succinogenes* biofilm experiments in the literature (Van Heerden & Nicol, 2013; Bradfield & Nicol, 2014; Maharaj, Bradfield & Nicol, 2014). The black box mass balances determined from these studies and from the current study are shown in FIGURE 6-6. It can be seen that the mass balances were approximately 10% under the expected value for nearly all the measurements. This indicates that an additional undetected catabolic fermentation product is likely in the outlet stream.

A probable candidate for this unknown catabolic product is pyruvic acid (PA), as this product has a high-performance liquid chromatograph (HPLC) peak at the same time as glucose, which means that it would be obscured for runs in which incomplete glucose conversion was observed. In addition, the production of PA could account for the additional NADH required for the observed SA/AA ratios above 3.93 $g.g^{-1}$ (Section 2.3.4).

The production of PA involves a net production of NADH (equation (6-14)), while the production of SA involves a net requirement of NADH (equation (6-1)). In this study, as well as the studies by both Bradfield and Nicol (2014) and Maharaj, Bradfield and Nicol (2014), a net NADH requirement was observed; the SA/AA ratios were significantly higher, for $C_{SA} > 10\ g.L^{-1}$, than the maximum possible value of 3.93 $g.g^{-1}$ during complete *pdh/fdh* production of AA. This indicated an additional source of NADH as the *pdh/fdh* route could not account for the additional NADH requirement during the SA production (see Section 2.3.4 on page 2-36 for an in-depth discussion on the respective studies).

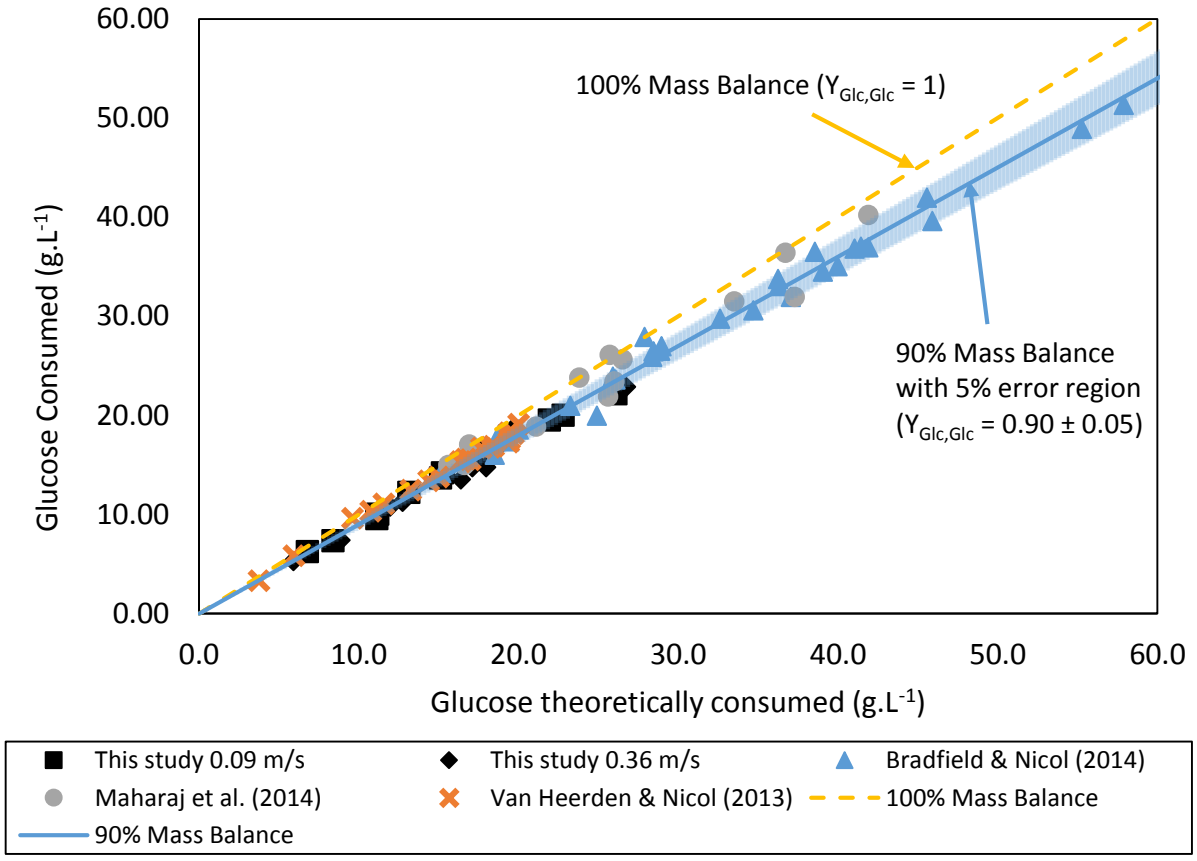

Figure 6-6: Black box mass balances for this study as well as results from the literature (Van Heerden & Nicol, 2013; Bradfield & Nicol, 2014; Maharaj, Bradfield & Nicol, 2014). The mass balances were calculated using equation *(B-26)* (Section *B.x* on page *B-13*).

The data in this study were limited to relatively low C_{SA} values. This was mostly a result of the extremely large D values used during the fermentations (Section *4.5.1* on page *4-11*), as well as of the limited biofilm fermentation periods (Section *4.5.2* on page *4-12*).

6.3.2 Results obtained from batch runs

In addition to the continuous fermentation results obtained, four separate batch runs were completed. The experimental methodology, including the biofilm growth, batch initiation and sampling method, is discussed in more detail in the *BATCH OPERATION* section on page *4-13*. The measured concentrations from the individual batch runs are summarised in *FIGURE 6-7*.

The batch results (*FIGURE 6-7*) indicate that extremely high SA titres (C_{SA}) were measured inside the reactors during batch operation. The highest $C_{SA} \approx 72$ g.L^{-1} was measured during Batch 3. However, maximum $C_{SA} > 60$ g.L^{-1} was measured for Batches 1 and 2, and maximum $C_{SA} \approx 55$

g.L^{-1} for Batch 4. These results are supported by the measured C_{SA} = 68.4 ± 0.2 g.L^{-1} during *A. succinogenes* batch runs in a fibrous bed bioreactor performed by Yan et al. (2014).

The results in FIGURE 6-7 were, however, subject to dilution as a result of the NaOH dosed to control the pH, as well as the periodic removal of reactor volume due to sampling, which increased the diluting effect of the NaOH. The actual masses of produced SA (m_{SA}) were calculated by converting the concentration values to mass values while taking the removal of sample volume from the reactor into account (equations (B-27) and (B-28)); the results are shown in FIGURE B-11.

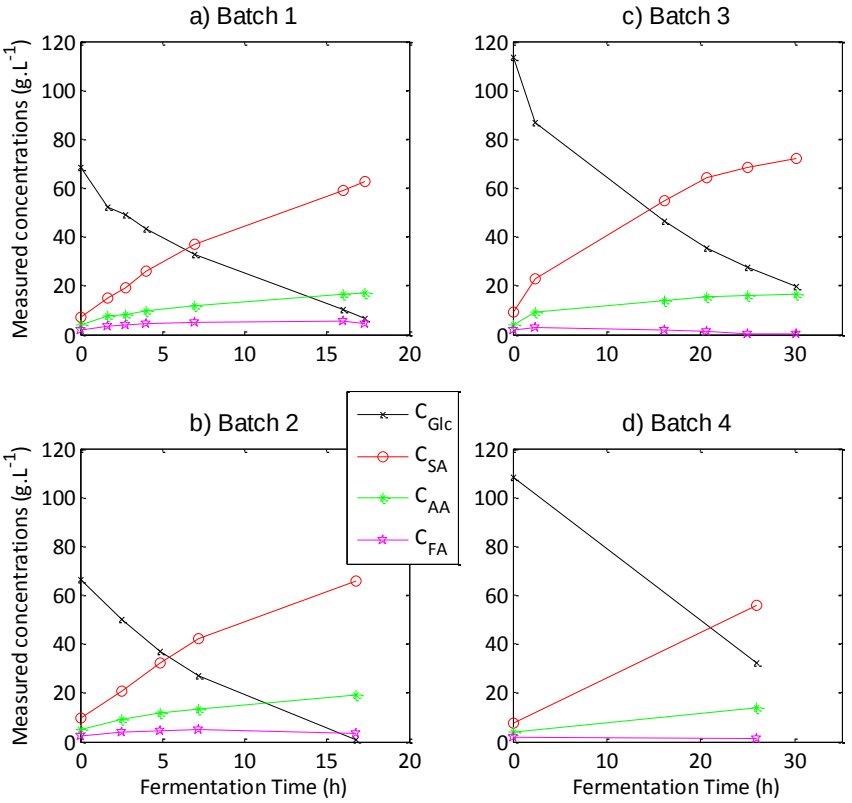

Figure 6-7: Concentration measurements obtained during the 4 individual batch runs. The figure shows the measured concentrations of Glc (C_{Glc}), SA (C_{SA}), AA (C_{AA}), and FA (C_{FA}) measured at different fermentation times during the respective batch runs.

In addition to the measured concentrations as shown in FIGURE 6-7, the NaOH dosing was logged as a function of fermentation time and is shown in FIGURE B-10 (Section B.XI on page B.XI). The adjusted results from FIGURE 6-7, using equations (B-27) and (B-28), were correlated to the accumulated NaOH dosing. This correlation is shown in FIGURE B-11 (Section B.XI on page B-14) and indicates a distinct increase in mass of SA produced with increasing NaOH

dosed. This is a result of the increased yield of SA to glucose, with increasing fermentation time, as can be seen in *FIGURE 6-7*.

Combining the NaOH dosing, shown in *FIGURE B-10*, with the correlation of the SA production against NaOH dosing (*FIGURE B-11*) and dividing the results by an average reactor volume over all the batch runs (49.6 ± 1.4 mL) yielded *FIGURE 6-8*, a representation of the true SA produced over time. Using this figure it was possible to determine the production rate of SA within the batch reactor more accurately than using the results from *FIGURE 6-7*.

An important observation from *FIGURE 6-8* is the significant correspondence between the SA produced in Batches 1, 3 and 4, indicating almost identical production rates over time, whereas the SA produced in Batch 2 was slightly higher, possibly corresponding to the higher cellular mass and the longer biofilm growth period in Batch 2 (*TABLE 4-4*).

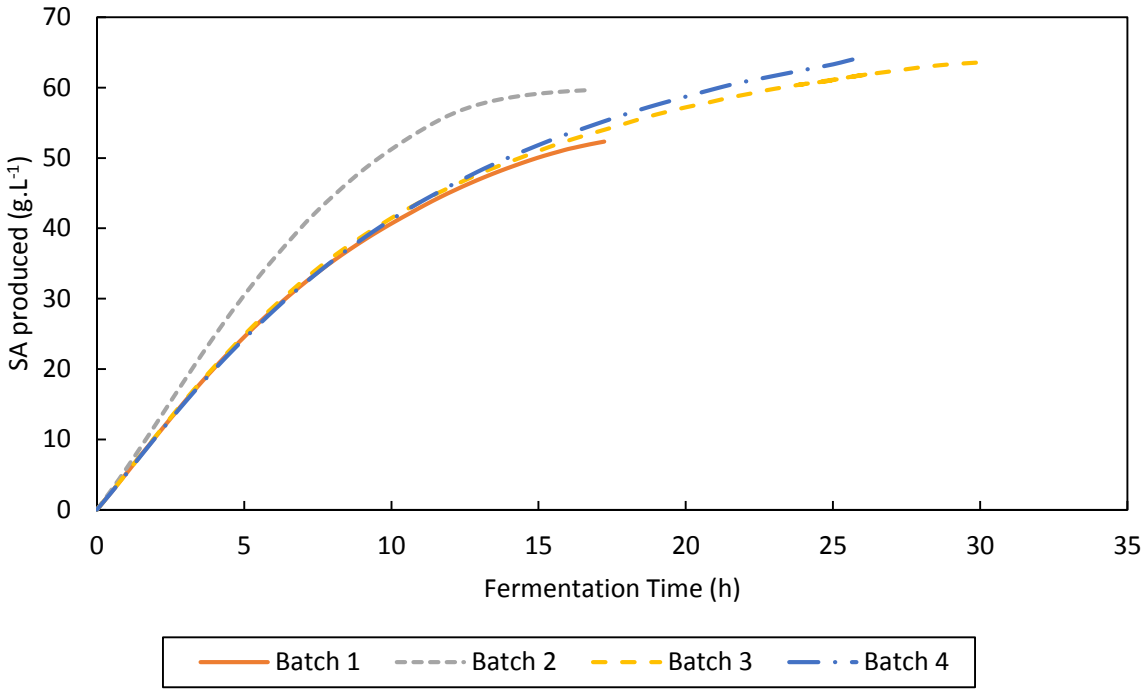

Figure 6-8: The resulting SA production profiles over time as determined using equations *(B-27)* and *(B-28)* and applied to the NaOH dosing profiles as shown in *FIGURE B-10*. The figure clearly shows that Batch 2 had the highest productivity, while Batches 1, 3 and 4 produced nearly identical SA amounts. It should be noted that the concentrations shown in this figure do not represent the measured concentrations, but rather the calculated masses of SA per average volume of reactor.

6.3.3 Production characteristics

Productivity is considered an integral part of bioreactor design as this quantifies the utilisation of the production capacity. Productivity in bioreactors is generally categorised according to

the basis used in the rate expressions. To determine the intrinsic properties of the microbial species within the biofilm, it is required that the specific production rate (r_p) be determined. This property is based on the cellular biomass in the reactor and gives information on the energetics, growth rates and sensitivity to the environment of the specific organism under consideration (Villadsen, Nielsen & Lidén, 2011: 179).

In contrast, the most commonly used basis is the total reactor volume with the corresponding volumetric production rate (q_P) defined as the mass of product formed per volume of reactor per time. The use of the volumetric production rate to measure the reactor productivity facilitates the design of the reactor, which is in most cases based on volumetric considerations (Villadsen, Nielsen & Lidén, 2011: 390).

Specific/Cell-based productivity

The cell-based productivity (r_p) in this study was determined after base hydrolysis and removal of the EPS from the biofilm biomass (Section 4.5.9 on page 4-17). This was done in order to determine the specific rates of SA production based on the cellular biomass (r_{SA}*), and therefore the intrinsic production capabilities of the bacteria within the biofilm. The r_{SA}* measured for the two different shear conditions in the biofilm reactor, as well as the r_{SA} as determined from the chemostat runs (the product of equations (6-10) and (6-12)), are shown in FIGURE 6-9.

FIGURE 6-9 indicates a distinct split between the r_{SA}* of the two different shear conditions for $C_{SA} < 10$ g.L^{-1}, while for $C_{SA} \geq 10$ g.L^{-1} the r_{SA}* appeared to meet and subsequently continued within the same band of values. The reason for the split between the r_{SA}* values is unsure: the cell-based productivities for the 0.09 m.s^{-1} scenario are much higher than predictions from the chemostat analysis and this raises the question as to whether the EPS that was removed contained active cellular material. However, the abnormally high rates occurred only in the growth region ($C_{SA} < 10$ g.L^{-1}), whereas the results for the maintenance region ($C_{SA} > 10$ g.L^{-1}) followed the same trend in both the 0.09 m.s^{-1} and 0.36 m.s^{-1} runs. The experimental results from the 0.09 m.s^{-1} run were fitted by an exponential decay function that was positively displaced on the r_{SA}*-axis (equation (6-13)). This displacement of 0.59 g.L^{-1}.h^{-1} represents the

maintenance production of SA by the organism (m_{SA}*) for $C_{SA} \gg 10$ g.L^{-1}, as can be seen in FIGURE 6-9.

$$r_{SA}* = 7.4exp(-0.3C_{SA}) + 0.59 \quad (6\text{-}13)$$

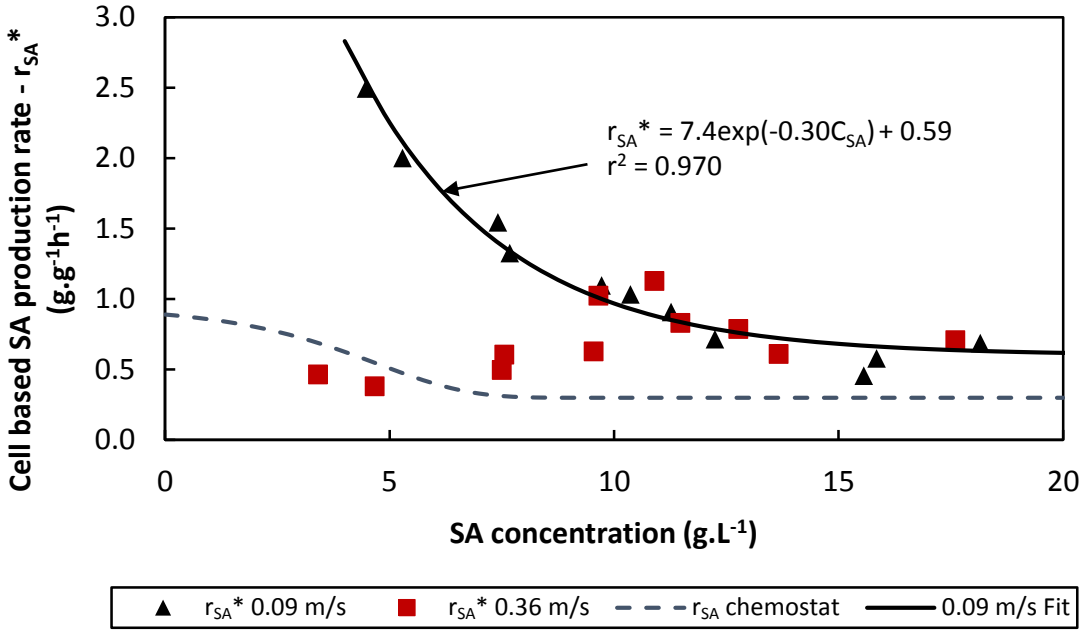

Figure 6-9: Specific production rate of cellular biomass (EPS removed) as a function of SA concentration, with an exponential fit to the results from the 0.09 m.s^{-1} run. The exponential fit was displaced on the r_{SA}*-axis by a value of 0.55 g.L^{-1}.h^{-1}, representing the maintenance SA production of the biofilm. In addition, the figure shows the chemostat r_{SA}, determined by multiplying equation (6-10) by equation (6-12). The r_{SA} of the chemostat clearly displays the m_{SA} = 0.31 g.L^{-1}.h^{-1} for C_{SA} > 7 g.L^{-1}.

FIGURE 6-9 shows that as the $C_{SA} \gg 10$ g.L^{-1}, the cells tend to produce SA mostly via maintenance or non-growth metabolism. This result corresponds to the observations made by Maharaj, Bradfield and Nicol (2014), as well as those of Bradfield and Nicol (2014) who found that at significantly high C_{SA}, the growth ceases and most of the SA production is linked to maintenance metabolism. This means that the cellular biomass produces the minimum amount of product, and therefore ATP, in order to maintain the basic cellular functions, while growth of biomass, i.e. multiplication and biomass production, is discontinued.

Comparison of the biofilm r_{SA}* with the chemostat r_{SA} (FIGURE 6-3) shows that the biofilm maintenance productivity was significantly higher (m_{SA}* = 0.59 g.g^{-1}.h^{-1}) than the $m_{SA} \approx 0.31$ g.g^{1}.h^{-1} as measured in the chemostat system (equation (6-10)). This could indicate an increased maintenance requirement of cells in the biofilm, possibly as a result of biofilm conservation. It should, however, be noted that the values of m_{SA} and m_{SA}* are extremely reliant

on the experimental fits as shown in *FIGURE 6-3* and *FIGURE 6-9*, and can therefore be significantly affected by the assumptions used. An example is the assumption that the biomass in the chemostat was virtually EPS-free and therefore represented the cellular biomass. If the biomass contained a fraction of EPS, then the r_{SA} for the chemostat would increase, moving closer to the m_{SA}*. Alternatively, the positive displacement along the r_{SA}*-axis might be less than fitted using the available experimental data, leading to a lower asymptote and a value closer to the m_{SA} measured in the chemostat.

The r_{ATP}* was analysed to determine how the maintenance ATP requirements for cellular mass compared between the chemostat and biofilm reactors. The ATP in the biofilm was determined using equations *(6-1)* to *(6-3)* and *(6-14)*, which assume that the mass imbalance as shown in *FIGURE 6-6* is accounted for in the production of pyruvic acid.

$$v_5: CH_2O\ (Glc) \rightarrow CH_{\frac{4}{3}}O\ (PA) + \frac{1}{3}NADH + \frac{1}{3}ATP \qquad (6\text{-}14)$$

The r_{ATP}* against C_{SA} is shown in *FIGURE 6-10* and indicates the dependence of the r_{ATP}* on the C_{SA}. This figure is similar to *FIGURE 6-9*, which could be expected considering that SA is the main product during fermentation. The data from the 0.09 $m.s^{-1}$ runs were fitted using an exponential decay curve, similar to equation *(6-13)*, that was positively displaced along the r_{ATP}*-axis (equation *(6-15)*). In the case of *FIGURE 6-9* it was assumed that the displacement represents the m_{SA}* = 0.60 $g.g^{-1}.h^{-1}$. Therefore, in this case it was assumed that the displacement represented the m_{ATP}* = 16.1 mmol $ATP.g^{-1}.h^{-1}$.

$$r_{ATP}* = 217exp(-0.3C_{SA}) + 16.1 \qquad (6\text{-}15)$$

The m_{ATP}* = 16.1 mmol $ATP.g^{-1}.h^{-1}$ indicates the minimum energy requirements per gram of dry cellular mass, i.e. without EPS. As was the case for the r_{SA}* (*FIGURE 6-9*), the chemostat maintenance was determined to be lower than the biofilm maintenance, possibly as a result of energy requirements for biofilm preservation. However, if the assumption was incorrect that all chemostat biomass was EPS-free and therefore represented the total biomass, then the r_{ATP} would increase with a corresponding increase in the m_{ATP}.

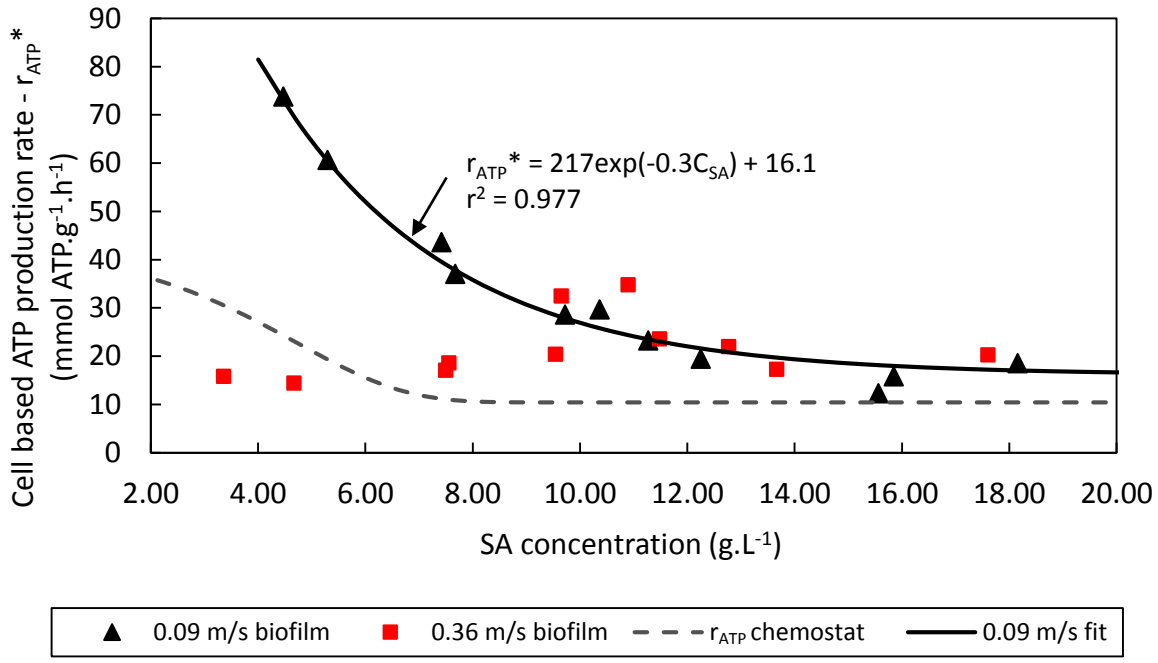

Figure 6-10: The catabolic ATP production calculated from the product distributions using equations *(6-1)* to *(6-3)* and *(6-14)*, divided by the cellular biomass (x_t*) measured during fermentations, plotted against the C_{SA}. The data for the 0.09 m.s^{-1} run were fitted using an exponential decay curve with displacement on the r_{ATP}*-axis, representing the m_{ATP}*. The m_{ATP} = 10.4 mmol.g^{-1}.h^{-1} are shown as a comparison between the maintenance requirments in the batch system and in the biofilm reactor.

In order to test the influence of high C_{SA} on the transient behaviour of r_{SA}*, the batch r_{SA}* values were plotted together with the fit obtained from the 0.09 m.s^{-1} runs (equation *(6-13)*) in *FIGURE 6-11*. Interestingly, the initial r_{SA}*values for the respective batch runs, i.e. the steady state values after the continuous biofilm growth period, corresponded well with the fit obtained in the 0.09 m.s^{-1} biofilm runs. The figure indicates that the r_{SA}* in the batch system maintained higher values than that in the continuous reactor, up to C_{SA} values of 40–45 g.L^{-1}. This indicates a significant lag in the inhibition of the SA production in the batch system. The individual batch runs initially followed considerably different paths, generally maintaining a constant rate with increasing C_{SA}, up to a C_{SA} of between 20 and 35 g.L^{-1}, depending on the specific batch run considered. At C_{SA} > 20–35 g.L^{-1}, the r_{SA}* started declining linearly with increasing C_{SA}. The r_{SA}* values from the four batch runs "met" at around 40–45 g.L^{-1} at approximately 0.59 g.g^{-1}.h^{-1}, the same point where the batch data cross the predicted m_{SA}* value. For C_{SA} > 45 g.L^{-1}, all the batch r_{SA}* values continued within a narrow band. This eventual decrease in r_{SA}* values might represent the eventual product inhibition of the r_{SA}* of *A. succinogenes*, with termination of production at C_{SA} values between 60 and 70 g.L^{-1}. This observation is supported by the results in the literature on *A. succinogenes* – maximum titres

of 64 g.L^{-1} and 68 g.L^{-1} were measured during continuous and batch biofilm fermentation respectively (Yan, Zheng, Dong, et al., 2014; Yan, Zheng, Tao, et al., 2014). The authors estimated a critical C_{SA} of approximately 60 g.L^{-1}, using a Ierusalimskii inhibition function (Egamberdiev & Ierusalimskii, 1968), after which the SA inhibition of the organism increased disproportionately, effectively "choking" the organism's ability to metabolise glucose.

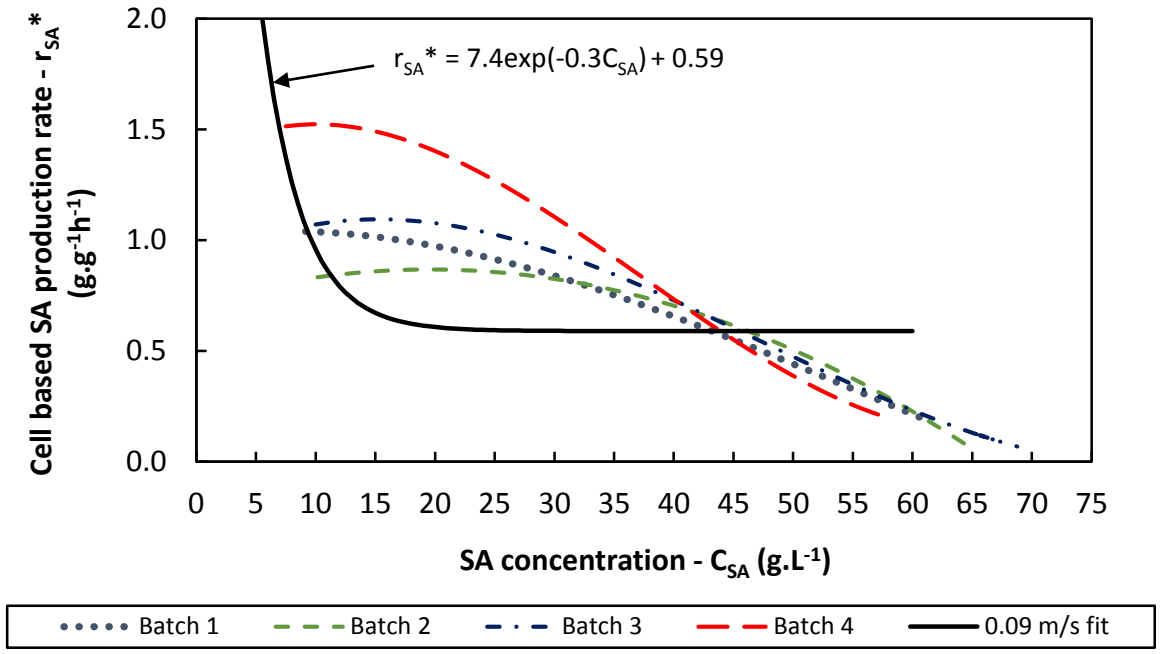

Figure 6-11: The specific rate of SA production based on cellular biomass (r_{SA}*) plotted as a function of C_{SA}. This figure also shows the fit to the 0.09 m.s^{-1} biofilm runs, shown in *FIGURE 6-9*; it is significant to observe the similarities between the fit and the steady-state values measured at the initiation of the respective batch runs. Interestingly, the r_{SA}* start at different initial rates, yet converge and follow similar values for C_{SA} > 45 g.L^{-1}.

Volume-based productivity

FIGURE 6-12 and *FIGURE 6-13* show the volumetric production rates of various continuous studies from the literature as well as the results obtained in this study against dilution rate (*FIGURE 6-12*) and C_{SA} (*FIGURE 6-13*). *FIGURE 6-12* and *FIGURE 6-13* show that the volumetric production rates appear to be bounded from above. In the case of *FIGURE 6-12* this boundary appears to continue increasing with increasing D. Arguably the maximum value measured in *FIGURE 6-12* of 17.1 g.L^{-1}.h^{-1} could indicate the maximum production rate possible and also indicate a subsequent decrease in q_{SA} with increased D. However, within the scope of industrial application, the measured SA titre of 7.67 g.L^{-1} at this q_{SA} (*FIGURE 6-13*) is far below that required by industry and therefore the interest lies in the region of higher SA titres, i.e. on the right hand side

of *FIGURE 6-13*. In this region the data appear to decrease constantly, with a boundary described by a hyperbolic function (equation *(6-16)*).

$$q_{SA}^{max} = \frac{170}{C_{SA}} \tag{6-16}$$

Due to a lack of experimental data, equation *(6-16)* is only applicable in the region 10 $g.L^{-1}$ < C_{SA} < 58 $g.L^{-1}$; it is uncertain whether the productivity maintains the same boundary outside of these C_{SA} values. The result from Yan et al. (2014) showed a marked decline in productivity at a C_{SA} > 58 $g.L^{-1}$. However, it cannot be ascertained with certainty whether this is representative of the q_{SA}^{max} boundary.

The data appear to have a boundary of minimum q_{SA}-values, which are designated by the chemostat values (*FIGURE 6-3*). It is important to observe the marked difference between the maximum and minimum q_{SA} values measured during the chemostat operation; it appears that a continuum of possible q_{SA} values is likely within these extreme values. The specific values of the q_{SA} for the respective studies appear to be dependent on the specific reaction system and on the support structure used for biofilm growth. The various studies (Van Heerden & Nicol, 2013; Bradfield & Nicol, 2014; Maharaj, Bradfield & Nicol, 2014; Yan, Zheng, Tao, et al., 2014) seemed to concentrate within particular regions within the continuum. These individual regions appeared mostly unaffected by dilution rate (*FIGURE 6-12*) and C_{SA} (*FIGURE 6-13*) as the q_{SA} values remained relatively constant as a function of both D and C_{SA}, while the boundary values of q_{SA} (q_{SA}^{max}) were observed to have a strong dependence on C_{SA}.

Equation *(6-16)* illustrates the strong correlation between the upper bound of q_{SA} and C_{SA} in the reactor, hinting at significant product inhibition of the cells in the biofilm. This was interesting as q_{SA} are based on reactor volume and therefore inhibition as a result of C_{SA} is an indication that there might be a global control mechanism controlling the SA production (see the section on *GLOBAL MICROBIAL REGULATION* on page *2-8*).

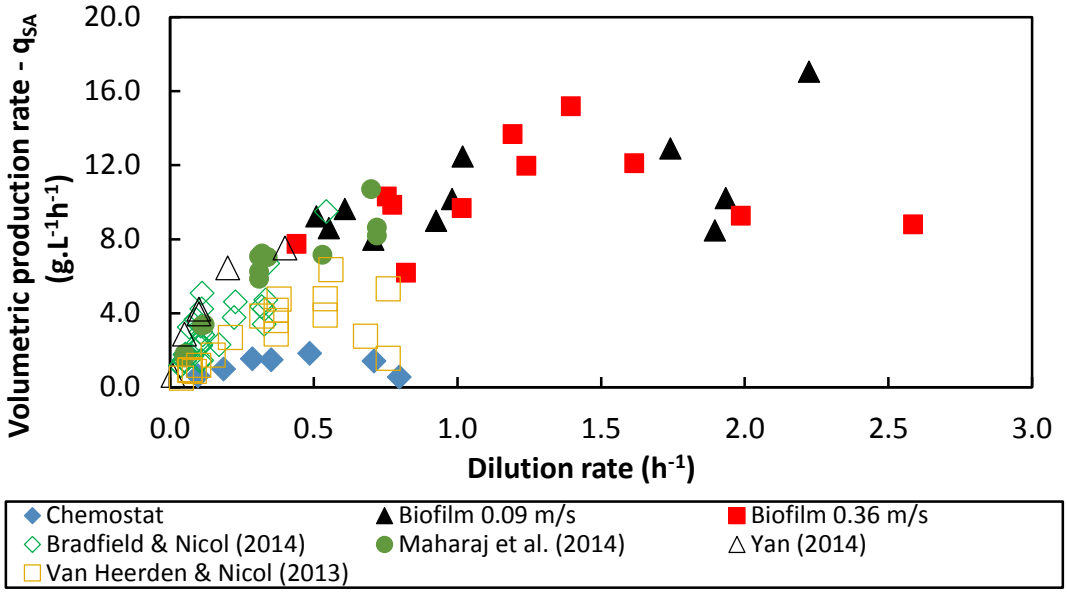

Figure 6-12: Volumetric productivities of *A. succinogenes* continuous studies from the literature (Van Heerden & Nicol, 2013; Bradfield & Nicol, 2014; Maharaj, Bradfield & Nicol, 2014; Yan, Zheng, Tao, et al., 2014)**, as well as results from this study, against dilution rate. The figure shows that the results appear to be bounded within a specific region.**

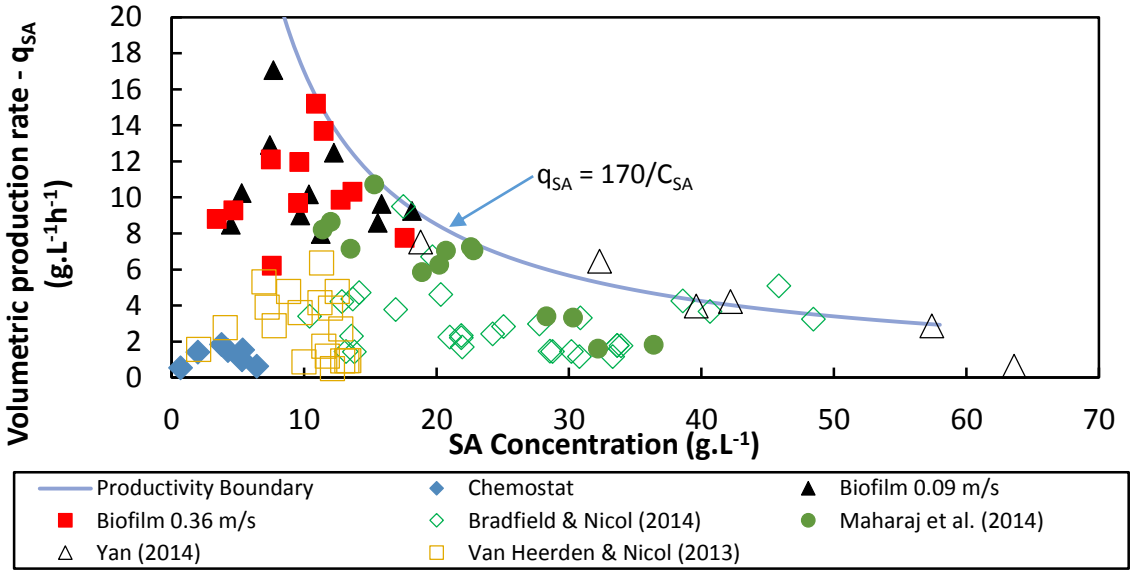

Figure 6-13: Volumetric productivities of *A. succinogenes* continuous studies from the literature (Van Heerden & Nicol, 2013; Bradfield & Nicol, 2014; Maharaj, Bradfield & Nicol, 2014; Yan, Zheng, Tao, et al., 2014)**, as well as results from this study, against C_{SA}. A productivity boundary, described by equation *(6-16)*, was fitted to the results. It appears that the q_{SA} for specific studies remained relatively "flat" as a function of the C_{SA}.**

By comparing the r_{SA}* (*FIGURE 6-9*) and q_{SA} (*FIGURE 6-13*) against the C_{SA}, it was observed that the r_{SA}* values followed significantly clearer trends and remained within narrower bands of results as opposed to the q_{SA} values measured. However, looking at the general shape of the q_{SA} results in this study (*FIGURE 6-13*), it appeared that under biomass growth conditions, i.e.

for C_{SA} < 10 g.L^{-1} both the shear runs exhibited a decrease in q_{SA} from a maximum at around 10 g.L^{-1}, with a decrease in C_{SA}. This section of the figure corresponded to the section of the r_{SA}* curve (*FIGURE 6-9*) in which a clear split in the r_{SA}* values was observed; the r_{SA}* of the 0.09 m.s^{-1} runs increased exponentially with decreasing C_{SA}, while that of the 0.36 m.s^{-1} runs decreased, from about 1.0 g.g^{-1}.h^{-1} to about 0.5 g.g^{-1}.h^{-1}, with decreasing C_{SA}. The 0.09 m.s^{-1} runs had a significantly lower amount of x_t* (*TABLE 6-4*) when compared with the 0.36 m.s^{-1} runs (*TABLE 6-5*): values of x_t* = 3.4–12.9 g.L^{-1} were reported in the 0.09 m.s^{-1} runs for C_{SA} < 10 g.L^{-1}, while values of x_t* = 15.4–24.4 g.L^{-1} were observed in the 0.36 m.s^{-1} runs for C_{SA} < 10 g.L^{-1}. This indicates that the q_{SA} is not a function of the total biomass amount in the system under growth conditions.

For C_{SA} > 10 g.L^{-1}, the q_{SA} exhibited a much greater spread in values, from a minimum of about 8 g.L^{-1}.h^{-1} up to the maximum described by equation *(6-16)*, while the r_{SA}* for both shear runs (for C_{SA} > 10 g.L^{-1}) followed the exponential decay curve (equation *(6-13)*) up to the maximum measured C_{SA} = 18.2 g.L^{-1}. This shows that q_{SA} is a function of the biomass in the system up to the maximum q_{SA}, because the cellular biomass appears to produce SA at the same r_{SA}*, while the q_{SA} fluctuates depending on the cellular biomass. The observation that the r_{SA}* values were the same for both shear conditions, although the q_{SA} values were bounded from above, indicated that the maximum amount of cells in the reactor was limited and therefore any additional cells were expelled. This conclusion concurs with the observation that the r_{SA}* followed equation *(6-13)*, irrespective of the q_{SA} or C_{SA}. The maximum x_t* can be determined as the quotient of the q_{SA}^{max} and the r_{SA}*, because the relationship between q_{SA} and r_{SA}* is the x_t*. Therefore x_t* can be calculated using equation *(6-17)*, which is the quotient of equations *(6-16)* and *(6-13)*.

$$x_t^* = \frac{q_{SA}^{max}}{r_{SA}^*} = \frac{170}{C_{SA}} \frac{1}{7.4\exp(-0.3C_{SA}) + 0.59}, for\ C_{SA} > 10\ g.L^{-1} \qquad (6\text{-}17)$$

The graphical representation of this equation and the maximum q_{SA} values from the experimental results (*TABLE 6-4* and *TABLE 6-5*) are shown in *FIGURE 6-14*. This figure shows that the range of the x_t* is predicted reasonably well (between 14 and 18 g.L^{-1}) and indicates that the x_t* values are controlled within a specified range by the C_{SA} in the reactor.

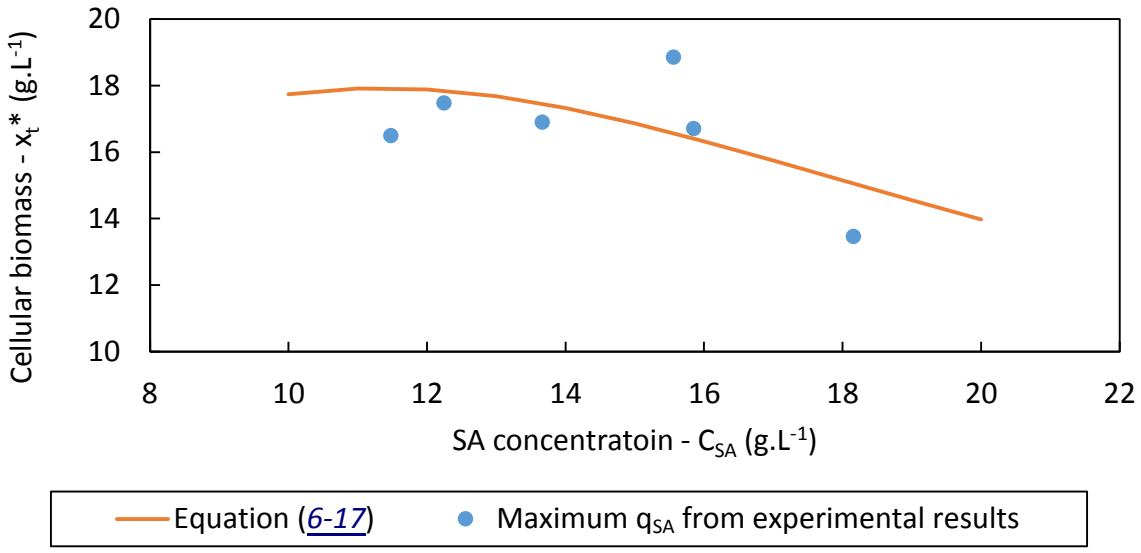

Figure 6-14: Graphical representation of equation (6-17) against C_{SA}, in comparison with the q_{SA}^{max} measured in the 0.09 m.s^{-1} and 0.36 m.s^{-1} runs. The graph shows that equation (6-17) predicts the range of x_t^{max} reasonably well.

In order to determine whether the same inhibition effect as in the continuous reactor systems was present in transient systems, as shown in FIGURE 6-13, the q_{SA} of the batch systems, together with batch results from Yan et al. (2014), were plotted against the measured C_{SA} in the respective systems (FIGURE 6-15). The batch q_{SA} results from this study were calculated as the slope of the respective curves in FIGURE 6-8, while the C_{SA} values were interpolated from the measured C_{SA} values in FIGURE 6-7.

Most of the batch q_{SA} results remained within the continuous q_{SA} boundary (equation (6-16)). However, the q_{SA} of Batch 2 appeared to cross the q_{SA} boundary due to a significantly higher q_{SA} at the initiation of batch conditions. As was the case in the batch r_{SA}* results as shown in FIGURE 6-11, the q_{SA} values remained almost constant as the C_{SA} increased to values between 20 and 40 g.L^{-1}, depending on the specific batch considered. The q_{SA} then almost linearly decreased with increases in the C_{SA} up to a C_{SA} value of between 60 and 70 g.L^{-1}, at which point the q_{SA} apparently terminated. This might indicate that the productivity boundary abandons the hyperbolic shape and drops to a productivity close to zero, for C_{SA} > 60 g.L^{-1}.

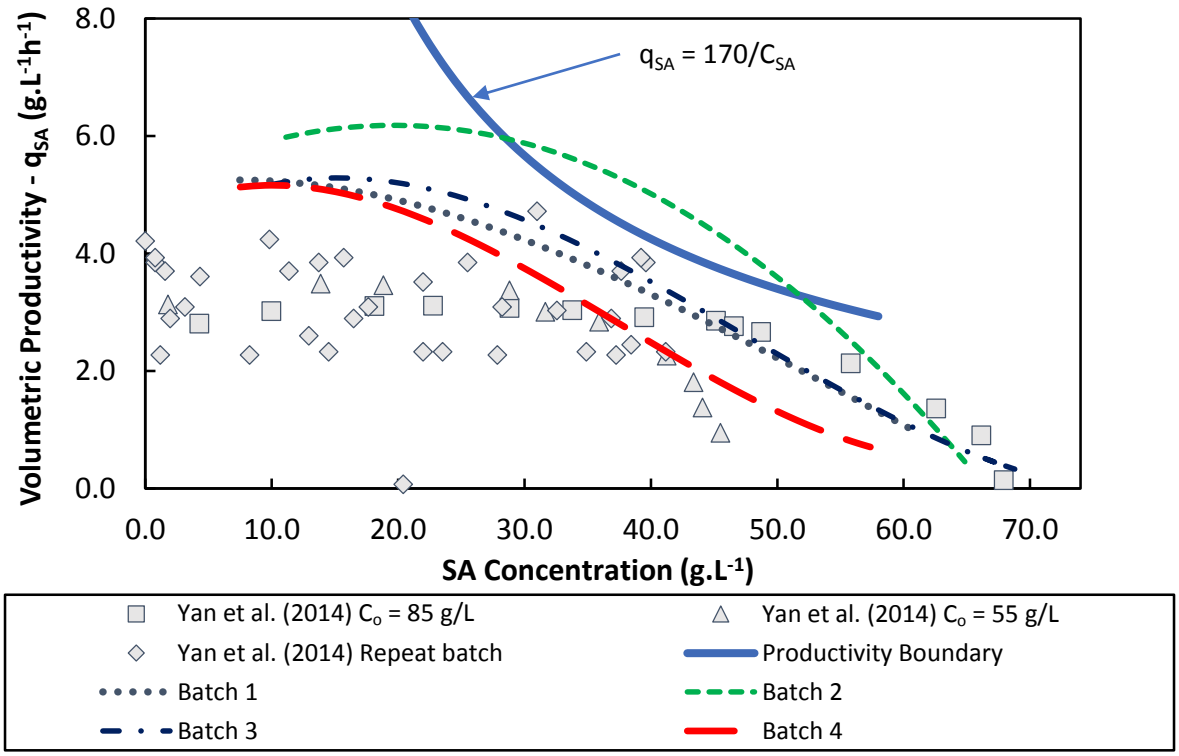

Figure 6-15: Volumetric productivities of batch runs from the literature (Yan, Zheng, Tao, et al., 2014) **and results from this study. In addition, the q_{SA}^{max} boundary, as described by equation *(6-16)*, is shown. The results remain largely within the q_{SA} boundary, except for Batch 2 which overshoots slightly. The results appear to support the observation that the production terminates at a C_{SA} between 60 and 70 g.L^{-1}.**

These results indicate that the biofilm experienced a lag in reacting to the C_{SA} increase in the biofilm reactor. It was apparent that the batch work done by Yan et al. (2014) followed very nearly the same trend as observed in the batch work done in this study.

It is interesting to observe the comparison between the r_{SA}* (*FIGURE 6-11*) and the q_{SA} (*FIGURE 6-15*) as a function of C_{SA}. The r_{SA}* values started on the line representing equation *(6-13)*. As the C_{SA} increased, the r_{SA}* remained largely constant until C_{SA} values of between 15 and 25 g.L^{-1}, were reached, at which point the product inhibition appeared to start affecting the r_{SA}*. All the r_{SA}* values then decreased linearly, with about the same slope, combining at C_{SA} of approximately 40–45 g.L^{-1} and continuing with this trend until the r_{SA}* terminated at a C_{SA} of approximately 60–70 g.L^{-1}. The nearly equal values of the r_{SA}* at C_{SA} > 45 g.L^{-1} indicate that at these values the cellular biomass in the batch reactors produced SA at equal rates per gram of biomass. Therefore, as was the case in the continuous runs, the q_{SA} for C_{SA} > 45 g.L^{-1} was dependent only on the total x_t* present in the reactor. However, for the C_{SA} values from the batch initiation until C_{SA} ≈ 45 g.L^{-1}, the r_{SA}* values were more dependent on the initial r_{SA}* value, i.e. at initiation of the batch run. This meant that Batch 4, which had the lowest initial

C_{SA} value, started at the highest r_{SA}*. Due to the lag in the product inhibition observed in the batch reactor, the high r_{SA}* was maintained and therefore the average r_{SA}* was significantly higher than in the equivalent continuous reactor. The reason that Batch 4 had the lowest q_{SA} was a result of the extremely low x_t* in the reactor. In the case of Batch 2, the measured q_{SA} crossed the q_{SA}^{max} boundary as a result of the lag in inhibition observed for C_{SA} up to 30 $g.L^{-1}$. However, Batch 2 did not show a significantly high r_{SA}* due to a high initiation C_{SA} (equation *(6-13)*). This means that the high observed q_{SA} was a result of the high x_t* value in the reactor. From this observation it was concluded that if Batch 4 had had an x_t* of larger magnitude, e.g. the maximum x_t* predicted by equation *(6-17)*, the q_{SA} could have been as high as the q_{SA}^{max} boundary. From here it could have maintained the q_{SA} and the r_{SA}* for a significant range of C_{SA} values due to the lag in inhibition. In this case an average q_{SA} significantly higher than that in a continuous biofilm reactor would be possible at much higher C_{SA} values.

Assuming that the hypothesis that additional cellular biomass is expelled from the fermenter during continuous operation, yielding the maximum x_t* function shown in *FIGURE 6-14* is correct, it would follow that the maximum x_t* function would be exceeded for increasing C_{SA} under transient conditions. This is due to the fact that the biomass remains constant within the batch volume and is not expelled as in the case of continuous operation. However, because the biofilm is grown during continuous operation, the maximum x_t* shown in *FIGURE 6-14* will be the maximum initial x_t* value at which the batch operation could commence. It is therefore a limiting condition within the fermenter for continuous and batch fermentation.

6.3.4 Metabolic product distribution

The metabolism of *A. succinogenes* was shown in Chapter 2 (see *FIGURE 2-5*) and was summarised in equations *(6-1)* to *(6-4)*. The expected metabolic products are SA, AA, FA and CO_2; the measured concentrations of these products for the current study, as well as from continuous biofilm studies from the literature (Van Heerden & Nicol, 2013; Bradfield & Nicol, 2014; Maharaj, Bradfield & Nicol, 2014), are shown in *FIGURE 6-16*. These results demonstrate the reproducibility of the experimental results for various different reactor configurations, as a function of the ΔGlc. It should be noted that the literature results shown here were generated using a very similar medium composition, i.e. a rich medium with YE and CSL as nitrogen sources, and a similar mineral salt composition.

From FIGURE 6-16 it can be seen that the product concentrations are represented by equations (6-18) to (6-20). The second term in the second part of equation (6-20) represents the amount of FA directed towards CO_2 by the *pdh/fdh* pathway. Therefore, the theoretical amount of FA if all fermentation took place via the *pfl* route would yield the equimolar amount of 0.77 $g.g^{-1}$, while the amount subtracted from the theoretical maximum would represent the CO_2 produced during fermentation.

$$C_{SA} = \begin{cases} 0.65\Delta Glc, \Delta Glc < 17\ g.L^{-1} \\ 0.92\Delta Glc - 4.2, \Delta Glc \geq 17\ g.L^{-1} \end{cases} \quad (6\text{-}18)$$

$$C_{AA} = \begin{cases} 0.29\Delta Glc, \Delta Glc < 17\ g.L^{-1} \\ 0.12\Delta Glc + 2.7, \Delta Glc \geq 17\ g.L^{-1} \end{cases} \quad (6\text{-}19)$$

$$C_{FA} = \begin{cases} 0.77C_{AA} = 0.22\Delta Glc, \Delta Glc < 17\ g.L^{-1} \\ 0.77C_{AA} - (0.17\Delta Glc - 2.4) = -0.08\Delta Glc + 4.48, \Delta Glc \geq 17\ g.L^{-1} \end{cases} \quad (6\text{-}20)$$

The piecewise-defined functions indicate a change in the metabolism at ΔGlc > 17 $g.L^{-1}$. This value corresponds to a $C_{SA} \approx 10\ g.L^{-1}$ and is therefore an indication of growth and non-growth metabolism. As shown in FIGURE 6-5, the growth of *A. succinogenes* ceases at a $C_{SA} \approx 10\ g.L^{-1}$.

Using the correlations as shown in equations (6-18) to (6-20), an attempt was made to elucidate the metabolic flux within the bacteria. Initially, the respective yields of the products to glucose consumption were determined from the correlations by dividing equations (6-18) to (6-20), as well as the experimental results, by the ΔGlc (equations (6-21) to (6-23)); this was to validate the accuracy of the correlations with regard to the yields.

$$Y_{Glc,SA} = \begin{cases} 0.65, \Delta Glc < 17\ g.L^{-1} \\ 0.92 - \dfrac{4.2}{\Delta Glc}, \Delta Glc \geq 17\ g.L^{-1} \end{cases} \quad (6\text{-}21)$$

$$Y_{Glc,AA} = \begin{cases} 0.29, \Delta Glc < 17\ g.L^{-1} \\ 0.12 + \dfrac{2.7}{\Delta Glc}, \Delta Glc \geq 17\ g.L^{-1} \end{cases} \quad (6\text{-}22)$$

$$Y_{Glc,FA} = \begin{cases} 0.22, \Delta Glc < 17\ g.L^{-1} \\ -0.08 + \dfrac{4.48}{\Delta Glc}, \Delta Glc \geq 17\ g.L^{-1} \end{cases} \quad (6\text{-}23)$$

FIGURE 6-17 shows the experimentally determined yields from the correlations (equations *(6-21)* to *(6-23)*), from this study and from the literature (Van Heerden & Nicol, 2013; Bradfield & Nicol, 2014; Maharaj, Bradfield & Nicol, 2014). From *FIGURE 6-17* it can be seen that the correlation-derived yield values and the experimentally determined values were in good agreement (< 10% error) for most of the data. This is significant as any errors in the correlation could be significantly magnified by using division to calculate the yield values.

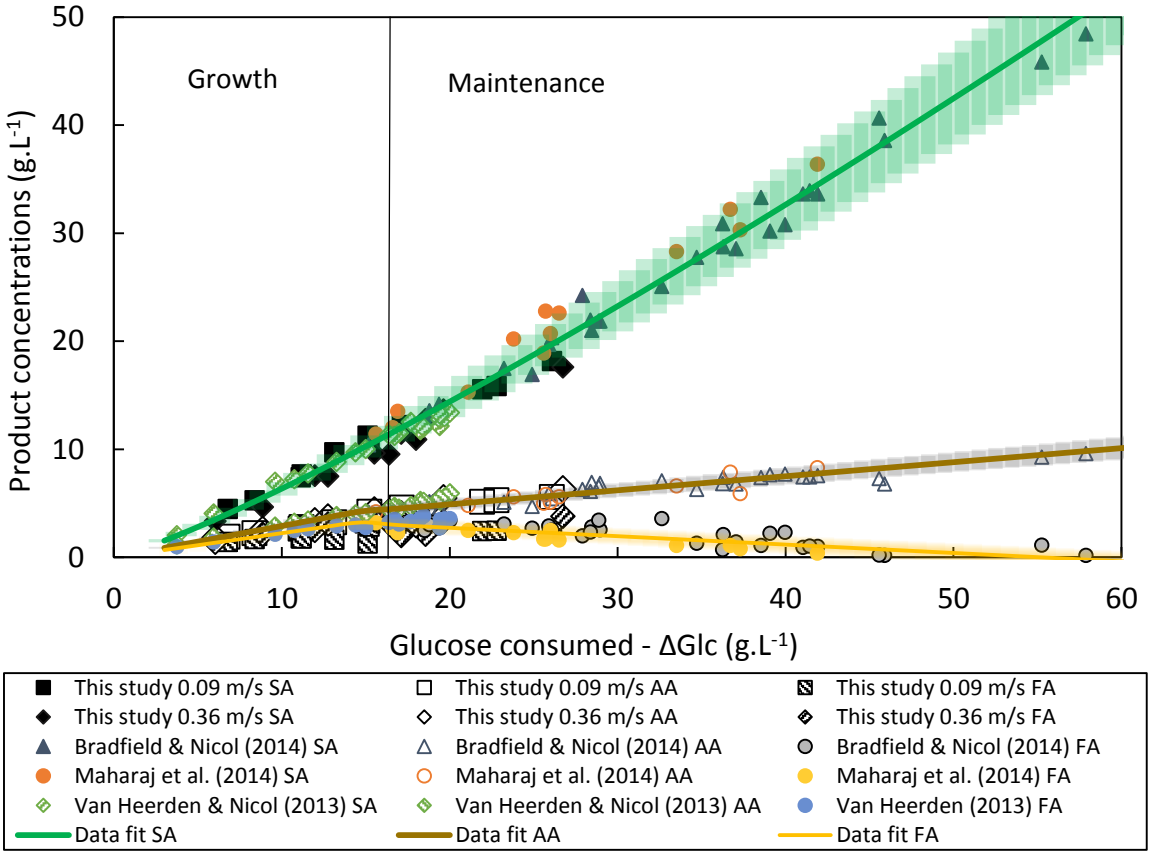

Figure 6-16: Measured concentrations for this study and from the literature (Van Heerden & Nicol, 2013; Bradfield & Nicol, 2014; Maharaj, Bradfield & Nicol, 2014), as well as empirically fitted curves (equations *(6-18)* to *(6-20)*) against the respective ΔGlc. The empirical curves show the 10% absolute relative error region.

From *FIGURE 6-15* and *FIGURE 6-16* it can be observed that during the growth metabolism (ΔGlc < 17 g.L^{-1}), the lower shear condition (0.09 m.s^{-1}) had a slightly higher $Y_{Glc,SA}$ (0.63–0.73 g.g^{-1}) compared with the higher shear condition which had a lower $Y_{Glc,SA}$ (0.53–0.63 g.g^{-1}). This is

similar to the metabolic shift as a function of shear velocity observed in *FIGURE 5-3* (Section *5.2.2* on page *5-5*). For the maintenance-driven metabolism (ΔGlc > 17 $g.L^{-1}$), the distinct separation between the results disappeared, indicating that the shear conditions played a significantly smaller role in the metabolism.

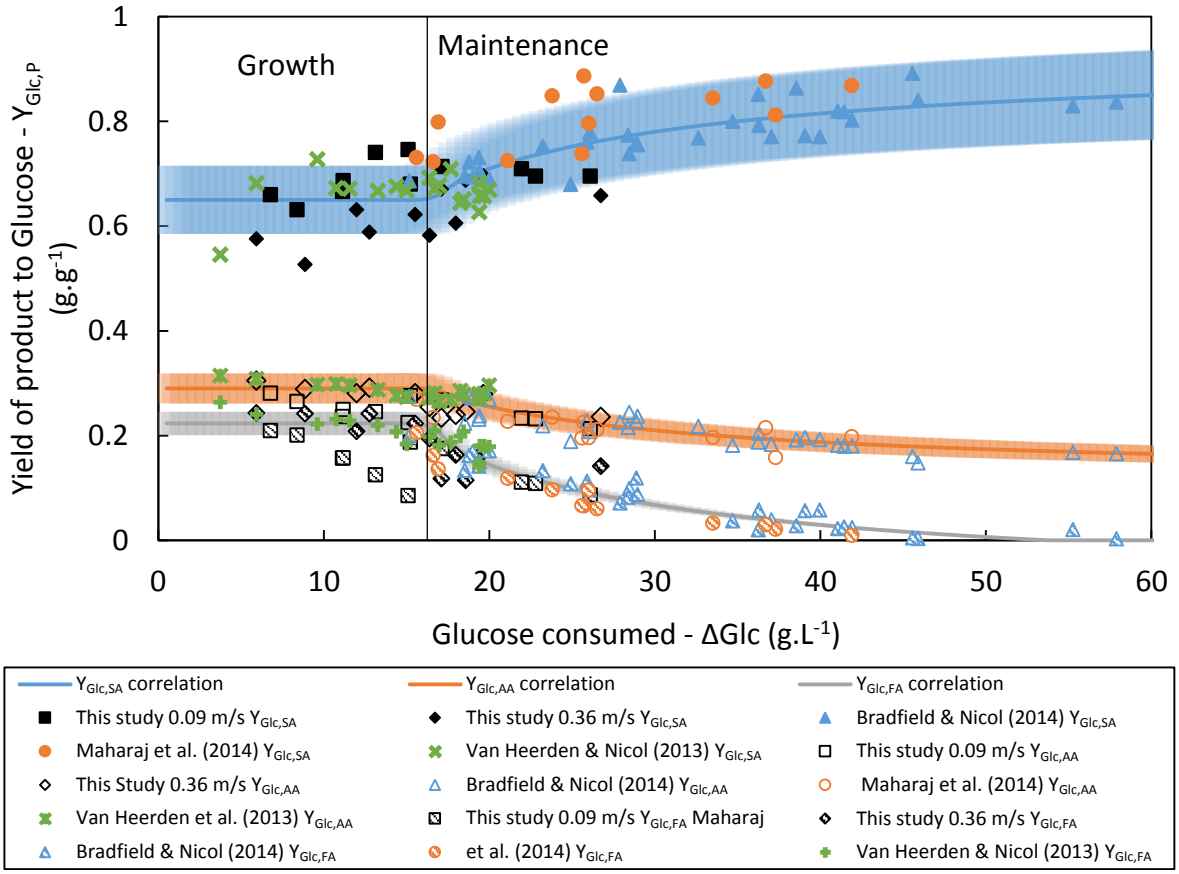

Figure 6-17: Product yield from glucose as a function of the consumed glucose for this study and from studies in the literature (Van Heerden & Nicol, 2013; Bradfield & Nicol, 2014; Maharaj, Bradfield & Nicol, 2014). In addition, the theoretical yield curves (equations *(6-21)* to *(6-23)*) are shown, as well as the ± 10% error regions.

In order to determine the metabolic flux of components within the reactor, a black box component balance was performed over the system (Section *B.XII* on page *B-16*). This was similar to the black box model shown in Section *B.X* on page *B-13*. However, in this case PA was included in the calculation due to the significant underprediction when the mass balance was calculated using only the products SA, AA, FA, CO_2 and H_2O (*FIGURE 6-6*). The black box model is described in Section *B.XII* on page *B-16* and the unknown yields ($Y_{Glc,PA}$, Y_{CO2}, Y_{H2O}) were determined using matrix solution software to solve equation *(B-31)* by specifying the product yields calculated from equations *(6-21)* to *(6-23)*. The results are shown in *FIGURE 6-18*. This figure indicates the increase in $Y_{Glc,SA}$, with the corresponding decrease in $Y_{Glc,AA}$ and $Y_{Glc,FA}$, observed in *FIGURE 6-17*. Interestingly, the theoretical $Y_{Glc,PA}$ remained nearly constant (a slight

increase was observed), supporting the observation that the mass balances were constantly underpredicted by approximately the same fraction for all values of ΔGlc.

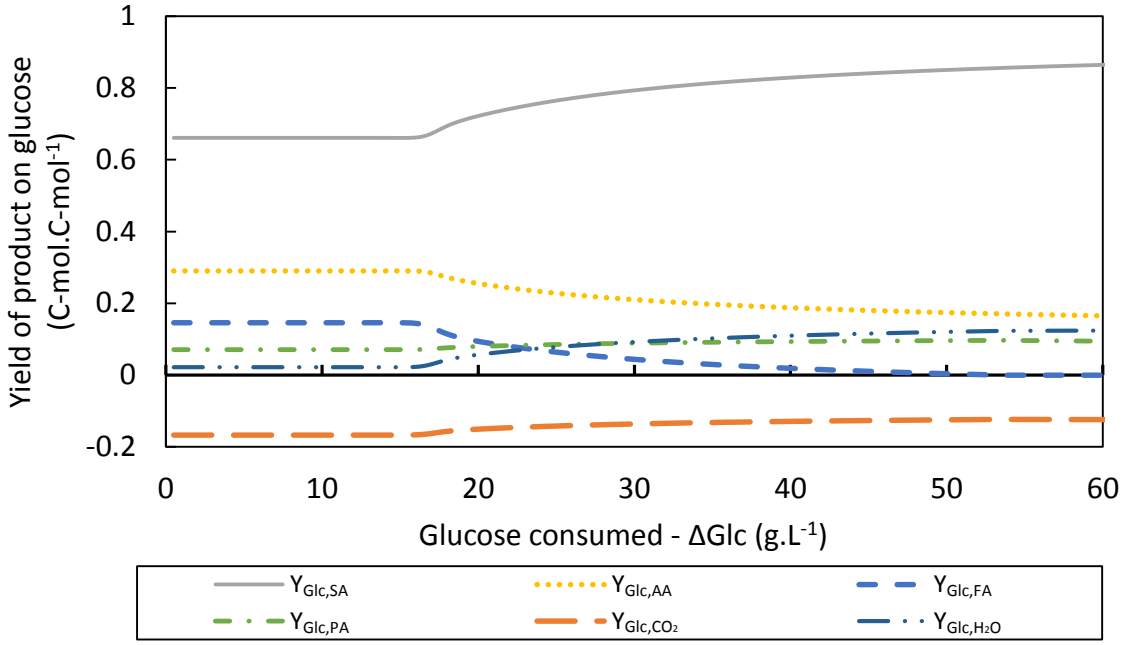

Figure 6-18: Yields of all catabolic products as solved from the black box mass balance by solving equation *(B-31)*. The $Y_{Glc,SA}$, $Y_{Glc,AA}$ and $Y_{Glc,FA}$ were specified from equations *(6-21)* to *(6-23)*, while the $Y_{Glc,PA}$, $Y_{GLc,CO2}$ and $Y_{Glc,H2O}$ were determined from the black box mass balance.

An additional analysis, using the data obtained in *FIGURE 6-18*, is a flux analysis of the glucose in the system. Using equations *(6-1)* to *(6-3)* and *(6-14)*, the flux of glucose as directed towards the various products gave a clearer visualisation of the metabolism in the cells within the reactor. The flux equations are repeated below as a visual aid:

$$v_1: CH_2O\ (Glc) + \frac{1}{3}CO_2 + \frac{1}{3}NADH \rightarrow \frac{4}{3}CH_{\frac{3}{2}}O(SA) + \frac{5}{9}ATP \quad (6\text{-}1)$$

$$v_2: CH_2O\ (Glc) \rightarrow \frac{2}{3}CH_2O\ (AA) + \frac{1}{3}CO_2 + \frac{2}{3}NADH + \frac{2}{3}ATP \quad (6\text{-}2)$$

$$v_3: CH_2O\ (Glc) \rightarrow \frac{2}{3}CH_2O\ (AA) + \frac{1}{3}CH_2O_2(FA) + \frac{1}{3}NADH + \frac{2}{3}ATP \quad (6\text{-}3)$$

$$v_5: CH_2O\ (Glc) \rightarrow CH_{\frac{4}{3}}O\ (PA) + \frac{1}{3}NADH + \frac{1}{3}ATP \quad (6\text{-}14)$$

The flux distribution within the reactor is shown in *FIGURE 6-19*, from which it can be seen that the flux of glucose during the growth phase was almost equally distributed between the formation of AA via the *pfl* route (v_3) and the production of SA (v_1). As the growth ceased (at ΔGlc > 17 g.L^{-1}), the distribution of glucose changed, with a significantly larger v_1 and a marked

decrease in the overall production of AA ($v_2 + v_3$). The flow of glucose via v_3 terminated, while the total flux of AA via the *pdh/fdh* route (v_2) increased to a value of approximately half of the original value at the ΔGlc ≈ 17 $g.L^{-1}$. The flux of glucose to pyruvate (v_5) increased slightly from about 0.07 $g.g^{-1}$ to around 0.1 $g.g^{-1}$.

The slight inflection observed in v_2 after the point when v_3 becomes inactive is a result of the continuously increased v_1, as well as a slight increase in the flux of glucose towards excess CO_2 production (equation *(6-24)*). The excess CO_2 is defined as the amount of CO_2 predicted in the black box mass balance that cannot be accounted for in the flux model (equations *(6-1)* to *(6-3)* and *(6-14)*). The excess CO_2 was calculated using equation *(6-24)*.

$$excess\ CO_2 = \frac{1}{3}v_2 - \frac{1}{3}v_1 \qquad (6\text{-}24)$$

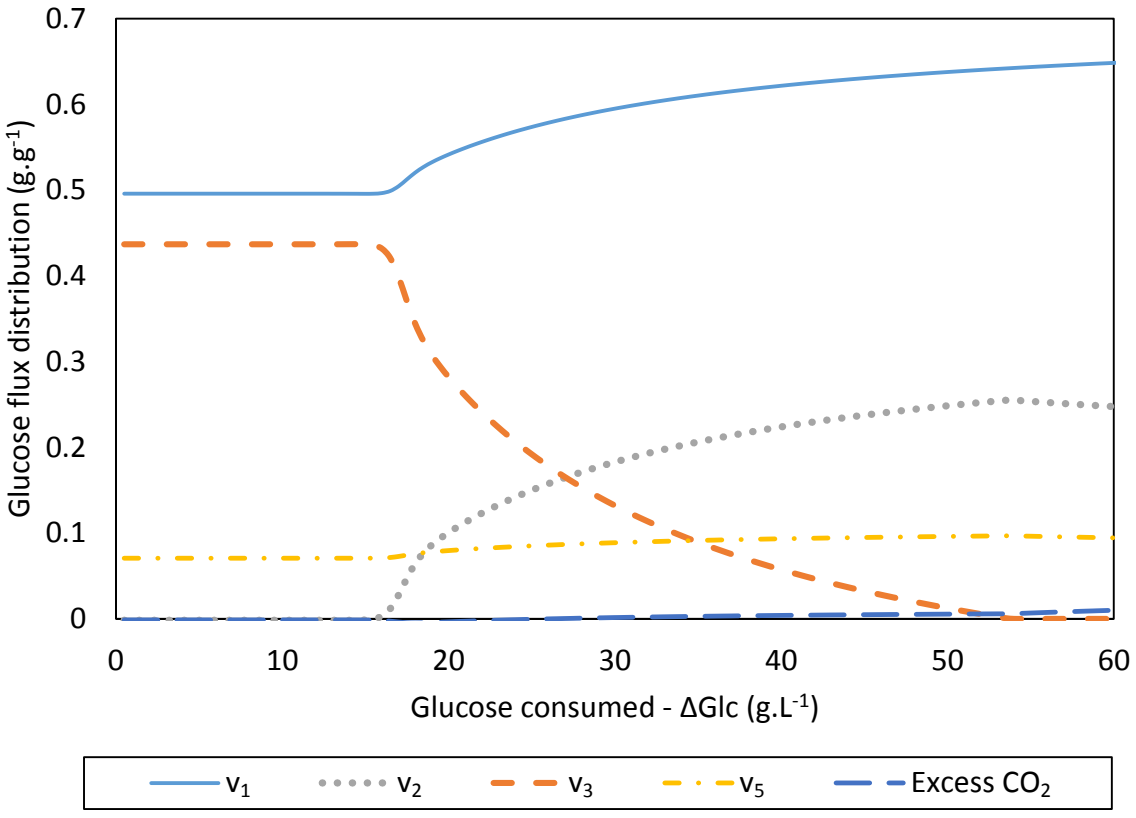

Figure 6-19: Flux distribution of glucose directed to SA (v_1), AA via *pdh/fdh* (v_2), AA via *pfl* (v_3), PA (v_5) and excess CO_2, as determined from the black box mass balance, and calculated using equation *(6-24)*.

The source of the excess CO_2 is uncertain. However, it could possibly be a result of activity in the pentose phosphate pathway (PPP), which was found to be active during ^{13}C pathway analysis performed by McKinlay et al. (2007). The flux model for the PPP is shown in equation

(6-25). The NADPH can consequently be converted to NADH using the transhydrogenase enzyme which was found to be active in *A. succinogenes* (McKinlay et al., 2007; McKinlay & Vieille, 2008). According to Bradfield and Nicol (2014), an active PPP is highly desirable within the metabolism of *A. succinogenes* as this provides a significant boost in reducing power (equation *(6-25)*) and could therefore increase $Y_{Glc,SA}$ significantly.

$$CH_2O\ (Glc) \rightarrow CO_2 + 2NADPH \tag{6-25}$$

To verify that the source of the CO_2 was the PPP, an NADH balance was performed over the system. If the influence of excess CO_2 production on the overall NADH balance was found to be insignificant (< 5%), the excess would be classified as experimental/numerical errors. However, in the case of a significant NADH imbalance (> 5%), this CO_2 could not be ignored and might very well play a significant role in the metabolism. *FIGURE 6-20* shows the ratio of produced over consumed NADH. A ratio of one indicates a perfect balance between the produced and consumed NADH.

From *FIGURE 6-20* it can be seen that at low ΔGlc, there is an overproduction of NADH. This overproduction is approximately 2%, with an increase to about 5% at the critical ΔGlc ≈ 17 $g.L^{-1}$. An overproduction of NADH is not unexpected within the region where growth is possible as is has been shown that NADH is required for growth of the bacterium. At ΔGlc > 17 $g.L^{-1}$ the overproduction decreases to zero and then becomes an underproduction of NADH. Up to ΔGlc ≈ 50 $g.L^{-1}$, the NADH balance was observed to be > 95% of the perfect NADH balance. This shows that the assumption that PA is produced during fermentation is highly likely to be correct due to the mass balance and NADH balance which are satisfied by this component.

An NADH underprediction of greater than 5% was observed for ΔGlc > 50 $g.L^{-1}$ and an underprediction of as much as 10% was observed for ΔGlc ≈ 60$g.L^{-1}$. This indicates that the PPP might very well be a significant pathway for additional NADH production. Especially at significantly high ΔGlc values, the production of NADH via v_5 is not sufficient to account for the increase in SA yield at ΔGlc > 50 $g.L^{-1}$, and an additional source such as the PPP might also play a role. This is, however, not certain as the production of PA itself is an educated guess that needs to be thoroughly tested before the influence of the PPP can be properly estimated.

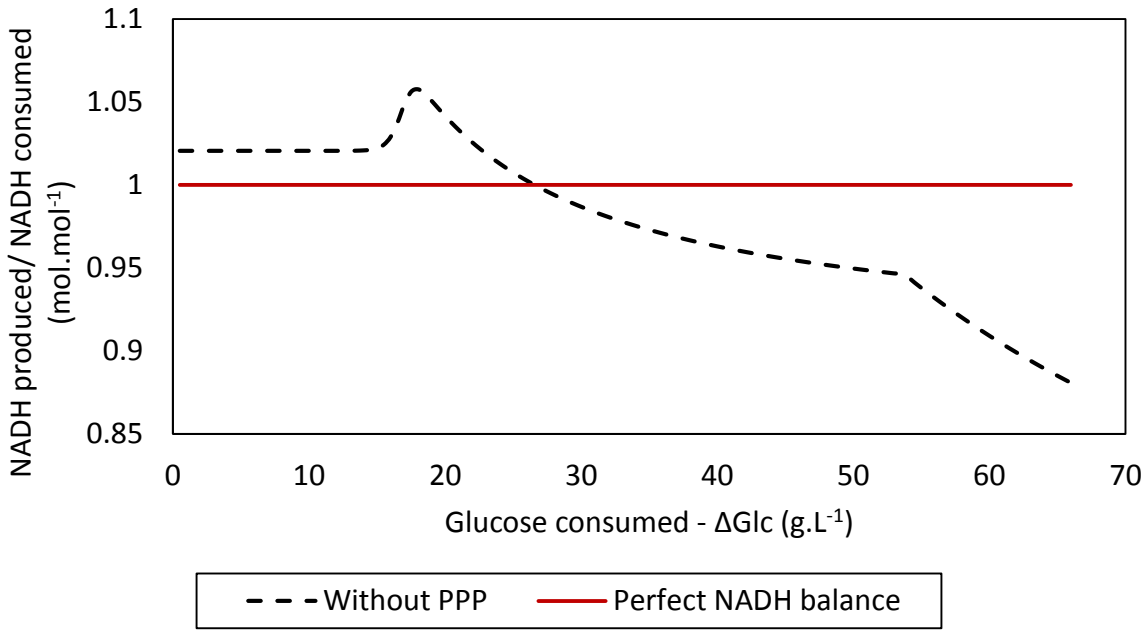

Figure 6-20: Ratio of NADH produced to NADH consumed during fermentation, against the glucose consumed, assuming no PPP activity (equation *(6-25)*). The line designated "Perfect NADH balance" is the line at which all NADH produced is consumed within the catabolism.

Assuming that PA was produced in addition to the measured products, namely SA, AA and FA, the total ATP produced in this study as well as in studies from the literature (Van Heerden & Nicol, 2013; Bradfield & Nicol, 2014; Maharaj, Bradfield & Nicol, 2014) was calculated from equations *(6-1)* to *(6-3)* and *(6-14)*, and the results are shown in *FIGURE 6-21*. The PA for each individual data point was calculated by applying the black box mass balance, as discussed in Section *B.XII* on page *B-16*, to the measurements.

$$v_1: CH_2O\ (Glc) + \frac{1}{3}CO_2 + \frac{1}{3}NADH \rightarrow \frac{4}{3}CH_{\frac{3}{2}}O(SA) + \frac{5}{9}ATP \quad (6\text{-}1)$$

$$v_2: CH_2O\ (Glc) \rightarrow \frac{2}{3}CH_2O\ (AA) + \frac{1}{3}CO_2 + \frac{2}{3}NADH + \frac{2}{3}ATP \quad (6\text{-}2)$$

$$v_3: CH_2O\ (Glc) \rightarrow \frac{2}{3}CH_2O\ (AA) + \frac{1}{3}CH_2O_2(FA) + \frac{1}{3}NADH + \frac{2}{3}ATP \quad (6\text{-}3)$$

$$v_5: CH_2O\ (Glc) \rightarrow CH_{\frac{4}{3}}O\ (PA) + \frac{1}{3}NADH + \frac{1}{3}ATP \quad (6\text{-}14)$$

It should be stressed that the values used in the black box model were the experimental measurements (C_{SA}, C_{AA}, C_{FA}) and not the correlations (equations *(6-21)* to *(6-23)*) determined in *FIGURE 6-16*. *FIGURE 6-21* clearly illustrates that a near-perfect linear fit of the yield of ATP to ΔGlc (r^2 = 0.997) was obtained, $Y_{Glc,ATP}$ = 18.9 mmol ATP.(g ΔGlc). This result is supported by

the observation in equations (6-1) to (6-3) that the ATP production was nearly equal (5/9 mol ATP.(C-mol ΔGlc)$^{-1}$ vs 2/3 mol ATP.(C-mol ΔGlc)$^{-1}$) and therefore a change in metabolism in which more SA is produced with increasing ΔGlc (FIGURE 6-16) is probably not linked to energetic considerations. If the metabolism change was a result of a change in the energy requirements, a significant shift in the ATP yield from ΔGlc would have been observed.

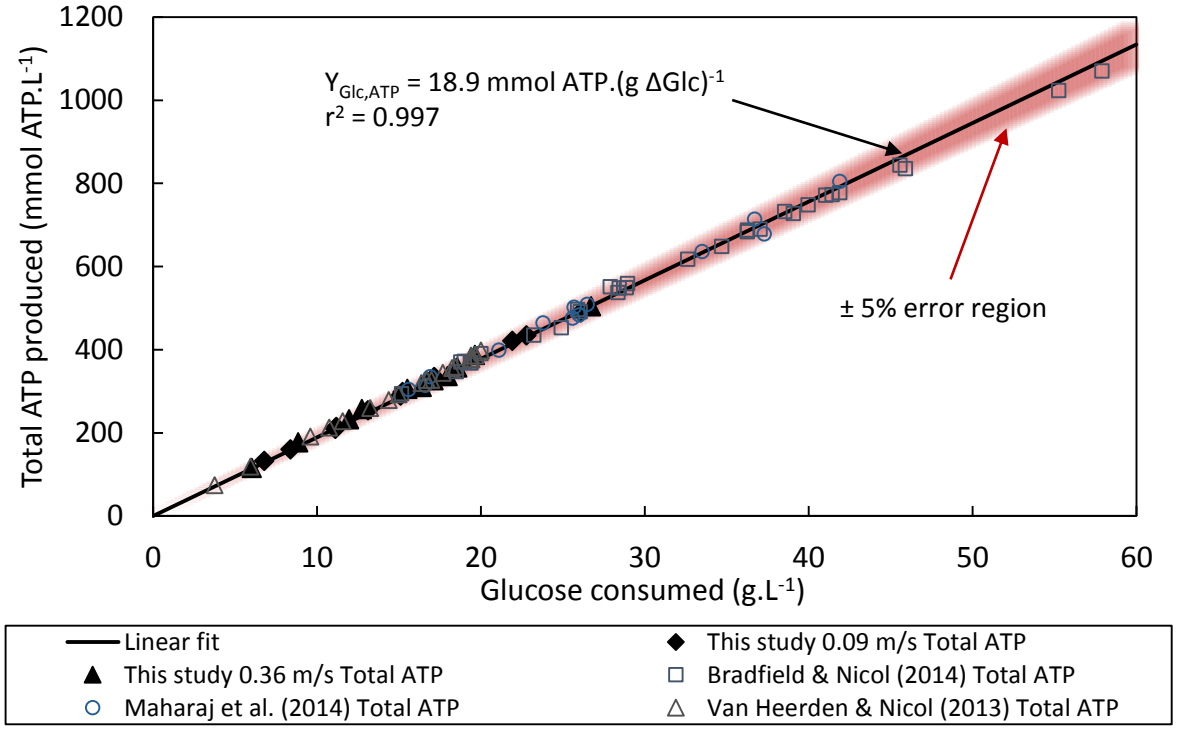

Figure 6-21: The total calculated ATP produced (equations (6-1) to (6-3) and (6-14)) in this study and in studies from the literature (Van Heerden & Nicol, 2013; Bradfield & Nicol, 2014; Maharaj, Bradfield & Nicol, 2014). It was assumed that PA was produced as a by-product and it was calculated by solving the black box model in Section B.XII on page B-16. Linear fits of the data and of the ± 5% error region are shown.

6.4 Conclusions

This study showed that biofilms of *A. succinogenes* provide a dual advantage when compared with chemostat fermentation of the same organism. The volumetric productivities (q_{SA}) of the reactor during biofilm conditions were as much as an order of magnitude greater than during chemostat conditions (FIGURE 6-12). This was due largely to significantly higher cellular biomass concentrations in the biofilm reactor than in the chemostat reactor. In addition, a major increase in the yield of SA on glucose was observed during biofilm operation ($Y_{Glc,SA}$ > 0.65 g.g^{-1}) as opposed to chemostat conditions ($Y_{Glc,SA}$ ≈ 0.48 g.g^{-1}). The significant increases in yield were confirmed by other *A. succinogenes* biofilm studies (Van Heerden & Nicol, 2013;

Bradfield & Nicol, 2014; Maharaj, Bradfield & Nicol, 2014). With regard to the differences between shear conditions in the reactor, a significantly higher EPS fraction (0.50 ± 0.05 $g.g^{-1}$) at lower shear conditions, as opposed to the lower EPS fraction (0.16 ± 0.02 $g.g^{-1}$) during the higher shear runs, was observed during the experiments. This corresponds to the observations made in Chapter 5 with regard to the predicted decrease in EPS fraction with increasing shear velocities (TABLE 5-2). However, this change in EPS fraction for the respective biofilm runs did not represent a significant change in the metabolism, as postulated in Chapter 5. The difference between the observations in Chapter 5 and those in this chapter are probably a result of differences between the maintenance and growth metabolisms for the respective systems. The system discussed in Chapter 5 was a growing system, with biomass being removed and replenished continuously during fermentation. This reflected in the continuous NADH requirements in the system, and in the changes in metabolism observed as a function of the shear velocity.

In this chapter, the significant differences in observed metabolism between the chemostat and biofilm reactors were attributed to metabolic differences as a result of biomass growth conditions (C_{SA} < 10 $g.L^{-1}$) vs. maintenance conditions (C_{SA} > 10 $g.L^{-1}$). Chemostat fermentation was, per definition, mostly growth-related, and it was observed that significant amounts of complex nitrogen sources (NS) were incorporated into the planktonic biomass (TABLE 6-3). A significant catabolic overproduction of NADH (catabolic NADH produced/catabolic NADH consumed > 1) was observed in the chemostat reactor, indicating that the NADH requirements for biomass production were substantial. This observation was supported by the growth metabolism described in Chapter 5.

It was shown that the NADH and ATP requirements decreased with increasing reliance on NS for biomass production, indicating that the NADH/ATP was directed towards amino acid/protein synthesis (TABLE 6-3). The specific growth function (equation (6-12)) derived for the chemostat data is in close agreement with results from the literature (FIGURE 2-5). This growth function stresses the extreme product inhibition experienced by the organism, and therefore should be taken into account during initial biofilm growth/development periods.

The r_{SA}* in biofilm reactors, for C_{SA} > 10 $g.L^{-1}$, was shown to follow a similar trend (equation (6-13)), irrespective of the shear conditions in the reactor. The trend illustrated that sessile cells operate predominantly under maintenance conditions and that the metabolic activity of

the sessile cell populations (EPS excluded) decreased at higher acid titres. A comparison of the volumetric production of SA in this study and those from the literature (Van Heerden & Nicol, 2013; Bradfield & Nicol, 2014; Maharaj, Bradfield & Nicol, 2014; Yan, Zheng, Tao, et al., 2014) showed that a hyperbolic "productivity boundary", defined by equation *(6-16)*, was present for all studies analysed. This boundary defined a maximum q_{SA} (q_{SA}^{max}) possible within the *A. succinogenes* biofilm reactor system during continuous operation. Considering the q_{SA}^{max} related to the r_{SA}* (equation *(6-13)*) by a cellular biomass (x_t*), it was argued that an expression of the maximum x_t* as a function of the C_{SA} can be derived from the quotient of equations *(6-16)* and *(6-13)*. This expression was shown in equation *(6-17)* and it predicted the region for the experimentally determined cellular biomass amounts reasonably well (*FIGURE 6-14*).

In order to determine whether the r_{SA}* trend (equation *(6-13)*) or the q_{SA}^{max} (equation *(6-16)*) was applicable to transient conditions, batch operation using biofilm reactors was employed. The biofilm in the batch reactors was grown during continuous operation. It was shown that during batch fermentation, the r_{SA}* and q_{SA} in the respective runs initially remained relatively constant as the C_{SA} increased, before eventually decreasing as the C_{SA} increased. This indicated a lag in the inhibiting effect of the product on the transient organism, which resulted in a crossing of the volumetric productivity boundary during one of the batch runs. At a sufficiently high C_{SA} (C_{SA} > 45 g.L^{-1}), the batch runs had nearly the same r_{SA}*, indicating that the inhibition "caught up" with the transient behaviour and therefore all biomass performed the same for any further increase in C_{SA}.

This lag period, as well as a q_{SA} higher than the q_{SA}^{max}, indicated that, given a sufficiently high cellular biomass (equation *(6-17)*), a q_{SA}^{max}, i.e. on the productivity boundary, could be maintained for a significant increase in C_{SA} by using a batch or repeat-batch reaction system. The average q_{SA} would therefore be notably higher than that in an equivalent continuous biofilm reactor.

The metabolic product distribution was analysed using a black box mass balance (Section *B.X* on page *B-13*) and it was found that a constant underprediction of approximately 10% in the amount of glucose consumption was present in this study and in the studies from the literature (Van Heerden & Nicol, 2013; Bradfield & Nicol, 2014; Maharaj, Bradfield & Nicol, 2014). It was hypothesised that the "missing" glucose was produced in the form of pyruvic acid (PA),

which has an HPLC peak at the same time as glucose, is therefore obscured by the glucose peak and yields a net NADH during production. This net NADH could theoretically resolve the redox imbalance observed as a result of the increased SA to AA ratios.

The measured concentrations of SA, AA and FA for this study, as well as in the studies from the literature (Van Heerden & Nicol, 2013; Bradfield & Nicol, 2014; Maharaj, Bradfield & Nicol, 2014), were plotted against glucose consumption and showed remarkable similarities between the respective studies. Correlations of the data (equations *(6-18)* to *(6-20)*) were obtained and fitted the experimental results to within a 10% absolute relative error. It was observed that for growth conditions ($\Delta Glc < 17$ g.L^{-1}), the lower shear conditions in this study had a slightly higher $Y_{Glc.SA}$ (0.63–0.73 g.g^{-1}) than that for the higher shear($Y_{Glc.SA}$ = 0.53–0.63 g.g^{-1}). This corresponds to the results observed in Chapter 5. However, the constant yields observed for the maintenance metabolism ($\Delta Glc > 17$ g.L^{-1}) indicate an independence of $Y_{Glc,SA}$ with regard to the shear conditions in the reactor. This difference is probably a result of the maintenance metabolism in this system vs. the growth metabolism in Chapter 5.

From these correlations the yields of product on glucose (equations *(6-21)* to *(6-23)*) and glucose fluxes (*FIGURE 6-18*) to the various metabolic products, including PA, were determined using a black box mass balance (Section *B.XII* on page *B-16*). The results indicated that a significant portion of the glucose that directed towards AA at low glucose consumptions, was redirected towards SA and a very small increase in the production of PA at high glucose consumptions. The production of excess CO_2 (unaccounted-for CO_2) from the black box model prompted the hypothesis that the pentose phosphate pathway (PPP) produced small amounts of CO_2 during fermentation. This theory was tested and proved reasonable, for significantly high ΔGlc values ($\Delta Glc > 50$ g.L^{-1}), based on the NADH balance of the glucose fluxes shown in *FIGURE 6-18*.

Finally, the total ATP production for each individual experimental data point in this study and in the results from the literature (Van Heerden & Nicol, 2013; Bradfield & Nicol, 2014; Maharaj, Bradfield & Nicol, 2014) was calculated, using equations *(6-1)* to *(6-3)* and *(6-14)*. A black box mass balance (Section *B.XII* on page *B-16*) was used to calculate the PA at each point. These results were plotted against the glucose consumed (*FIGURE 6-21*) and showed

that the total ATP fitted a linear trend of 18.9 mmol ATP.(g ΔGlc) (r^2 = 0.997). The good agreement with the linear fits indicates that the change in metabolism with increasing ΔGlc (*FIGURE 6-16*) is probably not linked to energetic requirements.

From a general biofilm reactor perspective, this study has shed new light on the possible advantages of single-culture biofilm fermentation. The observed variations in the flux distributions between the growth and maintenance-related metabolisms of this organism might apply to other biofilm producers. High cell densities are naturally achieved by biofilm-forming species and cell-retainment equipment is accordingly redundant. This well-established advantage, in combination with higher carbon yields, will contribute to the favouring of the biofilm fermenter in years to come.

CHAPTER 7
CONCLUSIONS

This thesis has explored the behaviour of biofilm fermenters through comparison of the results from two case studies: a two-phase *L. rhamnosus* study and a three-phase *A. succinogenes* study. The studies were performed in a novel tubular fermenter which provided homogeneously controlled shear. Fundamental investigation of the respective biofilm fermentation systems was done through the *in situ* removal of the biofilm biomass. This was accomplished either by increasing the shear stresses in the reactor or by mechanical friction through the soft silicone tubing. In addition, the ability to control the shear velocity allowed chemostat operation under high-shear conditions, as well as the study of biofilms under varying shear stresses. The case studies focused specifically on the following four parameters: volumetric production characteristics, specific production characteristics, the metabolic product distributions with corresponding redox analysis, and biofilm compositions as a function of shear conditions.

With regard to the volumetric production rates of lactic acid (q_{LA}) in the *L. rhamnosus* case study, an increase in q_{LA} was observed to correspond to a decrease in shear stresses. Specifically, a maximum q_{LA} of 4.46 $g.L^{-1}.h^{-1}$ was measured in the chemostat, while maximum q_{LA} values of 5.97, 6.45 and 8.04 $g.L^{-1}.h^{-1}$ were obtained in the 0.55, 0.36 and 0.19 $m.s^{-1}$ biofilm runs respectively.

Concerning the succinic acid volumetric production rates (q_{SA}) in the *A. succinogenes* case study, the biofilm q_{SA} values were observed to be nearly an order of magnitude higher in comparison with the results obtained from chemostat operation. Whereas a maximum $q_{SA} \approx 1.8$ $g.L^{-1}.h^{-1}$ was measured for chemostat operation, q_{SA} values of between 7 and 17 $g.L^{-1}.h^{-1}$ were obtained from the biofilm fermenters. This increase was attributed to the observation that the cellular biomass concentrations in the latter fermenters were significantly higher than those in chemostat conditions. Notably, this improvement was significantly larger than

that observed during the *L. rhamnosus* fermentation, which was probably due to a significantly larger increase in biomass concentrations when comparing the chemostat with the biofilm conditions for the two case studies.

With regard to the specific production rates in the two case studies, the differences found were probably a result of the variations in their respective metabolic states. The *L. rhamnosus* system was shown to exhibit exclusively growth-related characteristics during fermentation, while the *A. succinogenes* fermentation study possessed both growth and maintenance-related metabolic features.

In the *L. rhamnosus* study, it was found that the specific lactic acid production rates, based on the total biomass concentration (including EPS) (r_{LA}), decreased with decreasing shear velocities. During chemostat operation a maximum $r_{LA} \approx 3.7$ g.g^{-1}.h^{-1} was measured, while in the lowest-shear biofilm runs, a maximum r_{LA} of less than 2 g.g^{-1}.h^{-1} was obtained. This indicated a change in the biofilm composition and predicted an increased fraction of inactive EPS in the biofilm with decreasing shear condition.

In the *A. succinogenes* study, the cell-based specific succinic acid production rates (r_{SA}*) under growth conditions ($C_{SA} > 10$ g.L^{-1}) were shown to be highly dependent on the shear conditions within the biofilm reactor; the r_{SA}* values exhibited an unexplained split in the trends between higher- and lower-shear conditions. In the lower-shear biofilm run, the r_{SA}* values increased exponentially with decreasing SA titre (C_{SA}) and a maximum r_{SA}* value of approximately 2.5 g.g^{-1}.h^{-1} was measured. During the higher-shear biofilm run, a decrease in the r_{SA}* values (1.0 to 0.4 g.g^{-1}.h^{-1}) corresponded to a decrease in C_{SA}.

In contrast, under maintenance conditions ($C_{SA} > 10$g.L^{-1}), the r_{SA}* and the r_{ATP}* values appeared to be independent of shear conditions in the biofilm fermenter. The results from both the shear conditions followed a positively displaced exponential decay curve which decreased from $r_{SA}^* \approx 1$ g.g^{-1}.h^{-1} and $r_{ATP}^* \approx 30$ mmol ATP.(g.h)$^{-1}$, at $C_{SA} \approx 10$ g.L^{-1}, to asymptotic values of $r_{SA}^* \approx 0.59$ g.g^{-1}.h^{-1} and $r_{ATP}^* \approx 16.1$ mmol ATP.(g.h)$^{-1}$ at significantly high succinic acid titres. The asymptotic values indicated the non-growth-related cellular production rates of *A. succinogenes*.

The metabolic product distributions in both the case studies were highly dependent on redox requirements. In the *L. rhamnosus* study, it was observed that there was a significant NADH

requirement for chemostat operation. This was satisfied by the production of acetoin in the metabolism: during the chemostat operation, a $Y_{Glc,LA}$ = 0.75 g.g^{-1} and a $Y_{Glc,Acn}$ = 0.074 g.g^{-1} were measured. As the shear velocities decreased, the NADH requirements also decreased and the metabolism shifted to produce more lactic acid during fermentation; at the lowest-shear conditions, a $Y_{Glc,LA}$ = 0.90 g.g^{-1} with a corresponding $Y_{Glc,Acn}$ = 0.017 g.g^{-1} was observed. It was hypothesised that the change in NADH requirements corresponded to the difference between cellular and EPS biosynthesis, with an increase in NADH requirements being linked to a higher cellular biomass production.

In the *A. succinogenes* study, there appeared to be a very distinct difference between the metabolic product distribution under growth (C_{SA} < 10 g.L^{-1}, ΔGlc < 17 g.L^{-1}) and maintenance (C_{SA} > 10 g.L^{-1}, ΔGlc > 17 g.L^{-1}) conditions. Under growth conditions, a significant increase in the yield of SA on glucose was observed with decreasing shear velocities, as was evident by comparing the chemostat ($Y_{Glc,SA}$ ≈ 0.48 g.g^{-1}), the higher-shear biofilm ($Y_{Glc,SA}$ ≈ 0.53–0.63 g.g^{-1}), and the lower-shear biofilm runs ($Y_{Glc,SA}$ ≈ 0.63–0.73 g.g^{-1}). During chemostat operation, a significant anabolic NADH consumption was observed, while for the biofilm study a decrease in the desired anabolic NADH was observed. This indicates a change in redox requirements, with a corresponding change in metabolic flux.

Under maintenance conditions (C_{SA} > 10 g.L^{-1}, ΔGlc > 17 g.L^{-1}), the results from this study and those from the literature (Van Heerden & Nicol, 2013; Bradfield & Nicol, 2014; Maharaj, Bradfield & Nicol, 2014) followed a remarkably similar trend, which appeared to be independent of the shear conditions in the biofilm reactor. Under these conditions a mass balance underprediction and an NADH underproduction were observed. It was hypothesised that the "lost" mass and required NADH could be accounted for by pyruvic acid, a metabolite. However, this change in metabolism, which necessitates the production of an additional component, illustrates the significant difference between the growth and maintenance metabolisms.

The biofilm compositions (EPS fractions) for both the case studies were strongly affected by the shear conditions in the fermenter. In the *L. rhamnosus* study, the EPS fractions at different shear velocities were estimated by using a simplified model. The estimated fractions of EPS increased with decreasing shear velocities, with the lowest EPS fraction (0.09 g.g^{-1}) predicted at the shear of 0.55 m.s^{-1}, increasing to an EPS fraction of 0.70 g.g^{-1} at a shear velocity of

0.19 $m.s^{-1}$. In the *A. succinogenes* study, an EPS quantification technique was developed in order to distinguish between the cellular biomass and the EPS by base-hydrolysis of the total biomass sample and subsequent separation of the EPS fraction. Examination of the EPS fraction at the different shear conditions showed that at lower-shear conditions, a significantly higher EPS fraction (0.50 ± 0.05 $g.g^{-1}$) was measured, as opposed to the lower EPS fraction (0.16 ± 0.02 $g.g^{-1}$) during the higher-shear runs. These observations correspond to the results obtained in the *L. rhamnosus* case study and indicate a significant change in the biofilm morphology as a result of the shear conditions in the reactor.

From a general biofilm fermenter perspective, the work presented in this thesis yielded original insights into the characteristics of biofilm fermenters with respect to the underlying mechanisms that govern single-culture biofilm fermentation.

CHAPTER 8
REFERENCES

Abdel-Rahman, M.A., Tashiro, Y. & Sonomoto, K. 2011. Lactic acid production from lignocellulose-derived sugars using lactic acid bacteria: Overview and limits. *Journal of biotechnology*. 156(4):286–301. DOI: 10.1016/j.jbiotec.2011.06.017.

Agathos, S.N., Hellin, E., Ali-Khodja, H., Deseveaux, S., Vandermesse, F. & Naveau, H. 1997. Gas-phase methyl ethyl ketone biodegradation in a tubular biofilm reactor: microbiological and bioprocess aspects. *Biodegradation*. 8(4):251–264. DOI: 10.1023/A:1008257729749.

An, M. & Lo, K. V. 2001. Domestic wastewater treatment using immobilized sludge fluidized-bed reactors. *Journal of environmental science and health, Part A*. 36(5):819–831. DOI: 10.1081/ESE-100103763.

Andrews, G.F. & Fonta, J.P. 1989. A fluidized-bed continuous bioreactor for lactic acid production. *Applied biochemistry and biotechnology*. 20-21(1):375–390. DOI: 10.1007/BF02936497.

Andries, M., Van Beveren, P.C., Goffin, O. & Masschelein, C.A. 1996. Design and application of an immobilized loop bioreactor for continuous beer fermentation. *Progress in biotechnology*. 11:672–678. DOI: 10.1016/S0921-0423(96)80091-8.

Annachhatre, A.P. & Bhamidimarri, S.M.R. 1992. Microbial attachment and growth in fixed-film reactors: Process startup considerations. *Biotechnology advances*. 10(1):69–91. DOI: 10.1016/0734-9750(92)91352-F.

Audet, P., Paquin, C. & Lacroix, C. 1988. Immobilized growing lactic acid bacteria with κ-carrageenan — locust bean gum gel. *Applied microbiology and biotechnology*. 29(1):11–18. DOI: 10.1007/BF00258344.

Badel, S., Bernardi, T. & Michaud, P. 2011. New perspectives for Lactobacilli exopolysaccharides. *Biotechnology advances*. 29(1):54–66. DOI: 10.1016/j.biotechadv.2010.08.011.

Bahrami, M. 2011. *Viscous flow in ducts*. Vancouver. Available: www.sfu.ca/~mbahrami/ENSC 283/Notes/Viscous Flow in Ducts.pdf.

Bai, G., Bee, J.S., Biddlecombe, J.G., Chen, Q. & Leach, W.T. 2012. Computational fluid dynamics (CFD) insights into agitation stress methods in biopharmaceutical development. *International journal of pharmaceutics*. 423(2):264–280. DOI: 10.1016/j.ijpharm.2011.11.044.

Bakke, R., Kommedal, R. & Kalvenes, S. 2001. Quantification of biofilm accumulation by an optical approach. *Journal of microbiological methods*. 44(1):13–26. DOI: 10.1016/S0167-7012(00)00236-0.

Bakker, D.P., Van der Plaats, A., Verkerke, G.J., Busscher, H.J. & Van der Mei, H.C. 2003. Comparison of velocity profiles for different flow chamber designs used in studies of microbial adhesion to surfaces. *Applied and environmental microbiology*. 69(10):6280–6287. DOI: 10.1128/AEM.69.10.6280–6287.2003.

Banerjee, S., Hassenklöver, E., Kleijn, J.M., Cohen Stuart, M.A. & Leermakers, F.A.M. 2013. Interfacial tension and wettability in water-carbon dioxide systems: experiments and self-consistent field modeling. *The journal of physical chemistry. B*. 117(28):8524–8535. DOI: 10.1021/jp400940s.

Beloin, C. & Ghigo, J.M. 2005. Finding gene-expression patterns in bacterial biofilms. *Trends in microbiology*. 13(1):16–19. DOI: 10.1016/j.tim.2004.11.008.

Beloin, C., Roux, A. & Ghigo, J.M. 2008. *Escherichia coli* biofilms. *Current topics in microbiology and immunology*. 322:249–289. DOI: 10.1007/978-3-540-75418-3_12.

Benito de Cardenas, I.L., Ledesma, O.V. & Oliver, G. 1989. Effect of lactic acid on diacetyl and acetoin production by *Lactobacillus casei* subsp. *rhamnosus* ATCC 7469. *Current microbiology*. 18(6):351–354. DOI: 10.1007/BF01571127.

Benito de Cárdenas, I.L., Ledesma, O.V. & Oliver, G. 1987. Utilization of pyruvate in *Lactobacillus casei* subsp. *rhamnosus* ATCC 7469. *Current microbiology*. 15(5):259–264. DOI: 10.1007/BF01589377.

Benthin, S., Schulze, U., Nielsen, J. & Villadsen, J. 1994. Growth energetics of *Lactococcus cremoris* FD1 during energy-, carbon-, and nitrogen-limitation in steady state and transient cultures. *Chemical engineering science*. 49(5):589–609. DOI: 10.1016/0009-2509(94)85006-2.

Berčič, G. & Pintar, A. 1997. The role of gas bubbles and liquid slug lengths on mass transport in the Taylor flow through capillaries. *Chemical engineering science*. 52(21-22):3709–3719. DOI: 10.1016/S0009-2509(97)00217-0.

Bergmaier, D., Champagne, C.P. & Lacroix, C. 2005. Growth and exopolysaccharide production during free and immobilized cell chemostat culture of *Lactobacillus rhamnosus* RW-9595M. *Journal of applied microbiology*. 98(2):272–284. DOI: 10.1111/j.1365-2672.2004.02462.x.

Berry, A., Franco, C., Zhang, W. & Middelberg, A. 1999. Growth and lactic acid production in batch culture of *Lactobacillus rhamnosus* in a defined medium. *Biotechnology letters*. 21(2):163–167. DOI: 10.1023/A:1005483609065.

Beyenal, H. & Lewandowski, Z. 2002. Internal and external mass transfer in biofilms grown at various flow velocities. *Biotechnology progress*. 18(1):55–61. DOI: 10.1021/bp010129s.

Bleau, C., Monges, A., Rashidan, K., Laverdure, J.-P., Lacroix, M., Van Calsteren, M.-R., Millette, M., Savard, R., et al. 2010. Intermediate chains of exopolysaccharides from *Lactobacillus rhamnosus* RW-9595M increase IL-10 production by macrophages. *Journal of applied microbiology*. 108(2):666–675. DOI: 10.1111/j.1365-2672.2009.04450.x.

Botrous, A.E.F., Dahab, M.F. & Mihăltz, P. 2004. Nitrification of high-strength ammonium wastewater by a fluidized-bed reactor. *Water science and technology*. 49(5-6):65–71. Available: http://www.ncbi.nlm.nih.gov/pubmed/15137408 [2014, December 18].

Bradfield, M.F.A. & Nicol, W. 2014. Continuous succinic acid production by *Actinobacillus succinogenes* in a biofilm reactor: Steady-state metabolic flux variation. *Biochemical engineering journal*. 85:1–7. DOI: 10.1016/j.bej.2014.01.009.

Branda, S.S., Chu, F., Kearns, D.B., Losick, R. & Kolter, R. 2006. A major protein component of the *Bacillus subtilis* biofilm matrix. *Molecular microbiology*. 59(4):1229–1238. Available: http://dx.doi.org/10.1111/j.1365-2958.2005.05020.x.

Bretherton, F.P. 1961. The motion of long bubbles in tubes. *Journal of fluid mechanics*. 10(2):166–188. DOI: 10.1017/S0022112061000160.

Brink, H.G. & Nicol, W. 2014a. The influence of shear on the metabolite yield of *Lactobacillus rhamnosus* biofilms. *New biotechnology*. 31(5):460–467. DOI: 10.1016/j.nbt.2014.06.003.

Brink, H.G. & Nicol, W. 2014b. Succinic acid production with *Actinobacillus succinogenes*: rate and yield analysis of chemostat and biofilm cultures. *Microbial cell factories*. 13:111. DOI: 10.1186/s12934-014-0111-6.

Broadbent, J.R., McMahon, D.J., Welker, D.L., Oberg, C.J. & Moineau, S. 2003. Biochemistry, genetics, and applications of exopolysaccharide production in *Streptococcus thermophilus*: a review. *Journal of dairy science*. 86(2):407–23. DOI: 10.3168/jds.S0022-0302(03)73619-4.

Bruno-Bárcena, J.M., Ragout, A.L., Córdoba, P.R. & Siñeriz, F. 1999. Continuous production of L(+)-lactic acid by *Lactobacillus casei* in two-stage systems. *Applied microbiology and biotechnology*. 51(3):316–24. DOI: 10.1007/s002530051397.

Cai, W., Zhang, J., Zhang, X., Wang, Y. & Qi, X. 2013. Enhancement of CO_2 absorption under Taylor Flow in the presence of fine particles. *Chinese journal of chemical engineering*. 21(2):135–143. DOI: 10.1016/S1004-9541(13)60451-6.

Campesi, A., Cerri, M.O., Hokka, C.O. & Badino, A.C. 2009. Determination of the average shear rate in a stirred and aerated tank bioreactor. *Bioprocess and biosystems engineering*. 32(2):241–8. DOI: 10.1007/s00449-008-0242-4.

Cao, N., Du, J., Chen, C., Gong, C.S. & Tsao, G.T. 1997. Production of fumaric acid by immobilized *rhizopus* using rotary biofilm contactor. *Applied biochemistry and biotechnology*. 63-65:387–394. DOI: 10.1007/BF02920440.

Carvalho, M., Matos, M., Roca, C. & Reis, M. a M. 2014. Succinic acid production from glycerol by *Actinobacillus succinogenes* using dimethylsulfoxide as electron acceptor. *New biotechnology*. 31(1):133–139. DOI: 10.1016/j.nbt.2013.06.006.

Çengel, Y.A. & Cimbala, J.M. 2006. *Fluid mechanics: fundamentals and applications*. First ed. New York: McGraw Hill.

Cerning, J. 1990. Exocellular polysaccharides produced by lactic acid bacteria. *FEMS microbiology reviews*. 7(1-2):113–130. DOI: 10.1111/j.1574-6968.1990.tb04883.x.

Champagne, C.P., Gardner, N.J. & Lacroix, C. 2007. Fermentation technologies for the production of exopolysaccharide-synthesizing *Lactobacillus rhamnosus* concentrated cultures. *Electronic journal of biotechnology*. 10(2). DOI: 10.2225/vol10-issue2-fulltext-10.

Chapman, J., Lawlor, A., Weir, E., Quilty, B. & Regan, F. 2010. Phthalate doped PVC membranes for the inhibition of fouling. *Journal of membrane science*. 365(1-2):180–187. DOI: 10.1016/j.memsci.2010.09.003.

Chen, K., Jiang, M., Wei, P., Yao, J. & Wu, H. 2010. Succinic acid production from acid hydrolysate of corn fiber by *Actinobacillus succinogenes*. *Applied biochemistry and biotechnology*. 160(2):477–485. DOI: 10.1007/s12010-008-8367-0.

Chen, L., Tian, Y.S. & Karayiannis, T.G. 2006. The effect of tube diameter on vertical two-phase flow regimes in small tubes. *International journal of heat and mass transfer*. 49(21-22):4220–4230. DOI: 10.1016/j.ijheatmasstransfer.2006.03.025.

Chen, L., Zhang, Y., Li, S., Wang, X., Li, N., Wang, Y., Guo, X., Zhao, S., et al. 2014. Effect of plasma components on the stability and permeability of microcapsule. *Journal of biomedical materials research. Part A*. 102(7):2408–2416. DOI: 10.1002/jbm.a.34907.

Cheng, K.-C., Catchmark, J.M. & Demirci, A. 2009. Enhanced production of bacterial cellulose by using a biofilm reactor and its material property analysis. *Journal of biological engineering*. 3:12. DOI: 10.1186/1754-1611-3-12.

Cheng, K.-C., Demirci, A. & Catchmark, J.M. 2010. Advances in biofilm reactors for production of value-added products. *Applied microbiology and biotechnology*. 87(2):445–456. DOI: 10.1007/s00253-010-2622-3.

Chisholm, D. 1967. A theoretical basis for the Lockhart-Martinelli correlation for two-phase flow. *International journal of heat and mass transfer*. 10(12):1767–1778. DOI: 10.1016/0017-9310(67)90047-6.

Choi, M., Al-Zahrani, S.M. & Lee, S.Y. 2014. Kinetic model-based feed-forward controlled fed-batch fermentation of *Lactobacillus rhamnosus* for the production of lactic acid from Arabic date juice. *Bioprocess and biosystems engineering*. 37(6):1007–1015. DOI: 10.1007/s00449-013-1071-7.

Chowdary, K. & Panguluri, S. 2008. Evaluation of ethyl cellulose as microencapsulating agent for controlled release of glimepiride. *Asian journal of chemistry*. 20(8):5924–5930. Available: http://www.asianjournalofchemistry.co.in/user/journal/viewarticle.aspx?ArticleID=20_8_18 [2014, September 04].

Cloete, E. & Atlas, R. 2006. *Basic and applied microbiology*. Pretoria: Van Schaik Publishers.

Colas, A., Malczewski, R. & Ulman, K. 2004. *Silicone tubing for pharmaceutical processing*. Available: http://www.dowcorning.com/content/publishedlit/52-1067-01.pdf [2014, September 10].

Coleman, J.W. & Garimella, S. 1999. Characterization of two-phase flow patterns in small diameter round and rectangular tubes. *International journal of heat and mass transfer*. 42(15):2869–2881. DOI: 10.1016/S0017-9310(98)00362-7.

Coleman, J.W. & Garimella, S. 2003. Two-phase flow regimes in round, square and rectangular tubes during condensation of refrigerant R 134a. *International journal of refrigeration*. 26(1):117–128. DOI: 10.1016/S0140-7007(02)00013-0.

Collins, M.D., Phillips, B.A. & Zanoni, P. 1989. Deoxyribonucleic acid homology studies of *Lactobacillus casei*, *Lactobacillus paracasei* sp. Nov., subsp. *Paracasei* and subsp. *Tolerans*, and *Lactobacillus Rhamnosus* sp. Nov., comb. Nov. *International journal of systematic bacteriology*. 39(2):105–108. DOI: 10.1099/00207713-39-2-105.

Corona-Gonzalez, R.I., Bories, A., González-Alvarez, V., Snell-Castro, R., Toriz-González, G. & Pelayo-Ortiz, C. 2010. Succinic acid production with *Actinobacillus succinogenes* ZT-130 in the presence of succinic acid. *Current microbiology*. 60(1):71–77. DOI: 10.1007/s00284-009-9504-x.

Corona-González, R.I., Bories, A., González-Álvarez, V. & Pelayo-Ortiz, C. 2008. Kinetic study of succinic acid production by *Actinobacillus succinogenes* ZT-130. *Process biochemistry*. 43(10):1047–1053. DOI: 10.1016/j.procbio.2008.05.011.

Costerton, J.W. 1989. A Citation classic commentrary on “How bacteria stick”. *Citation classic*. 48:18.

Costerton, J.W., Geesey, G.G. & Cheng, K.-J. 1978. How bacteria stick. *Scientific American*. 238(1):86–95. DOI: 10.1038/scientificamerican0178-86.

Costerton, J.W., Lewandowski, Z., Caldwell, D.E., Korber, D.R. & Lappin-Scott, H.M. 1995. Microbial biofilms. *Annual review of microbiology*. 49:711–745. DOI: 10.1146/annurev.mi.49.100195.003431.

Cotton, J., Pometto, A.L. & Gvozdenovic-Jeremic, J. 2001. Continuous lactic acid fermentation using a plastic composite support biofilm reactor. *Applied microbiology and biotechnology*. 57(5-6):626–630. DOI: 10.1007/s002530100820.

Cuthbertson, L., Mainprize, I.L., Naismith, J.H. & Whitfield, C. 2009. Pivotal roles of the outer membrane polysaccharide export and polysaccharide copolymerase protein families in export of extracellular polysaccharides in gram-negative bacteria. *Microbiology and molecular biology reviews*. 73(1):155–177. DOI: 10.1128/MMBR.00024-08.

Czaczyk, K. & Myszka, K. 2007. Biosynthesis of extracellular polymeric substances (EPS) and its role in microbial biofilm formation. *Polish journal of environmental studies*. 16(6):799–806. Available: http://6csnfn.pjoes.com/pdf/16.6/799-806.pdf [2014, August 14].

Dagher, S.F., Ragout, A.L., Siñeriz, F. & Bruno-Bárcena, J.M. 2010. Cell immobilization for production of lactic acid: biofilms do it naturally. *Advances in applied microbiology*. 71:113–148. DOI: 10.1016/S0065-2164(10)71005-4.

Danese, P.N., Pratt, L.A. & Kolter, R. 2000. Exopolysaccharide production is required for development of *Escherichia coli* K-12 biofilm architecture. *Journal of bacteriology*. 182(12):3593–3596. DOI: 10.1128/JB.182.12.3593-3596.2000.

Das, T., Sharma, P.K., Busscher, H.J., Van der Mei, H.C. & Krom, B.P. 2010. Role of extracellular DNA in initial bacterial adhesion and surface aggregation. *Applied and environmental microbiology*. 76(10):3405–3408. DOI: 10.1128/AEM.03119-09.

De Beer, D., Stoodley, P., Roe, F. & Lewandowski, Z. 1994. Effects of biofilm structures on oxygen distribution and mass transport. *Biotechnology and bioengineering*. 43(11):1131–1138. DOI: 10.1002/bit.260431118.

Degeest, B., Vaningelgem, F. & De Vuyst, L. 2001. Microbial physiology, fermentation kinetics, and process engineering of heteropolysaccharide production by lactic acid bacteria. *International dairy journal*. 11(9):747–757. DOI: 10.1016/S0958-6946(01)00118-2.

De Lathouder, K.M., Bakker, J., Kreutzer, M.T., Kapteijn, F., Moulijn, J.A. & Wallin, S.A. 2004. Structured reactors for enzyme immobilization: advantages of tuning the wall morphology. *Chemical engineering science*. 59(22-23):5027–5033. DOI: 10.1016/j.ces.2004.07.047.

Demirci, A., Pometto, A.L. & Johnson, K.E. 1993. Lactic Acid production in a mixed-culture biofilm reactor. *Applied and environmental microbiology*. 59(1):203–207. Available: http://www.pubmedcentral.nih.gov/articlerender.fcgi?artid=202078&tool=pmcentrez&rendertype=abstract [2012, October 23].

Dervakos, G.A. & Webb, C. 1991. On the merits of viable-cell immobilisation. *Biotechnology advances*. 9(4):559–612. DOI: 10.1016/0734-9750(91)90733-C.

Djukić-Vuković, A.P., Mojović, L. V, Jokić, B.M., Nikolić, S.B. & Pejin, J.D. 2013. Lactic acid production on liquid distillery stillage by *Lactobacillus rhamnosus* immobilized onto zeolite. *Bioresource technology*. 135:454–458. DOI: 10.1016/j.biortech.2012.10.066.

Donlan, R.M. 2002. Biofilms: microbial life on surfaces. *Emerging infectious diseases*. 8(9):881–890. DOI: 10.3201/eid0809.020063.

Donlan, R. & Costerton, J. 2002. Biofilms: survival mechanisms of clinically relevant microorganisms. *Clinical microbiology reviews*. 15(2):167–193. DOI: 10.1128/CMR.15.2.167.

Doran, P.M. 2013. *Bioprocess Engineering Principles*. Waltham: Academic Press.

Du, C., Lin, S.K.C., Koutinas, A., Wang, R. & Webb, C. 2007. Succinic acid production from wheat using a biorefining strategy. *Applied microbiology and biotechnology*. 76(6):1263–1270. DOI: 10.1007/s00253-007-1113-7.

Du, C., Lin, S.K.C., Koutinas, A., Wang, R., Dorado, P. & Webb, C. 2008. A wheat biorefining strategy based on solid-state fermentation for fermentative production of succinic acid. *Bioresource technology*. 99(17):8310–8315. DOI: 10.1016/j.biortech.2008.03.019.

Du, J., Cao, N., Gong, C.S., Tsao, G.T. & Yuan, N. 1997. Fumaric acid production in airlift loop reactor with porous sparger. *Applied biochemistry and biotechnology*. 63-65(1):541–556. DOI: 10.1007/BF02920452.

Dumsday, G., Zhou, B., S, B., GA, S. & NB., P. 1997. Continuous ethanol production by *Escherichia coli* KO11 in continuous stirred tank and fluidized bed fermenters. *Australasian biotechnology*. 7(4):300–303. Available: http://www.bioline.org.br/request?au97039 [2014, December 18].

Dunne, W. 2002. Bacterial adhesion: seen any good biofilms lately? *Clinical microbiology reviews*. 15(2):155–166. DOI: 10.1128/CMR.15.2.155-166.2002.

Dupont, I., Roy, D. & Lapointe, G. 2000. Comparison of exopolysaccharide production by strains of Lactobacillus rhamnosus and Lactobacillus paracasei grown in chemically defined medium and milk. *Journal of industrial microbiology & biotechnology*. 24(4):251–255. DOI: 10.1038/sj.jim.2900810.

Ebihara, T. & Bishop, P.L. 2002. Effect of acetate on biofilms utilized in PAH bioremediation. *Environmental engineering science*. 19(5):305–319. DOI: 10.1089/10928750260418944.

Edwards, S.J. & Kjellerup, B. V. 2013. Applications of biofilms in bioremediation and biotransformation of persistent organic pollutants, pharmaceuticals/personal care products, and heavy metals. *Applied microbiology and biotechnology*. 97(23):9909–9921. DOI: 10.1007/s00253-013-5216-z.

Egamberdiev, N.B. & Ierusalimskii, N.D. 1968. Studies of the dynamics of the continuous must fermentation processes with the yeast *Saccharomyces vini* (Race PR-1) to produce dry wines. In *Continuous cultivation of microorganisms, Proceedings of the 4th symposium, Prague*. I. Malek & A. Voltova, Eds. Czechoslovak academy of sciences. 517–527.

Engineering Workshop. 2013. *Flash evaporation*. Available: http://en.citizendium.org/wiki/Flash_evaporation/Citable_Version [2014, September 23].

Ercan, D. & Demirci, A. 2015. Current and future trends for biofilm reactors for fermentation processes. *Critical reviews in biotechnology*. 35(1):1–14. DOI: 10.3109/07388551.2013.793170.

Espinoza, D.N. & Santamarina, J.C. 2010. Water-CO_2-mineral systems: Interfacial tension, contact angle, and diffusion-Implications to CO_2 geological storage. *Water resources research*. 46(7):W07537. DOI: 10.1029/2009WR008634.

Fajardo-Solache, N. 1999. Detection of genes encoding glucosyl-transferases in *Lactobacillus rhamnosus* ATCC 9595 (eps+). Laval University.

Fischer, N.O., Blanchette, C.D., Chromy, B.A., Kuhn, E.A., Segelke, B.W., Corzett, M., Bench, G., Mason, P.W., et al. 2009. Immobilization of His-tagged proteins on nickel-chelating nanolipoprotein particles. *Bioconjugate chemistry*. 20(3):460–465. DOI: 10.1021/bc8003155.

Flemming, H.-C. & Wingender, J. 2010. The biofilm matrix. *Nature reviews. Microbiology*. 8(9):623–633. DOI: 10.1038/nrmicro2415.

Flemming, H.-C.C., Neu, T.R. & Wozniak, D.J. 2007. The EPS matrix: The “house of biofilm cells”. *Journal of bacteriology*. 189(22):7945–7947. DOI: 10.1128/JB.00858-07.

Frank, M.J.W., Kuipers, J.M.A. & Van Swaaij, W.P.M. 1996. Diffusion coefficients and viscosities of $CO_2 + H_2O$, $CO_2 + CH_3OH$, $NH_3 + H_2O$, and $NH_3 + CH_3OH$ liquid mixtures. *Journal of chemical & engineering data*. 41(2):297–302. DOI: 10.1021/je950157k.

Franklin, M.J. & Ohman, D.E. 1993. Identification of *algF* in the alginate biosynthetic gene cluster of *Pseudomonas aeruginosa* which is required for alginate acetylation. *Journal of bacteriology*. 175(16):5057–5065. Available: http://www.ncbi.nlm.nih.gov/pmc/articles/PMC204972/.

Frederici, F. & Petruccioli, M. 1996. Production of fumaric acid by Rhizopus arrhizus on polyurethane sponge. In *Immobilized cells: Basics and applications volume 11 of progress in Biotechnology*. R.M. Buitelaar, C. Bucke, J. Tramper, & R.H. Wijffels, Eds. Amsterdam: Elsevier B.V. 655–660.

Galaction, A.-I., Kloetzer, L., Turnea, M., Webb, C., Vlysidis, A. & Caşcaval, D. 2012. Succinic acid fermentation in a stationary-basket bioreactor with a packed bed of immobilized *Actinobacillus succinogenes*: 1. Influence of internal diffusion on substrate mass transfer and consumption rate. *Journal of industrial microbiology & biotechnology*. 39(6):877–888. DOI: 10.1007/s10295-012-1095-z.

Gayen, K., Gupta, M. & Venkatesh, K. V. 2007. Elementary mode analysis to study the preculturing effect on the metabolic state of *Lactobacillus rhamnosus* during growth on mixed substrates. *In silico biology*. 7(2):123–139. Available: http://www.ncbi.nlm.nih.gov/pubmed/17688437.

Gloag, E.S., Turnbull, L., Huang, A., Vallotton, P., Wang, H., Nolan, L.M., Mililli, L., Hunt, C., et al. 2013. Self-organization of bacterial biofilms is facilitated by extracellular DNA. *Proceedings of the National Academy of Sciences of the United States of America*. 110(28):11541–11546. DOI: 10.1073/pnas.1218898110.

Goldstone, R.J., Popat, R., Fletcher, M.P., Crusz, S.A. & Diggle, S.P. 2012. Quorum sensing and social interactions in microbial biofilms. In *Microbial biofilms: Current research and applications*. G. Lear & G. Lewis, Eds. Norfolk: Caister Academic Press. 1–24.

Gompertz, B. 1825. On the nature of the function expressive of the law of human mortality, and on a new mode of determining the value of life contingencies. *Philosophical transactions of the Royal Society of London*. 115:513–583. DOI: 10.1098/rstl.1825.0026.

Gonçalves, L.M.D., Barreto, M., Xavier, A.M.B.R., Carrondo, M. & Klein, J. 1992. Inert supports for lactic acid fermentation - a technological assessment. *Applied microbiology and biotechnology*. 38(3):305–311. DOI: 10.1007/BF00170077.

Gross, R., Hauer, B., Otto, K. & Schmid, A. 2007. Microbial biofilms: new catalysts for maximizing productivity of long-term biotransformations. *Biotechnology and bioengineering*. 98(6):1123–1134. DOI: 10.1002/bit.21547.

Gross, R., Lang, K., Bühler, K. & Schmid, A. 2010. Characterization of a biofilm membrane reactor and its prospects for fine chemical synthesis. *Biotechnology and bioengineering*. 105(4):705–717. DOI: 10.1002/bit.22584.

Gross, R., Schmid, A. & Buehler, K. 2012. Catalytic biofilms: A powerful concept for future bioprocesses. In *Microbial biofilms: Current research and applications*. G. Lear & G. Lewis, Eds. Norfolk: Caister Academic Press. 193–222.

Guettler, M., Rumler, D. & Jain, M. 1999. *Actinobacillus succinogenes* sp. nov., a novel succinic-acid-producing strain from the bovine rumen. *International journal of systematic bacteriology*. 49:207–216. DOI: 10.1099/00207713-49-1-207.

Guettler, M.V., Jain, M.K. & Rumler, D. 1996. *Patent No. US5573931 A*. United States: Google Patents. Available: http://www.google.com/patents/US5573931 [2011, September 09].

Guoqiang, D., Kaul, R. & Mattiasson, B. 1992. Immobilization of *Lactobacillus casei* cells to ceramic material pretreated with polyethylenimine. *Applied microbiology and biotechnology*. 37(3):305–310. DOI: 10.1007/BF00210983.

Guttenplan, S.B., Blair, K.M. & Kearns, D.B. 2010. The *EpsE* flagellar clutch is bifunctional and synergizes with EPS biosynthesis to promote *Bacillus subtilis* biofilm formation. *PLoS genetics*. 6(12):e1001243. DOI: 10.1371/journal.pgen.1001243.

Halan, B., Schmid, A. & Buehler, K. 2010. Maximizing the productivity of catalytic biofilms on solid supports in membrane aerated reactors. *Biotechnology and bioengineering*. 106(4):516–527. DOI: 10.1002/bit.22732.

Hall, E.R. 1987. Biofilm reactors in anaerobic wastewater treatment. *Biotechnology advances*. 5(2):257–269. DOI: 10.1016/0734-9750(87)90321-1.

Hanafizadeh, P., Saidi, M.H., Nouri Gheimasi, a. & Ghanbarzadeh, S. 2011. Experimental investigation of air–water, two-phase flow regimes in vertical mini pipe. *Scientia Iranica*. 18(4):923–929. DOI: 10.1016/j.scient.2011.07.003.

Hansen, P.A. 1968. *Type strains of* Lactobacillus *species: A report by the taxonomic subcommittee on* Lactobacilli *and closely related organisms. A subcommittee of the International Committee on Nomenclature of Bacteria of the International Association of Microb*. Manassas: American Type Culture Collection.

Harutoshi, T. 2013. Exopolysaccharides of lactic acid bacteria for food and colon health applications. In *Lactic acid bacteria - R & D for food, health and livestock purposes*. J. Marcelino Kongo, Ed. Rijeka: InTech. 515–538. DOI: 10.5772/50839.

Heukelekian, H. & Heller, A. 1940. Relation between food concentration and surface for bacterial growth. *Journal of bacteriology*. 40(4):547–558. Available: http://www.ncbi.nlm.nih.gov/pmc/articles/PMC374658/ [2014, August 22].

Ho, K., Pometto, A., Hinz, P.N. & Demirci, A. 1997a. Nutrient leaching and end product accumulation in plastic composite supports for L-(+)-lactic acid biofilm fermentation. *Applied and environmental microbiology*. 63(7):2524–2532. Available: http://aem.asm.org/content/63/7/2524.short [2015, January 05].

Ho, K.L., Pometto, A.L., Hinz, P.N., Dickson, J.S. & Demirci, A. 1997b. Ingredient selection for plastic composite supports for L-(+)-lactic acid biofilm fermentation by *actobacillus casei* subsp. *rhamnosus*. *Applied and environmental microbiology*. 63(7):2516–2523. Available: http://www.ncbi.nlm.nih.gov/pmc/articles/PMC168549/ [2014, February 06].

Horiuchi, J.-I., Tabata, K., Kanno, T. & Kobayashi, M. 2000. Continuous acetic acid production by a packed bed bioreactor employing charcoal pellets derived from waste mushroom medium. *Journal of bioscience and bioengineering*. 89(2):126–130. DOI: 10.1016/S1389-1723(00)88725-3.

Huang, W.-C., Ramey, D.E. & Yang, S.-T. 2004. Continuous production of butanol by *Clostridium acetobutylicum* immobilized in a fibrous bed bioreactor. *Applied biochemistry and biotechnology*. 115(1-3):887–898. DOI: 10.1385/ABAB:115:1-3:0887.

Hyde, F.W., Hunt, G.R. & Errede, L.A. 1991. Immobilization of bacteria and *Saccharomyces cerevisiae* in poly(tetrafluoroethylene) membranes. *Applied and environmental microbiology*. 57(1):219–222. Available: http://aem.asm.org/content/57/1/219.

Idris, A. & Suzana, W. 2006. Effect of sodium alginate concentration, bead diameter, initial pH and temperature on lactic acid production from pineapple waste using immobilized *Lactobacillus delbrueckii*. *Process biochemistry*. 41(5):1117–1123. DOI: 10.1016/j.procbio.2005.12.002.

Itoh, N., Nakamura, M., Inoue, K. & Makino, Y. 2007. Continuous production of chiral 1,3-butanediol using immobilized biocatalysts in a packed bed reactor: promising biocatalysis method with an asymmetric hydrogen-transfer bioreduction. *Applied microbiology and biotechnology*. 75(6):1249–1256. DOI: 10.1007/s00253-007-0957-1.

Jarpa, M., Pozo, G., Baeza, R., Martínez, M. & Vidal, G. 2012. Polyhydroxyalkanoate biosynthesis from paper mill wastewater treated by a moving bed biofilm reactor. *Journal of environmental science and health. Part A, Toxic/hazardous substances & environmental engineering*. 47(13):2052–2059. DOI: 10.1080/10934529.2012.695699.

Jassim, E., Newell, T. & Chato, J. 2006. Probabilistic Determination of Two-Phase Flow Regimes Utilizing an Automated Image Recognition Technique. In *International refrigeration and air conditioning conference at Purdue, July 17-20, 2006*. Purdue: Purdue University. Available: http://docs.lib.purdue.edu/cgi/viewcontent.cgi?article=1825&context=iracc [2014, September 18].

Jepson, W.P. & Taylor, R.E. 1993. Slug flow and its transitions in large-diameter horizontal pipes. *International journal of multiphase flow*. 19(3):411–420. DOI: 10.1016/0301-9322(93)90057-2.

Jyoti, B.D., Suresh, A.K. & Venkatesh, K. V. 2004. Effect of preculturing conditions on growth of *Lactobacillus rhamnosus* on medium containing glucose and citrate. *Microbiological research*. 159(1):35–42. DOI: 10.1016/j.micres.2004.01.008.

Kant, R., Rintahaka, J., Yu, X., Sigvart-Mattila, P., Paulin, L., Mecklin, J.-P., Saarela, M., Palva, A., et al. 2014. A comparative pan-genome perspective of niche-adaptable cell-surface protein phenotypes in *Lactobacillus rhamnosus*. *PloS one*. 9(7):e102762. DOI: 10.1371/journal.pone.0102762.

Karel, S.F., Libicki, S.B. & Robertson, C.R. 1985. The immobilization of whole cells: Engineering principles. *Chemical engineering science*. 40(8):1321–1354. DOI: 10.1016/0009-2509(85)80074-9.

Kashinsky, O.N., Kurdyumov, a. S. & Randin, V. V. 2006. Wall shear stress in an upward slug flow in a vertical tube. *Thermophysics and aeromechanics*. 13(3):381–385. DOI: 10.1134/S0869864306030073.

Katzbauer, B., Narodoslawsky, M. & Moser, A. 1995. Classification system for immobilization techniques. *Bioprocess engineering*. 12(4):173–179. DOI: 10.1007/BF01767463.

Kennedy, J.F., Humphreys, J.D., Alan Barker, S. & Greenshields, R.N. 1980. Application of living immobilized cells to the acceleration of the continuous conversions of ethanol (wort) to acetic acid (vinegar)—Hydrous titanium(IV) oxide-immobilized *Acetobacter* species. *Enzyme and microbial technology*. 2(3):209–216. DOI: 10.1016/0141-0229(80)90049-6.

Khezry, M. 2012. Mapping the distribution of the EPS matrix within mixed microbial flocs. University of Guelph.

Kilonzo, P.M., Margaritis, A. & Bergougnou, M. a. 2010. Hydrodynamic characteristics in an inverse internal-loop airlift-driven fibrous-bed bioreactor. *Chemical engineering science*. 65(2):692–707. DOI: 10.1016/j.ces.2009.09.023.

Kim, J.-U., Kim, Y., Han, K.-S., OH, S., Whang, K.-Y., Kim, J.-N. & Kim, S.-H. 2006. Function of cell-bound and released exopolysaccharides produced by *Lactobacillus rhamnosus* ATCC 9595. *Journal of microbiology and biotechnology*. 16(6):939–945.

Kim, M. Il, Kim, N.J., Shang, L., Chang, Y.K., Lee, S.Y. & Chang, H.N. 2009. Continuous production of succinic acid using an external membrane cell recycle system. *Journal of microbiology and biotechnology*. 19(11):1369–1373. DOI: 10.4014/jmb.0903.03034.

Kim, S.-Lk., Park, P.-J. & Byun, H.-G. 2002. Continuous production of citric acid from dairy wastewater using immobilized *Aspergillus niger* ATCC 9142. *Biotechnology and bioprocess engineering*. 7(2):89–94. DOI: 10.1007/BF02935885.

Kokare, C., Chakraborty, S., Khopade, A.N. & Mahadik, K.R. 2009. Biofilm: Importance and applications. *Indian journal of biotechnology*. 8(2):159–168.

Krischke, W., Schröder, M. & Trösch, W. 1991. Continuous production of L-lactic acid from whey permeate by immobilized *Lactobacillus casei* subsp. *casei*. *Applied microbiology and biotechnology*. 34(5):573–578. DOI: 10.1007/BF00167901.

Kunduru, M.R. & Pometto, A.L. 1996a. Continuous ethanol production by *Zymomonas mobilis* and *Saccharomyces cerevisiae* in biofilm reactors. *Journal of industrial microbiology*. 16(4):249–256. DOI: 10.1007/BF01570029.

Kunduru, M.R. & Pometto, A.L. 1996b. Evaluation of plastic composite-supports for enhanced ethanol production in biofilm reactors. *Journal of industrial microbiology*. 16(4):241–248. DOI: 10.1007/BF01570028.

Kwon, S., Lee, P.C., Lee, E.G., Keun Chang Y & Chang, N. 2000. Production of lactic acid by *Lactobacillus rhamnosus* with vitamin-supplemented soybean hydrolysate. *Enzyme and microbial technology*. 26(2-4):209–215. DOI: 10.1016/S0141-0229(99)00134-9.

Landersjö, C., Yang, Z., Huttunen, E. & Widmalm, G. 2002. Structural studies of the exopolysaccharide produced by *Lactobacillus rhamnosus* strain GG (ATCC 53103). *Biomacromolecules*. 3(4):880–4. DOI: 10.1021/bm020040q.

Laspidou, C.S. & Rittmann, B.E. 2002. A unified theory for extracellular polymeric substances, soluble microbial products, and active and inert biomass. *Water research*. 36(11):2711–2720. DOI: 10.1016/S0043-1354(01)00413-4.

Lawrence, J.R., Swerhone, G.D.W., Kuhlicke, U. & Neu, T.R. 2007. In situ evidence for microdomains in the polymer matrix of bacterial microcolonies. *Canadian journal of microbiology*. 53(3):450–458. DOI: 10.1139/W06-146.

Lazzi, C., Turroni, S., Mancini, A., Sgarbi, E., Neviani, E., Brigidi, P. & Gatti, M. 2014. Transcriptomic clues to understand the growth of *Lactobacillus rhamnosus* in cheese. *BMC microbiology*. 14:28. DOI: 10.1186/1471-2180-14-28.

Lebeer, S., De Keersmaecker, S.C.J., Verhoeven, T.L.A., Fadda, A.A., Marchal, K. & Vanderleyden, J. 2007. Functional analysis of *luxS* in the probiotic strain *Lactobacillus rhamnosus* GG reveals a central metabolic role important for growth and biofilm formation. *Journal of bacteriology*. 189(3):860–871. DOI: 10.1128/JB.01394-06.

Lebeer, S., Verhoeven, T.L.A., Perea Vélez, M., Vanderleyden, J. & De Keersmaecker, S.C.J. 2007. Impact of environmental and genetic factors on biofilm formation by the probiotic strain *Lactobacillus rhamnosus* GG. *Applied and environmental microbiology*. 73(21):6768–6775. DOI: 10.1128/AEM.01393-07.

Lebeer, S., Verhoeven, T.L.A., Francius, G., Schoofs, G., Lambrichts, I., Dufrêne, Y., Vanderleyden, J. & De Keersmaecker, S.C.J. 2009. Identification of a gene cluster for the biosynthesis of a long, galactose-rich exopolysaccharide in *Lactobacillus rhamnosus* GG and functional analysis of the priming glycosyltransferase. *Applied and environmental microbiology*. 75(11):3554–3563. DOI: 10.1128/AEM.02919-08.

Lebeer, S., Claes, I.J.J., Verhoeven, T.L. a, Vanderleyden, J. & De Keersmaecker, S.C.J. 2011. Exopolysaccharides of Lactobacillus rhamnosus GG form a protective shield against innate immune factors in the intestine. *Microbial biotechnology*. 4(3):368–74. DOI: 10.1111/j.1751-7915.2010.00199.x.

Lee, H.K. & Maddox, I.S. 1986. Continuous production of 2,3-butanediol from whey permeate using *Klebsiella pneumoniae* immobilized in calcium alginate. *Enzyme and microbial technology*. 8(7):409–411. DOI: 10.1016/0141-0229(86)90147-X.

Lee, K.-J., Kim, J.-A., Hwang, W., Park, S.-J. & Lee, K.-H. 2013. Role of capsular polysaccharide (CPS) in biofilm formation and regulation of CPS production by quorum-sensing in *Vibrio vulnificus*. *Molecular microbiology*. 90(4):841–857. DOI: 10.1111/mmi.12401.

Lee, P.C., Lee, S.Y. & Chang, H.N. 2008. Cell recycled culture of succinic acid-producing *Anaerobiospirillum succiniciproducens* using an internal membrane filtration system. *Journal of microbiology and biotechnology*. 18(7):1252–1256. Available: http://www.ncbi.nlm.nih.gov/pubmed/18667853 [2011, September 09].

Lee, S.-M., Cho, M.O., Park, C.H., Chung, Y.-C., Kim, J.H., Sang, B.-I. & Um, Y. 2008. Continuous butanol production using suspended and immobilized *Clostridium beijerinckii* NCIMB 8052 with supplementary butyrate. *Energy & fuels*. 22(5):3459–3464. DOI: 10.1021/ef800076j.

Leewenhoeck, A. 1684. An abstract of a letter from mr. Anthony leewenhoeck at Delft, dated Sep 17 1683 containing some microscopical observations, about animals in the scurf of the teeth, the substance call'd worms in the nose, the cuticula consisting of scales. *Philosophical transactions of the Royal Society of London*. 14(155-166):568–574. DOI: 10.1098/rstl.1684.0030.

Leng, D.E., Katti, S.S. & Atiemo-Obeng, V. 2008. Industrial mixing technology. In *Albright's chemical engineering handbook*. L. Albright, Ed. Boca Raton: CRC Press.

Li, J., Jiang, M., Chen, K., Shang, L., Wei, P., Ying, H., Ye, Q., Ouyang, P., et al. 2010. Enhanced production of succinic acid by *Actinobacillus succinogenes* with reductive carbon source. *Process biochemistry*. 45(6):980–985. DOI: 10.1016/j.procbio.2010.03.001.

Li, Q., Wang, D., Wu, Y., Yang, M., Li, W., Xing, J. & Su, Z. 2010. Kinetic evaluation of products inhibition to succinic acid producers *Escherichia coli* NZN111, AFP111, BL21, and *Actinobacillus succinogenes* 130Z^{T}. *Journal of microbiology (Seoul, Korea)*. 48(3):290–296. DOI: 10.1007/s12275-010-9262-2.

Li, X.Z., Hauer, B. & Rosche, B. 2007. Single-species microbial biofilm screening for industrial applications. *Applied microbiology and biotechnology*. 76(6):1255–1262. DOI: 10.1007/s00253-007-1108-4.

Lin, S.K.C., Du, C., Koutinas, A., Wang, R. & Webb, C. 2008. Substrate and product inhibition kinetics in succinic acid production by *Actinobacillus succinogenes*. *Biochemical engineering journal*. 41(2):128–135. DOI: 10.1016/j.bej.2008.03.013.

Ling, L.S., Mohamad, R., Rahim, R.A., Wan, H.Y. & Ariff, A. Bin. 2006. Improved production of live cells of Lactobacillus rhamnosus by continuous cultivation using glucose-yeast extract medium. *Journal of microbiology (Seoul, Korea)*. 44(4):439–446.

Lísal, M., Smith, W.R. & Aim, K. 2004. Analysis of Henry's constant for carbon dioxide in water via Monte Carlo simulation. *Fluid phase equilibria*. 226:161–172. DOI: 10.1016/j.fluid.2004.06.062.

Liu, T.-J. 1997. Investigation of the wall shear stress in vertical bubbly flow under different bubble size conditions. *International journal of multiphase flow*. 23(6):1085–1109. DOI: 10.1016/S0301-9322(97)00030-X.

Liu, Y. & Tay, J.-H. 2002. The essential role of hydrodynamic shear force in the formation of biofilm and granular sludge. *Water research*. 36(7):1653–1665. DOI: 10.1016/S0043-1354(01)00379-7.

Liu, Y.-P., Zheng, P., Sun, Z.-H., Ni, Y., Dong, J.-J. & Wei, P. 2008. Strategies of pH control and glucose-fed batch fermentation for production of succinic acid by *Actinobacillus succinogenes* CGMCC1593. *Journal of chemical technology & biotechnology*. 83(5):722–729. DOI: 10.1002/jctb.1862.

Looijesteijn, P.J., van Casteren, W.H.M., Tuinier, R., Doeswijk-Voragen, C.H.L. & Hugenholtz, J. 2000. Influence of different substrate limitations on the yield, composition and molecular mass of exopolysaccharides produced by Lactococcus lactis subsp. cremoris in continuous cultures. *Journal of applied microbiology*. 89(1):116–122. DOI: 10.1046/j.1365-2672.2000.01082.x.

López, D., Vlamakis, H. & Kolter, R. 2010. Biofilms. *Cold Spring Harbor perspectives in biology*. 2(7):a000398. DOI: 10.1101/cshperspect.a000398.

Lovley, D.R. & Lonergan, D.J. 1990. Anaerobic oxidation of toluene, phenol, and *p*-cresol by the dissimilatory iron-reducing organism, GS-15. *Applied and environmental microbiology*. 56(6):1858–1864. Available: http://www.ncbi.nlm.nih.gov/pmc/articles/PMC184522/.

Luedeking, R. & Piret, E.L. 1959. A kinetic study of the lactic acid fermentation. Batch process at controlled pH. *Journal of biochemical and microbiological technology and engineering*. 1(4):393–412.

Lux, R., Li, Y., Lu, A. & Shi, W. 2004. Detailed three-dimensional analysis of structural features of *Myxococcus xanthus* fruiting bodies using confocal laser scanning microscopy. *Biofilms*. 1(4):293–303. DOI: 10.1017/S1479050505001559.

Ma, Y., Zhang, Y., Liu, Y., Chen, L., Li, S., Zhao, W., Sun, G., Li, N., et al. 2013. Investigation of alginate-ε-poly-L-lysine microcapsules for cell microencapsulation. *Journal of biomedical materials research. Part A*. 101(5):1265–1273. DOI: 10.1002/jbm.a.34418.

Macedo, M.G., Lacroix, C., Gardner, N.J. & Champagne, C.P. 2002. Effect of medium supplementation on exopolysaccharide production by *Lactobacillus rhamnosus* RW-9595M in whey permeate. *International dairy journal*. 12(5):419–426. DOI: 10.1016/S0958-6946(01)00173-X.

Maharaj, K., Bradfield, M.F.A. & Nicol, W. 2014. Succinic acid-producing biofilms of *Actinobacillus succinogenes*: reproducibility, stability and productivity. *Applied microbiology and biotechnology*. 98(17):7379–7386. DOI: 10.1007/s00253-014-5779-3.

Mahmud, T., Haque, J.N., Roberts, K.J., Rhodes, D. & Wilkinson, D. 2009. Measurements and modelling of free-surface turbulent flows induced by a magnetic stirrer in an unbaffled stirred tank reactor. *Chemical engineering science*. 64(20):4197–4209. DOI: 10.1016/j.ces.2009.06.059.

Malczewski, R., Inman, W. & Cadieux, B. 2004. Burst Strength of Silicone Tubing. *Innovations in pharmaceutical technology*. February. Available: http://iptonline.com/articles/public/dcolarticle0204b.pdf [2014, September 10].

Malczewski, R.M., Inman, W.D. & Cadieux, B.L. 2003. *Burst strength testing of DOW CORNING ® brand pharma tubings*.

Manderson, G.J. & Doelle, H.W. 1972. The effect of oxygen and pH on the glucose metabolism of *Lactobacillus casei* var. *rhamnosus* ATCC 7469. *Antonie van Leeuwenhoek*. 38(1):223–240. DOI: 10.1007/BF02328095.

Manolov, T., Kristina, H. & Benoit, G. 2005. Continuous acetonitrile degradation in a packed-bed bioreactor. *Applied microbiology and biotechnology*. 66(5):567–574. DOI: 10.1007/s00253-004-1744-x.

Marques, S., Santos, J.A.L., Gírio, F.M. & Roseiro, J.C. 2008. Lactic acid production from recycled paper sludge by simultaneous saccharification and fermentation. *Biochemical engineering journal*. 41(3):210–216. DOI: 10.1016/j.bej.2008.04.018.

Martin, G.J.O., Knepper, A., Zhou, B. & Pamment, N.B. 2006. Performance and stability of ethanologenic *Escherichia coli* strain FBR5 during continuous culture on xylose and glucose. *Journal of industrial microbiology & biotechnology*. 33(10):834–844. DOI: 10.1007/s10295-006-0129-9.

May, T. & Okabe, S. 2011. Enterobactin is required for biofilm development in reduced-genome *Escherichia coli*. *Environmental microbiology*. 13(12):3149–3162. DOI: 10.1111/j.1462-2920.2011.02607.x.

McCarthy, D.A., Field, M., Mumford, P., Pell, B.K., Holborow, E.J. & Maini, R.N. 1985. The production of small IgG aggregates by glutaraldehyde cross-linking. *Journal of immunological methods*. 82(2):349–358. DOI: 10.1016/0022-1759(85)90367-9.

McKinlay, J.B. & Vieille, C. 2008. ^{13}C-metabolic flux analysis of *Actinobacillus succinogenes* fermentative metabolism at different $NaHCO_3$ and H_2 concentrations. *Metabolic engineering*. 10(1):55–68. DOI: 10.1016/j.ymben.2007.08.004.

McKinlay, J.B., Zeikus, J.G. & Vieille, C. 2005. Insights into *Actinobacillus succinogenes* fermentative metabolism in a chemically defined growth medium. *Applied and environmental microbiology*. 71(11):6651–6656. DOI: 10.1128/AEM.71.11.6651-6656.2005.

McKinlay, J.B., Shachar-Hill, Y., Zeikus, J.G. & Vieille, C. 2007. Determining *Actinobacillus succinogenes* metabolic pathways and fluxes by NMR and GC-MS analyses of ^{13}C-labeled metabolic product isotopomers. *Metabolic engineering*. 9(2):177–192. DOI: 10.1016/j.ymben.2006.10.006.

McKinlay, J.B., Laivenieks, M., Schindler, B.D., McKinlay, A.A., Siddaramappa, S., Challacombe, J.F., Lowry, S.R., Clum, A., et al. 2010. A genomic perspective on the potential of *Actinobacillus succinogenes* for industrial succinate production. *BMC genomics*. 11:680. DOI: 10.1186/1471-2164-11-680.

Medina de Figueroa, R., Oliver, G. & Benito de Cárdenas, I.L. 2001. Influence of temperature on flavour compound production from citrate by *Lactobacillus rhamnosus* ATCC 7469. *Microbiological research*. 155(4):257–262. DOI: 10.1016/S0944-5013(01)80002-1.

Mehaia, M.A. & Cheryan, M. 1987. Immobilization of *Lactobacillus bulgaricus* in a hollowfiber bioreactor for production of lactic acid from acid whey permeate. *Applied biochemistry and biotechnology*. 14(1):21–27. DOI: 10.1007/BF02798495.

Mel, M., Karim, M.I.A., Salleh, M.R.M. & Amin, N.A.M. 2008. Optimizing media of Lactobacillus rhamnosus for lactic acid fermentation. *Journal of applied sciences*. 8(17):3055–3059. DOI: jas.2008.3055.3059.

Meyer, A. & Wallis, F.M. 1997. Development of microbial biofilms on various surfaces for the treatment of heavy metal containing effluents. *Biotechnology techniques*. 11(12):859–863. DOI: 10.1023/A:1018497813505.

Migneault, I., Dartiguenave, C., Bertrand, M.J. & Waldron, K.C. 2004. Glutaraldehyde: behavior in aqueous solution, reaction with proteins, and application to enzyme crosslinking. *BioTechniques*. 37(5):790–802. Available: http://www.ncbi.nlm.nih.gov/pubmed/15560135.

Millsap, K.W., Reid, G., Van der Mei, H.C. & Busscher, H.J. 1997. Adhesion of *Lactobacillus* species in urine and phosphate buffer to silicone rubber and glass under flow. *Biomaterials*. 18(1):87–91. DOI: 10.1016/S0142-9612(96)00105-6.

Mishima, K. & Hibiki, T. 1996. Some characteristics of air-water two-phase flow in small diameter vertical tubes. *International journal of multiphase flow*. 22(4):703–712. DOI: 10.1016/0301-9322(96)00010-9.

Moreno-Castilla, C. & Pérez-Cadenas, A.F. 2010. Carbon-based honeycomb monoliths for environmental gas-phase applications. *Materials*. 3(2):1203–1227. DOI: 10.3390/ma3021203.

Morita, H., Toh, H., Oshima, K., Murakami, M., Taylor, T.D., Igimi, S. & Hattori, M. 2009. Complete genome sequence of the probiotic *Lactobacillus rhamnosus* ATCC 53103. *Journal of bacteriology*. 191(24):7630–7631. DOI: 10.1128/JB.01287-09.

Mostafa, N. 1996. Production of lactic acid from whey with agar immobilized cells in a continuous packed tubular reactor. *Energy conversion and management*. 37(3):253–260. DOI: 10.1016/0196-8904(95)00184-0.

Mousavi, S.M., Shojaosadati, S. a., Golestani, J. & Yazdian, F. 2010. CFD simulation and optimization of effective parameters for biomass production in a horizontal tubular loop bioreactor. *Chemical engineering and processing: process intensification*. 49(12):1249–1258. DOI: 10.1016/j.cep.2010.09.013.

Murtaza, G. 2012. Ethylcellulose microparticles: a review. *Acta poloniae pharmaceutica*. 69(1):11–22. Available: http://www.ncbi.nlm.nih.gov/pubmed/22574502.

Muzychka, Y.S. & Awad, M.M. 2010. Asymptotic generalizations of the Lockhart–Martinelli method for two phase flows. *Journal of fluids engineering*. 132(3):031302. DOI: 10.1115/1.4001157.

Nakamura, L.K. 1982. Deoxyribonucleic acid homologies of *Lactobacillus amylophilus* and other homofermentative species. *International journal of systematic bacteriology*. 32(1):43–47. DOI: 10.1099/00207713-32-1-43.

Nakoryakov, V.E., Kashinsky, O.N., Burdukov, A.P. & Odnoral, V.P. 1981. Local characteristics of upward gas-liquid flows. *International journal of multiphase flow*. 7(1):63–81. DOI: 10.1016/0301-9322(81)90015-X.

Nakoryakov, V.E., Kashinsky, O.N. & Kozmenko, B.K. 1986. Experimental study of gas-liquid slug flow in a small-diameter vertical pipe. *International journal of multiphase flow*. 12(3):337–355. DOI: 10.1016/0301-9322(86)90012-1.

Nicolella, C., Van Loosdrecht, M.C.M. & Heijnen, J.J. 2000a. Wastewater treatment with particulate biofilm reactors. *Journal of biotechnology*. 80(1):1–33. DOI: 10.1016/S0168-1656(00)00229-7.

Nicolella, C., Van Loosdrecht, M.C. & Heijnen, S.J. 2000b. Particle-based biofilm reactor technology. *Trends in biotechnology*. 18(7):312–320. DOI: 10.1016/S0167-7799(00)01461-X.

Nielsen, P.H. & Jahn, A. 1999. Extraction of EPS. In *Microbial Extracellular Polymeric Substances Characterization, Structure and Function*. V. 69. J. Wingender, T.R. Neu, & H.-C. Flemming, Eds. Berlin, Heidelberg: Springer Berlin Heidelberg. 49–72. DOI: 10.1007/978-3-642-60147-7.

Nyvad, B. & Fejerskov, O. 1989. Structure of dental plaque and the plaque-enamel interface in human experimental caries. *Caries Research*. 23(3):151–158. DOI: 10.1159/000261169.

Olde Damink, L.H.H., Dijkstra, P.J., Van Luyn, M.J.A., Van Wachem, P.B., Nieuwenhuis, P. & Feijen, J. 1995. Glutaraldehyde as a crosslinking agent for collagen-based biomaterials. *Journal of materials science: Materials in medicine*. 6(8):460–472. DOI: 10.1007/BF00123371.

Oldenburg, H. 1665. The Introduction. *Philosophical transactions of the Royal Society of London*. 1(1-22):1–2. DOI: 10.1098/rstl.1665.0002.

Oliveira, A.P., Nielsen, J. & Förster, J. 2005. Modeling *Lactococcus lactis* using a genome-scale flux model. *BMC microbiology*. 5:39. DOI: 10.1186/1471-2180-5-39.

Oriel, P. 1988. Immobilization of recombinant *Escherichia coli* in silicone polymer beads. *Enzyme and microbial technology*. 10(9):518–523. DOI: 10.1016/0141-0229(88)90043-9.

Ozmihci, S. & Kargi, F. 2007. Continuous ethanol fermentation of cheese whey powder solution: effects of hydraulic residence time. *Bioprocess and biosystems engineering*. 30(2):79–86. DOI: 10.1007/s00449-006-0101-0.

Ozmihci, S. & Kargi, F. 2008. Ethanol production from cheese whey powder solution in a packed column bioreactor at different hydraulic residence times. *Biochemical engineering journal*. 42(2):180–185. DOI: 10.1016/j.bej.2008.06.017.

Ozmihci, S. & Kargi, F. 2009. Fermentation of cheese whey powder solution to ethanol in a packed-column bioreactor: effects of feed sugar concentration. *Journal of chemical technology & biotechnology*. 84(1):106–111. DOI: 10.1002/jctb.2013.

Papagianni, M., Mattey, M. & Kristiansen, B. 2003. Design of a tubular loop bioreactor for scale-up and scale-down of fermentation processes. *Biotechnology progress*. 19(5):1498–1504. DOI: 10.1021/bp030002y.

Park, Y.S. & Toda, K. 1992. Multi-stage biofilm reactor for acetic acid production at high concentration. *Biotechnology letters*. 14(7):609–612. DOI: 10.1007/BF01023950.

Park, J.-B., Bühler, B., Panke, S., Witholt, B. & Schmid, A. 2007. Carbon metabolism and product inhibition determine the epoxidation efficiency of solvent-tolerant *Pseudomonas* sp. strain VLB120ΔC. *Biotechnology and bioengineering*. 98(6):1219–1229. DOI: 10.1002/bit.21496.

Park, S.H., Xing, R. & Whitman, W.B. 1995. Nonenzymatic acetolactate oxidation to diacetyl by flavin, nicotinamide and quinone coenzymes. *Biochimica et biophysica acta (BBA) - General subjects*. 1245(3):366–370. DOI: 10.1016/0304-4165(95)00103-4.

Paul, E., Ochoa, J.C., Pechaud, Y., Liu, Y. & Liné, A. 2012. Effect of shear stress and growth conditions on detachment and physical properties of biofilms. *Water research*. 46(17):5499–5508. DOI: 10.1016/j.watres.2012.07.029.

Péant, B., LaPointe, G., Gilbert, C., Atlan, D., Ward, P. & Roy, D. 2005. Comparative analysis of the exopolysaccharide biosynthesis gene clusters from four strains of *Lactobacillus rhamnosus*. *Microbiology (Reading, England)*. 151(6):1839–51. DOI: 10.1099/mic.0.27852-0.

Pelletier, C., Bouley, C., Cayuela, C., Bouttier, S., Bourlioux, P. & Bellon-Fontaine, M.N. 1997. Cell surface characteristics of *Lactobacillus casei* subsp. *casei*, *Lactobacillus paracasei* subsp. *paracasei*, and *Lactobacillus rhamnosus* strains. *Applied and environmental microbiology*. 63(5):1725–1731. Available: http://www.ncbi.nlm.nih.gov/pmc/articles/PMC168469/.

Petrov, K.K., Yankov, D.S. & Beschkov, V.N. 2005. Lactic acid fermentation by cells of *Lactobacillus rhamnosus* immobilized in polyacrylamide gel. *World journal of microbiology and biotechnology*. 22(4):337–345. DOI: 10.1007/s11274-005-9039-7.

Petrov, K.K., Petrova, P.M. & Beschkov, V.N. 2007. Improved immobilization of *Lactobacillus rhamnosus* ATCC 7469 in polyacrylamide gel, preventing cell leakage during lactic acid fermentation. *World journal of microbiology and biotechnology*. 23(3):423–428. DOI: 10.1007/s11274-006-9242-1.

Petrova, O.E. & Sauer, K. 2012. Sticky situations: key components that control bacterial surface attachment. *Journal of bacteriology*. 194(10):2413–2425. DOI: 10.1128/JB.00003-12.

Peyton, B.M. 1996. Effects of shear stress and substrate loading rate on *Pseudomonas aeruginosa* biofilm thickness and density. *Water research*. 30(1):29–36. DOI: 10.1016/0043-1354(95)00110-7.

Peyton, B.M. & Characklis, W.G. 1993. A statistical analysis of the effect of substrate utilization and shear stress on the kinetics of biofilm detachment. *Biotechnology and bioengineering*. 41(7):728–735. DOI: 10.1002/bit.260410707.

Pham, P.L., Dupont, I., Roy, D., Lapointe, G. & Cerning, J. 2000. Production of exopolysaccharide by *Lactobacillus rhamnosus* R and analysis of its enzymatic degradation during prolonged fermentation. *Applied and environmental microbiology*. 66(6):2302–2310. DOI: 10.1128/AEM.66.6.2302-2310.2000.

Poolman, M.G., Venkatesh, K. V, Pidcock, M.K. & Fell, D.A. 2004. A method for the determination of flux in elementary modes, and its application to *Lactobacillus rhamnosus*. *Biotechnology and bioengineering*. 88(5):601–612. DOI: 10.1002/bit.20273.

Prasertmanakit, S., Praphairaksit, N., Chiangthong, W. & Muangsin, N. 2009. Ethyl cellulose microcapsules for protecting and controlled release of folic acid. *AAPS PharmSciTech*. 10(4):1104–1112. DOI: 10.1208/s12249-009-9305-3.

Qureshi, N. & Maddox, I.S. 1988. Reactor design for the ABE fermentation using cells of *Clostridium acetobutylicum* immobilized by adsorption onto bonechar. *Bioprocess engineering*. 3(2):69–72. DOI: 10.1007/BF00369330.

Qureshi, N. & Schripsema, J. 2000. Continuous solvent production by *Clostridium beijerinckii* BA101 immobilized by adsorption onto brick. *World journal of microbiology and biotechnology*. 16(4):377–382. DOI: 10.1023/A:1008984509404.

Qureshi, N., Lai, L.L. & Blaschek, H.P. 2004. Scale-up of a high productivity continuous biofilm reactor to produce butanol by adsorbed cells of *Clostridium beijerinckii*. *Food and Bioproducts Processing*. 82(2):164–173. DOI: 10.1205/0960308041614891.

Qureshi, N., Annous, B.A., Ezeji, T.C., Karcher, P. & Maddox, I.S. 2005. Biofilm reactors for industrial bioconversion processes: employing potential of enhanced reaction rates. *Microbial cell factories*. 4:24. DOI: 10.1186/1475-2859-4-24.

Raihan, S., Ahmed, N., Macaskie, L.E. & Lloyd, J.R. 1997. Immobilisation of whole bacterial cells for anaerobic biotransformations. *Applied microbiology and biotechnology*. 47(4):352–357. DOI: 10.1007/s002530050939.

Reij, M.W. & Hartmans, S. 1996. Propene removal from synthetic waste gas using a hollow-fibre membrane bioreactor. *Applied microbiology and biotechnology*. 45(6):730–736. DOI: 10.1007/s002530050755.

Reynolds, O. 1895. On the dynamical theory of incompressible viscous fluids and the determination of the criterion. *Philosophical transactions of the Royal Society A: Mathematical, physical and engineering Sciences*. 186:123–164. DOI: 10.1098/rsta.1895.0004.

Rieder, A., Ladnorg, T., Wöll, C., Obst, U., Fischer, R. & Schwartz, T. 2011. The impact of recombinant fusion-hydrophobin coated surfaces on *E. coli* and natural mixed culture biofilm formation. *Biofouling: The journal of bioadhesion and biofilm research*. 27(10):1073–1085. DOI: 10.1080/08927014.2011.631168.

Riscaldati, E., Moresi, M., Federici, F. & Petruccioli, M. 2002. Ammonium fumarate production by free or immobilised Rhizopus arrhizus in bench- and laboratory-scale bioreactors. *Journal of chemical technology and biotechnology*. 77(9):1013–1024. DOI: 10.1002/jctb.672.

Roberts, I.S. 1996. The biochemistry and genetics of capsular polysaccharide production in bacteria. *Annual review of microbiology*. 50:285–315. DOI: 10.1146/annurev.micro.50.1.285.

Rogl, H., Kosemund, K., Kühlbrandt, W. & Collinson, I. 1998. Refolding of *Escherichia coli* produced membrane protein inclusion bodies immobilised by nickel chelating chromatography. *FEBS letters*. 432(1-2):21–26. DOI: 10.1016/S0014-5793(98)00825-4.

Rosche, B., Li, X.Z., Hauer, B., Schmid, A. & Buehler, K. 2009. Microbial biofilms: a concept for industrial catalysis? *Trends in biotechnology*. 27(11):636–643. DOI: 10.1016/j.tibtech.2009.08.001.

Roy, D., Goulet, J. & Le Duy, A. 1987. Continuous Production of Lactic Acid from Whey Perméate by Free and Calcium Alginate Entrapped *Lactobacillus helveticus*. *Journal of dairy science*. 70(3):506–513. DOI: 10.3168/jds.S0022-0302(87)80035-8.

Ruas-Madiedo, P. & De los Reyes-Gavilán, C.G. 2005. *Invited review*: methods for the screening, isolation, and characterization of exopolysaccharides produced by lactic acid bacteria. *Journal of dairy science*. 88(3):843–856. DOI: 10.3168/jds.S0022-0302(05)72750-8.

Ryu, H.W. & Wee, Y.J. 2001. Characterization of bioconversion of fumarate to succinate by alginate immobilized *Enterococcus faecalis* RKY1. *Applied biochemistry and biotechnology*. 91-93(1-9):525–535. DOI: 10.1385/ABAB:91-93:1-9:525.

Ryu, C.S., Czajka, J.W., Sakamoto, M. & Benno, Y. 2001. Characterization of the *Lactobacillus casei* group and the *Lactobacillus acidophilus* group by automated ribotyping. *Microbiology and immunology*. 45(4):271–275. DOI: 10.1111/j.1348-0421.2001.tb02618.x.

Saini, R. & Vieth, W.R. 2007. Reaction kinetics and mass transfer in glucose isomerisation with collagen-immobilised whole microbial cells. *Journal of applied chemistry and biotechnology*. 25(2):115–141. DOI: 10.1002/jctb.5020250206.

Sajc, L., Grubisic, D. & Vunjak-Novakovic, G. 2000. Bioreactors for plant engineering: an outlook for further research. *Biochemical engineering journal*. 4(2):89–99. DOI: 10.1016/S1369-703X(99)00035-2.

Sakai, T., Oishi, K., Asahara, T., Takada, T., Yuki, N., Matsumoto, K., Nomoto, K. & Kushiro, A. 2010. M-RTLV agar, a novel selective medium to distinguish *Lactobacillus casei* and *Lactobacillus paracasei* from *Lactobacillus rhamnosus*. *International journal of food microbiology*. 139(3):154–160. DOI: 10.1016/j.ijfoodmicro.2010.03.019.

Salman, W., Gavriilidis, A. & Angeli, P. 2006. On the formation of Taylor bubbles in small tubes. *Chemical engineering science*. 61(20):6653–6666. DOI: 10.1016/j.ces.2006.05.036.

Sánchez Pérez, J.A., Rodríguez Porcel, E.M., Casas López, J.L., Fernández Sevilla, J.M. & Chisti, Y. 2006. Shear rate in stirred tank and bubble column bioreactors. *Chemical engineering journal*. 124(1-3):1–5. DOI: 10.1016/j.cej.2006.07.002.

Sander, R. 2014. Compilation of Henry's law constants, version 3.99. *Atmospheric chemistry an physics discussions*. 14(21):29615–30521. DOI: 10.5194/acpd-14-29615-2014.

Sankpal, N. V, Joshi, A.P. & Kulkarni, B.D. 2001. Citric acid production by Aspergillus niger immobilized on cellulose microfibrils: influence of morphology and fermenter conditions on productivity. *Process biochemistry*. 36(11):1129–1139. DOI: 10.1016/S0032-9592(01)00155-8.

Sano, Y. & Usui, H. 1985. Interrelations among mixing time, power number and discharge flow rate number in baffled mixing vessels. *Journal of chemical engineering of Japan*. 18(1):47–52. DOI: 10.1252/jcej.18.47.

Schindler, B.D., Joshi, R. V & Vieille, C. 2014. Respiratory glycerol metabolism of *Actinobacillus succinogenes* 130Z for succinate production. *Journal of industrial microbiology & biotechnology*. 41(9):1339–1352. DOI: 10.1007/s10295-014-1480-x.

Schmid, A., Dordick, J.S., Hauer, B., Kiener, A., Wubbolts, M. & Witholt, B. 2001. Industrial biocatalysis today and tomorrow. *Nature*. 409(6817):258–268. DOI: 10.1038/35051736.

Senthuran, A., Senthuran, V., Hatti-Kaul, R. & Mattiasson, B. 1999. Lactic acid production by immobilized *Lactobacillus casei* in recycle batch reactor: a step towards optimization. *Journal of biotechnology*. 73(1):61–70. DOI: 10.1016/S0168-1656(99)00133-9.

Silva, E.M. & Yang, S.-T. 1995. Kinetics and stability of a fibrous-bed bioreactor for continuous production of lactic acid from unsupplemented acid whey. *Journal of biotechnology*. 41(1):59–70. DOI: 10.1016/0168-1656(95)00059-Y.

Singh, R., Paul, D. & Jain, R.K. 2006. Biofilms: implications in bioremediation. *Trends in microbiology*. 14(9):389–397. DOI: 10.1016/j.tim.2006.07.001.

Sobieszuk, P., Pohorecki, R., Cygański, P. & Grzelka, J. 2011. Determination of the interfacial area and mass transfer coefficients in the Taylor gas–liquid flow in a microchannel. *Chemical engineering science*. 66(23):6048–6056. DOI: 10.1016/j.ces.2011.08.029.

Stenroos, S.-L., Linko, Y.-Y. & Linko, P. 1982. Production of l-lactic acid with immobilized *Lactobacillus delbrueckii*. *Biotechnology letters*. 4(3):159–164. DOI: 10.1007/BF00144317.

Stewart, P.S. 1998. A review of experimental measurements of effective diffusive permeabilities and effective diffusion coefficients in biofilms. *Biotechnology and bioengineering*. 59(3):261–272. DOI: 10.1002/(SICI)1097-0290(19980805)59:3<261::AID-BIT1>3.0.CO;2-9.

Stojkovič, G. & Žnidaršič-Plazl, P. 2012. Continuous synthesis of l-malic acid using whole-cell microreactor. *Process biochemistry*. 47(7):1102–1107. DOI: 10.1016/j.procbio.2012.03.023.

Stoodley, P., Yang, S., Lappin-Scott, H. & Lewandowski, Z. 1997. Relationship between mass transfer coefficient and liquid flow velocity in heterogenous biofilms using microelectrodes and confocal microscopy. *Biotechnology and bioengineering*. 56(6):681–688. DOI: 10.1002/(SICI)1097-0290(19971220)56:6<681::AID-BIT11>3.0.CO;2-B.

Su, Y., Zhang, M., Zhu, X., Hu, Q. & Geng, Y. 2010. Measurements of wall shear stress in horizontal air–water bubbly flows. *Flow measurement and instrumentation*. 21(3):373–381. DOI: 10.1016/j.flowmeasinst.2010.04.008.

Sutherland, I. 2001a. Biofilm exopolysaccharides: a strong and sticky framework. *Microbiology (Reading, England)*. 147(1):3–9. Available: http://www.ncbi.nlm.nih.gov/pubmed/11160795.

Sutherland, I.W. 2001b. The biofilm matrix-an immobilized but dynamic microbial environment. *Trends in microbiology*. 9(5):222–227. DOI: 10.1016/S0966-842X(01)02012-1.

Tan, C.H., Koh, K.S., Xie, C., Tay, M., Zhou, Y., Williams, R., Ng, W.J., Rice, S. a, et al. 2014. The role of quorum sensing signalling in EPS production and the assembly of a sludge community into aerobic granules. *The ISME journal*. 8(6):1186–1197. DOI: 10.1038/ismej.2013.240.

Tang, H., Cao, T., Liang, X., Wang, A., Salley, S.O., McAllister, J. & Ng, K.Y.S. 2009. Influence of silicone surface roughness and hydrophobicity on adhesion and colonization of *Staphylococcus epidermidis*. *Journal of biomedical materials research. Part A*. 88(2):454–463. DOI: 10.1002/jbm.a.31788.

Tay, A. & Yang, S.-T. 2002. Production of L(+)-lactic acid from glucose and starch by immobilized cells of *Rhizopus oryzae* in a rotating fibrous bed bioreactor. *Biotechnology and bioengineering*. 80(1):1–12. DOI: 10.1002/bit.10340.

Teodósio, J.S., Simões, M., Melo, L.F. & Mergulhão, F.J. 2011. Flow cell hydrodynamics and their effects on *E. coli* biofilm formation under different nutrient conditions and turbulent flow. *Biofouling: The journal of bioadhesion and biofilm research*. 27(1):1–11. DOI: 10.1080/08927014.2010.535206.

Terada, A., Okuyama, K., Nishikawa, M., Tsuneda, S. & Hosomi, M. 2012. The effect of surface charge property on *Escherichia coli* initial adhesion and subsequent biofilm formation. *Biotechnology and bioengineering*. 109(7):1745–1754. DOI: 10.1002/bit.24429.

Tielen, P., Strathmann, M., Jaeger, K.-E., Flemming, H.-C. & Wingender, J. 2005. Alginate acetylation influences initial surface colonization by mucoid *Pseudomonas aeruginosa*. *Microbiological research*. 160(2):165–176. DOI: 10.1016/j.micres.2004.11.003.

Triplett, K.A., Ghiaasiaan, S.M., Abdel-Khalik, S.I. & Sadowski, D.L. 1999. Gas–liquid two-phase flow in microchannels Part I: two-phase flow patterns. *International journal of multiphase flow*. 25(3):377–394. DOI: 10.1016/S0301-9322(98)00054-8.

Tuli, A., Sethi, R.P., Khanna, P.K., Marwaha, S.S. & Kennedy, J.F. 1985. Lactic acid production from whey permeate by immobilized *Lactobacillus casei*. *Enzyme and microbial technology*. 7(4):164–168. DOI: 10.1016/0141-0229(85)90058-4.

Urbance, S.E., Pometto, A.L., DiSpirito, A.A. & Demirci, A. 2003. Medium evaluation and plastic composite support ingredient selection for biofilm formation and succinic acid production by *Actinobacillus succinogenes*. *Food biotechnology*. 17(1):53–65. DOI: 10.1081/FBT-120019984.

Urbance, S.E., Pometto, A.L., DiSpirito, A.A. & Denli, Y. 2004. Evaluation of succinic acid continuous and repeat-batch biofilm fermentation by *Actinobacillus succinogenes* using plastic composite support bioreactors. *Applied microbiology and biotechnology*. 65(6):664–670. DOI: 10.1007/s00253-004-1634-2.

Ürküt, Z., Dağbağlı, S. & Göksungur, Y. 2007. Optimization of pullulan production using Ca-alginate-immobilized *Aureobasidium pullulans* by response surface methodology. *Journal of chemical technology & biotechnology*. 82(9):837–846. DOI: 10.1002/jctb.1750.

Vallejos, J.R., Kostov, Y., Ram, A., French, J.A., Marten, M.R. & Rao, G. 2006. Optical analysis of liquid mixing in a minibioreactor. *Biotechnology and bioengineering*. 93(5):906–911. DOI: 10.1002/bit.20785.

Van Calsteren, M.R., Pau-Roblot, C., Bégin, A. & Roy, D. 2002. Structure determination of the exopolysaccharide produced by *Lactobacillus rhamnosus* strains RW-9595M and R. *Biochemical journal*. 363(1):7–17. Available: http://www.ncbi.nlm.nih.gov/pmc/articles/PMC1222445/ [2011, October 26].

Van der Werf, M.J., Guettler, M. V, Jain, M.K. & Zeikus, J.G. 1997. Environmental and physiological factors affecting the succinate product ratio during carbohydrate fermentation by *Actinobacillus* sp. 130Z. *Archives of microbiology*. 167(6):332–342. DOI: 10.1007/s002030050452.

Vandu, C.O., Liu, H. & Krishna, R. 2005. Mass transfer from Taylor bubbles rising in single capillaries. *Chemical engineering science*. 60(22):6430–6437. DOI: 10.1016/j.ces.2005.01.037.

Van Heerden, C.D. & Nicol, W. 2013. Continuous succinic acid fermentation by *Actinobacillus succinogenes*. *Biochemical engineering journal*. 73:5–11. DOI: 10.1016/j.bej.2013.01.015.

Van Loosdrecht, M.C.M., Eikelboom, D., Gjatelma, A., Mulder, A., Tijhuis, L. & Heijnen, J.J. 1995. Biofilm structures. *Water science and technology*. 32(8):35–43. DOI: 10.1016/0273-1223(96)00005-4.

Van Loosdrecht, M.C.M., Picioreanu, C. & Heijnen, J.J. 1997. A more unifying hypothesis for biofilm structures. *FEMS microbiology ecology*. 24(2):181–183. DOI: 10.1111/j.1574-6941.1997.tb00434.x.

Van Loosdrecht, M.C.M., Heijnen, J.J., Eberl, H., Kreft, J. & Picioreanu, C. 2002. Mathematical modelling of biofilm structures. *Antonie van Leeuwenhoek*. 81(1-4):245–256. DOI: 10.1023/A:1020527020464.

Vilain, S., Pretorius, J.M., Theron, J., Brözel, V.S. & Broezel, V.S. 2009. DNA as an adhesin: *Bacillus cereus* requires extracellular DNA to form biofilms. *Applied and environmental microbiology*. 75(9):2861–2868. DOI: 10.1128/AEM.01317-08.

Villadsen, J., Nielsen, J. & Lidén, G. 2011. *Bioreaction Engineering Principles*. 3rd ed. Boston, MA: Springer US. DOI: 10.1007/978-1-4419-9688-6.

Vlysidis, A., Binns, M., Webb, C. & Theodoropoulos, C. 2011. Glycerol utilisation for the production of chemicals: Conversion to succinic acid, a combined experimental and computational study. *Biochemical engineering journal*. 58-59:1–11. DOI: 10.1016/j.bej.2011.07.004.

Vu, B., Chen, M., Crawford, R.J. & Ivanova, E.P. 2009. Bacterial extracellular polysaccharides involved in biofilm formation. *Molecules (Basel, Switzerland)*. 14(7):2535–2554. DOI: 10.3390/molecules14072535.

Walker, J.T., Mackerness, C.W., Rogers, J. & Keevil, C.W. 1995. Heterogeneous mosaic biofilm—a haven for waterborne pathogens. In *Microbial Biofilms*. H.M. Lappin-Scott & J.W. Costerton, Eds. Cambridge: Cambridge University Press. 196–204.

Wang, A.Y., Leong, S., Liang, Y.-C., Huang, R.C.C., Chen, C.S. & Yu, S.M. 2008. Immobilization of growth factors on collagen scaffolds mediated by polyanionic collagen mimetic peptides and its effect on endothelial cell morphogenesis. *Biomacromolecules*. 9(10):2929–2936. DOI: 10.1021/bm800727z.

Wang, C.-C., Zhu, L.-W., Li, H.-M. & Tang, Y.-J. 2012. Performance analyses of a neutralizing agent combination strategy for the production of succinic acid by *Actinobacillus succinogenes* ATCC 55618. *Bioprocess and biosystems engineering*. 35(4):659–664. DOI: 10.1007/s00449-011-0644-6.

Wang, F., Hayter, J. & Wilson, L.J. 1996. Salt-induced aggregation of lysozyme studied by cross-linking with glutaraldehyde: implications for crystal growth. *Acta crystallographica. Section D, Biological crystallography*. 52(5):901–908. DOI: 10.1107/S0907444996005227.

Wang, R., Neoh, K.G., Shi, Z., Kang, E.-T., Tambyah, P.A. & Chiong, E. 2012. Inhibition of *Escherichia coli* and *Proteus mirabilis* adhesion and biofilm formation on medical grade silicone surface. *Biotechnology and bioengineering*. 109(2):336–345. DOI: 10.1002/bit.23342.

Watnick, P.I., Kolter, R. & Watnik, P.I. 1999. Steps in the development of a *Vibrio cholerae* El Tor biofilm. *Molecular microbiology*. 34(3):586–595. DOI: 10.1046/j.1365-2958.1999.01624.x.

Webb, C., Fukuda, H. & Atkinson, B. 1986. The production of cellulase in a spouted bed fermentor using cells immobilized in biomass support particles. *Biotechnology and bioengineering*. 28(1):41–50. DOI: 10.1002/bit.260280107.

Wecker, A. & Onken, U. 1991. Influence of dissolved oxygen concentration and shear rate on the production of pullulan by *Aureobasidium pullulans*. *Biotechnology letters*. 13(3):155–160. DOI: 10.1007/BF01025810.

Wee, Y.-J., Yun, J.-S., Kang, K.-H. & Ryu, H.-W. 2002. Continuous production of succinic acid by a fumarate-reducing bacterium immobilized in a hollow-fiber bioreactor. In *Biotechnology for fuels and chemicals*. M. Finkelstein, J.D. McMillan, & B.H. Davison, Eds. New York, NY: Humana Press. 1093–1104. DOI: 10.1007/978-1-4612-0119-9_88.

Werpy, T. & Petersen, G.R. 2004. *Top value added chemicals from biomass. Volume 1-results of screening for potential candidates from sugars and synthesis gas*. Oak Ridge. Available: http://www.nrel.gov/docs/fy04osti/35523.pdf [2011, September 09].

West, T.P. 2011. Effect of carbon source on polysaccharide production by alginate-entrapped *Aureobasidium pullulans* ATCC 42023 cells. *Journal of basic microbiology*. 51(6):673–677. DOI: 10.1002/jobm.201100048.

Weuster-Botz, D. 1993. Continuous ethanol production by *Zymomonas mobilis* in a fluidized bed reactor. Part I. Kinetic studies of immobilization in macroporous glass beads. *Applied microbiology and biotechnology*. 39(6):679–684. DOI: 10.1007/BF00164449.

Weuster-Botz, D., Aivasidis, A. & Wandrey, C. 1993. Continuous ethanol production by *Zymomonas mobilis* in a fluidized bed reactor. Part II: Process development for the fermentation of hydrolysed B-starch without sterilization. *Applied microbiology and biotechnology*. 39(6):685–690. DOI: 10.1007/BF00164450.

Whitchurch, C.B., Tolker-Nielsen, T., Ragas, P.C. & Mattick, J.S. 2002. Extracellular DNA required for bacterial biofilm formation. *Science*. 295(5559):1487. DOI: 10.1126/science.295.5559.1487.

Whitfield, C. 1988. Bacterial extracellular polysaccharides. *Canadian journal of microbiology*. 34(4):415–420. DOI: 10.1139/m88-073.

Wimpenny, J.W.T. & Colasanti, R. 1997. A unifying hypothesis for the structure of microbial biofilms based on cellular automaton models. *FEMS microbiology ecology*. 22(1):1–16. DOI: 10.1111/j.1574-6941.1997.tb00351.x.

Wingender, J., Neu, T.R. & Flemming, H.-C. 1999. What are bacterial extracellular polymeric substances? In *Microbial extracellular polymeric substances*. J. Wingender, T.R. Neu, & H.-C. Flemming, Eds. Berlin, Heidelberg: Springer Berlin Heidelberg. 1–24. DOI: 10.1007/978-3-642-60147-7.

Wongwises, S., Pornsee, A. & Siroratsakul, E. 1999. Gas-wall shear stress distribution in horizontal stratified two-phase flow. *International communications in heat and mass transfer*. 26(6):849–860. DOI: 10.1016/S0735-1933(99)00073-1.

Xi, Y., Chen, K.-Q., Xu, R., Zhang, J.-H., Bai, X.-F., Jiang, M., Wei, P. & Chen, J.-Y. 2012. Effect of biotin and a similar compound on succinic acid fermentation by *Actinobacillus succinogenes* in a chemically defined medium. *Biochemical engineering journal*. 69:87–92. DOI: 10.1016/j.bej.2012.08.016.

Xiao, Z. & Xu, P. 2007. Acetoin metabolism in bacteria. *Critical reviews in microbiology*. 33(2):127–140. DOI: 10.1080/10408410701364604.

Xu, G., Chu, J., Wang, Y., Zhuang, Y., Zhang, S. & Peng, H. 2006. Development of a continuous cell-recycle fermentation system for production of lactic acid by *Lactobacillus paracasei*. *Process biochemistry*. 41(12):2458–2463. DOI: 10.1016/j.procbio.2006.05.022.

Yahiro, K., Takahama, T., Park, Y.S. & Okabe, M. 1995. Breeding of *Aspergillus terreus* mutant TN-484 for itaconic acid production with high yield. *Journal of fermentation and bioengineering*. 79(5):506–508. DOI: 10.1016/0922-338X(95)91272-7.

Yan, Q., Zheng, P., Tao, S.-T. & Dong, J.-J. 2014. Fermentation process for continuous production of succinic acid in a fibrous bed bioreactor. *Biochemical engineering journal*. 91:92–98. DOI: 10.1016/j.bej.2014.08.002.

Yan, Q., Zheng, P., Dong, J.-J. & Sun, Z.-H. 2014. A fibrous bed bioreactor to improve the productivity of succinic acid by *Actinobacillus succinogenes*. *Journal of chemical technology & biotechnology*. 89(11):1760–1766. DOI: 10.1002/jctb.4257.

Yang, Z., Li, S., Zhang, X., Zeng, X., Li, D., Zhao, Y. & Zhang, J. 2010. Capsular and slime-polysaccharide production by Lactobacillus rhamnosus JAAS8 isolated from Chinese sauerkraut: potential application in fermented milk products. *Journal of bioscience and bioengineering*. 110(1):53–57. DOI: 10.1016/j.jbiosc.2009.12.010.

Yazdian, F., Shojaosadati, S., Nosrati, M., Mehrnia, M. & Vasheghani-Farahani, E. 2009. Study of geometry and operational conditions on mixing time, gas hold up, mass transfer, flow regime and biomass production from natural gas in a horizontal tubular loop bioreactor. *Chemical engineering science*. 64(3):540–547. DOI: 10.1016/j.ces.2008.09.031.

Yazdian, F., Hajiabbas, M.P., Shojaosadati, S. a., Nosrati, M., Vasheghani-Farahani, E. & Mehrnia, M.R. 2010. Study of hydrodynamics, mass transfer, energy consumption, and biomass production from natural gas in a forced-liquid vertical tubular loop bioreactor. *Biochemical engineering journal*. 49(2):192–200. DOI: 10.1016/j.bej.2009.12.013.

Yu, M.-C., Wang, R.-C., Wang, C.-Y., Duan, K.-J. & Sheu, D.-C. 2007. Enhanced production of l(+)-lactic acid by floc-form culture of *Rhizopus oryzae*. *Journal of the Chinese institute of chemical engineers*. 38(3-4):223–228. DOI: 10.1016/j.jcice.2007.02.005.

Zeguai, S., Chikh, S. & Tadrist, L. 2013. Experimental study of two-phase flow pattern evolution in a horizontal circular tube of small diameter in laminar flow conditions. *International journal of multiphase flow*. 55:99–110. DOI: 10.1016/j.ijmultiphaseflow.2013.04.008.

Zhang, S., Norrlöw, O., Wawrzynczyk, J. & Dey, E.S. 2004. Poly(3-hydroxybutyrate) biosynthesis in the biofilm of *Alcaligenes eutrophus*, using glucose enzymatically released from pulp fiber sludge. *Applied and environmental microbiology*. 70(11):6776–6782. DOI: 10.1128/AEM.70.11.6776-6782.2004.

Zhang, W., Sileika, T.S., Chen, C., Liu, Y., Lee, J. & Packman, A.I. 2011. A novel planar flow cell for studies of biofilm heterogeneity and flow-biofilm interactions. *Biotechnology and bioengineering*. 108(11):2571–2582. DOI: 10.1002/bit.23234.

Zhang, Y., Ma, Y., Yang, F. & Zhang, C. 2009. Continuous acetone-butanol-ethanol production by corn stalk immobilized cells. *Journal of industrial microbiology & biotechnology*. 36(8):1117–1121. DOI: 10.1007/s10295-009-0582-3.

Zheng, P., Dong, J.-J., Sun, Z.-H., Ni, Y. & Fang, L. 2009. Fermentative production of succinic acid from straw hydrolysate by *Actinobacillus succinogenes*. *Bioresource technology*. 100(8):2425–2429. DOI: 10.1016/j.biortech.2008.11.043.

Zheng, P., Zhang, K., Yan, Q., Xu, Y. & Sun, Z. 2013. Enhanced succinic acid production by *Actinobacillus succinogenes* after genome shuffling. *Journal of industrial microbiology & biotechnology*. 40(8):831–840. DOI: 10.1007/s10295-013-1283-5.

Zou, W., Zhu, L.-W., Li, H.-M. & Tang, Y.-J. 2011. Significance of CO_2 donor on the production of succinic acid by *Actinobacillus succinogenes* ATCC 55618. *Microbial cell factories*. 10:87. DOI: 10.1186/1475-2859-10-87.

Appendix A: Two-phase biofilm fermenter

A.i *Hydrodynamic entry length criteria*

According to Çengel & Cimbala (2006: 326) the hydrodynamic entry length is the length of pipe required for fully developed flow. According to Bahrami (2011), in a pipe with length 1 000 times greater than its diameter all the entrance effects would negligible, inferring the entire length of tube can be analysed as fully developed flow. This means that the total length of the tubing had to be at least 1 000 times the diameter of the tubing to ensure near perfect mixing within the reactor and therefore CSTR characteristics.

A.ii *Area to volume ratio of a tube*

For a tube of constant diameter, the area to volume ratio is an intrinsic characteristic, independent of the external dimensions. The value of A/V can be expressed as equation *(A-1)*:

$$\frac{\mathrm{A}}{\mathrm{V}} = \frac{\pi d L}{\frac{\pi d^2 L}{4}} = \frac{4}{d} \tag{A-1}$$

A.iii *Pressure drop in tubes*

The minimum pressure drop (ΔP_{min}) in a tube is calculated using equation *(A-2)*, with f the Darcy-Weisbach friction factor, L the length of the tube, d the diameter, ρ the density of the fluid and u_{avg} the average superficial velocity in the line.

$$\Delta P_{min} = f \frac{L}{d} \frac{\rho u_{avg}^2}{2} \tag{A-2}$$

A.iv *Hydrodynamic flow regimes in tubes*

Hydrodynamic flow in tubes can be described as laminar (*FIGURE A-1*a) or turbulent (*FIGURE A-1*b) with a transitional regime between these flow regimes. The laminar regime is characterised by smooth streamlines with highly ordered movement of the fluid, while the turbulent regime is characterised by significant velocity fluctuations as well as highly disordered motion in the liquid. The transitional regime fluctuates between laminar and turbulent flow and

therefore possesses characteristics of both these regimes (Çengel & Cimbala, 2006: 323). The flow regime in tubes is characterised using the Reynolds number (Re) defined by equation *(A-3)* (Reynolds, 1895):

$$\mathrm{Re} = \frac{\rho d u}{\mu_L} \tag{A-3}$$

The regimes are usually defined as laminar for Re ≤ 2300 and turbulent for Re ≥ 4000, with transitional flow 2 300 < Re < 4 000 (Çengel & Cimbala, 2006: 324–325). The shear stresses experienced at the tube wall are highly dependent on the hydrodynamic flow regime in the tube, this is due to the significant difference in the velocity profiles of laminar and turbulent flows as shown in *FIGURE A-1* (Çengel & Cimbala, 2006: 328,338).

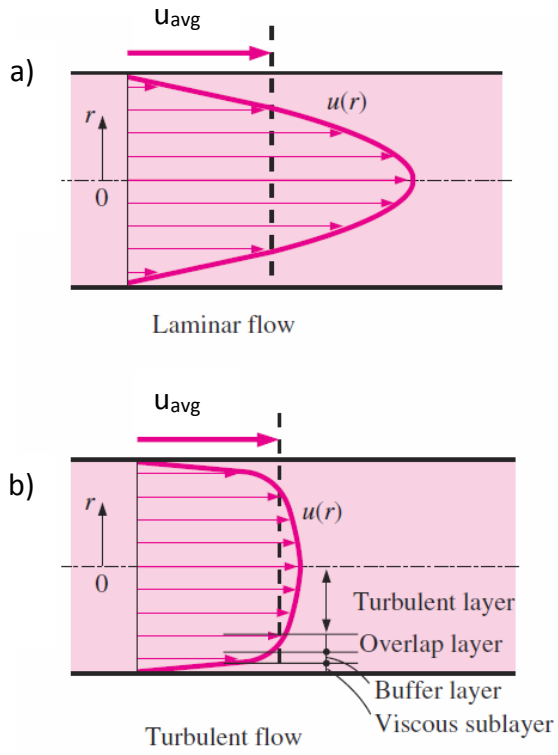

Figure A-1: Velocity profiles in a) laminar and b) turbulent flow in pipes (Çengel & Cimbala, 2006: 338). The velocity profile in the laminar flow regime has a parabolic shape which is proportional to the average velocity and inversely proportional to the square of the tube radius. This means that the τ_W is a linear function of the average velocity and inversely proportional to the tube diameter. The τ_W in the turbulent regime is non-linearly proportional to the average velocity because it is inversely proportional to the viscous sublayer thickness which in turn is inversely affected by the average velocity.

A.i *Wall shear stresses in a tube*

The shear stresses at the tube wall can be expressed by equation *(A-4)* with τ_W the shear stresses at the wall, μ_L the dynamic viscosity of water, and $\partial u/\partial y$ the slope of the velocity profile of the liquid in the tube (Çengel & Cimbala, 2006: 337).

$$\tau_W = \mu_L \left(\frac{\partial u}{\partial y}\right)_{y=0} \quad \text{(A-4)}$$

From equation *(A-4)* can be seen that τ_W is directly proportional to ∂u/∂y at the wall with μ_L the proportionality constant; in aqueous medium the fluid behaves as a Newtonian fluid with a constant μ_L (7×10^{-4} Pa.s).

In the case of laminar flow in tubes (*FIGURE A-1*a), it can be proven that the velocity profile is parabolic and can be expressed in terms of the radius (r), total tube radius (R) and average superficial velocity (u_{avg}) as shown in equation *(A-5)*.

$$u(r) = 2u_{avg}\left(1 - \frac{r^2}{R^2}\right) \quad \text{(A-5)}$$

Applying equation *(A-4)* to equation *(A-5)* and setting r = R yields equation *(A-6)* in terms of tube diameter (d):

$$\tau_W = \mu_L \left(\frac{\partial u}{\partial y}\right)_{y=0} = \mu_L \left(\frac{\partial u}{\partial r}\right)_{r=R} = -\frac{4\mu_L u_{avg}}{R} = -\frac{8\mu_L u_{avg}}{d} \quad \text{(A-6)}$$

This equation shows that for laminar flow conditions the shear stresses in the reactor are directly proportional to the average superficial velocity in the tube and inversely proportional to the tube diameter.

In the case of turbulent flow conditions (*FIGURE A-1*b), the velocity profile in the tube bulges out significantly which leads to a significantly increased slope and therefore a much larger shear stress at the wall. From *FIGURE A-1*b can be seen that the flow in the turbulent regime can be divided into four sublayers; viscous, buffer, overlap and turbulent (Çengel & Cimbala, 2006: 338). The viscous sublayer is the most important for this study as this layer dictates the shear stress at the wall, the parameter which would dictate biofilm inhibition or removal. The viscous sublayer is usually extremely thin, typically much less than one percent of the tube diameter, yet this layer plays a dominant role in the shear stresses as a result of the very large velocity gradient present in this layer. The wall dampens eddy effects in this layer and therefore the flow is nearly laminar, leading to laminar shear stresses on the wall (Çengel & Cimbala, 2006: 338). The velocity gradient at the wall remains nearly constant at ∂u/∂y = u/y therefore yielding equation *(A-7)*, where u_δ is the velocity at the edge of the viscous sublayer and y_δ is the thickness of the viscous sublayer (Çengel & Cimbala, 2006: 338).

$$\tau_W = \mu_L \left(\frac{\partial u}{\partial y}\right)_{y=0} = \mu_L \frac{u_\delta}{y_\delta} \quad \text{(A-7)}$$

Experimentally, it has been found that the viscous sublayer is suppressed at higher u_{avg} and therefore y_δ becomes smaller, while u_δ is closely related to the u_{avg}. From this can be concluded that as the velocity increases in the turbulent regime, the wall shear increases non-linearly as a result of the increasing u_δ and the decreasing y_δ. Unlike laminar regime, the wall shear stresses are independent of the diameter of the tube.

A.ii *Shear stress requirements to inhibit microbial attachment or biofilm removal*

It has been shown that shear stresses of 6–8 Pa are sufficient in inhibiting *Pseudomonas fluorescens* growth while shear stresses of 12–13 Pa are sufficient to remove attached cells (Bakker et al., 2003; Paul et al., 2012). Teodósio et al. (2011) used computational fluid dynamics to simulate the shear stresses present in silicone tubing of 8 mm diameter and found that at a superficial velocity of 2.2 $m.s^{-1}$ the average shear stress was estimated as 15 Pa, with a maximum shear stress of 18 Pa. These values are well in excess of the 12 Pa required for cell removal as well as the 6–8 Pa required for biofilm inhibition. This was verified by the absence of *Escherichia coli* biofilms in these tubes during fermentation, while there were biofilms observed in flow cells present in the rest of the system (Teodósio et al., 2011).

By analysing the results from Teodósio et al. (2011), it was found that the tubing had a Re ≈ 17 500, indicating fully turbulent conditions. This means that the average shear stress, at 2.2 $m.s^{-1}$, of 15.3 Pa estimated in this study would be applicable to silicone tubing of any diameter with equivalent viscosity. Increasing the superficial velocity would non-linearly increase the shear. This was supported by work done by Liu (1997) and Su et al. (2010) which will be described in the *WALL SHEAR IN A TAYLOR FLOW SYSTEM* section in *APPENDIX B*.

Appendix B: Three-phase biofilm fermenter

B.i *Gas–liquid flow in tubes*

Gas–liquid flow in tubes have been extensively studied due to its importance in industrial applications, e.g. petroleum oil transport, refrigerant transport, steam–water flow as well as multiphase chemical reactors (Jepson & Taylor, 1993; Coleman & Garimella, 1999, 2003; Triplett et al., 1999; Wongwises, Pornsee & Siroratsakul, 1999; Chen, Tian & Karayiannis, 2006; Jassim, Newell & Chato, 2006; Hanafizadeh et al., 2011; Zeguai, Chikh & Tadrist, 2013). The flow in these tube are characterised with respect to the observed flow patterns and interphase interactions observed at different gas or liquid superficial velocities, with various different regimes reported depending on the criteria used in the respective study. *TABLE B-1* shows the most prominent flow-regimes within small-channels (Section *B.II* on page *B-3*) (Coleman & Garimella, 1999; Triplett et al., 1999; Chen, Tian & Karayiannis, 2006) as well as the main flow-patterns within these flow-regimes. The visually observed flow-patterns are shown in *FIGURE B-1* with the corresponding regime transition boundaries shown in *FIGURE B-2*.

Table B-1: The major flow-regimes in small-channel gas–liquid flow, identified in the literature (Coleman & Garimella, 1999; Chen, Tian & Karayiannis, 2006).

Major Flow Regimes	Flow patterns
Intermittent	Slug flow (Taylor bubble)
	Churn
Annular	Wavy annular
	Annular
Dispersed/Bubble flow	Bubble
	Dispersed bubble

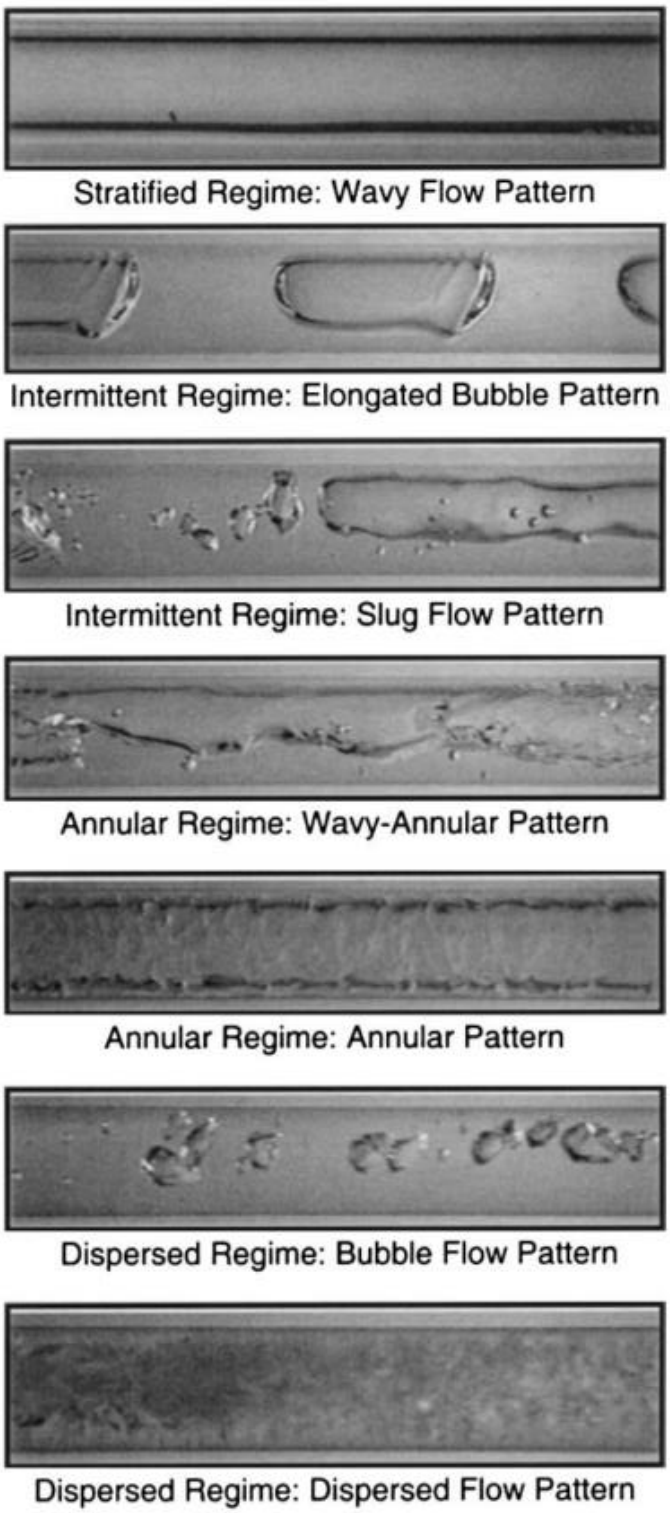

Figure B-1: The visually observed flow-patterns in present in gas–liquid flow within small channel systems (Coleman & Garimella, 1999).

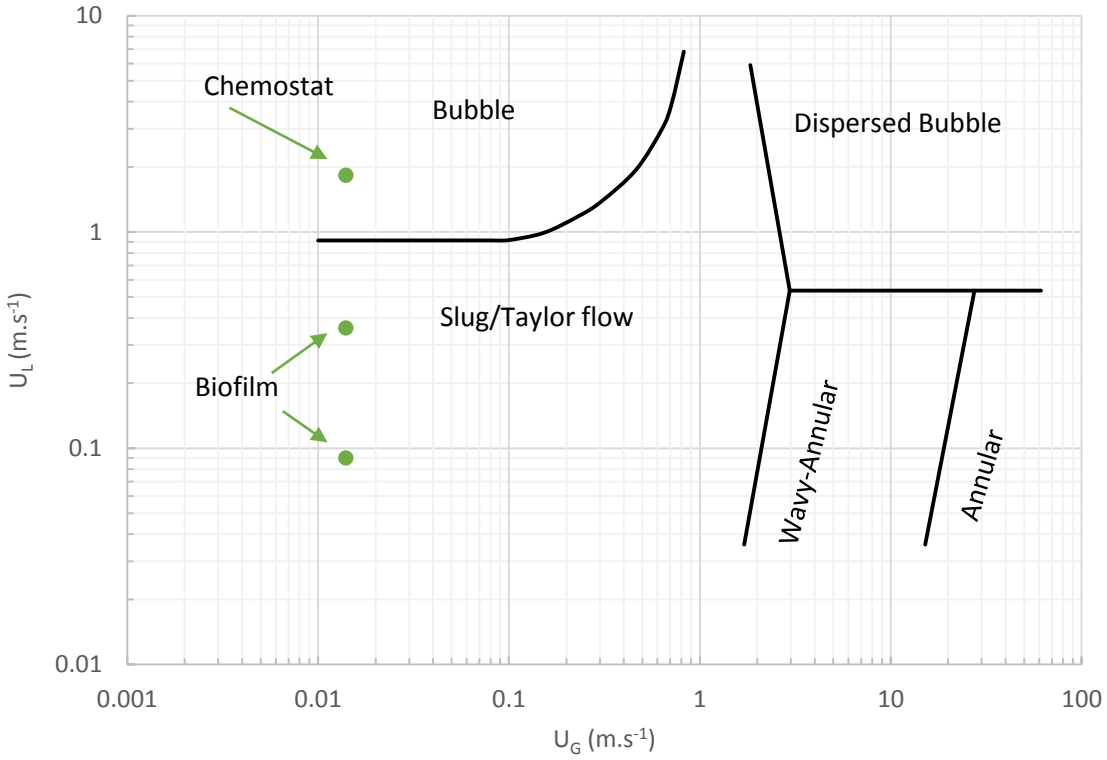

Figure B-2: The gas–liquid flow-regime map (Coleman & Garimella, 1999; Triplett et al., 1999), showing the different flow-regimes present within gas–liquid multiphase flow. In addition, the operating points within this study are shown as green points, it can clearly be seen that the biofilm runs were operated within the slugging flow (Taylor flow) regime, while the chemostat operated in the bubble flow regime,

From *FIGURE B-2* can be seen that at relatively low gas superficial velocities ($u_g \lessapprox 2$ m.s^{-1}) there are only two applicable flow regimes, i.e. the plug/slug flow (Taylor bubble) and the bubble/dispersed flow regimes. At liquid superficial velocities (u_L) $\lessapprox 1$ m, the Taylor bubble regime dominates while for $u_L \gtrapprox 1$ m.s^{-1} the flow is predominantly dispersed/bubble regime.

The experimental operating points are shown in *FIGURE B-2* and indicates that the biofilm runs were operated within the slugging (Taylor flow) regime, while the chemostat was operated within the bubble flow regime.

B.ii *Small-channel flow assessment in experimental design*

Small-channel, two-phase flow is defined by the criterion in *EQUATION (B-1)*, in which g is the gravitational acceleration, ρ_{H2O} and ρ_{H2O} the densities of the two phases, Water and CO_2, d is the diameter of the tube and σ is the interfacial tension. In the case of small-channels there is no observable difference between horizontal and vertical tubes as it was shown that effect of gravity on the gas behaviour in the tubes were negligible (Bretherton, 1961)

$$\frac{g\left(\rho_{H_2O} - \rho_{CO_2}\right)d^2}{\sigma} < 3.37 \qquad \text{(B-1)}$$

In order to ensure the system could be defined as a small-channel system, the system was assessed according to the criterion in equation *(B-1)* (Bretherton, 1961) using the parameters in *TABLE B-2*. The value for the dimensionless group yielded 1.25 which is significantly smaller than 3.37 and therefore the system can be defined as small-channel, two-phase flow capable of Taylor flow at medium to low superficial velocities (Salman, Gavriilidis & Angeli, 2006). Therefore the system should not be affected by gravitational effects and the gas–liquid flow regime map (*FIGURE B-2*) is applicable.

Table B-2: System parameters used to verify that the system can be classified as a small-channel system and are therefore not affected by gravity

Parameter	Value
g	9.81 $m.s^{-2}$
ρ_{H2O} (37 °C)	992 $kg.m^{-3}$
ρ_{CO2} (37 °C)	1.8 $kg.m^{-3}$
d	0.003 m
σ	0.07 $N.m^{-1}$ (Espinoza & Santamarina, 2010; Banerjee et al., 2013)

B.iii *Gas–liquid mass transfer in Taylor flow*

In a system dominated by Taylor flow (*FIGURE B-3*), the gas-phase consists of elongated capsular bubbles, with equivalent diameter ≫ d, separated by liquid slugs (Salman, Gavriilidis & Angeli, 2006; Cai et al., 2013). A significant benefit of this form of two-phase flow is a significant improvement in heat and mass transfer between the liquid and wall as well as improvement in the interfacial gas–liquid mass transfer between the bubble and the liquid slug (Berčič & Pintar, 1997). Berčič & Pintar (1997) developed a simple correlation (equation *(B-2)*) for determining the gas–liquid mass transfer in Taylor flow.

$$k_L a = \frac{0.111(u_G + u_L)^{1.19}}{\left((1 - \epsilon_G)L_{UC}\right)^{0.57}} \qquad \text{(B-2)}$$

This was followed by another correlation derived by Vandu, Liu & Krishna (2005) which took into account the effect of tube diameter (equation *(B-3)*):

$$k_L a = \frac{1}{d}\sqrt{\frac{\mathfrak{D} u_G}{L_{UC}}} \tag{B-3}$$

According to Cai et al. (2013), the overall gas–liquid mass transfer coefficient ($k_L a$) can be expressed by equation *(B-4)*. The parameters a_{cap} and a_{Film} can be calculated using equations *(B-5)* and *(B-6)* (Sobieszuk et al., 2011; Cai et al., 2013), while the parameters $k_{L,Cap}$ and $k_{L,Film}$ can be calculated using equations *(B-7)* to *(B-11)* (Sobieszuk et al., 2011; Cai et al., 2013).

$$k_L a = k_{L,Cap} a_{Cap} + k_{L,Film} a_{Film} \tag{B-4}$$

$$a_{Cap} = \frac{4}{L_{UC}} \tag{B-5}$$

$$a_{Film} = \frac{4L_b}{L_{UC} d} \tag{B-6}$$

The parameters L_{UC} and L_B can be evaluated experimentally as shown in *FIGURE B-3*.

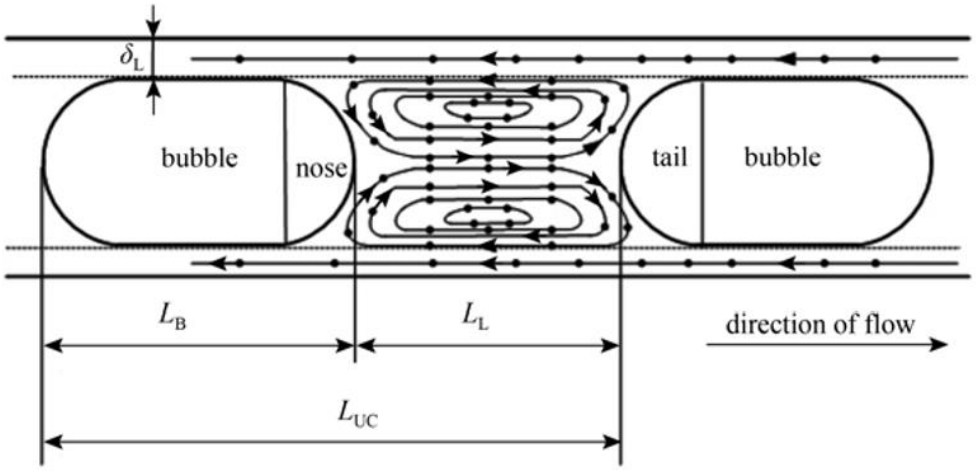

Figure B-3: Diagram showing a visualisation of the flow patterns within a slugging or Taylor flow system (Cai et al., 2013)

$$k_{L,Cap} = \frac{4}{\pi}\sqrt{\frac{\mathfrak{D} u_b}{d}} \tag{B-7}$$

$$k_{L,Film} = 2\sqrt{\frac{\mathfrak{D}u_b}{\pi L_b}} \tag{B-8}$$

$$\frac{L_b}{d} = 1.637\epsilon_G^{0.107}(1-\epsilon_G)^{-1.05}Re^{-0.075}Ca^{-0.0687} \tag{B-9}$$

$$u_b = u_{TP}\frac{1}{1-0.61Ca^{0.33}} \tag{B-10}$$

$$Ca = \frac{u_{TP}\mu_L}{\sigma} \tag{B-11}$$

The total k_La of the system was solved using both the simple correlations of Berčič & Pintar (1997) (equation *(B-2)*), and Vandu, Liu & Krishna (2005) (equation *(B-3)*), as well as the more complicated system (equations *(B-4)* to *(B-11)*) for various gas flow rates at a liquid velocity of 0.09 m.s^{-1} using parameters as shown in *TABLE B-3*. The results are shown in *FIGURE B-4*. In determining the L_{UC} it was assumed that the peristaltic pump forms three individual slug during a single revolution, this assumption is based on the design of the pump head which uses three individual equispaced rollers. This means that at 10 rpm (u_L = 0.09 m.s^{-1}) there would form a slug every two seconds, therefore $L_{UC} = 2(u_L + u_G)$. The gas hold-up in the system was assumed to be predicted by the equation $\epsilon_G = u_G/(u_L + u_G)$.

Table B-3: Parameters used to calculate the k_La values in the system using correlations from the literature (Berčič & Pintar, 1997; Vandu, Liu & Krishna, 2005; Cai et al., 2013)

Parameter	Value	Reference
$\mathfrak{D}$	2.49 × 10^{-9} m^2.s^{-1}	(Frank, Kuipers & Van Swaaij, 1996)
ρ	992 kg.m^{-3}	
μ_L	0.0007 Pa.s	(Frank, Kuipers & Van Swaaij, 1996)
σ	0.07 N.m^{-1}	(Espinoza & Santamarina, 2010; Banerjee et al., 2013)

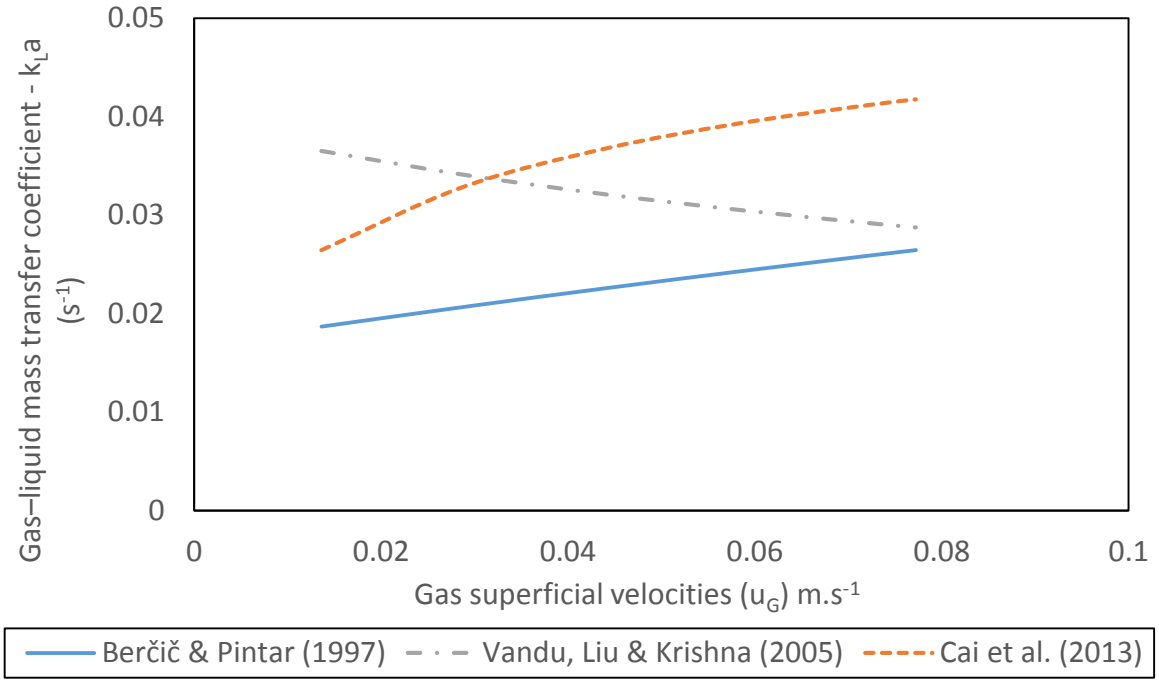

Figure B-4: Calculated k_La values in a Taylor flow system, using the parameters shown in *TABLE B-3* and correlations from the literature (Berčič & Pintar, 1997; Vandu, Liu & Krishna, 2005; Cai et al., 2013) as a function of the gas superficial velocity.

These correlations show that the k_La value of the system falls within a narrow range of values, between 0.02 s^{-1} – 0.04 s^{-1} for u_G values between 0.014 – 0.078 $m.s^{-1}$.

B.iv *Wall shear in a Taylor flow system*

It has been shown that that the wall shear in a Taylor flow systems can be expressed by equation *(B-12)*; τ_{W0} is defined as the wall shear stress in single phase flow under the same operational conditions and α_m are the actual void fraction in the reactor (equation *(B-13)*) (Nakoryakov et al., 1981; Nakoryakov, Kashinsky & Kozmenko, 1986; Kashinsky, Kurdyumov & Randin, 2006).

$$\tau_W = \tau_{W0}(1-\alpha_m)^{-1.53} \quad \text{(B-12)}$$

$$\alpha_m = \frac{0.833u_g}{u_g + u_L} \quad \text{(B-13)}$$

From equation *(B-12)* can be seen that as $\alpha_m \rightarrow 0$, $\tau_W \rightarrow \tau_{W0}$, indicating that the shear in the system tends to approximate that in a liquid system under the same conditions as the ratio of gas to liquid superficial velocities decrease. This observation was supported by a number of authors (Liu, 1997; Su et al., 2010; Teodósio et al., 2011) for shear stress measurements in which the $u_L \gg u_g$. *FIGURE B-5* shows that at several different u_g for constant values for u_L,

very similar τ_W values were measured. The measurements in *FIGURE B-5* were done in the Taylor flow and bubble flow regime in gas–liquid systems, as well as turbulent flow regime in single phase systems (u_g = 0, Re > 4 000).

From *FIGURE B-5* can be seen that τ_W in a bubble flow regime and a turbulent regime can be predicted by equation *(B-14)*.

$$\tau_W = 4.56 u_L^{1.34} \qquad \text{(B-14)}$$

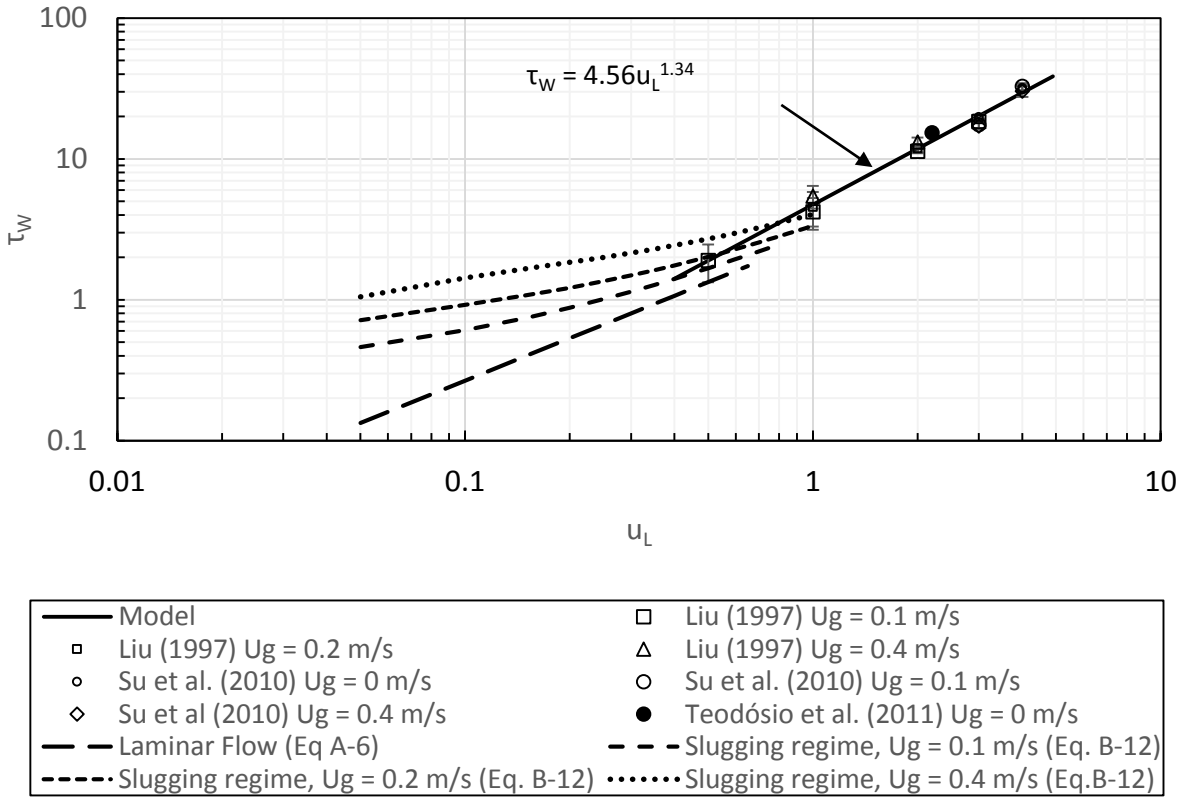

Figure B-5: Correlation of the wall shear in gas–liquid flow system using data from the literature (Liu, 1997; Su et al., 2010; Teodósio et al., 2011), as compared to correlations presented elsewhere (equations *(A-6)* and *(B-12)*).

It is interesting that the wall shear measured in turbulent, liquid systems (Su et al., 2010; Teodósio et al., 2011) fit the correlation quite well and was therefore used to estimate the wall shear in the two-phase reactor system during chemostat operation as well as during scrubbing procedures (section 3.4.1 on page 3-7).

B.v *Pressure drop in a two phase flow system*

Determining the pressure drop in two-phase flow systems is more complicated than in a single-phase system, due to the additional friction and turbulence caused by the gas phase in

the system. According to Chisholm (1967), Mishima & Hibiki (1996) and Muzychka & Awad (2010) the pressure drop in a two-phase system can be determined using a multiplier φ^2_L defined by equation *(B-15)*.

$$\phi_L^2 = \frac{\Delta P_{total}}{\Delta P_L} \tag{B-15}$$

With ΔP_{total} and ΔP_L the total pressure drop and the pressure drop in a single-phase liquid system (equation *(A-2)*) respectively. The multiplier can be evaluated using equations *(B-16)*, *(B-17)* and *(B-18)*, ΔP_G is defined as the pressure drop in the same system for single-phase gas flow (equation *(A-2)*), C is the Chisholm parameter (Chisholm, 1967) and d the tube diameter in mm.

$$\phi_L^2 = 1 + \frac{C}{X} + \frac{1}{X^2} \tag{B-16}$$

$$X^2 = \frac{\Delta P_L}{\Delta P_G} \tag{B-17}$$

$$C = 21(1 - e^{-0.333d}) \tag{B-18}$$

B.vi *Gas–liquid separation*

Industrially gas bubbles and liquid slugs are separated using what is referred to as gas–liquid separators (GLS), flash-drums, knock-out drums or “slug-catchers”. The main objective in the design of the GLS is to ensure total separation of gas and liquid ensuring that no accumulation of gas in the system occurs. *FIGURE B-6* shows a typical design for a vapour liquid separator (Engineering Workshop, 2013).

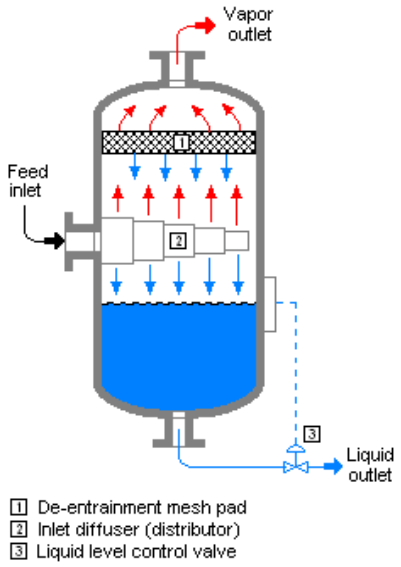

Figure B-6: Design of a gas–liquid separation vessel in industry (Engineering Workshop, 2013)

B.vii *Mixing in a stirred vessel*

The mixing regime in a stirred vessel can be expressed using the impeller Reynolds number (Re_i) defined by equation *(B-19)* (Leng, Katti & Atiemo-Obeng, 2008: 920; Doran, 2013: 204), The variables in equation *(B-19)* are defined as: Re_i – the impeller Reynolds number; N – the stirring speed of the impeller (s^{-1}); d_i – the impeller diameter (m); ρ – the liquid density ($kg.m^{-3}$) and μ_L – the liquid dynamic viscosity (Pa.s).

$$Re_i = \frac{d_i^2 N \rho}{\mu_L} \qquad \text{(B-19)}$$

The regimes in the case of a stirred vessel are defined as (Leng, Katti & Atiemo-Obeng, 2008: 924; Doran, 2013: 205):

- Laminar: $Re_i < 10$
- Transition: $10 < Re_i < 10^4$
- Turbulent: $Re_i > 10^4$

Vallejos et al. (2006) found that the non-dimensionalised mixing time ($N.\Theta_M$) in a "minibioreactor" of volume ≈ 12.5 mL was directly proportional ($r^2 = 0.99$) to the Re_i in the reactor with the relationship as shown in equation *(B-20)*.

$$N\Theta_M = 0.34 Re_i + 35 \qquad \text{(B-20)}$$

Making Θ_M the subject of equation *(B-20)* yields equation *(B-21)*.

$$\Theta_M = \frac{0.34 d^2 \rho}{\mu_L} + \frac{35}{N} \qquad \text{(B-21)}$$

Equation *(B-21)* shows that the mixing time is inversely dependent of N for N → 0 and independent of N as N→ ∞, therefore for a fixed set of operational conditions and impeller size the mixing time is a constant value at high enough N. This observation was supported by Sano & Usui (1985) who found that in the turbulent regime ($Re_i > 10^4$) the Θ_M was independent of N and therefore only a function of d_i, ρ and μ_L. This is demonstrated in *FIGURE B-7* in which can be seen that at an N ≥ 500 rpm the Θ_M value is within 1 % of the final value as predicted in equation *(B-21)*; D_i = 0.025 m, ρ = 1000 kg.m^{-3} and μ_L = 0.001 Pa.s.

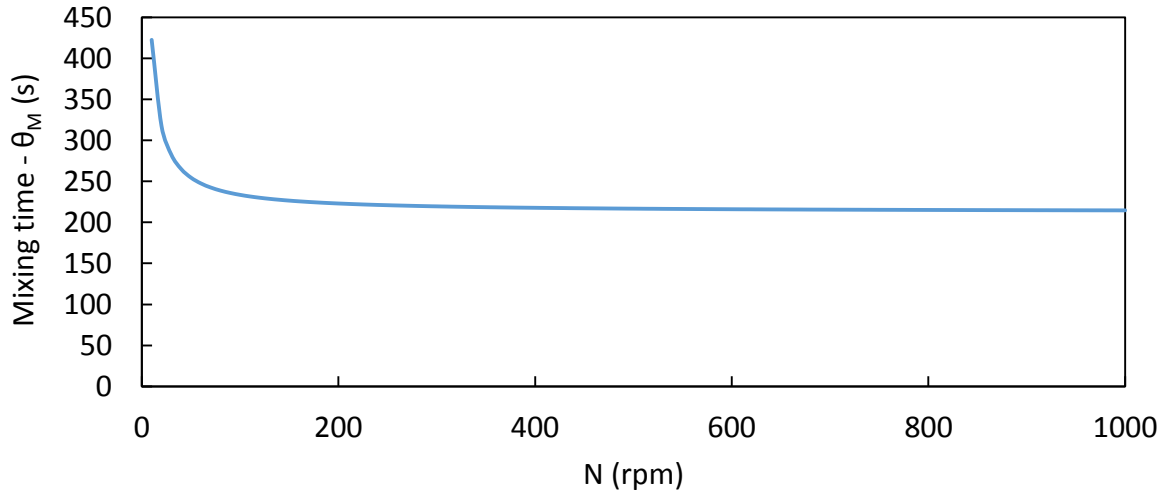

Figure B-7: Mixing time in a stirred vessel as a function of stirring rate (N) calculated using equation *(B-21)*; D_i = 0.025 m, ρ = 1000 kg.m^{-3} and μ = 0.001 Pa.s. It is clear that the mixing time become is within 1% of the final value for N > 500 r.min^{-1}.

B.viii *Wall shear in the GLS*

Due to the small size of the reactor volume, the stirring in the GLS would be done by magnetic stirrer. *FIGURE B-8* shows work done by Mahmud et al.(2009) and Bai et al. (2012) in determining the wall shear at the glass-liquid interface of magnetically stirred reactors. The Re_i of the study by Bai et al. (2012) were in the range 56 000 < Re < 150 000 (fully turbulent regime); the Re_i of the Mahmud et al.(2009) study were in the range 350 < Re_i < 3500 (transitional regime). The shear in stirred vessels can be expressed by equation *(B-22)*, with k_i a constant dependent on the stirrer/impeller as well as system characteristics (Wecker & Onken, 1991; Sánchez Pérez et al., 2006; Campesi et al., 2009).

$$\tau_W = k_i N \tag{B-22}$$

From *FIGURE B-8* can be seen that the characteristic equations for the Mahmud et al. (2009) and Bai et al. (2012) systems can be expressed as equations *(B-23)* and *(B-24)* respectively.

$$\tau_W = 1.5 \times 10^{-2} N \tag{B-23}$$

$$\tau_W = 5.5 \times 10^{-3} N \tag{B-24}$$

The vessel in the Mahmud et al. (2009) study had a diameter (d_T) of 0.15 m with a stirrer of d_i = 0.113 m, while the d_T of the Bai et al. (2012) study was only 0.01455 m with d_i = 0.008 m. The observations of the wall shear in these respective studies showed that the wall shear remained within 1 order of magnitude even though the volumes, stirrer bar lengths and flow regimes differed significantly. It could therefore be reasoned that a system that lay between these measured system-parameters (d_T, d_i, Re_i) would exhibit a wall shear between the values in these two studies. In comparison to work done in 6 L and 30 L laboratory scale bioreactors using four blade turbines (Wecker & Onken, 1991), the measured wall shear stresses were very similar as shown by the triangles in *FIGURE B-8*.

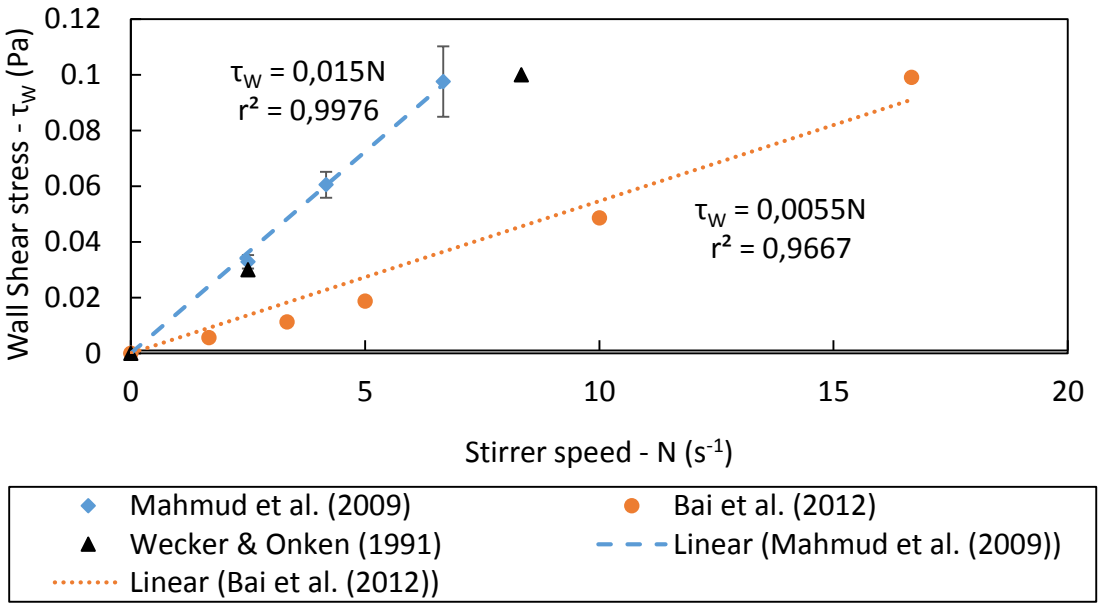

Figure B-8: Measured shear stresses in stirred vessels, as a function of stirrer speed (N) from the literature (Wecker & Onken, 1991; Mahmud et al., 2009; Bai et al., 2012). It is clear from these that the wall shear reaches a maximum value of less than 0.1 Pa for almost all stirring speeds.

The shear stresses measured in these studies were approximately two orders of magnitude smaller than the required shear of 6–8 Pa to inhibit cellular attachment or the 12 Pa required for cellular removal (Bakker et al., 2003; Teodósio et al., 2011), indicating that the require-

ment to inhibit cellular growth on the vessel walls by shear alone would be unrealistic. Assuming equation *(B-23)* holds for the system to be designed, at the maximum rotation of 2 500 r.min^{-1} (N ≈ 42 s^{-1}) a maximum wall shear stress of $\tau_W \approx 0.63$ Pa could be achieved which remains significantly smaller than the $\tau_W >$ 6–8 Pa required.

B.ix *Volume calibration of the GLS system*

The liquid volume in the GLS was calibrated against the liquid level in the vessel as measured by calliper for a non-stirred vessel, the measurement was taken from the bottom of the vessel. The calibration is shown in *FIGURE B-9* and shows a coefficient of determination (r^2) of 0.9997, indicating an almost perfect linear relationship between height and volume. This calibration was used to determine the total volume of the reactor after removal of the biofilm (scrubbing) as the entire contents of the reactor was pumped into the GLS before sampling.

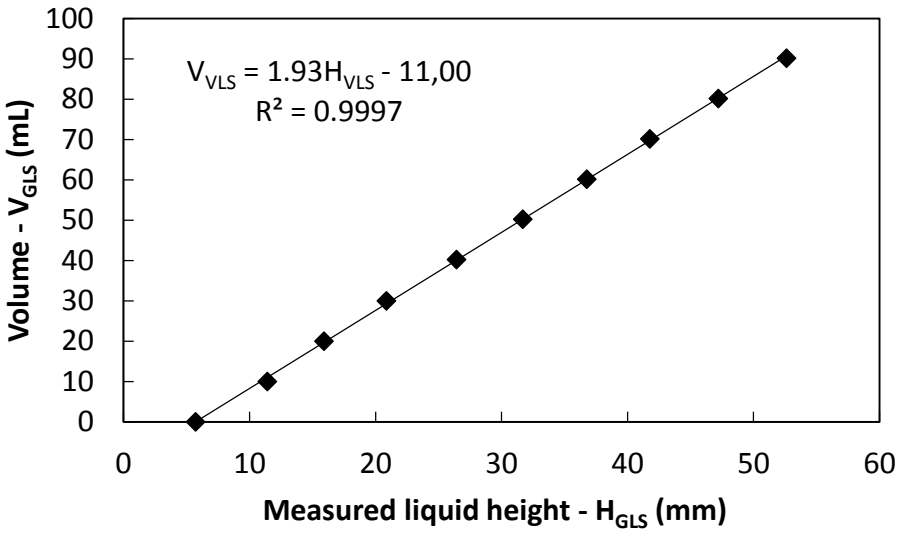

Figure B-9: The total volume in the GLS as a function of the liquid height in the vessel. The calibrations was used to determine the volume of liquid in the reactor during operation as well as at the end of the fermentation runs.

B.x *Black box mass balance in* A. succinogenes *fermentation system*

The black box mass balance treats the system as a "black box" and balances the overall flux of reagents and products (Villadsen, Nielsen & Lidén, 2011: 63). This method permits the description of reagent to product conversion by a single stoichiometric equation, the black box model. From the mass balance the respective stoichiometric coefficients in the black box model are calculated; the balance is based upon three component balances (C, H, O) and the

specification of a number of compound stoichiometric coefficients reducing the degrees of freedom to zero (Villadsen, Nielsen & Lidén, 2011: 96).

The overall black box model (in C-mol units) of the *A. succinogenes* system, given the metabolic map in FIGURE 2-4, is described by equation (B-25).

$$Y_{Glc,Glc}CH_2O(Glc) + Y_{Glc,CO_2}CO_2 \rightarrow Y_{Glc,SA}CH_{\frac{3}{2}}O(SA) + Y_{Glc,AA}CH_2O(AA) + Y_{Glc,FA}(FA) + Y_{Glc,H_2O}H_2O \quad \text{(B-25)}$$

In this system the specified yields (measured variables) were the $Y_{Glc,SA}$, $Y_{Glc,AA}$ and $Y_{Glc,FA}$. The calculated variables were the mass balance of glucose, calculated by determining the stoichiometric coefficient $Y_{Glc,Glc}$, the $Y_{Glc,CO2}$ as well as $Y_{Glc,H2O}$. Assuming that the mass balance closed perfectly, the value of $Y_{Glc,Glc}$ would equal one, i.e. all glucose directed to the predicted products. However a value lower than one would indicate an additional product and a value higher than one would indicate an additional reagent.

The black box mass balance was solved using matrix solution software and solving the vector $\bar{y}$ from equation (B-26)

$$\bar{b} = A\bar{y}$$

$$A = \begin{bmatrix} 1 & 1 & 1 & 1 & 0 & 1 \\ 1.5 & 2 & 2 & 0 & 2 & 2 \\ 1 & 1 & 2 & 2 & 1 & 1 \\ 1 & 0 & 0 & 0 & 0 & 0 \\ 0 & 1 & 0 & 0 & 0 & 0 \\ 0 & 0 & 1 & 0 & 0 & 0 \end{bmatrix}, y = \begin{bmatrix} Y_{Glc,SA} \\ Y_{Glc,AA} \\ Y_{Glc,FA} \\ Y_{Glc,CO_2} \\ Y_{Glc,H_2O} \\ Y_{Glc,Glc} \end{bmatrix}, \quad \text{(B-26)}$$

$$\bar{b} = \begin{bmatrix} 0 & 0 & 0 & Y_{Glc,SA} & Y_{Glc,AA} & Y_{Glc,FA} \end{bmatrix}$$

B.xi *Calibration of NaOH dosing to SA concentration during batch runs*

The accumulated dosing of the NaOH for the pH control was continually logged and are shown in FIGURE B-10.

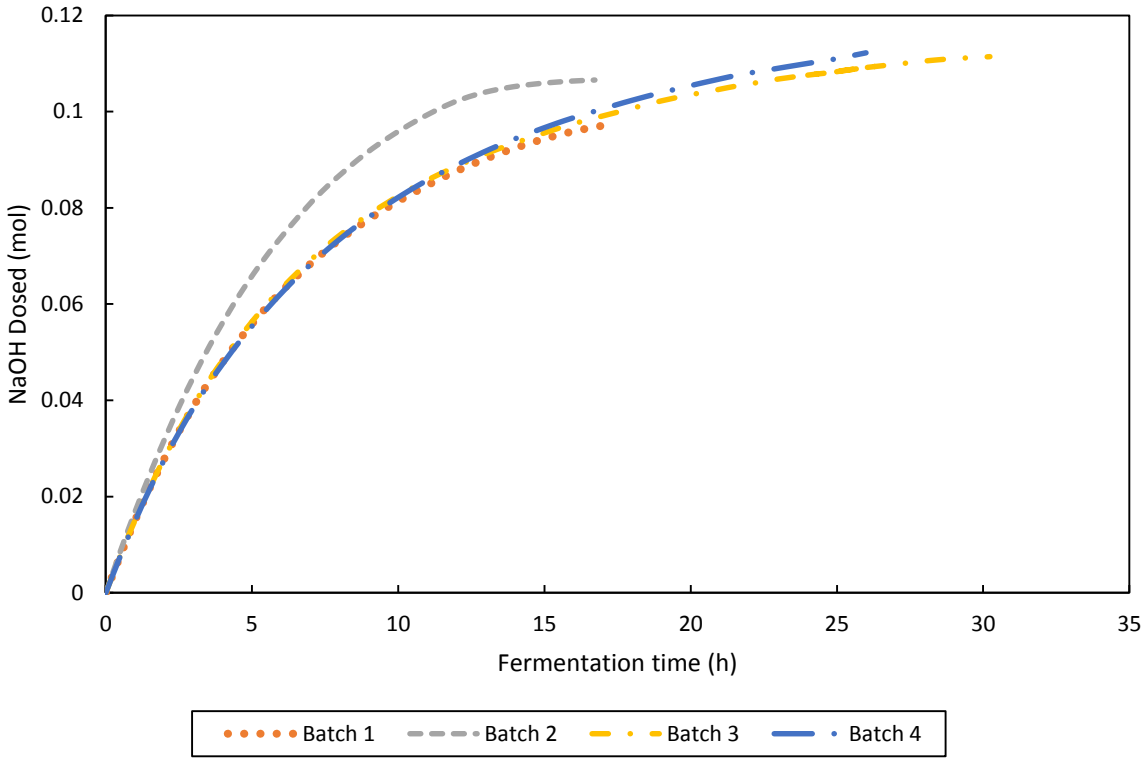

Figure B-10: Cumulative NaOH dosed during batch runs as a function of fermentation time. It is significant to note the similarities between Batches 1, 3 and 4 in terms of the NaOH dosing, while Batch 2 had a significantly higher rate of NaOH dosing (slope of the curve).

The data from *FIGURE B-10* was correlated to the produced SA, as determined from the measured concentrations (*FIGURE 6-7*), and are shown in *FIGURE B-11*. The produced SA was adjusted for the volume of sample taken during the batch run by equation *(B-27)*. The dosed $NaOH_i$ was determined as the total NaOH dosed from the time of batch initiation to the time the sample was taken (equation.

$$\Delta m_{SA,i} = \left(C_{SA,measured,i}\right)(V_i) - \left(C_{SA,measured,i-1}\right)\left(V_{i-1} - V_{Sample}\right) \quad \text{(B-27)}$$

$$m_{SA,i} = \sum_{i}^{0} \Delta m_{SA,i} \quad \text{(B-28)}$$

The total SA produced ($C_{SA,i}$ from equation *(B-28)*) was higher than the measured concentration within the reactor due to the dilution effect of the NaOH as well as the volume reduction during sampling.

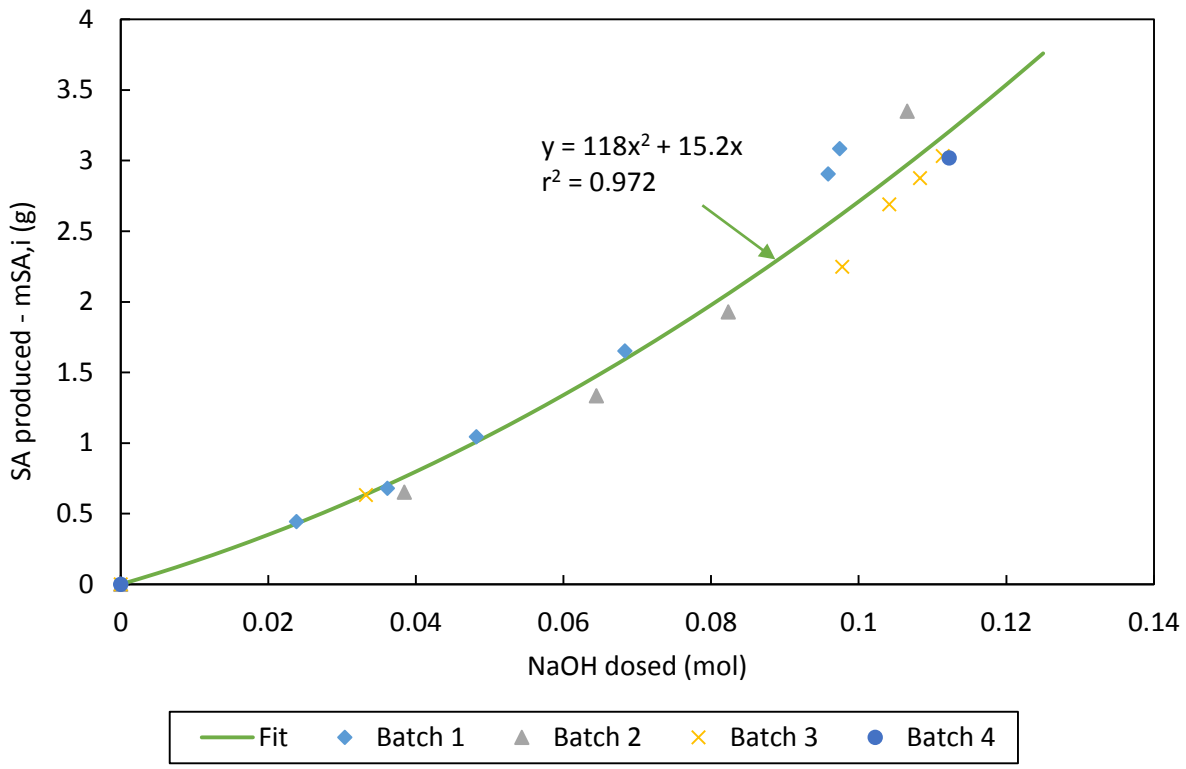

Figure B-11: The SA produced during the batch fermentation runs, as a function of the cumulative NAOH dosed. The upward trend of the function indicates the increasing SA fraction of the total produced acids; the difference is a result of the diprotic nature of SA as opposed to the monoprotic nature of both AA and FA.

The relationship between the $C_{SA,i}$ and the NaOH dosed can be expressed as equation *(B-29)*.

$$m_{SA,i} = 118(NaOH_i)^2 + 15.2(NaOH_i) \quad \text{(B-29)}$$

B.xii *Black box mass balance for system which includes pyruvic acid (PA) as a metabolic product*

The black box model assumed the production of SA, AA, FA, CO_2, H_2O as well as PA, as additional by-product in the system, and is described by equation *(B-30)*. The model is expressed with respect to carbon moles of product, i.e. all products are shown with respect to a single carbon atom and its corresponding ratios of H and O bound to the carbon.

$$\begin{aligned} CH_2O\ (Glc) \rightarrow\ & Y_{Glc,SA}CH_{\frac{3}{2}}O\ (SA) + Y_{Glc,AA}CH_2O\ (AA) \\ & + Y_{Glc,FA}CH_2O_2\ (FA) + Y_{Glc,PA}CH_{\frac{4}{3}}O\ (PA) \\ & + Y_{Glc,CO_2}CO_2 + Y_{Glc,H_2O}H_2O \end{aligned} \quad \text{(B-30)}$$

As was the case with the black box model in section *B.x* on page *B-13*, the black box mass balance was solved using matrix solution software and solving the vector $\bar{y}$ from equation *(B-31)*

$$\bar{b} = A\bar{y}$$

$$A = \begin{bmatrix} 1 & 1 & 1 & 1 & 0 & 1 & 1 \\ 1.5 & 2 & 2 & 0 & 2 & 2 & 4/3 \\ 1 & 1 & 2 & 2 & 1 & 1 & 1 \\ 1 & 0 & 0 & 0 & 0 & 0 & 0 \\ 0 & 1 & 0 & 0 & 0 & 0 & 0 \\ 0 & 0 & 1 & 0 & 0 & 0 & 0 \\ 0 & 0 & 0 & 1 & 0 & 0 & 0 \end{bmatrix}, y = \begin{bmatrix} Y_{Glc,SA} \\ Y_{Glc,AA} \\ Y_{Glc,FA} \\ Y_{Glc,Glc} \\ Y_{Glc,CO_2} \\ Y_{Glc,H_2O} \\ Y_{Glc,PA} \end{bmatrix}, \quad \text{(B-31)}$$

$$\bar{b} = [0\ 0\ 0\ Y_{Glc,SA}\ Y_{Glc,AA}\ Y_{Glc,FA}\ Y_{Glc,Glc}]$$

In this case, the mass balance was assumed to solve completely and therefore the $Y_{Glc,Glc}$ was specified as 1 C-mol/C-mol. This was not possible in the previous case (section *B.x*) as the system had no degrees of freedom and therefore did not allow the specification of the $Y_{Glc,Glc}$. The unknowns solved in this case were $Y_{Glc,PA}$, $Y_{Glc,CO2}$ and $Y_{Glc,H2O}$.